DEVELOPMENT OF YTTRIUM / TiB$_2$ REINFORCED AA2024 MATRIX COMPOSITES WITH SUPERIOR MECHANICAL PROPERTIES

Ph.D. THESIS

By

CH. SURESH VIDYASAGAR

METALLURGICAL AND MATERIALS ENGINEERING DEPARTMENT
INDIAN INSTITUTE OF TECHNOLOGY ROORKEE
ROORKEE – 247 667 (INDIA)
MARCH, 2019

DEVELOPMENT OF YTTRIUM / TiB$_2$ REINFORCED AA2024 MATRIX COMPOSITES WITH SUPERIOR MECHANICAL PROPERTIES

A THESIS

Submitted in partial fulfilment of the requirements for the award of the degree

of

DOCTOR OF PHILOSOPHY

In

METALLURGICAL AND MATERIALS ENGINEERING

by

CH. SURESH VIDYASAGAR

**METALLURGICAL AND MATERIALS ENGINEERING DEPARTMENT
INDIAN INSTITUTE OF TECHNOLOGY ROORKEE
ROORKEE – 247 667 (INDIA)
MARCH, 2019**

INDIAN INSTITUTE OF TECHNOLOGY ROORKEE
ROORKEE

<u>CANDIDATE'S DECLARATION</u>

I hereby certify that the work which is being presented in the thesis entitled "**DEVELOPMENT OF YTTRIUM / TiB$_2$ REINFORCED AA2024 MATRIX COMPOSITES WITH SUPERIOR MECHANICAL PROPERTIES**" in partial fulfilment of the requirements for the award of the Degree of Doctor of Philosophy and submitted in the Department of Metallurgy and Materials Engineering of the Indian Institute of Technology Roorkee, Roorkee, is an authentic record of my own work carried out during a period from July, 2013 to March, 2019 under the supervision of Dr. D. Benny Karunakar, Associate Professor, Department Mechanical and Industrial Engineering, Indian Institute of Technology Roorkee, Roorkee.

The matter presented in this thesis has not been submitted by me for the award of any other degree of this or any other Institution.

(**CH. SURESH VIDYASAGAR**)

This is to certify that the above statement made by the candidate is correct to the best of my knowledge.

(D. Benny Karunakar)

Supervisor

The Ph.D Viva-Voce Examination of Mr. CH. Suresh Vidyasagar, Research Scholar, has been held on _____

Signature of supervisor   Chairman, SRC   External Examiner

Head of Department

DEDICATION

To

My former supervisor

Late. Prof. Vijaya Agarwala

"Do you know that a woman is "not dead" while her name is still spoken?"

—**Terry Pratchett.**

ACKNOWLEDGEMENTS

ABSTRACT

Composites are a class of materials developed by reinforcing one or more materials to the matrix. The properties of a composite mainly depend on the factors like reinforcement material and processing method. Though the reinforcing material has the potential to improve the properties of a composite, the drawbacks and challenges encountered during the production stage deteriorate the properties of the end product. Hence, the present work is emphasized to investigate the influence of a few factors like processing techniques, minor reinforcements of a rare earth element (yttrium) and a ceramic material (TiB_2) on the mechanical properties of AA2024 matrix composites.

In the present work, initially, three batches of each comprising five different AA2024 matrix composites reinforced with varying amounts of micro yttrium ranging from 0.1 to 0.5 wt% are developed through stir casting, cold compaction and spark plasma sintering (SPS). It is revealed that the reinforcement of micro yttrium in small amounts has improved the mechanical properties of AA2024 matrix composites processed through stir casting, cold compaction and SPS. However, the composites developed through SPS showed better properties when compared to those of the composites developed through stir casting and cold compaction. Among the SPSed composite samples, the composite reinforced with 0.3 wt% micro yttrium showed highest values of hardness, UTS, YS and EL which are found to be 114 HV, 315 MPa, 262 MPa and 22.3% respectively. Hence, based on the present work, the processing methods can be rated as SPS > cold compaction > stir casting with respect to the mechanical properties attained in the composites.

In a similar way, a batch of five different AA2024 matrix nano composites reinforced with varying amounts of nano yttrium ranging from 0.1 to 0.5 wt% are also developed through SPS. It is worthwhile to note that AA2024 matrix composite samples with minor reinforcement of nano yttrium showed better mechanical properties compared to those of the composites with reinforced with micro yttrium. From these investigations, it is also found that the composite reinforced with 0.3 wt% nano yttrium showed better properties among the other nano composite samples. Highest hardness, UTS, YS and EL are found to be 130 HV, 462 MPa, 382 MPa and 16.8% respectively for the composite reinforced with 0.3 wt% nano yttrium. These investigations confirmed that reinforcing rare earth element in small amounts to an aluminium

matrix significantly improves its mechanical properties through grain refinement and acceleration of precipitation kinetics.

Finally, a batch of five different AA2024 matrix hybrid composites reinforced with a fixed amount of TiB_2 (1.0 wt%) and varying amounts of nano yttrium ranging from 0.1 to 0.5 wt% are developed through spark plasma sintering. These investigations revealed that the formation of the brittle Al_3Ti phase is supressed and the ductility is retained. As an evidence of grain refinement, ultra fine grains, nano grains and nano precipitation are observed in the microstructures of the composite reinforced with 1.0 wt% TiB_2 and 0.3 wt% nano yttrium. The composite reinforced with 1.0 wt% TiB_2 and 0.3 wt% nano yttrium showed better mechanical properties. Highest hardness, UTS, YS and EL are found to be 137 HV, 496 MPa, 438 MPa and 15.8% respectively in the composite with 1.0 wt% TiB_2 and 0.3 wt% nano yttrium.

In addition, the composites developed through SPS reinforced with varying amounts of micro yttrium ranging from 0.1-0.5 wt% are further subjected to cryo rolling. The mechanical properties of the cryo rolled composites followed the same trend as those of the un rolled composites. Cryo rolling improved the strength of the composites remarkably, but at the cost of ductility.

From the investigations carried out in the present work, it is found that 0.3 wt% yttrium (micro as well as nano) reinforcement seems to create a favourable condition in all the composite samples processed through stir casting, cold compaction and SPS to yield superior mechanical properties. In the composites reinforced with 1.0 wt% TiB_2 along with varying amounts of nano yttrium, formation of Al_3Ti phase is supressed and hence, the ductility of the composites is retained. It is also found that the nano yttrium reinforced composites processed through SPS attained improved mechanical properties when compared to their micro yttrium counter parts. Based on the present work, the processing methods can be rated as SPS > cold compaction > stir casting with respect to the mechanical properties attained in the composites.

Key words: AA2024 matrix, Yttrium reinforcement, Stir casting, Spark plasma sintering, Cold compaction, Mechanical properties, TiB_2 reinforcement, Hybrid composites, Cryo rolling.

INDEX

LIST OF FIGURES

LIST OF TABLES

Symbols, Formulae and Abbreviations

Ψ	-	Densification Parameter
ρ_t	-	Theoretical Density
ρ_s	-	Sintered Density
ρ_g	-	Green Densities
AA	-	Aluminium Alloy
AMC	-	Aluminium Matrix Composite
AMHC	-	Aluminium Matrix Hybrid Composite
AMMC	-	Aluminium Metal Matrix Composite
ASTM	-	American Society for Testing and Materials
ARB	-	Accumulative Roll Bonding
BFS	-	Blast Furnace Slag
BLA	-	Banana Leaf Ash
CI	-	Cast Iron
CMC	-	Ceramic Matrix Composite
CNT	-	Carbon Nano Tubes
COF	-	Coefficient of Friction
CR	-	Cryo Rolling
DCT	-	Deep Cryogenic Treatment
DTA	-	Differential Thermal Analyzer
EDX	-	Energy Dispersive X-rays Spectroscopy
EDM	-	Electric Discharge Machining
EDS	-	Energy Dispersive Spectrum
FA	-	Fly Ash
FE-SEM	-	Field Emission Scanning Electron Microscope
FSP	-	Friction Stir Processing
FSW	-	Friction Stir Welding
FWHM	-	Full Width at Half Maximum
GBF	-	Granulated Blast Furnace
GNP	-	Graphene Nano Platelets
HEBM	-	High Energy Ball Mill
HMMC	-	Hybrid Metal Matrix Composites
HRTEM	-	High Resolution Transition Electron Microscopy
HV	-	Vicker's Hardness
MIG	-	Metal Inert Gas
MMC	-	Metal Matrix Composite
OM	-	Optical Microscopy
PM	-	Powder Metallurgy
PMC	-	Polymer Matrix Composite
RE	-	Rare Earth
RM	-	Red Mud
RT	-	Room Temperature
SCT	-	Shallow Cryogenic Treatment
SDAS	-	Secondary Dentric Arm Spacing
SEM	-	Scanning Electron Microscope
SHT	-	Solution Artificially aged
SPD	-	Severe Plastic Deformation
SPS	-	Spark Plasma Sintering

ST	-	Solution Treatment
TM	-	Transition Metal
UTS	-	Ultimate Tensile Strength
WR	-	Warm Rolling
XRD	-	X-ray Diffraction

1.1 Introduction to composites

The development of materials and their processing technologies reflect the capability and understanding of human beings to deal with new things, which is marked throughout human history. The development of materials began with stone age followed by development of bronze, iron, steel, aluminium and its alloys. The major purpose of alloying the metals is to improve their properties by refining their respective microstructures.

The pressure of developing better materials, which can be used in the field of transportation, aerospace, automobile and other engineering applications, is mounting day-by-day [1]. As it is said, "Need is the mother of all inventions", researchers made it possible to push the limits towards developing new materials and processing techniques which yield better properties [2]. Henceforth, advanced engineering applications demand/require stronger, lighter and cheaper materials, which can perform better with minimum utilization of resources. The intense and dedicated efforts put by the researchers in studying and understanding the fundamental nature of materials and structure-properties relationship led to the development of new generation materials.

Enhanced performance and cost effectiveness are two major conflicting, yet driving forces leading to the development of new materials. This may be achieved by adopting advance processing techniques and also by combining two or more materials with superior qualities. Most of the engineering materials derive superior properties from a combination of components rather than a single component. These materials made up of a combination of two or more phases dispersed on a microscopic scale to obtain optimum/tailored properties are the new generation materials, which are called composites. In technical terms, composite can be defined as a combination of two or more materials mixed or bonded together (matrix, reinforcement, resin, filler, etc.), differing in form or composition on a macro/nano scale. The constituents retain their identities, i.e. they do not dissolve or merge into each other, although they act in co-ordination. Normally, the components can be physically identified which exhibit an interface between each other. The pictorial definition of a composite is shown in Fig. 1.1.

| MATRIX | + | REINFORCEMENT | = | COMPOSITE |

Fig. 1.1 Pictorial definition of a composite.

There are other definitions for a composite available in the literatures, which are mostly similar. However, a few definitions contradict with each other.

Suchetclan [3] explained a composite as a heterogeneous material consisting of two or more solid phases, which are in contact with each other on a microscopic scale. It can also be considered as a homogeneous material on a macroscopic scale in the sense that any portion of it will have the same physical properties.

On the other hand, **Kelly** [4] stated that "composites should not be regarded as a simple combination of two materials. In a broader significance, the combination has its own distinctive properties. In terms of properties and other desirable qualities, composites are better than either of the components alone or radically different from either of them".

1.1.1 Types of composites

These new composite materials include high performance Polymer Matrix Composites (PMC's), Ceramic Matrix Composites (CMC's), Metal Matrix Composites (MMC's), etc. Continuous advancements of these composite materials qualified them to be used in more diversified applications. Out of over 1800 engineering materials available in the market today, more than 200 are composite materials, which reflect their importance.

Generally, composites are classified based on two main factors.

(a)   Matrix material

(b)   Type of reinforcement

The classification of composite materials is shown in Fig. 1.2 and Fig. 1.3.
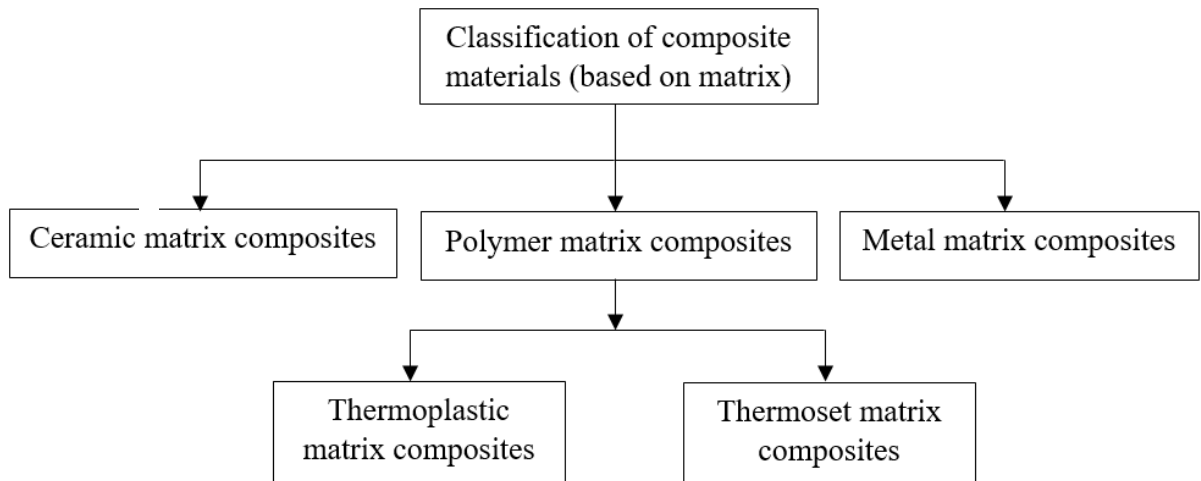
Fig. 1.2 Classification of composites based on matrix material.
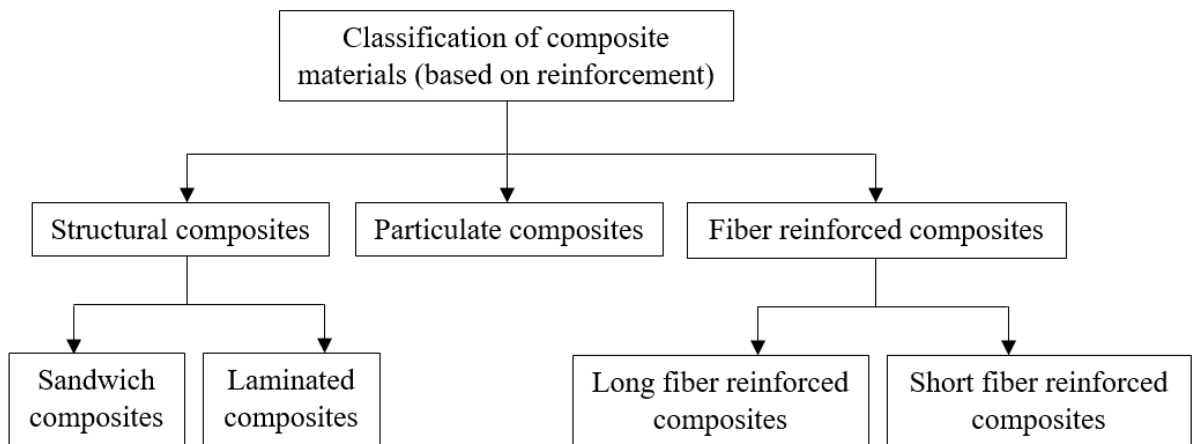
Fig. 1.3 Classification of composites based on reinforcing material.

1.1.2 Advantages and applications of composites

The advantages of a composite are mainly based on the properties of the constituent material phases, their distribution and the interaction between them. Apart from the characteristics of the constituent materials, the geometry of the material (size, shape and distribution) also affect the properties of a composite to a great extent. The orientation and concentration of the reinforcement also affect the properties. The main advantages of composites are listed below [5].

- Dimensional accuracy
- Tight tolerance, repeatable mouldings
- Low post mould shrinkage
- Chemical resistance

3

- Corrosion resistance
- Design flexibility
- Durability
- High flexural modulus to carry demanding loads
- High impact strength
- High performance at elevated temperatures
- Naturally flame resistance
- Creep resistance
- Superior mechanical properties
- Superior thermal stability
- Lighter weight than metal or alloy
- Comparatively lower manufacturing costs
- Moulded in colour
- Moulded in inserts
- Outstanding electrical insulation
- Ability to quench

Applications of composite materials only began in aerospace industry in 1970's [6]. Just after three decades, the applications of the composites have spread very wide in several industries. Fig. 1.4 shows typical applications of composites.

Fig. 1.4 Typical applications of composites. (Source: Slideshare.net.)

Other areas of applications of composites are listed below.

1) Aerospace
2) Automotive
3) Medical

4) Electrical

5) Sports and recreation

6) Chemical Industry

7) Other **-** Composites have long been used in the construction for industrial supports, buildings, long span roof structures, tanks, bridge components and complete bridge systems.

1.2 Aluminium metal matrix composites

Aluminium is the most abundant metal in the Earth's crust, and the third most abundant element, after oxygen and silicon. It makes up about 8.3% by weight of the Earth's solid surface. Due to its high strength to weight ratio, easy availability, easy machinability, durability, ductility and malleability, aluminium is the most widely used non-ferrous alloy [7]. Soviet leader Joseph Stalin wrote a letter to the then U.S. president Franklin Roosevelt in 1941 saying "give me 30,000 tonnes of aluminium, and I will win the war" [8]. Aluminium is also theoretically 100% recyclable without losing its original nature and the use of recycled aluminium is environmentally and economically compelling. Development and modification of aluminium alloys for industrial applications is a never-ending process. Modifications of these alloys mainly depend on either altering the fabrication method or changing the elemental proportions of basic and well-known alloy series [9].

The most common matrix materials of MMCs are aluminium, titanium, magnesium, copper, nickel and various alloys of these metals. The main purpose involved in designing a metal matrix composite material is to combine the desirable properties of matrix material and reinforcement. However, most of the commercial work on MMCs has focussed on aluminium as the matrix material.

Aluminium Metal Matrix Composites (AMMCs), also called as Aluminium matrix composites (AMCs) in short, were developed as a viable and practical solution to the shortcomings of the alloys. The major advantages of AMCs compared to their un-reinforced counter parts are as follows [10, 11].

- Improved high temperature properties
- Better strength
- Better density
- Improved stiffness

5

- Tailored thermal expansion co-efficient
- Improved wear resistance
- Improved abrasion resistance
- Better thermal management
- Higher electrical properties
- Improved damping capabilities etc.

In AMCs, one of the constituent is aluminium/aluminium alloy. In AMCs aluminium is used as the matrix material and most commonly, the materials such as Al_2O_3, SiC, TiB_2, TiC, TiO_2, B_4C, fly ash, TM, graphite, nano materials, etc, are used as the reinforcements. Properties of AMCs can be tailored by varying the constituents and the amount of volume fraction [12].

In general, over monolithic alloys, the Al-MMCs are reputed to have better elastic modulus, tensile and fatigue strength [13]. The yield strength increases after heat treatment in case of heat treatable Al-alloys and their composites by improving the precipitation hardening [14, 49] and reducing the cracking tendency [15]. After fabrication, these materials are artificially aged to peak aged condition to attain better properties [16]. When these reinforcements like ceramics are combined with Al matrix, the resulting composite exhibits significant improvement in its hardness, strength, fracture toughness and wear resistance [17]. Metal bonded ceramic materials are also used as grinding tools to grind materials, which have high wear resistance [18]

Manufacturing is integrally linked with the development of civilization. Some of the important manufacturing processes are machining, metal forming, casting, joining, powder metallurgy, and 3D printing. Some of the important secondary processes are warm rolling, cryo rolling, forging, Friction Stir Processing (FSP), etc. Recently, FSP under rapid cooling conditions is also employed to develop aluminium alloys [19].

1.3 Introduction to work plan

The main objective of the present work is to develop AMCs with superior mechanical properties for aerospace applications such that they would possess lower density, which could be achieved by reinforcing rare earth materials like yttrium in an extremely small proportion in an appropriate aluminium matrix. As a part of this work, some preliminary experiments have been done to optimize the parameters of the processing techniques used in the present study. Materials like AA2024 ingot and powder were used as the matrix materials. Materials like

yttrium and TiB_2 (micro/nano) and were used as the reinforcements. Different batches of composite samples were developed with varying amounts of reinforcement and different processing techniques. The composite samples thus produced were tested for metallurgical/mechanical properties and physical properties.

1.3.1 Development of AA2024 + yttrium composite

Three batches of AA2024 + yttrium composites (five samples in each batch) with varying amount of yttrium ranging from 0.1 to 0.5 wt% were developed using three different processing techniques, viz. stir casting process, cold compaction and spark plasma sintering (SPS). In addition, a set of five composites with varying amount of nano yttrium were also developed through SPS.

In the case of stir casting, AA2024 ingot was used as the matrix and in the case of PM processes AA2024 was used as the matrix in the powder form. Yttrium in the form of chips was used as the reinforcement in all the processes. An attempt was also made to evaluate the density, hardness, strength and ductility of all the composites developed and co-relate them to their respective microstructures and x-ray diffraction patterns. Pure AA2024 samples were also fabricated as a benchmark in each process and the results were compared to assess the effect of yttrium reinforcement. In addition, the composite samples developed through SPS were cryo-rolled and their mechanical properties are evaluated.

Among all the three processing methods, it was found that an optimum amount of yttrium reinforcement (0.3 wt%) could create a favorable condition for optimum precipitation, grain refinement and intermetallic growth in the composites developed, which led to the improvement of mechanical properties. Composites reinforced with nano yttrium and processed through SPS exhibited better mechanical properties compared to others including full density.

1.3.2 Development of AA2024 + nano yttrium + TiB₂ hybrid composites

Five AA2024 matrix composite samples reinforced with different proportions of nano yttrium along with 1.0 wt% TiB_2 to each sample were developed through SPS. The main objective of adding TiB_2 to Al-Y powders was to evaluate the effect of TiB_2 on the mechanical properties of the hybrid composite thus developed. By processing the powders through SPS, the formation of brittle Al_3Ti phase was suppressed and hence the ductility of the composites was retained. Dual grain size was also observed in the composite with 0.3 wt% yttrium. Even in these hybrid

7

composites, it was found that an optimum amount of yttrium reinforcement (0.3 wt %) could create favourable conditions for the formation of nano grains and nano precipitates, thus achieves superior mechanical properties in the composite, compared to Al-Y composites.

1.4 Overview of processes used

The processes used in the present study are summarised below.

1.4.1 Stir casting

In a stir casting process, the reinforcing material (usually in powder form) is distributed into the matrix by stirring the melt mechanically. **Ray** [20] initiated stir casting of metal matrix composites in 1968, when he introduced alumina particles into aluminium melt by stirring molten aluminium. Stir casting process of aluminium matrix composite is illustrated in Fig. 1.5. Mechanical stirring in the furnace is a main element of this process. The resultant molten composite can then be used for die-casting, permanent mould casting, or sand casting. Stir casting is suitable for manufacturing composites with up to 30% volume fractions of reinforcement. However, hot tearing in casted samples is common which deteriorate their strength, but efforts have been made to eliminate it [21].
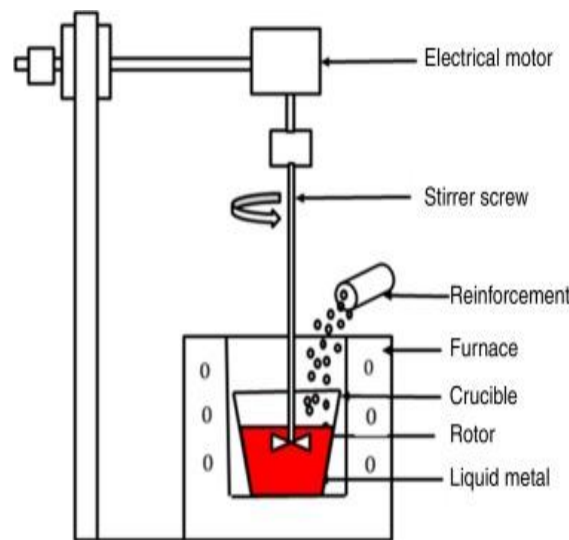
Fig. 1.5 Stir casting process [21].

One of the major barriers associated with the stir casting process is the agglomeration of reinforcing particles, which is caused due to settling of the particles at the bottom during the melting and solidification processes. The distribution of the particles in the final solid composite depends on matrix material properties and process parameters such as the wetting condition of

the reinforcement with the melt, relative density, rate of mixing, and rate of solidification. The distribution of the particles in the molten matrix also depends on the geometry of the stirrer, stirring speed, placement of the stirrer in the melt, melting temperature of the matrix, and the properties of the reinforcing particles added [22]. Compared to other well-established metal matrix composite fabrication methods, stir casting is the most economical and costs as little as one third to one tenth when mass produced [23]. Therefore, stir casting is currently the most popular commercial method of producing aluminium based composites. However, oxidation of the melt during solidification deteriorates the mechanical properties of the cast product.

1.4.2 Cold compaction

Powder metallurgy (PM) is the process of blending fine metal powders, pressing them into a desired shape (compacting), and then heating the compacted material in a controlled atmosphere to bond the powders together (sintering) [24]. The basic steps involved in powder metallurgy are shown in Fig. 1.6.
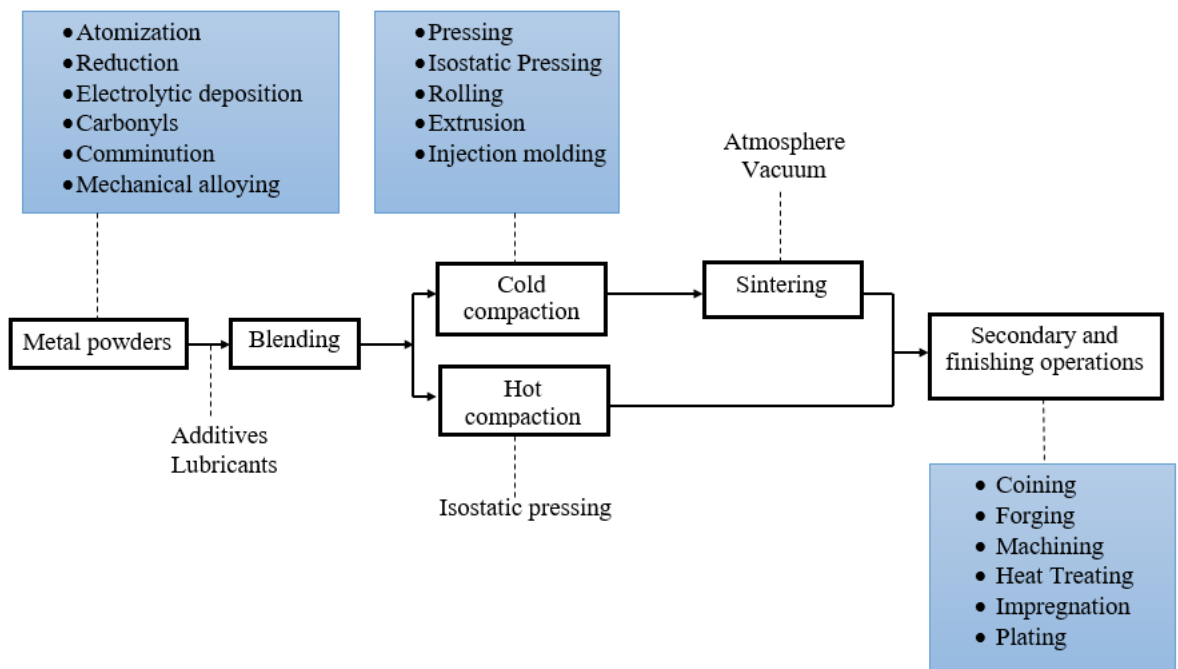
Fig. 1.6 Basic steps involved in powder metallurgy process [24].

The powder metallurgy process generally consists of four basic steps: (1) powder manufacture, (2) powder mixing and blending, (3) compacting, (4) sintering [25]. Compacting is generally performed at room temperature and the process of sintering at elevated temperature is usually conducted at atmospheric pressure.

Certain special metals that are difficult to be manufactured by other techniques can be shaped to full density by powder metallurgy. Important applications of PM include aerospace, automobile, lamp filaments, oil-impregnated bearings, gears, filters, etc., [28].

However, sintering of aluminium powder is a challenge as each powder particle forms a protective oxide layer around it to prevent the particle from further corrosion. **Davim et al.,** [26] sintered aluminium 6061 matrix powders in the presence of a gas comprising about 10 to 100% nitrogen by volume and a non-oxidizing gas like hydrogen or argon as the balance, which could prevent oxidation and enhance densification.

Mahesh et al., [27] investigated aluminium metal matrix composites produced through powder metallurgy route. Different composites are processed by adding different amounts of ZrB_2. The powder blend was compacted and sintered without external pressure at 550° C for 1 hour in a controlled argon gas atmosphere and concluded that the relative density of the sintered products was 90% approximately. Sintered preforms are used as the sample material for deformation study at different temperatures in order to determine the effect of temperature on the densification behaviour.

1.4.3 Spark plasma sintering

PM has certain limitations that large components and complex shapes cannot be fabricated effectively. Further, compaction and sintering of the composite cannot be done simultaneously causing a delay in the process. A new technique called spark plasma sintering (SPS) has emerged as an alternative consolidation technique to overcome this problem by enabling compacting and sintering simultaneously reducing the processing time.

Spark plasma sintering is an advanced sintering technology that has developed rapidly in the recent years. It is a solid consolidation sintering process that has the key advantage of obtaining a very high degree of densification at low-sintering temperatures and within a short time, compared to the conventional sintering methods. The processing mechanism of SPS is shown in Fig. 1.7.
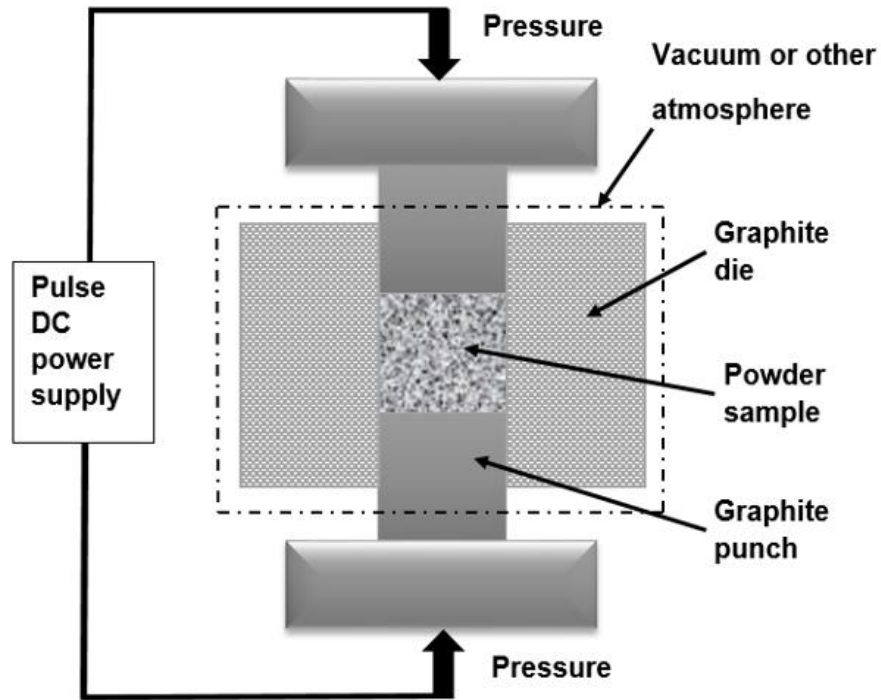
Fig. 1.7 Processing mechanism of SPS.

Unlike conventional PM route, SPS process simultaneously applies a low-voltage, high-intensity pulsed direct current and uni-axial pressure at the same time, which offers the possibilities of using rapid heating rates (e.g., achieving 1000º C/min) and very short holding times (3–5 min) to obtain highly dense samples [29]. However, in contrast to many reports of the experimental studies on the processing parameters for new material preparation, the mechanisms for densification of sintered compacts still remains unclear and systematic investigations on the mechanisms underlying the SPS features are limited in the literature. In some publications concerning the factors that contribute to the rapid densification process [30], it is frequently argued that during the initial stage of the sintering process, the ON–OFF pulsed direct current generates a spark discharge between the powder particles. The gases existing in the sample can be ionized and transformed into plasma.

During sintering, the generated spark and plasma promote the elimination of absorbed gases and oxide layers on the surface of powder particles; hence, the particle surfaces are cleaned and activated, which lead to a favourable diffusion bonding between the particles, thus accelerating the densification of the compact.

1.4.4 Cryo rolling

Cryo-rolling is a severe plastic deformation (SPD) process carried out at cryogenic temperatures (i.e. below −190 °C) and is used to obtain ultrafine grained nano structured materials with higher strength and hardness than in conventional cold rolling. Schematic diagram of cryo-rolling process is shown in Fig. 1.8.
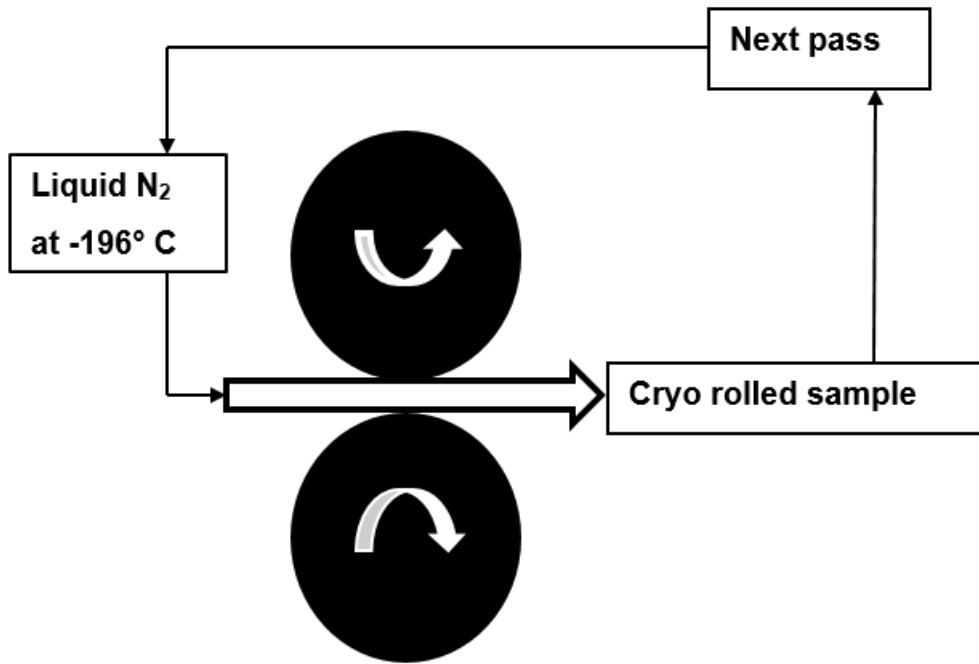
Fig. 1.8 Schematic diagram of cryo-rolling process.

However, it results in poor ductility and formability. Deformation in the strain hardened metals by cryo-rolling is preserved as a result of the suppression of the dynamic recovery. Hence, large strains can be maintained which lead to fine grained structure. Generally, cryo-rolling is a secondary process employed to bulk materials fabricated through other methods or processes. Cryogenic treatments of materials can be classified as follows:

1) Deep cryogenic treatments (DCT) (-196° C).
2) Shallow cryogenic treatments (SCT) (-77° C).

Different treatments are used for different applications. Some of the applications of cryo-rolling are aerospace, marine, military, cutting tools, medical equipment, musical instruments, etc, [31].

1.5 Overview of results

Addition of 0.3 wt% yttrium seems to create a favourable condition in all the composite samples developed using stir casting, cod compaction and SPS to yield superior mechanical properties. Composites reinforced with nano yttrium showed better mechanical properties compared to that of the composites reinforced with micro yttrium. Addition of 1.0 wt% TiB_2 in all the hybrid composites has made remarkable grain modifications in the composites. Cryo rolling increased the mechanical properties of the composites like hardness and tensile strength. However, dutility decreased drastically. The processing methods can be rated as SPS > cold compaction > stir casting, with respect to mechanical properties attained in the composites.

1.6 Organization of thesis

Different chapters of the present thesis are organized as follow.

Chapter 1: INTRODUCTION

This chapter introduces the concept of the composites in detail focusing on AMCs with different reinforcements. The work plan of the present research work, overview of the processes used and overview of the results obtained are presented in brief.

Chapter 2: LITERATURE REVIEW

This chapter critically reviews and puts forth the recent developments in AMCs using stir casting, cold compaction and SPS with various reinforcements focusing on their process parameters and mechanical properties. Structure-property relationship of the AMCs is extensively reviewed by comparing the metallurgical characterization with the corresponding mechanical properties. Critical literature review is done regarding reinforcing of Rare Earth (RE) to AMCs.

Chapter 3: EXPERIMENTAL PROCEDURE

This chapter introduces and discusses the equipments and instruments used for the present investigations elaboratively. Standard sample preperation (according to ASTM) for both mechanical and metallurgical characterization, and testing procedures at each stage are presented in detail.

Chapter 4: DEVELOPMENT OF AA2024 + YTTRIUM COMPOSITE

This chapter discusses different development routes, mechanical and metallographic characterization of AA2024 + Yttrium (micro/nano) composites in the light of the effect of reinforcements and process parameters by corelating microstrutures with mechanical properties.

Chapter 5: DEVELOPMENT OF AA2024 + YTTRIUM + TiB$_2$ HYBRID COMPOSITE

This chapter discusses the development of composite, mechanical and metallographic characterization of AA2024 + nano yttrium + TiB$_2$ composites including the role of reinforcements and process parameters in the formation of nano grains.

Chapter 6: GENERAL CONCLUSIONS

In this chapter, the cumulative and overall conclusions are presented from the entire research work. Some light is also thrown on the scope for future work. This chapter is followed by the list of references, vitae of the candidate and the list of publications of the candidate.

Chapter 2
LITERATURE REVIEW

This literature review is carried out as a part of the present research work to provide an overview on the development of second, third and fourth generation AMCs and their processing techniques. Different aluminium alloy matrices and reinforcing materials are thoroughly reviewed. Structure-property relationship of the AMCs is reviewed by comparing the metallurgical characterization with the corresponding mechanical properties. Processing techniques of AMCs are extensively studied focusing on stir casting, cold compaction, SPS and cryo rolling.

2.1 Review on reinforcing materials in aluminium metal matrix composites

In AMCs, aluminium is used as the matrix material, and the materials such as ceramics, fly ash, graphite, carbon nano tubes (CNTs), Transition Metals (TM), Rare Earth (RE), nano materials, etc., as reinforcements. The properties of AMCs can be tailored to fit the purpose by varying the type and amount of reinforcement. Some of the important reinforcing materials are characterised below.

A. Ceramic reinforcement

Generally, one of the most important reinforcing materials to AMC is ceramic material. Many researchers have incorporated several ceramic materials in various proportions to different series of aluminium alloys in order to increase their potential to load bearing capacity and durability.

The advantages of ceramic reinforcement can be quantified for better understanding and appreciation. For example, Young's modulus of pure aluminium can be enhanced from 69 GPa to 250 GPa by reinforcing with 60 vol% of continuous Al_2O_3 fibre. On the other hand, reinforcing 60 vol% Al_2O_3 fibre in pure aluminium reduces the thermal co-efficient from $25 \times 10^{-6}/°C$ to $6 \times 10^{-6}/°C$ [32]. Similarly, wear resistance of Al-9%Si-20%SiCp composite is equivalent or better than grey cast iron.

All these examples show that it is possible to alter many types of properties of aluminium and aluminium alloys by more than twice or thrice the order of magnitude by reinforcing with appropriate materials in suitable amounts.

The key advantages of AMCs in transportation sector are improved performances while maintaining low fuel consumption, less noise and lower airborne emissions with increasing strict environmental regulations [33].

The overall performance of a composite is the cumulative contribution of the shape and size of the individual constituents, their distribution and structural arrangement. For every composite, the factors that determine the properties are microstructure, volume fraction of the reinforcement, isotropy, homogeneity of the system, etc. For instance, density is the physical property that reflects the characteristics of composites. In general, the proportions of the matrix and reinforcement are expressed either as the weight fraction (w), which is convenient for fabrication, or as the volume fraction (v), which is commonly used in density calculations. Experimentally, the density of a composite is calculated by displacement technique, using a physical balance with density measuring kit as per ASTM: D 792-66 test method. However, density can also be calculated from porosity and apparent density values (sample mass and dimensions).

Miyajima et al., [34] reported that the density of Al 2024-SiC particle reinforced composite is higher than that of Al 2024-SiC whisker-reinforced composite. From the above investigation, the increase in density can be due to the fact that the ceramic particles possess higher density. Further, the increased volume fraction of these particles contributes in increasing the density of the composites. In addition, the authors have stated that the theoretical and measured density values of these composites match with each other (full density condition).

By the Archimedean principle, **Sahin and Murphy** [35] determined the density of SiC-coated unidirectional boron fibre-reinforced Al 2014 matrix composites. The mechanical properties like hardness increased linearly with increased volume percentage of reinforcements and the tensile strength of the base Al alloy was 172 MPa, whereas, tensile strength of the composites was in the range of 312 to 524 MPa.

Kalkanli and Yilmaz [36] also reported that the hardness of the composites was observed to be decreasing with an increase in porosity. They also concluded that the maximum hardness and tensile strength is obtained in the composite with 24 hours ageing and precipitation heat treatment at 120°C with 10 wt% SiC.

Deuis et al., [37] concluded that the factors affecting the hardness of composite containing hard ceramic particles are the size of reinforcement, interface bonding and structure of the constituents. Moreover, these composites exhibit excellent wear resistance due to the superior hardness due to uniformly distributed reinforcement. On the other hand, **Fang et al.,** [38] observed that an *in situ* formed Al-ceramic composite had low Vicker's hardness because of some reaction contamination and high porosity.

Lee et al., [39] have developed AA 6061/SiCp composites by the pressure less infiltration method under a nitrogen atmosphere and studied their microstructures and tensile properties. They concluded that the reaction layers (Al_4C_3) which were formed at the interface between SiCp and Al alloy matrix as a result of the in situ reaction has significantly affected the ductility rather than strength. **Veeresh et al.,** [34] reported that the tensile strength of Al 7075-SiC composites were found to be improved by increasing the volume percentage of ceramic phase but at the cost of reduced tensile ductility.

Klimowicz and Vecchio [41] found that the fracture toughness decreased and tensile strength increased with aging time in Al_2O_3 reinforced 6061 and 2014 matrix composites. However, the fracture toughness continued to decrease even in the over-aged condition where the strength was decreasing.

Whereas, **Deshmanya and Purohit** [42] concluded that the hardness of Al 7075-Al_2O_3 composites constantly decreased with an increase in the size of reinforcement because coarse grain size results in a lesser dense distribution of Al_2O_3 particles in the matrix. The hardness of the composites was reported to be dropped initially with an increase in the proportion of reinforcement. However, after about 8% addition of reinforcement, there was a substantial improvement in the hardness. A maximum hardness of 140 HV was observed for the composite containing 15% of Al_2O_3. With an increase in the reinforcement percentage, the ratio of reinforcement-to-matrix becomes richer, which imparts increased hardness to the composite. However, the authors did not explain clearly about the initial decrease in hardness.

Jayaram and Biswas [43], from their investigations, reported that porosity of the composite was the major influencing factor for the decrease in the hardness of Al_2O_3 and SiC reinforced Al matrix composites.

In another study, **Veeresh et al., [44]** reported that the micro-hardness (HV) of Al 6063-SiC and Al 7075-Al_2O_3 composites increased with an increase in the percentage of reinforcement addition. However, hardness and tensile strength of Al 7075-Al_2O_3 composites were observed to be more as compared to those of Al 6063-SiC composites. The UTS of Al 6063-SiC and Al 7075-Al_2O_3 composites increased with an increase in the percentage of reinforcement.

Selvaganesan et al [45] studied the production and characterization of Al-TiB_2 composites by stir casting method. The stir casting process, which was carried out at 750º C, was successfully utilized for casting Al-6061 matrix composites reinforced with TiB_2 particles. Aluminium composites so developed exhibited uniform distribution of the particles in the matrix and good interface bonding between the ceramic particles and the metallic matrix. The mechanical properties of the AMCs have improved when the proportion of TiB_2 was increased. The tensile strength increased significantly to 220MPa when the TiB_2 particles reached 9% of the composite. The hardness value of 12% TiB_2 increased by 50% compared to the unreinforced base alloy.

Ravi Kumar et al., [46] investigated the mechanical properties of AA 6082 composites reinforced with tungsten carbide (WC) particles (2, 4, 6, 8 and 10 wt%) by stir casting. The density, impact strength and elongation of the composites decreased with an increase in the addition of WC, while the hardness of composites increased with an increase in the addition of tungsten carbide. The tensile strength of the composites increased initially and then decreased.

Nie et al., [47] successfully developed and investigated boron carbide (B_4C) particulates reinforced 2024 aluminium matrix composites by mechanical alloying, followed by hot extrusion. A clean and strong interface bonding between B_4C and aluminium matrix was observed from the microstructures. The yield strength and Young's modulus values were improved significantly over the monolithic base 2024 alloy. A homogeneous distribution of B_4C particles was also observed throughout the matrix.

Jinfeng et al., [48] developed a kind of Al-TiB$_2$/TiC in situ composite using the melt reaction method and the accumulative roll-bonding (ARB) technique. It was found that the distribution of reinforcement particles became more homogenous with an increasing ARB cycle. Meanwhile, the mechanical properties showed great improvement during the ARB process. The ultimate tensile strength (UTS) and micro hardness of the composites were increased to 173.1 MPa and 63.3 HV respectively after two ARB cycles. **Alaneme and Aluko** [49] also observed that the strain to fracture was less affected by the volume fraction of reinforcement and heat treatment in Al 6061 matrix composites.

B. Metallic and intermetallic reinforcement

Recently, non-conventional compositions of rapidly solidified aluminium alloys reinforced with transmission metal-based alloys (RS-Al-TM), (TM = Transition Metal such as Fe, Ni, Cr, V, Zr, Ti, rare earth metals, etc.) attracted great interest of researchers. These RS-Al-TM alloys have been reported to achieve tensile strengths above 1000 MPa because of their ability to form amorphous or nano-crystalline structure through a suitable process, as shown in Fig 2.1.
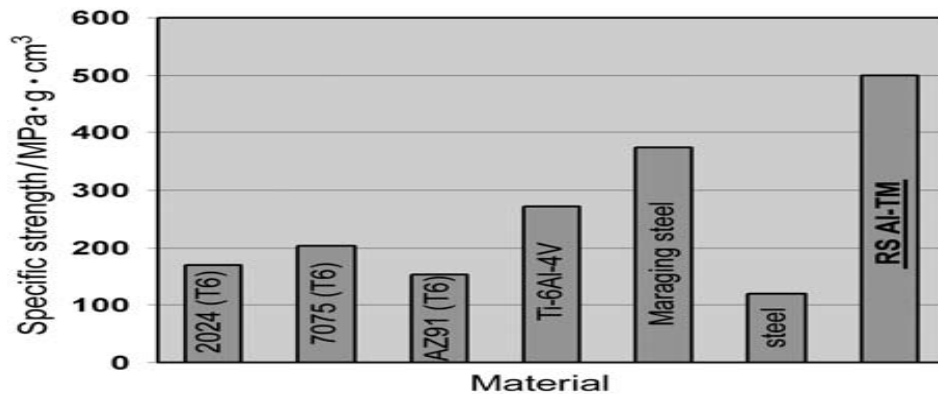
Fig. 2.1. Comparison of specific strength of various materials (**Veeresh et al,** [43]).

This ultra-high tensile strength is achieved through modifying the grain structure to amorphous state. It is reported that the tensile strengths of these aluminium alloys can go up to levels above 1200 MPa that are more than twice than that of the commercial high strength aluminium alloys [9]. In-situ method provides the possibility to refine the grain size in the matrix leading to improvement in physical and mechanical properties of aluminium composites [50].

Vijaya et al., [51] developed aluminium metal matrix composites reinforced with medium carbon steel short fibres by hot pressing with 50 MPa axial stress and subsequent sintering. Improved densification was achieved for up to 10 wt% reinforcement. A maximum hardness of

51 HV was achieved for 10 wt% at 550⁰ C for 15 min sintering time and it was concluded that the critical reinforcement is 10 wt%.

Davidson et al., [52] compacted and sintered aluminium–copper composite powders with 2 wt%, 4 wt% and 6 wt% copper content with different initial relative densities by applying recommended powder compaction pressures. The results showed that the amount of densification in the composite increased with an increase in copper content under similar working conditions. In another study, they reported the effect of ZrB_2 on Al-ZrB_2 composites using conventional sintering and concluded that increase in ZrB_2 content improved the strength of the composite [53].

Manikanta et al., [54] studied and compared the mechanical properties of Al 2024-gray cast iron (CI) composite with age hardening process. The composites were developed by reinforcing gray cast iron powder in AA2024 through double stir casting method. Heat treatment was given so as to tailor and improve the mechanical properties as per the requirement. The results revealed that artificial aging had a positive effect on hardness of both the composites. The tensile test result showed that 4 wt% gray C.I composite in peak-aged condition at 100⁰ C has the highest ultimate tensile strength. There is an increase in tensile strength for both as cast and peak aged specimens (both 100⁰ C and 200⁰ C) from 0% to 4 wt% and a decrease for 6 wt% of reinforcement.

Haribabu et al., [55] prepared Al–Cu composites by dispersing (5–15 wt%) copper powder in molten Al 2024 alloy by stir casting vortex method. Based on the results, the authors concluded that there was a homogeneous distribution of particles in the matrix phase without voids and discontinuities in the composites. From the microstructures, it was observed that Al_2Cu precipitation occurred in both the samples and grain refinement took place in the composite sample with 5 wt% Cu. The EDX analysis revealed that there was no contamination from the atmosphere in the composites due to the Nitrogen gas atmosphere employed during the process. The hardness of the composites increased with an increase in the amount of Cu to the base alloy.

Wang et al., [56] developed composites consisting of Al 2024 matrix reinforced with β-Al_3Mg_2 particles through powder metallurgy with the aim of reducing the density of the material, at the same time, increasing the strength of the matrix. The results revealed those the composite with 20 vol% reinforcement showed yield and compressive strengths exceeding that

of the unreinforced alloy by about 120 and 180 MPa, while retaining appreciable plastic deformation of about 30%. The strength of the material was further improved for the samples with 30 and 40 vol% of β-Al$_3$Mg$_2$ phase. However, the composites showed reduced elongation percentage of 11 and 4.5. Moreover, the addition of the low-density β-Al$_3$Mg$_2$ particles decreased the density of the materials below that of the base 2024 matrix, thus increasing the specific strength of the composites.

Jinwen et al., [57] developed ultrafine-grained in situ synthesized Al$_3$Ni particulate-reinforced composites by friction stir processing (FSP), introducing Ni powder into the stirred zone of 1100-H14 aluminium alloy. The XRD and EDS analyses showed that the Al–Ni in situ synthesizing product was Al$_3$Ni. When the specimen was stirred for two passes, the formed Al$_3$Ni was tiny to be detected. Al$_3$Ni subsequently became apparent when stirring for 4 to 6 passes and the fine Al$_3$Ni particles were dispersed homogeneously in the composites, which caused significant increase in the micro hardness and UTS of the composites.

In a similar study, **Hsu et al.,** [58] produced intermetallic-reinforced AMCs by FSP from elemental powder mixtures of Al–Cu and Al–Ti. The intermetallic phases were identified as Al$_2$Cu and Al$_3$Ti, which were formed in situ during FSP. The volume fraction of the intermetallic phases in the in situ composites may reach as high as ~ 0.5. The composites produced were fully dense with high strength, and the composite strength increased with an increase in the reinforcement.

Jayanthi et al., [59] focused on improving the specific strength of AA 2924 by reinforcing with entropy alloy particulate through stir casting route. Based on the experimental results, increase in reinforcement content enhanced all the mechanical properties such as yield strength, tensile strength and Young's modulus of elasticity. Specific hardness of the resultant metal–metal composites is much superior to conventional MMCs. The decrease in particle size with increasing reinforcement content enhances the surface area to volume ratio of the resultant particulates. Except ductility, an average increment of 62% is observed in mechanical properties of the composite compared to the base alloy.

C. Rare earth (RE) material reinforcement

Rare earth elements are called "vitamins" in metals, and their metal activity is second only to alkali metals and alkaline earth metals. Adding a small amount of rare earth material to a metal

can greatly improve its performance [60]. Many studies have shown that rare earth element modification can effectively improve the comprehensive mechanical properties of aluminium alloys [61, 62].

Qiu et al., [63] investigated the modification of near-eutectic Al-12Si alloys with Samarium and found that a good mechanical performance of the upgrade has been obtained when the addition of Samarium (Sm) was up to 0.6 wt %.

Kaur et al., [64] studied the influences of electromagnetic stirring and rare earth addition on reciprocating wear behaviour of hypereutectic Al-Si alloys and found that the process has significantly decreased the wear rates of the said alloys. Rare earth elements such as Lanthanum (La), Cerium (Ce), Yttrium (Y), and Misch metal (MM) were reported to act as effective modifiers. Misch metal contained 50-52% Cerium, 20-22% Lanthanum, 15-17% neodymium and 10-12% of other rare earth elements and its addition increases under cooling up to 25° K with 0.2% addition giving rise to modified precipitate shapes. Rare earth elements are used to modify Si phase from acicular needles to fibrous one and results in enhancing the tensile properties [65]. It is well known that trace element additions to aluminium alloys can strongly influence the precipitation process, including modifying the dispersion, morphology and crystal structure of the resulting precipitations [66-69]. Studies on rare earths as micro-alloying elements showed that they had beneficial effects on the mechanical properties of aluminium alloys. It was reported that addition of Ce to Al-Cu-Mg-Ag alloy improved the thermal stability of the Ω phase thus raising the service temperature of this alloy [67].

Li et al., [70] demonstrated that reinforcing 0.1%−0.2% (mass fraction) yttrium improved the tensile properties of 2519 alloy at room as well as elevated temperatures as addition of yttrium changed the size and density of θ′ phase. **Zhang et al.,** [71] indicated that Neodymium (Nd) was mainly distributed in form of intermediate compound AlCuNd, which exerted a restraining force on the grain boundaries and enhanced the mechanical properties of 2519 alloy at high temperature. Some recent researches showed that Yb was considered as an effective micro-alloying element in aluminium alloys. It was reported that Yttribium (Yb) addition improved the mechanical properties of Al-Cu-Mg-Ag alloy and Al-Zn-Mg-Cu-Zr alloy [72, 73]. Moreover, complex additions of Yb, Cr and Zr to Al-Zn-MgCu alloy significantly enhanced the resistance to recrystallization [74, 75].

Lim et al., [76] developed A356 aluminium composites by reinforcing scandium (Sc) in the proportions of 0.1, 0.2 and 0.3% by weight, using gravity die casting process. The results obtained in this work revealed that scandium could significantly enhance the mechanical properties of A356 matrix composite in terms of tensile strength, hardness and charpy impact strength. In conclusion, the addition of 0.2 wt% Sc in A356 alloy was able to achieve the maximum tensile strength of 172.94 MPa as compared to 136.03 MPa for the sample without reinforcement of Sc. No significant improvement in tensile strength was found when more than 0.3 wt% Sc was reinforced to the base alloy. As for the hardness, the sample with 0.3 wt% Sc attained the maximum Vicker's hardness of 86.60 HV, as compared to 76.48 HV for the unreinforced A356 alloy.

Zhang et al., [77] developed a new technology to improve the elongation of A365 alloy by reinforcing it with RE elements during melt processing. After the treatment, the elongation was 19.5% for A356 alloy with RE addition, which was much higher than that of 13% for the normal A356 alloy. Microstructure observation showed that the morphology of Si changed significantly from rod shape to spheroid. The improvement of elongation was attributed to the morphology change of α-Al and eutectic Si.

In a similar study, **Lim** [78] investigated the efficiency of yttrium on grain refinement of A356 aluminium alloy developed through gravity die casting. Yttrium was reinforced in proportions of 0.3 and 0.6 wt% to the base A356 alloy. The reinforcement of yttrium was found to reduce the primary coarse α-Al and refine the eutectic silicon phase to a finer and more fibrous structure. The grain size measured in μm^2 /grain was 65.2 for pure A356 alloy, 51.1 for Al-0.3 wt% Y and 57.3 for Al-0.6 wt% Y. The reinforcement of 0.3 wt% yttrium to A356 alloy was found to be the most optimal to achieve the finest grains and modify the coarse eutectic phase to be more fibrous. The grain refining efficiency of yttrium is attributed to its ability to reduce the growth of the coarse dendritic grains and clean the interface between α-Al and eutectic phase.

Wang et al., [79] synthesized in-situ $(Al_2O_3+Al_3Zr)$/A356 composites by melt reaction technology and investigated the effects of yttrium on microstructure and mechanical properties. The results indicated that the reinforced particulates Al_2O_3 and Al_3Zr became smaller in size about 0.5~2 μm with yttrium reinforcement and the distribution became more homogeneous. With 0.4 wt% yttrium reinforcement, the ultimate tensile strength and yield strength of the

composites reached to 388 MPa and 296 MPa respectively, which are 35.6% and 37.0% improvement compared to the composites without yttrium reinforcement respectively.

2.2 Review on aluminium metal matrix composites using stir casting

Casting of metals is one of the earliest processing techniques known to man. One of the major barriers associated with casting process for fabricating AMCs is the agglomeration of reinforcing particles, which is caused due to settling of reinforcement particles at the bottom during the melting and solidification process. The distribution of the reinforcing particles in the final solid composite depends on matrix material properties and process parameters such as the wetting condition of the reinforcement with the melt, relative density, rate of mixing, and rate of solidification. The distribution of the particles in the molten matrix also depends on the geometry of the stirrer, stirring speed, placement of the stirrer in the melt, melting temperature of the matrix, and the properties of the reinforcing particles [80, 81]. Stir casting is suitable for manufacturing composites with reinforcement up to 30% volume [82].

An interesting recent development in stir casting is a two-step mixing process [83]. In this process, the matrix material is melted and then cooled down to a temperature between the liquidus and solidus points and kept in a semi-solid state. Now, the preheated reinforcing particles are added and mixed to the matrix. The mixture is again heated to liquid state and mixed thoroughly. This two-step stirring process has been used in the production of aluminium A356 and 6061 matrix composites reinforced with SiC particles and the resulting microstructure has been found to be more uniform than the one processed through conventional stirring. The main advantage of stir casting is its applicability to mass and large scale production. Compared to other well-established metal matrix composite fabrication methods, stir casting is the most economical and it costs as little as one third to one tenth when mass produced [84, 85]. Therefore, stir casting is currently the most popular commercial method for producing aluminium based composites [86].

Poria et al., [87] studied the tribological characterization of stir-cast aluminium-TiB_2 metal matrix composites. In this study, friction and wear of aluminium matrix composites reinforced with TiB_2 micro particles processed through stir casting method rather than in-situ technique was considered. Different weight percentages of TiB_2 powders having average size of 5-40 microns were incorporated into molten LM4 aluminium matrix by stir casting method. Normal loads of 25-75 N and rotational speed of 400-600 RPM were used for investigating the friction

and wear behaviour. It was found that the friction and wear decrease with an increase in the percentage of TiB_2 reinforcement in the composite, while friction and wear increase with applied load and speed. Scanning electron microscopy revealed the presence of both abrasive and adhesive wear mechanisms, with abrasive wear being predominant.

Gao et al., [88] prepared in-situ 5 vol% TiB_2/Al–4.5Cu composites by the salt–metal reactions, assisted by improved mechanical stirring. The X-ray diffraction confirmed the formation of TiB_2 particles and no cluster or large precipitation of intermediate brittle phases like Al_3Ti and AlB_2 could be traced, which are difficult to machine [89]. Mechanical stirring could reduce the large agglomerations and finally eliminate them when the speed was raised to 540 RPM. Most of the TiB_2 particles were uniformly distributed along the grain boundaries in the matrix, and lots of dispersed particles with a size under 0.4 μm were also found. Yield stress and ultimate tensile strength of the composite were improved by 85% and 46% respectively.

Suresh et al., [90] developed aluminium MMC reinforced with micro and nano sized Al_2O_3 using stir casting method. Nano Al_2O_3 particulate reinforced AMC exhibited better hardness and strength when compared to the micro Al_2O_3 reinforced AMC. Moreover, uniform distribution of reinforcement particles was observed in both the AMCs. However, agglomeration was obvious. On the other hand, both the AMCs were found to have low porosity levels and hence exhibited improved strengths. By proper optimization of the process parameters, stir casting could be a promising and economically feasible route for the fabrication of nano particle reinforced AMCs.

Sreenivasan et al., [91] studied the microstructure and wear behaviour of Al-TiB_2 composites. Composites were prepared with 5, 10, and 15 wt% reinforcement of TiB_2 by stir casting method. The composite samples were tested for wear by pin-on-disc method at 100, 200, 300, 400 and 500 rpm on an EN 24 steel disc with varying loads of 10-60 N in steps of 10 N. The results showed that the wear rate increased with an increase in the load and the sliding speed for both the matrix and the reinforcement. The transition loads for the MMCs were much higher than that of the matrix material. The transition loads have increased with an increase in the reinforcement of TiB_2 and the same have decreased with an increase in the sliding speed. The improvement in hardness and wear of the composite are attributed to the uniform distribution of reinforcement in the matrix achieved through stir casting.

Hashim et al., [92] proposed a modified stir casting method to eliminate various deficiencies in the normal stir casting process. In the normal practice of stir casting technique, metal matrix composite (MMC) is produced by melting the matrix material in a furnace, and then the molten metal is stirred thoroughly to form a vortex and the reinforcement particles are introduced through the side of the vortex formed. From some point of view, this approach has certain disadvantages, mainly arising from the particle addition and the stirring methods. During particle addition there is undoubtedly local solidification of the melt induced by the particles, and this increases the viscosity of the slurry. A top reinforcement addition method introduced air into the slurry, which appears as air pockets among the particles.

Nabil et al., [93] compared the microstructure and mechanical properties of modified and un-modified stir-cast commercial aluminium alloys A-S7G03 and A-S4G. This stir-cast structure slightly improved the mechanical properties in comparison to those of the conventionally cast alloys. However, the fracture surfaces of the stir cast sample revealed inter granular brittle fracture. The addition of 0.02 wt% strontium, in the form of AI-5 wt% Sr master alloy, during stir casting modified the eutectic silicon into very fine spheroid morphology, while the phase particle showed the same morphology as the stir-cast alloy. This novel structure resulted in significant improvement of mechanical properties. The elongation of the modified stir-cast alloy was five times greater than that of the un-modified one.

Jayaseelan et al., [94] compared the extrusion characteristics of Al-SiC metal matrix composites produced by two methods, namely powder metallurgy and stir casting. Stir cast specimens exhibited finer microstructure and high hardness as compared to the specimens produced by powder metallurgy. They also possessed higher strength.

Alaneme et al., [95] evaluated the percent porosity of HAMCs reinforced with banana leaf ash (BLA) and SiC developed through two step stir casting process. The theoretical density was evaluated using the rule of mixtures, while the experimental density was determined by dividing the measured weight of the test sample with its volume. The porosity percent did not show any particular trend with an increase in the BLA content. However, the densities of the cast composites were observed to be reduced. For all the cast composites, the percent porosity was within the acceptable limiting value of 4%.

Gopalakrishnan and Murugan [96] investigated the production of metal matrix composite by enhanced stir-casting method for improved specific strength, high temperature and wear resistance applications. Al–TiC$_p$ composite was produced by an indigenously developed enhanced stir casting process. This process helps to minimise the problems associated with the conventional stir casting process. Cleaned AA6061 was placed inside the crucible. Temperature was set at 30 °C above the melting point of AA6061. After the complete melting of aluminium, once again the temperature was further raised by 50 °C to compensate the cooling effect produced due to stirring. TiC was introduced in the form of capsule (TiC wrapped in aluminium foil) during the mechanical stirring. Two step stirring method was adopted to ensure a thorough mixing of reinforcement. Magnesium (1%) was added during the stirring process to improve the wettability of TiC with the molten aluminium. Argon gas was used to prevent reaction of molten aluminium with the atmosphere after the addition of Magnesium. Difficulty associated with metal pouring was also drastically reduced in this process.

Naher et al., [97] produced Al-SiC composites by liquid and semi solid stir-casting techniques. Stirring speed was varied from 200 to 500 RPM. 10% volume of 30 micrometer diameter sized SiC particles was reinforced. The main aim was to achieve an uniform distribution of SiC in the aluminium matrix. Faster solidification after ceasing of mixing improved the uniformity of the SiC distribution significantly.

Boopathi et al., [98] developed aluminium hybrid composites by reinforcing SiC and fly ash through stir casting. Based on the results, they reported that the density of hybrid composites decreased with an increase in SiC content and non-uniformity in the distribution of reinforced particles was observed in the micrograph.

James et al., [99] prepared a hybrid metal matrix composite by reinforcing SiC and TiB$_2$ to aluminium matrix by stir casting route. Hardness test showed that addition of SiC and TiB$_2$ reinforcements to a certain level increased the hardness. However, beyond 15 wt% reinforcement, hardness tends to decrease. It has been observed from the tensile test results that the addition of SiC to the matrix added 20% strength to the composite but addition of TiB$_2$ reduced the strength by 50-60%. Wear test analysis has been performed to study the wear resistance characteristics of TiB$_2$ reinforced composite. Wear test analysis proved that the addition of TiB$_2$ increased the wear resistance of the composite.

Ravesh and Garg [100] developed fly ash and SiC reinforced hybrid aluminium composites through stir casting and reported that with an increase in the amounts of reinforcements, the hardness of the composites increased. For the Al 6061-T6 treated hybrid matrix composites reinforced with a constant 5 wt% fly ash and 2.5 wt%, 5 wt%, 7.5 wt% and 10 wt% of SiC, the Rockwell hardness on the C scale was observed to be 61, 70, 81 and 93 respectively.

In a similar work, **Mahajan et al.,** [101] developed hybrid Al 6061 composites by reinforcing 10 wt% SiC constant in all the composite samples and varying TiB_2 content in the order of 2.5 wt%, 5 wt% and 10 wt% and compared their mechanical properties. The two composites were developed using stir casting route with bottom pouring technique. The hardness comparison showed that the hardness of the SiC reinforced composite is higher than that of the TiB_2 reinforced composite. From the tensile test results, it has been observed that the tensile strength of the TiB_2 reinforced composite is 30% higher than that of the SiC composite. Wear test analysis proved that the wear resistance of TiB_2 reinforced composite is higher than that of the SiC reinforced composite. However, the wear resistance of all the composites increased up to certain extent and reduced drastically when the transition load is increased.

Ramkumar et al., [102] developed AA 7075-TiB_2-Gr in situ hybrid composite through stir casting route. This in situ method involved the formation of reinforcements within the matrix by the chemical reaction of two or more compounds, which also produced some changes in the matrix material within the vicinity. It was found that good/excellent mechanical properties were obtained in the AA 7075-TiB_2-Gr in situ hybrid composite compared to the base alloy due to particulate strengthening of TiB_2 ceramic particles in the matrix. Further, Al 7075- 3 wt% TiB_2-1 wt% Gr hybrid in situ composite exhibited improved machinability over the unreinforced base alloy and other composites due to self-lubricating property of Gr particles.

Poria et al., [103] studied the role of nano-graphite particles in determining wear and friction behavior of Al-TiB_2-nano-Gr hybrid composites. Ultrasonic cavitation assisted stir casting method has been used for the development of composites. Al-Si_5Cu_3 alloy was used as the base alloy along with micro sized TiB_2 hard ceramic particles (2.5 and 5.5 wt%) as reinforcement and nano-Gr particles (2 and 4 wt%) as solid lubricant additives. Wear resistance of the composites increased with incorporation of reinforcing phases together. Nano-Gr particles were easily sheared out from the sub-surface of the composite and provided a layer over the tribo-surface of the composite that enhanced friction and wear resistance. Wear resistance in

the composites is predominantly due to adhesion while abrasion and ploughing are prominent in the base alloy.

Rebba et al., [104] made an effort to enhance the mechanical properties of AMCs like tensile strength and hardness by reinforcing B_4C particles in 2024 Al matrix through stir casting method. Composites of different wt % of reinforcement (0%, 1%, 2%, 3%, 4% & 5%) of B_4C particles were developed. Homogeneous dispersion of B_4C particles in the matrix was observed by optical microscope. The reinforcement dispersion has also been identified with X-ray diffraction. The tensile strength and hardness were found to increase with an increase in wt. % of the reinforcement. The tensile strength and hardness of 2024 Al with 5% B_4C reinforcement showed highest value.

Bhaskar et al., [105] developed and investigated Al 2024–Beryl particulate composites by stir casting by varying the beryl particulates from 2 wt% to 10 wt% in steps of 2 wt%. The cast Al 2024 alloy and its composites have been subjected to solutionizing treatment at a temperature of 495° C for 2 hours, followed by ice quenching. The results revealed that the wear rate of the composites is lower than that of the base alloy. The wear rate increased with an increase in the applied load and sliding distance, and decreased with an increase in the sliding velocity.

Narayanan et al., [106] developed an aluminium metal matrix composite with tungsten carbide (WC) as reinforcement by low-cost stir casting technique and estimated the effect of friction stir processing (FSP) on microstructure and mechanical properties. The observed results were compared with those of the base Al 2024 alloy material. From the results, it was observed that the mechanical properties like hardness were improved due to surface modification by FSP when compared to the unreinforced base Al 2024 alloy.

Canakci et al., [107] modified the manufacturing process to develop an AMC in order to improve the incorporation of B_4C particles in 2024 aluminium alloy melt. Stir casting process was developed to produce aluminium alloy composites containing two different sizes and volume fractions of B_4C particles up to 10 vol%. They reported a novel pre-treatment process prior to stir casting process to reduce the processing temperature. The results showed that the treatment modified the surface condition of boron carbide powders by removing the oxide layers. The ratio between the added and incorporated particles (the yield rate) indicated that the amount of incorporated particles decreased with an increase in the volume fraction and

decreased size of B₄C particles. Microscopic observations of the microstructures showed that the dispersion of coarser particles was more uniform, while finer particles lead to agglomeration and porosity. The results also showed that the density of the composites decreased with an increase in the particle volume fraction and decreased particle size, whereas the porosity and hardness values increased with an increase in the particle volume fraction and decreased particle size.

Gowda et al., [108] developed AA2024 matrix composite reinforced with tungsten carbide (WC) via stir cast technique. WC particles were reinforced in AA2024 matrix ranging from 1 wt% to 5 wt% in increments of 1 wt %. The SEM observations of AA2024 matrix composites showed that WC was uniformly distributed in the matrix. Significant reduction in wear rate was observed with the reinforcement of WC during dry sliding process. Finally, the authors have concluded that the composite with 3 wt% WC could perform best for high load applications. Therefore, they have recommended the composite with 3 wt% WC reinforcement for engineering applications.

Bhandakkar et al., [109] evaluated the influence of fly ash reinforcement on hardness, tensile strength and fracture toughness in AA2024 matrix composites, using stir casting. They reported that the hardness of fly ash reinforced aluminium metal matrix composites increased with the addition of fly ash particulate reinforcement, while the tensile strength and fracture toughness of the composite decreased compared to those of the base alloy. Uniform distribution of fly ash and silicon carbide particles in the aluminium matrix was obtained by stir casting, followed by hot extrusion. The fracture toughness of AA2024 reinforced with fly ash is 18 MPa as compared to 21 MPa for unreinforced and re-melted base alloy.

Rao et al., [110] investigated the characteristics and mechanical properties of AA2024 matrix composite reinforced with 2 to 10 wt% fly ash developed by stir casting route. The microstructure observations reveal that there was a uniform distribution of fly ash particles in the matrix phase and also the existence of very good interfacial bonding between the matrix and the reinforcement particles. The density of the composites decreased, while the hardness increased with an increase in the reinforcement of fly ash. Increase in compression strength and enhanced pitting corrosion was observed with an increase in the amount of fly ash. The enhanced pitting corrosion of the composites was attributed to the introduction of nobler second

phase of fly ash particles. The composite reinforced with 10 wt% fly ash show highest compressive strength.

In a similar investigation, **Vijayalakshmi** and **Balaji** [111] developed AA2024 matrix composites reinforced with 10% fly ash by stir casting route. Finite Element Analysis (FEA) results revealed that the simulated values were closely in agreement with the experimental values with a maximum deviation of less than 5%. Hence, the FEA model adopted for solving the present upsetting analysis was validated with the analytical results.

Murthy et al., [112] utilized industrial wastes like fly ash and granulated blast furnace (GBF) slag to produce AA2024 matrix composite reinforced with 5 wt% fly ash and GBF slag by stir casting route. The microstructure studies revealed that there was a uniform distribution of fly ash and GBF slag particles in the matrix phase and also a very good interfacial bonding existed between the matrix and the reinforcement particles. Improved hardness and mechanical properties were observed for both the composites compared to the unreinforced alloy. This increase is higher for the Al-fly ash reinforced composite than the Al-GBF slag reinforced composite. The hardness of the composites increased while the density decreased with the addition of reinforcement, compared to the base alloy. Al-fly ash composites are harder than Al-GBF slag composite. Enhanced compressive properties were observed for both the composites than the unreinforced base alloy.

In another study, **Shivaprakash et al.,** [113] developed composites by reinforcing precipitator type fly ash having particle size below 45 μm in amounts of 2.5, 5, 7.5, 10 and 15% by weight to the wrought aluminium alloy AA2024 by stir casting. The composite samples and the non artificially aged alloy were tested for dry sliding wear behaviour on a pin-on-disc machine. For each specimen the wear test was conducted in the laboratory conditions by varying the speeds (200, 300 and 400 RPM) and by applying different normal loads like 10, 25 and 35 N. Experimental results displayed a good improvement in the wear resistance as well as hardness as the fly ash content was increased in the matrix. The increase in the wear resistance was associated with the increase in the hardness. On the other hand, co-efficient of friction was found to decrease as the content of fly ash increased but it showed some increasing and decreasing trends for an increase in the normal load for all the speeds. Finally, they concluded that the optimum quantity of fly ash reinforcement to AA2024 matrix for achieving peak mechanical properties falls between 10 and 15 wt%.

Reddy et al., [114] developed AA2024/ZrC metal matrix composite by stir casting method with bottom-up pouring technique to investigate the effect of agglomeration and porosity on mechanical and wear properties. The microstructures observations of AA2024/ZrC nano composites have revealed the occurrence of particle agglomeration and porosity. The normalized tensile strength and elastic modulus decreased with porosity and agglomeration of ZrC nano particles. The simulated results by FEM were compared with the experimental results and were found to be in close agreement.

In another study, **Mahendra et al.,** [115] developed aluminium-SiC-fly ash hybrid metal matrix composite by stir casting method, adding the reinforcements up to the ultimate level. Their objective was on to combine the strength of the reinforcement with the toughness of the matrix in order to achieve a combination of desirable properties not available in any single alloy or conventional material. When different proportions of silicon carbide and fly ash [5 wt% SiC + 10 wt% fly ash] and [10 wt% SiC +10 wt% fly ash] were reinforced with aluminium, it was fairly observed that the density of the composites decreased and the hardness increased. Correspondingly, an increase in tensile strength was also observed but elongation of the hybrid metal matrix composites in comparison with the unreinforced aluminium has decreased. Finally, the authors concluded that the aluminium-SiC-fly ash hybrid metal matrix composites significantly differed in all of the properties measured. Aluminium reinforced with SiC (10 wt%)-fly ash (10 wt%) was much harder when compared to the other combinations of aluminium-SiC and aluminium-fly ash composites.

Karuna et al., [116], to overcome the cost barrier for wide spread applications, evaluated the mechanical properties of 2024 T351 aluminium hybrid composites reinforced with Blast Furnace Slag (BFS) and Red Mud (RM) by stir casting technique. BFS particulates were reinforced in AA2024 matrix by decreasing from 4 to 1% by weight. Red mud particulates were reinforced in AA2024 matrix varying between 1 to 4% by weight. The experimental results showed that 2% BFS and 3% RM were the optimum amounts of reinforcements to obtain peak mechanical properties in the hybrid composite. They also reported that the reinforcements were uniformly distributed in the matrix phase.

Jayanthi et al., [117] focused on improving the specific strength of AA 2924 matrix by reinforcing it with ternary alloy particulates by stir casting route. Based on the experimental results, increase in reinforcement material enhanced all the mechanical properties such as yield

strength, tensile strength and Young's modulus of elasticity. Specific hardness of the resultant metal–metal composites was much superior to those of the conventional MMCs. The decrease in particle size and increase in reinforcement proportion enhanced the surface area to volume ratio of the resultant composite. Except ductility, an average increment of 62% was observed in the mechanical properties of the composites, compared to the unreinforced base alloy. However, agglomeration of reinforced particles during solidification due to settling down was a major barrier in stir casting to develop AMCs. A few researchers have come up with some solution to this problem.

For example, **Chen et al.,** [118] used a vertical-injection squeeze casting machine to cast Al-7Si-0.3Mg alloy where the molten metal was injected under pressure into the mould. The original billet surface layer was found to be largely confined to the surface layer in the biscuit, except for the top of the billet surface, which flowed to the upper surface of the casting. As a consequence, the incidence of oxide inclusions within the casting was very low, leading to high elongation values with low scatter. Significant lower strength and higher elongation values were observed in the biscuit. This effect was attributed to there being a significantly lower concentration of the solute elements in the biscuit compared to the casting.

2.3 Review on AMCs using cold compaction

Recent developments have made it possible to use rapid manufacturing techniques which use metal powders for making the products. In this technique, the powder was sintered but not melted and better mechanical strength could be accomplished. Powder metallurgy (PM) is a highly evolved method of manufacturing reliable near net shaped components by blending elemental or pre-alloyed powders together, compacting this blend in a die, and sintering or heating the compact in a controlled atmosphere to bond the particles metallurgically. The PM process is a unique part fabrication method that is highly cost effective in producing simple or complex parts at or close to final dimensions. PM processing provides the following advantages.

- Production of complex shapes
- Very close dimensional tolerances
- High density
- Minimum scrap loss
- Fewer secondary machining operations
- Less processing time, etc.,

Physical and mechanical properties of the components can be tailored through close control of starting materials and process parameters. Specific properties can be improved through secondary processing operations such as heat treatment and cold/hot forming. The advantages of this processing method include the capability of incorporating a relatively high volume fraction of reinforcement and fabrication of composites with matrix and reinforcement systems that are otherwise immiscible by liquid casting. However, this method requires metal powders that are generally more expensive than the bulk material, and involves complicated processes during powder processing.

Sagar et al., [119] developed Al−SiCp composite with 10, 15, 20, and 25 wt% of SiCp through die compaction of powders and subsequent sintering at 580° C. Valve seat inserts from these composites were also developed through gravity die casting process. The hardness, density, radial crushing load and surface roughness of the Al−SiCp composites (with different wt% of SiCp) and those of the steel valve seat inserts (presently used in engines) were measured and compared. The hardness and radial crushing load of the composites reinforced with 15, 20, and 25 wt% of SiCp were higher than those of the steel valve seat inserts. The microstructures of the cast as well as powder metal Al-SiCp composites were also studied.

Ramachandra et al., [120] developed a pure aluminium matrix composite reinforced with nano ZrO_2 using powder metallurgy technique and studied its hardness and wear resistance. Microstructure of the nano composite revealed a near uniform distribution of nano ZrO_2 particles with a little agglomeration. The microstructure also revealed good interfacial bonding between matrix and nano ZrO_2 particles. Addition of nano ZrO_2 particles to aluminium matrix lead to the production of nano aluminium composites with better hardness, wear resistance and other mechanical properties. These composites can find applications in automotive components such as cylinder liners, pistons and connecting rods.

Khorshid et al., [121] highlighted the importance of powder metallurgy route while synthesizing aluminium matrix nano composites reinforced with graphene nano platelets (GNPs). The authors investigated the tribological behaviour of the said composite at different percentages of reinforcement. The experimental results showed some changes in the morphology of Al-1 wt% GNPs powder with 6 hours of milling time. The shape changed from regular platelets to flaky, as a result, the coefficient of friction (COF) varied with normal load at constant sliding speed of 100 RPM. The results showed that due to insufficient solid lubricant

available at the contact surface, the COF does not change significantly by adding 0.1 wt% of GNP to aluminium matrix. Finally, they concluded that the wear rate of Al-1 wt% GNP is higher at higher normal loads when compared to lower normal loads, and the COF of Al-1 wt% GNP is lower at higher normal load.

Abdizadeh et al., [122] developed Al nano composites by reinforcing varying amounts of MgO nano particles (1.5, 2.5 and 5 vol %) to A356 aluminium alloy matrix using powder metallurgy route. Different processing temperatures of 575, 600, and 625º C were considered and the authors concluded through the results that 625º C is the optimum processing temperature to achieve better mechanical properties.

Nassar et al., [123] developed Al/TiO_2 composites by powder metallurgy process and studied its properties. TiO_2 nano powder with volume fractions of 0.5, 1.5, 2.5, 3.5 and 4.5% were mixed with Al powder by ball milling. The powder mixtures were compressed at room temperature at a pressure of 104 N/cm^2 for 6 minutes. The resultant green compacts were conventionally sintered at 450º C in argon atmosphere. The experimental results showed great improvement in tensile strength due to low degree of porosity and fine distribution of particles achieved by ball milling and powder metallurgy route. Mechanical blending and alloying of powders lead to uniform distribution of TiO_2 particles and less air gaps between the grains. Experimental results of tensile strength, hardness, and density showed that the porosity and the tensile strength of composites increased with an increase in volume fraction of nano particles. However, ductility of composites decreased. Wear test revealed that composites offer superior wear resistance compared to the base alloy. Multi-directional grain refinement was also observed in the composite through optical microstructure.

Umma et al., [124] focused on some important methods of Al-CNT nano composite development. Among all the development methods of Al-CNT nano composites, they found that PM is the most efficient process. Therefore, this PM process route with optimum process parameters could help to develop a new nano composite material with good functional and mechanical properties. Therefore, the lightweight industries, such as aerospace, automotive, sports and other industries would be attracted to use this material for many structural and tribological applications.

Aoshuang., [125] developed aluminium matrix hybrid composites (AMHCs) reinforced with 10 wt% SiC micro particles and 1, 3 and 5 wt% TiB_2 nano particles through powder metallurgy

35

route. The results showed that the mechanical properties of the hybrid composites were improved with an increase in the proportion of TiB_2 nano particles. Compared to aluminium matrix composites reinforced with micro SiC particles alone, the ultimate tensile and yield strengths of the AMHCs with 5 wt% TiB_2 nano particles were improved by 64% and 23% respectively.

Rajmohan et al., [126] studied the sintering process of hybrid micro and nano composites reinforced with SiC and CuO nano particles in aluminium matrix. Atomized 99.5% pure aluminium powder was used as the matrix material and micro silicon carbide (SiC 10wt %) particles and nano copper oxide (CuO 0-2wt %) particles were used as the hybrid reinforcements. Characterization was done by fixed weight percentage of micro particles and varying percentage of nano particles. Finally, they concluded that the reinforcement of nano CuO particles in the AMC improves the structure and properties of the composite material.

Subrahmanyam et al., [127] developed AA2024 matrix composites through powder metallurgy by reinforcing fly ash (FA) in the proportions of 2, 4, 6, 8 and 10% by weight. The obtained composites were cut into small specimens and tested for hardness, wear, density and corrosion. Based on their studies, the authors concluded that the addition of FA increased the hardness and other mechanical properties of the composites. Thus, this industrial waste (FA) can be converted into industrial wealth by using it as a reinforcement. These lightweight aluminium fly ash composites can be used for automobile industries and aerospace applications.

Ovali et al., [128] produced Al 2024/10Al_2O_3, Al 2024/10Al_2O_3/3MgO, Al 2024/10Al_2O_3/6MgO, Al 2024/10Al_2O_3/3MgO/1.5 Gr, Al 2024/10Al_2O_3/3MgO/3Gr hybrid metal matrix composites by powder metallurgy process. The composite powders were separately mixed in a 3-dimentional tubular mixer for 30 minutes. The mixed compositions were pressed at 300 MPa and sintered at 550° C for 1 hour. After that, the three materials were extruded at the same temperature. Experimental results showed that the Al 2024/10Al_2O_3/3MgO/3Gr hybrid metal matrix composites (HMMCs) has better wear resistance than the other two composites because of higher hardness and Gr behaves as a lubricant during wear process and concluded that wear resistance of HMMCs could be optimized by controlling the reinforcement type and its proportion.

Krishnamaraju et at., [129] made investigations on the mechanical properties of aluminium 2024 based hybrid composites reinforced with silicon carbide and Al_2O_3 by powder metallurgy technique. The authors concluded that the hardness, density and compression strength increased with an increase in the hard ceramic reinforcements. The increase in the properties was also attributed to the grain refinement of the matrix, due to the addition of SiC and Al_2O_3.

Kumar et al., [130] developed hybrid nano composites of AA2024 matrix reinforced with weight fractions of nano SiC particles ranging from 5 to 10 wt% and also 5 wt% Graphite particles constant in each case. The hybrid composites were produced by blend– press–sinter methodology. The green compacts were sintered at 530°C for 60 min. The results showed that by increasing the reinforcement content, the hardness and wear resistance of the hybrid nano composites were considerably increased. Good interface bonding was observed between the matrix and the reinforcement. The nano hybrid composite with 5 wt% Gr and 10 wt % SiC showed a significant improvement in tribological performance. Finally, they concluded that the tribological behaviour of the hybrid composite depends on the hardness of the composite, the structure of the solid lubricating film deposited on the worn surface, the rate of graphite particles release and the structure of the wear debris.

2.4 Review on AMCs using spark plasma sintering

The main challenge in producing composites is to uniformly distribute the reinforcement particles in the matrix. As the particle size of the reinforcement decreases (sub-micron/nano), its uniform distribution becomes more complicated due to the agglomeration of the reinforcement. Agglomeration of reinforcement leads to anisotropy in the composite. Some researchers reported that localized agglomeration of reinforced particles is unavoidable in process like stir casting [131].

PM gives a viable solution to this problem, as it restricts the movement of reinforced particles once they are placed in the die and ready to be compacted. However, proper mixing of composite powders is essential before further processing. Generally, ball milling is used for blending or mechanically alloying the composite powder. During mechanical alloying, both advantageous and disadvantageous like intermetallic phases including contamination are reported [132, 133]. Hence, the step of blending or mechanical alloying primarily depends on the characteristics of the composite powders and also the desired properties of the end product.

On the other hand, sintering of aluminium powder is a difficult task as the powder particles form protective layer around them when exposed to atmosphere. This oxide layer protects the particles from further corrosion. During sintering, the same protective layer hinders the particle-particle contact and degrades the diffusion and hence densification of the composite [134]. Therefore, aluminium green composites need different atmospheres like argon, nitrogen, etc., for sintering. Another drawback of conventional cold compaction is that the compaction and sintering are done separately and require high temperatures and holding times. To overcome these challenges, novel and advanced sintering technique was developed called Spark plasma sintering (SPS). Some of the AMCs processed through SPS are summarised below.

One of the early investigations on sintering aluminium powder was attempted by **Guoqiang et al.,** [135] by sintering pure aluminium powder through spark plasma sintering, varying sintering temperature and loading pressure and investigated relative density and mechanical properties. The authors also studied the interface behaviour between particles after SPS and reported that two types of interfaces namely, metal-metal and metal-oxide layer-metal were observed as shown in Fig. 2.2. The properties of the powder compact depended on the behaviour of the oxide layer between the powder particles. The increase in sintering temperature and loading pressure improved the relative density and mechanical properties of the composite as shown in Fig. 2.2. The authors recommended a few sintering processing parameters such as sintering temperature above 873 K and loading pressure above 23.5 MPa could breakdown the oxide layer and increase the metal-metal bonding leading to better mechanical properties of the composite. This was proven by electrical conduction test where composite with more number of metal-metal contacts showed better electric conduction.
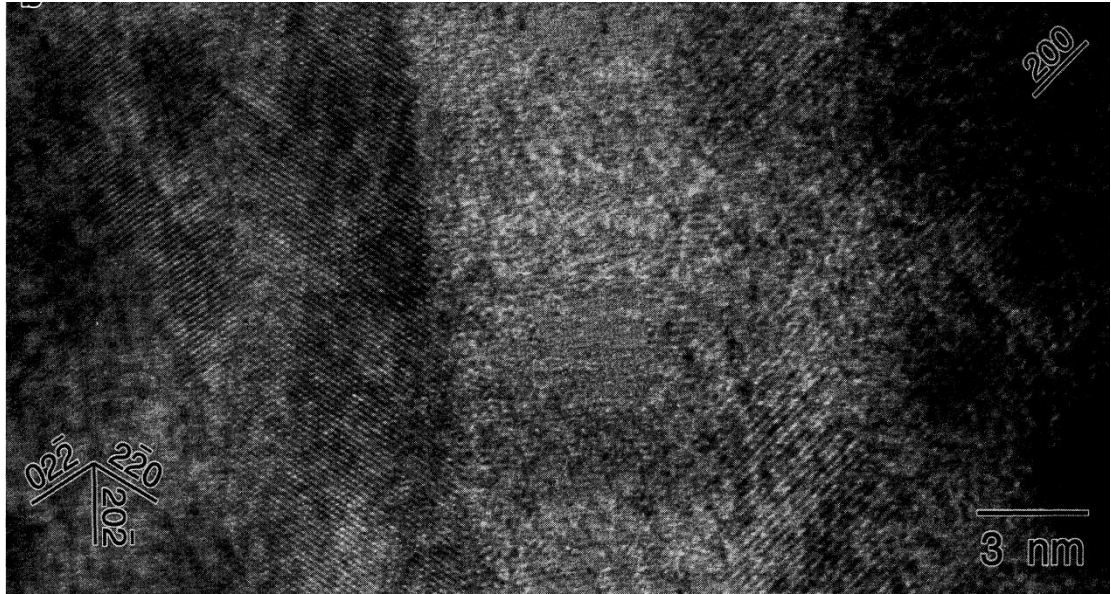
Fig. 2.2. HRTEM of the typical metal-oxide layer-metal bonding in the composite sample using SPS [135].

Muthuchamy et al., [136] successfully produced Al-20Cu-15Mn alloy using powder metallurgy route and various sintering processes. Al, Cu and Mn powders were mixed in a tubular mixer for one hour. The resultant powder blend was sintered using conventional sintering, microwave sintering and SPS. The sintered density was highest with spark plasma sintering, followed by microwave and conventional sintering processes. Mechanical properties were also found to be highest in spark plasma sintered samples followed by microwave and conventional sintered samples. Microwave and spark plasma sintering produce finer microstructure and smaller pores than the conventionally sintered sample. Corrosion resistance was highest for spark plasma sintered sample followed by conventional and microwave sintered samples. The grain size of the composite samples varied as 36, 24 and 15µ for conventional, microwave and SPS processes respectively.

Ehsan et al., [137] developed pure aluminium-zircon composite through spark plasma sintering at a low sintering temperature of 450° C. A full dense aluminium metal matrix composite with mechanical properties such as bending strength of 284±21 MPa and micro Vickers hardness of 171±14 were obtained. The authors concluded that the application of SPS could result in producing an aluminium-zircon composite with full density, uniform microstructure and improved mechanical properties.

Mallik et al., [138] produced in-situ aluminium metal matrix composite reinforcing nano sized Fe_2O_3 powder by SPS. During the SPS, temperature was varied at 700, 800 and 900° C under vacuum, with an uniaxial pressure of 50 MPa and a holding time of 10 minutes. The powder compact was subjected to cycles of very rapid heating and cooling with very short holding time at the given sintering temperature, lower than that in normal conventional hot pressing. In-situ reinforcements were formed during SPS by exothermal reaction between aluminium and nano-size Fe_2O_3 particles at the interface. Micro hardness measurement of the composite shows significant increase in hardness with an increase in SPS temperature and volume fraction of secondary phase. Further, the starting temperature of the in-situ reaction decreased considerably with the use of nano-sized Fe_2O_3 powder.

Sweet et al., [139] developed aluminium based metal matrix composites (AMCs) containing SiC, aluminium nitride (AlN), silicon nitride (Si_3N_4) and boron nitride (BN) as the reinforcements through spark plasma sintering. SiC, AlN and Si_3N_4 proved to be responsive to this type of processing. Full densification of AMCs that incorporated finer ceramic particles was complicated due to the presence of ceramic agglomeration and the extent to which aluminium could be forced into these regions. AMCs that incorporated coarser ceramic particles were more easily densified, but their hardness benefits were inferior. SiC reinforced composites outperformed AlN reinforced AMC samples in bend tests. Excellent ductility and bend strength were developed at low temperatures for all composites.

In another study, **Ehsan et al.,** [140] developed aluminium metal matrix composite reinforced with graphene nano particles (GNP) and carbon nano tubes (CNT), through SPS, microwave (MW) and conventional techniques in order to evaluate and differentiate their mechanical properties. Three initial compositions of Al-1 wt% CNT, Al-1 wt% GNP and Al-1 wt% CNT– 1 wt% GNP were mixed by a high energy ultrasonic device and mixer mill to achieve homogenous dispersion. SPS, MW and conventional sintering processes were carried out at approximately 450, 600 and 700°C respectively. A maximum relative density (99.7 ± 0.2% of theoretical density) and bending strength (337 ± 11 MPa) were obtained by SPS, while a maximum Vickers micro hardness of 221 ± 11 was achieved by microwave sintering for Al-1 wt% CNT–1 wt% GNP hybrid composite. Processing through SPS produced high density composites at minimum temperature and less processing time.

Yet in another study, **Ehsan et al.,** [141] investigated the mechanical properties and microstructure of Al-15 wt % TiC composite samples. The sintering processes were carried out by SPS, microwave and conventional sintering processes at approximately 400, 600, and 700°C respectively. The results showed that the samples processed by SPS have the highest relative density (99% of theoretical density), bending strength (291 ± 12 MPa), and hardness (253 ± 23 HV). The X-ray diffraction investigations showed the formation of TiO_2 from the surface layer decomposition of TiC particles. Scanning electron microscopy micrographs demonstrated uniform distribution of reinforcement particles in all sintered samples. SEM/EDS analysis revealed the formation of TiO_2 around the porous TiC particles. The SPS method with the applied pressure and the low sintering temperature simultaneously led to proper microstructure and mechanical properties, in comparison to the other sintering methods. In microwave and conventional sintering process, the higher sintering temperature and time resulted in the decomposition of TiC and the formation of TiO_2 and CO_2. The CO_2 gas formed during sintering produced porosities in the microstructure of the samples. The SPS sintered samples achieved almost full density with the highest mechanical properties at a lower sintering temperature and processing time than the microwave and conventional sintered samples. Fig. 2.3 shows the time versus temperature curves for the conventional, microwave and SPS processed samples.
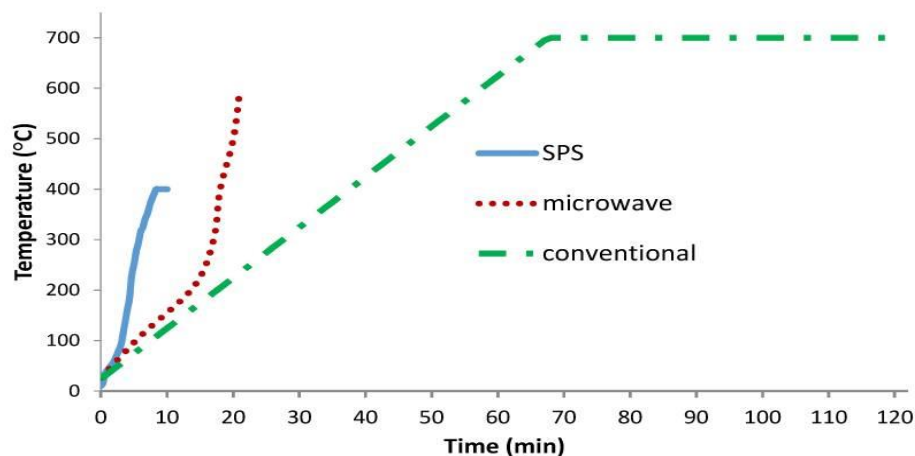
Fig. 2.3. Time-temperature curves for the conventional, microwave and SPS processed samples [141].

Cavaliere et al., [142] investigated the effect of 0.5 and 1 wt% of CNTs reinforcement on the mechanical and microstructural behaviour of Al based metal matrix composites produced by SPS. The results showed that the CNT addition resulted in an increase in porosity and strength when compared to pure SPSed aluminium.

Ridvan et al., [143] studied and reported the effect of sintering parameters and eutectic phase on densification during sintering through SPS in aluminium based SiC reinforced composite. Experiments were conducted by varying pressure, sintering temperature and heating rate. Based on the experimental results, the authors concluded that the eutectic phase consisting of Al_2Cu and Mg_2Si affect the sintering of the composite because of the lower melting point of aluminium. High heating rates were generated at the particle boundaries during spark sintering of the composite particles due to Joule effect and electric discharge. Localized temperature raise at the contact points caused eutectic melting along the particle boundaries, resulting in a higher relative density. Fig. 2.4 shows the schematic model of the eutectic phase effect during SPS.
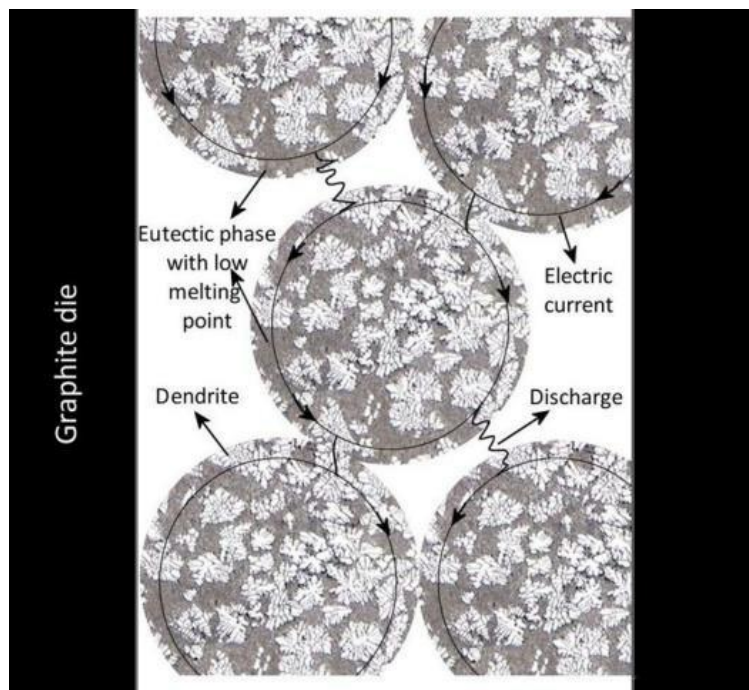
Fig. 2.4. Eutectic phase affecting the sintering of composite [143].

A liquid phase in the material during the process activates the sintering. At a higher temperature ($500°C$), a separation was observed between liquid and solid due to the pressure applied during the SPS process. Almost all the liquid was separated from the composite material, leaving large pores behind. Therefore, the temperature was decreased to 400 and $450°C$ for further analysis. An increase in the amount of the liquid phase due to an increase in the sintering temperature caused an increase in densification at those temperatures. The density of the composite material increased with an increase in sintering temperature, accompanied by raise in the pressure. High heating rate caused a decrease in the density. However, high heating rate with increased

pressure resulted in high density. Full (100%) relative density was obtained at 450°C with 5 minutes holding time, 100°C/min heating rate and 50 MPa pressure. High heating rate, especially at high temperatures promoted eutectic melting in the composite, resulting in a high relative density. However, the authors did not discuss the role of reinforcement in densification.

Firestein et al., [144] developed Al-based composites reinforced with micro/nano boron nitride (BN) particles up to 10 wt% through SPS. The Al-BN powder mixtures were prepared using ball milling. A dramatic increase in the tensile strength of the composite was observed compared to pure Al samples during tensile tests at both room temperature and 500° C. The composite reinforced with micro particles was found to be more favourable for reinforcement compared to reinforcement of nano particles, due to improved homogeneous distribution and formation of uniform morphologies. An impressive tensile strength of 170 MPa at 500° C was achieved for the Al-7 wt% micro BN reinforced composite, as compared to that of the pure Al, which is only 33 MPa for a SPS processed sample. The SPS composites were analysed metallurgically to determine the role of reinforcements. Micro scale BN and intermetallics like AlB_2 and AlN acted within Al-matrices in the form of Orowan strengthening mechanism. Moreover, pre-formed intermetallics during ball milling of Al-BN powder mixtures finally crystallized during SPS processing and rejuvenate the adequately improved tensile strength and hardness of the resultant composites.

Behzad et al., [145] developed Al-based composites by reinforcing 3 and 6wt% of SiO_2 nano particles using SPS to evaluate their mechanical properties and microstructure. The properties were evaluated in the light of SPS process parameters such as sintering temperature, heating rate and pressure. The results reflected that lower proportion of SiO_2 nano particles were very effective for improving the mechanical properties. Increase in the reinforcement of SiO_2 content resulted in agglomeration and deteriorated the mechanical properties of the composites.

Baisong et al., [146], in order to provide guidance for manufacturing the flat products of Al/CNTs composites with high strength and good ductility, conducted studies on carbon nano tubes reinforced pure aluminium matrix composites using spark plasma sintering and hot rolling. The effects of sintering temperature, sintering mechanism and CNTs content on the microstructures and mechanical properties of the composites were studied. Based on the results, it has been shown that the composite sintered at 630° C reinforced with 0.75 vol% CNTs showed the best comprehensive mechanical properties, due to the combined positive

43

effects of the good Al-CNTs interfacial bonding, full densification of the composite and uniform dispersion of CNTs in the matrix. It has been found that the load transfer strengthening and dispersion strengthening of CNTs are the dominant strengthening mechanisms in the composites.

Ehsan et al., [147] developed Aluminium-10 wt% TiO_2 metal matrix composites using conventional, microwave, and spark plasma sintering processes. Aluminium and nano-sized TiO_2 powders were mixed using a high-energy mixer and the sintering process was carried out at 450° C for spark plasma sintering and at 600° C for both microwave and conventional sintering. Based on the experimental results, it was found that microwave sintering led to form flaky shape Al_3Ti intermetallic compounds. Investigations by X-ray diffraction and scanning electron microscope revealed and confirmed that conventional heating also lead to the formation of brittle Al_3Ti phase at the same sintering temperature. However, in the nano-sized TiO_2 particles reinforced composite developed through SPS, no additional phases were obtained at the lowest sintering temperature. A maximum bending strength of 254 ± 12 MPa and Vickers hardness of 235 ± 13 were measured for the samples developed by microwave sintering as a consequence of brittle Al_3Ti formation. The SEM and energy-dispersive X-ray spectroscopy analyses showed uniform distribution of Al_3Ti particles in the microstructure of microwave sintered samples and non uniform distribution of agglomerated Al_3Ti particles and porosities in the samples sintered by conventional heating.

Liao et al., [148] reported development of Al-CNT composites (up to 2 wt% CNTs) using SPS, followed by hot extrusion. The improvement in the hardness with CNT reinforcement was not significant (~10%) due to pronounced agglomeration of CNTs in the composites. It is clear that the dispersion of CNTs in the starting powder blend is important to gain the advantages of SPS processing.

Thomas et al., [149] developed AA 2219 matrix composite by reinforcing 0.75 wt% CNT through conventional sintering and SPS. Due to the lack of good interface bonding between CNT and Al matrix, there was no appreciable improvement in the properties. An additional coating to CNT was suggested by the authors to improve the interface bonding. However, un-reinforced compacts processed by SPS showed good properties compared to the conventional sintered compacts. Advantage of SPS is seen with substantial increase in hardness and density. Hardness of the matrix has increased to almost 24.6 % whereas the effect is not as significant

with reinforcement. The reasons are clearly seen in optical micrographs, shown in Fig. 2.5. However, efforts need to be made to achieve an effective bonding between the matrix and the reinforcement. It was found that SPS consolidated samples showed the most promising results with improved mechanical properties, as well as the finest microstructure.
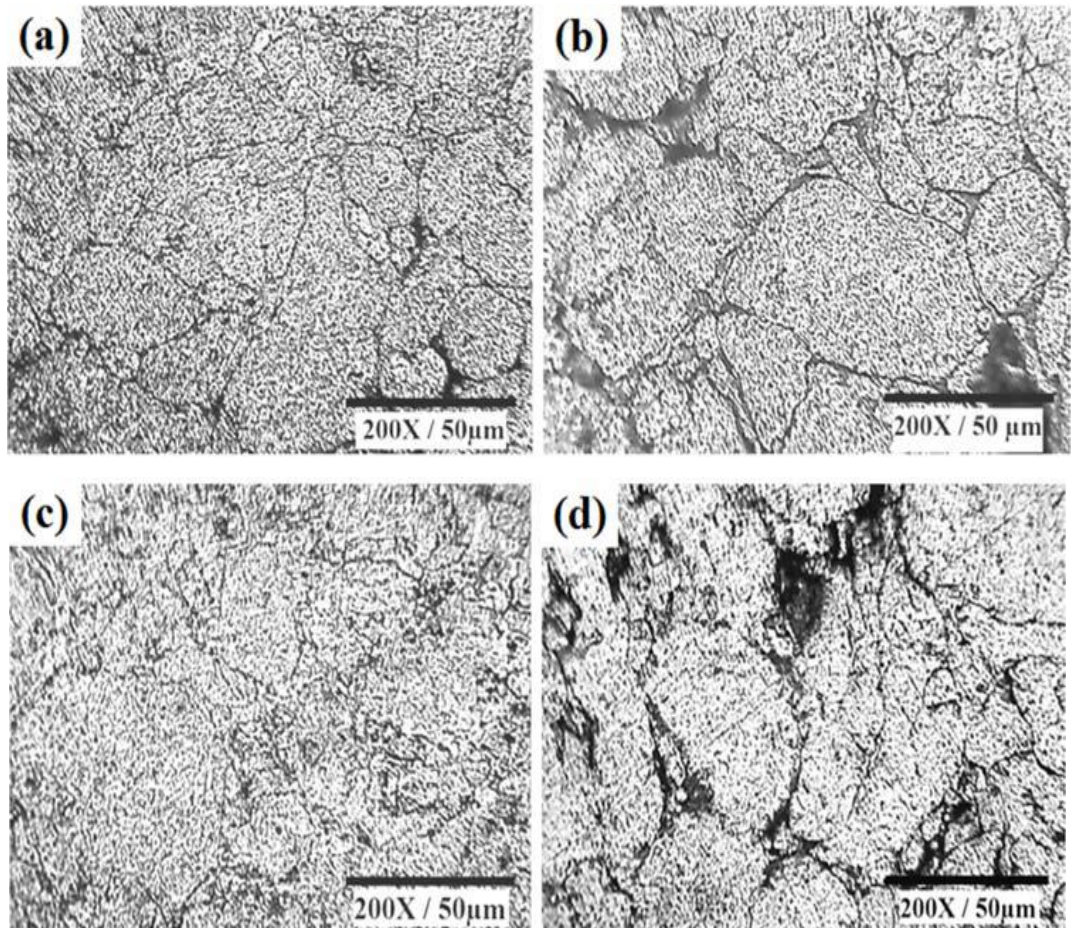
Fig. 2.5. Etched optical microstructure of (a) AA 2219 unreinforced conventional sintered sample, (b) AA 2219 + 0.75wt% CNT conventional sintered sample, (c) AA 2219 unreinforced spark plasma sintered sample, and (d) AA2219 + 0.75 wt% CNT spark plasma sintered sample [149].

Micro hardness of spark plasma sintered AA 2219 sample decreased with 0.75 wt% reinforcement of CNT due to the clustering of CNT and it was increasing in conventional method. 0.75 wt% CNT reinforced samples show equal hardness in both the processing methods. SPS could achieve better densification and sinterability. Pores formation associated with incoherency of CNT-AA 2219 composite brings the actual density lower than the theoretical density.

Song et al., [150] studied the densification process in SPS and concluded that a self-adjusting mechanism leads to uniform distribution of current intensity and hence improves the relative density, as shown in Fig. 2.6 and 2.7.
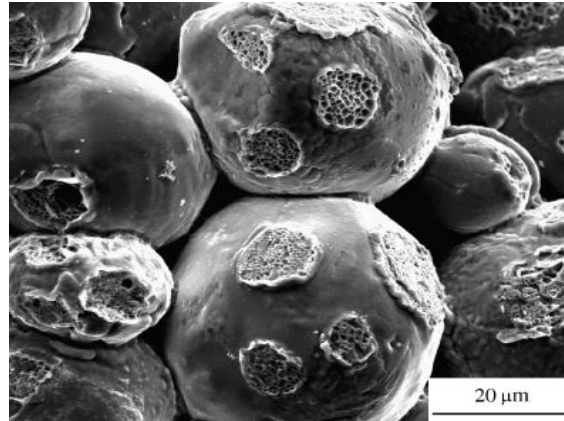
Fig. 2.6. Homogeneous distribution of neck sizes observed during the spark plasma sintering process. [150]
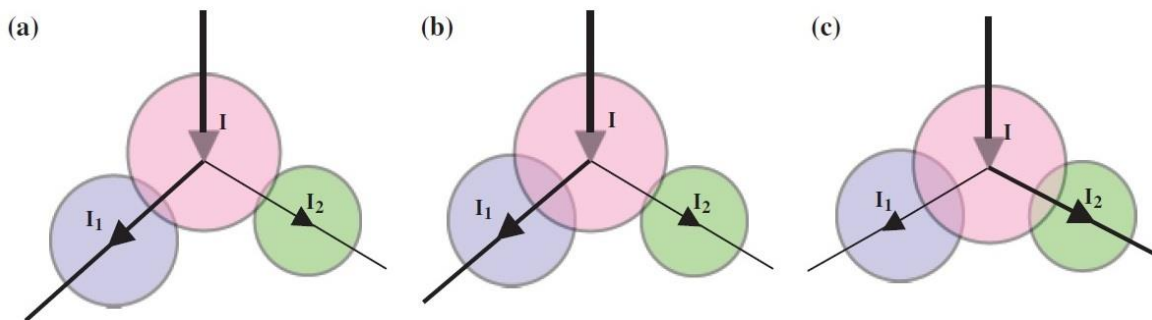
Fig. 2.7. Diagram showing the distribution of the local current intensity and the neck growth between particles (a) stage 1, (b) stage 2, and (c) stage 3. [150]

The authors also proposed a severe plastic deformation (SPD) that takes place at high temperature along with applied pressure that leads to grain refinement, as shown in Fig. 2.8.
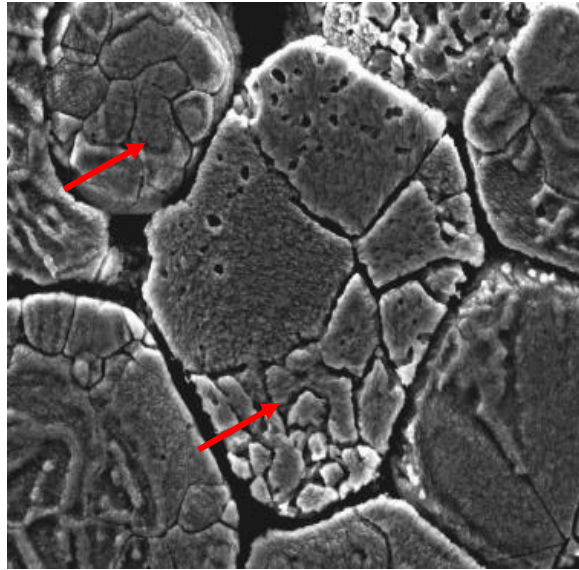
Fig. 2.8. Grain structures of powder particles observed on the polished surfaces of the samples sintered at (a) 550°C and (b) 660°C. (The arrows indicate the fine grains formed in the neck zones) [150].

In addition, **Johnson et al.,** [151] also observed grain size reduction from 10 μm to 0.51 μm in 8 mol% yttria stabilized zirconia (8YSZ) composite developed through SPS.

2.5 Review on AMCs using cryo rolling

As discussed in section 1.4.4 in Chapter 1, cryo rolling is a secondary severe plastic deformation process carried out at cryogenic temperature. The main aim of cryo rolling is to deform the material to form ultrafine/nano grains and create more number of dislocations, while the dynamic re-crystallization step is suppressed or bypassed. Due to reduction in grain size, more number of dislocations and formation of nano precipitates arise through which the material's mechanical properties improve. However, some properties like ductility deteriorate, which need further treatment like heat treatment, etc. Some of the investigations carried out by researchers on the role of improvement in mechanical properties by cryo rolling are summarised below.

Krishna et al., [152] investigated on cryo rolling of Al−4wt%Cu−3wt%TiB$_2$ in situ composite, followed by short annealing at 175 °C and ageing at 125°C, which resulted in an ultra-high yield strength of about 800 MPa with 9% total elongation. It was estimated that the maximum contribution to the improvement of properties was from grain refinement due to cryo rolling,

47

followed by precipitation and dispersion strengthening. The grain refinement achieved due to cryo rolling played an important role in improving the yield strength.

Markushev et al., [153] investigated the effect of cryo rolling on D16 aluminium alloy and concluded that the deformation structure of the D16 alloy formed during cryogenic rolling was relatively stable upon further short term annealing up to ~200° C. Upon annealing in the temperature range 200–300° C, this structure transformed into a mixed one consisting of regions with recrystallized nano grains inside. However, an increase in the annealing temperature to 450° C lead to noticeable coarsening of recrystallized grains and the formation of a fully recrystallized coarse grained structure lead to a decrease in mechanical properties.

Cryogenic rolling of the alloy increased its hardness from ~100 to 180 HV, which is higher than the level achieved for the standard state artificially aged alloy. The authors also concluded that cryo rolling of the preliminarily quenched alloy accelerates its subsequent artificial aging. As a result, the maximum alloy hardness (~200 HV) was reached at a lower temperature or in a shorter time as compared to the conventional hardening heat treatment used for the maximum strength. However, further annealing in the temperature range 230-450° C reduced its hardness to 90 HV because of the recrystallization and grain growth.

Jayaganthan et al., [154] investigated the effect of cryo rolling followed by warm rolling (CR+WR) on strength and ductility of Al-Mg-Si alloys. An ultrafine grained Al 6063 alloy was developed through cryo rolling up to 80% reduction in thickness and with warm rolling up to 50% reduction in thickness at 200° C, followed by ageing at 100°C for 22 hours. It was compared with the material processed through cryo rolling, followed by low temperature ageing. By implementing this new approach, simultaneous improvement in strength (290 MPa) and ductility (15%) was achieved in Al 6063 alloys. The ultrafine grain structure with 150-300 nm was observed in CR+WR sample. Strength, hardness and ductility of CR+WR samples were found to be superior to CR sample after peak ageing treatment. The improvement in strength was attributed to the decrease in dislocation density further by annihilation of dislocations due to static recovery effect and precipitation of remnant excess solid solution from the matrix.

Das et al., [155] studied the effects of cryo rolling and heat treatment (short annealing + ageing) on tensile behaviour of Al 7075 alloy. The Al 7075 alloy was rolled for different thickness

reductions (40% and 70%) at cryogenic (liquid nitrogen) temperature. The cryo rolled Al alloy after 70% thickness reduction exhibited ultrafine grain structure, as observed from its FE-SEM micrographs. It was observed that the yield strength of the cryo rolled material (up to 70% thickness reduction) has increased by 108%, compared to the starting material. The improved tensile strength of the cryo rolled Al alloy was credited to grain refinement, grain fragments with high angle boundaries, and ultrafine grain formation by multiple cryo rolling passes. Cryo rolled samples were subjected to short annealing for 5 min at 170° C and 150° C, followed by ageing at 140° C and 120° C for both 40% and 70% reduced samples. The combined effect of short annealing and ageing improved the strength and ductility of cryo rolled samples, which was due to precipitation hardening and sub-grain coarsening mechanism respectively. However, impact strength of the cryo rolled Al alloy has decreased due to high strain rate involved during impact loading.

Panigrahi et al., [156] investigated the effects of rolling temperature and rolling strain on the mechanical properties and microstructural refinement of Al 6063 alloy. A solution treated bulk Al 6063 alloy samples were subjected to cryo rolling and room temperature rolling to produce sheets with different strain levels viz., 0.4, 2.3 and 3.8. Prior to cryo rolling and room temperature rolling, the initial conditions such as solution treatment temperature, and sample immersion duration time in liquid nitrogen were optimized by Electron back scattered diffraction (EBSD). Based on the significant precipitation hardening response in Al 6063 alloy evident from EBSD microstructures, among all the solution treatment (ST) temperatures, 520° C was selected as an ideal ST temperature for Al 6063 alloy prior to cryo rolling and room temperature rolling. With an increase in sample immersion duration time in liquid nitrogen, an improvement in strength was observed and it stabilized after 30 min. The severe strain induced at very low temperature facilitated the formation and retention of high concentration of defects (dislocation), which acted as a driving force for the formation of substructures, followed by ultrafine grains. It was found that, for cryo rolled (CR) samples a strain value of 3.8 is desirable for producing the ultrafine-grained Al 6063 alloys with the high angle grain boundaries. However, in case of room temperature rolled samples, the sub-grains were not recrystallized up to this strain.

Hailiang et al., [157] developed aluminium alloy 6061 sheets using the accumulative roll bonding (ARB) technique, followed by cryo rolling. Grain size and precipitations affecting the strength and ductility of ultrafine-grained materials were studied. In this study, the ARB-

processed sheets were subjected to cryo rolling, followed by asymmetric cryo rolling. The sheets were further aged at 100°C for 48 hours. Mechanical tests showed that a combination of asymmetric cryo rolling and ageing results in significant improvement in both the ductility and the strength of the ARB processed sheets.

Vigneshwaran et al., [158] successfully rolled different aluminium sheets (AA 5083, AA 6061 and pure-Al) under room temperature (RT) and at liquid nitrogen temperature. Rolling reduction along with liquid nitrogen (LNR) resulted in strength improvement in AA 6061 and pure Al, where as, in the case of AA 5083, the evolution of second phase Al_6Mn resulted in better strength in room temperature rolling (RTR) condition than that of the LNR condition. The work hardening rate of AA 5083 was higher in all the process conditions due to the effect of solid solution and the presence of fine second phase, but the average solid solution was comparatively lower for AA 6061 and CP-Al. The relative slip distance was lower for LNR 75 condition irrespective of the alloy system; whereas the slip distance was marginally higher for AA 5083 due to solute pinning down and annihilated dislocation that resulted in increase in relative slip distance. The void coalescence analysis showed high void size and void area for AA 5083 compared to other Al alloys for a given strain tri-axialaity. The work hardening rate was also high for AA 5083 than that of the other Al alloys. The higher fracture limit of AA 5083 alloy with for 50% reduction may be due to the effect of orientation of precipitates under SPD. However, for the alloy with 75% reduction enhanced fracture strain was shown due to solute clustering and presence of Al_6Mn, which resulted in better strengthening.

Fitsum et al., [159] made an attempt to improve the formability of cryo rolled AA5083 alloy sheets, followed by annealing process at 275°C for 15 minutes. Flat bottom square cup shaped parts were made by deep drawing through hydro forming. Generally, cryo rolling degrades the ductility and malleability of an alloy. Hence, the minimum corner radius and the maximum depth that could be achieved without failure and the maximum thinning at the corners have been considered as the measures of formability. The results have been compared with those of the conventional deep drawing. The simulation results have also been validated with experimental work in both hydro forming and conventional forming. A process window with optimum combination of peak sealing force and peak pressure has been identified to form the cups up to full depth of the die without failure at die entry or bottom corners. Lubrication between the die and the blank reduced the minimum possible corner radius to nearly 16 mm with thinning less than 6%. In conventional forming, only 70% of the full depth could be

obtained before failure with 16 mm punch corner radius, due to excessive thinning at the corners. Enhanced formability in hydro forming is mainly due to higher uniform strain distribution and hydrostatic stress, which suppresses the rate of void growth and hence delays the onset of necking or failure. The authors concluded that by hydro forming, formability of high strength cryo rolled Al alloy sheets could be enhanced due to lower thinning and higher uniform strain distribution. This process route (cryo rolling followed by hydro forming) is recommended as a potential technique to produce complex parts made up of lightweight and high strength Al alloy sheets, due to enhanced formability.

Vineet et al., [160] concluded that the CR alloy showed better precipitation strengthening and higher density while investigating the effect of cryo rolling and room temperature rolling with subsequent annealing on tensile behaviour of 6082 Al alloys with different thickness reductions i.e. 40%, 70% and 90%. A significant improvement in the yield strength, ultimate tensile strength of the CR and RTR aluminium alloy was observed. This could be attributed to the high dislocation density, sliding of grain boundaries and grain refinement. For the same amount of thickness reductions, the mechanical properties of CR alloys were better than those of the RTR alloys due to higher dislocation density as well as formation of sub-grain structures in CR alloy. It was seen that grain refinement is not a key factor for an increased strength after ageing, as only a portion of the grains was recrystallized.

In another study, **Yua, et al.,** [161] investigated the mechanical properties of the Ti-6Al-4V alloy sheets using cold rolling, asymmetric rolling and asymmetric cryo rolling and were characterized by subjecting it to tensile test and micro hardness test. Results show that the Ti-6Al-4V alloy sheets subjected to asymmetrical cryo rolling with low rolling speed ratio have the highest tensile strength and micro hardness. The tensile stress of the alloy samples was found to be 1008 MPa after cold rolling, 1046 MPa after asymmetric rolling, and 1113 MPa after asymmetric cryo rolling. The highest Vickers hardness (395 HV) was achieved by asymmetric cryo rolling. The improvement in mechanical properties when subjected to asymmetric cryo rolling was due to the criteria of grain size reduction, size of second phase as well as improved dislocation density.

Shivaprasad et al., [162] severely plastic deformed Al-3Mg-0.25Sc alloy sheets by rolling at room and cryogenic temperatures to 50% and 75% reduction in thickness respectively and subjected to solution heat treatment (SHT) at 530° C for 1 hour. The results revealed the

formation of a bimodal microstructure. The grain size distribution based on electron backscattered diffraction analyses showed an enhanced fraction of ultra-fine grains with nearly 100 nm in cryo rolled samples whereas; room temperature rolled samples exhibited sub-micron grains with 300 nm. The transmission electron microscopy studies revealed some dense dislocation cell structures for cryo rolled samples due to the restriction of dynamic recovery. Better forming and fracture limit strains were noticed for cryo rolled samples compared to room temperature rolled ones. There was a better accumulation of plastic deformation and improved formability of cryo rolled samples. Further, due to cryo rolling, the reduction in the aspect ratio (L/W) of the void signified a delayed fracture behaviour in the samples when compared to that of the room temperature rolled samples. It also showed better fracture resistance. It could be appreciated that cryo rolling enhanced the strength leading to better fracture resistance and significant ductility in cryo rolled samples, which resulted in better formability compared to RTR samples.

Kumar et al., [163] successfully rolled Al–4Cu–5TiB$_2$ in situ composite sheets at both room temperature and cryogenic temperature to a true strain of 0.6. Aging kinetics and peak hardness of Al–4Cu–5TiB$_2$ in situ composite was improved by rolling. Room and cryogenic rolling and subsequent peak aging of the composite have developed hardness of 138 and 143 HV, respectively, i.e., approximately 25% increase in hardness in comparison to the as cast and peak aged composites. There was no significant influence of rolling temperature on the hardness of the composite in the present experimental range, i.e., rolling strain of 0.6. The wear resistances of the rolled and peak aged samples were higher than those of the as-cast and as-rolled samples.

2.6 Discussion and gap areas

From the literature review, it is found that, if one wants to design a composite having ultra high strength, then, such a composite should consist of

> ➢ Extremely fine grains

> ➢ High volume fraction of fine inter-metallic phases

> ➢ Optimum volume fraction of well distributed reinforcement

> ➢ Suitable processing method

> ➢ Suitable secondary processing and treatment.

However, the properties of a composite mainly depend on some factors like reinforcement material and processing method. Though the reinforcing material has the potential to improve the properties of a composite, the drawbacks and challenges encountered during the production stage deteriorate the properties of the end product. Unfortunately, very well-known and popular conventional processing techniques like stir casting and PM possess certain drawbacks while processing aluminium metal matrix composites. On the other hand, over the years, utilization of various types of reinforcing materials in aluminium metal matrix composites has increased. With an increase in the reinforcement wt% in the composite, certain factors like agglomeration, formation of undesirable phases, ductility reduction and cost increase.

Few researchers have used rare earth metals as reinforcements to enhance the mechanical properties of aluminium matrix composites. For example, reinforcement of small amounts of Sm [64], Ce [62, 65] Cd [67], Nd [71], Yb [72-75], Sc [76], Y [70, 78, 79], etc., are reported to improve the mechanical properties, promote grain refinement and accelerate precipitation kinetics of various aluminium alloys.

The existing literature shows that enough investigations have been done on improving the mechanical properties of various aluminium alloys through reinforcement with TiB_2. However, in most of the cases, formation of brittle Al_3Ti phase is observed, which deteriorated the ductility of the composites. Later, some researchers have put efforts in suppressing the formation of such phases and succeeded. In addition, literature also gives evidences of improvement in tensile strength of the aluminium matrix composite through cryo rolling.

Based on the above literature review, the gap areas can be summarized as follows

2.6.1 Gap areas related to reinforcing materials

- Enough investigations have been carried out to develop composites by reinforcing ceramics, graphite, carbon nano tubes, etc. Though some attempts have been made to develop the composites by reinforcing certain rare earth materials, enough investigations have not been made with rare earth materials, especially with yttrium.

- Enough investigations have been carried out to develop aluminium nano composites by reinforcing aluminium with nano ceramics, metallic, graphite, CNT, etc. However, no attempt has been made to develop aluminium nano composite by reinforcing nano yttrium.

- Some investigations have been carried out to develop aluminium hybrid composite and by reinforcing TiC, nano carbon tubes, SiC, B_4C, Al_2O_3, etc. However, no attempt has been made to develop hybrid composites by reinforcing nano rare earth material and TiB_2.

2.6.2 Gap areas related to processing methods

- Enough investigations have been carried out to develop composites with various reinforcing materials using stir casting method. However, the advantages and limitations of stir casting in developing Al-RE composites have not been explored so far.

- Enough investigations have been carried out to develop composites using conventional cold compaction. However, investigations on the reinforcement of RE in Al matrix using cold compaction are limited.

- Several researchers have made investigations to develop the composites of aluminium-copper alloy materials using different processing methods with different reinforcements but very little work has been attempted using SPS.

- Enough investigations have been carried out to develop the composites using standard processing methods like casting, forming, rolling, etc. However, no attempt has been made to develop the hybrid composite using SPS.

- Some investigations have been carried out on the cryo rolling of aluminium alloys. However, no attempt has been made to investigate the cryo rolling of Al-Cu alloy matrix composites developed by SPS.

2.7 Objectives of the present investigations

- To develop a composite material of aluminium metal matrix with the reinforcement of rare earth material (yttrium) through stir casting.

- To develop a composite material of aluminium metal matrix with the reinforcement of rare earth material (yttrium) powder (micro/nano) through cold compaction.

- To develop a composite material of aluminium metal matrix with the reinforcement of a rare earth material (yttrium) through SPS.

- To develop a hybrid composite by using some hard ceramic material with good wear resistance as a second reinforcement in addition to the rare earth material to the above said matrix through SPS.

- To investigate the effect of cryo rolling on the aluminium metal matrix composites with the reinforcement of rare earth material (yttrium) through SPS.

- To investigate the morphology of the above said composites using optical microscopy, Field Emission Scanning Electron Microscope (FE-SEM) and X-ray Diffraction (XRD).

- To evaluate the mechanical properties of the composites developed in each of the above said cases.

The flow chart of the present work plan is shown in Fig. 2.9.
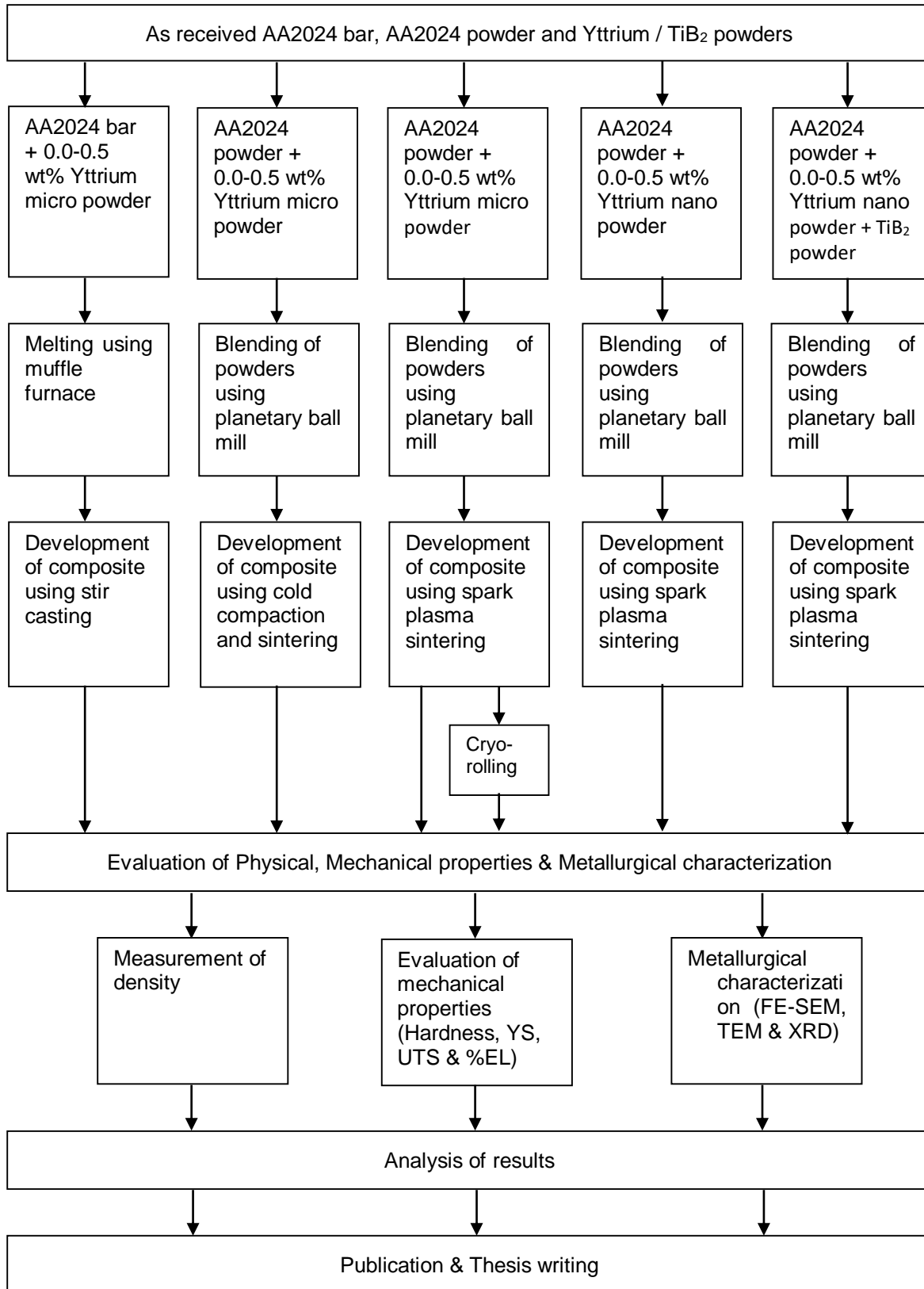
Fig. 2.9 Flow chart of work plan

This chapter introduces and discusses about various details of the starting materials, processing methods, characterization techniques, instruments and equipment used in the present investigations. The properties of the staring powders, morphology, and structure are presented in detail. Different aspects of characterization techniques like metallurgical characterization, mechanical characterization, etc., are elaborated. The instruments used for various measurements, standard sample preparation along with their specifications are discussed in detail.

3.1 Preparation of materials

In this experimental work, the materials chosen were 2024 aluminium alloy (AA2024) cylindrical bar, the powders of AA2024 and the powders of yttrium (Y), titanium boride (TiB_2), and nano yttrium produced through ball milling. The chemical composition of the as-received aluminium 2024 alloy powder is shown in Table 3.1. This AA2024 powder was used as the matrix material, which was procured from Alfa Aesar, United States. The average particle size was 60 microns.

Table 3.1 Chemical composition of the as- received AA2024 powder.

Element	Si	Cu	Fe	Zn	Mg	Ti	V	Mn	Al
Wt%	0.16	4.67	0.47	0.14	1.71	0.05	0.001	0.80	Balance

Yttrium powder of particle size 400 microns and titanium boride powder of average particle size 10 μm were used as the reinforcement materials to AA2024 matrix. This yttrium powder (99.6% purity) and titanium boride (99.9% purity) powders were also procured from Alfa Aesar, United States.

Five batches of composites each comprising of five samples were developed in the present work. In the first three batches, AA2024 matrix was reinforced with varying amounts of micro yttrium ranging from 0.1 to 0.5 wt%. Among these three batches, first batch composites were developed by reinforcing varying amounts of micro yttrium to AA2024 melt, processed through stir casting. The second and third batch composites were developed through cold compaction and Spark Plasma Sintering (SPS) respectively by reinforcing varying amounts of

micro yttrium powder in AA2024 matrix powder. The fourth batch composites were developed through SPS by reinforcing varying amounts of micro yttrium powder in AA2024 matrix powder. The fifth batch composites were developed through SPS by reinforcing a constant amount of 1.0 wt% TiB_2 and varying amounts of nano yttrium in AA2024 matrix powder.

3.1.1 Preparation of composite matrix material

Fig. 3.1 shows the as-received AA2024 cylindrical bars used in the development of composites through stir casting process. The AA2024 cylindrical bars were also procured from Alfa Aesar. These bars were cut into small pieces and used as matrix material in stir casting.

Fig. 3.1 As-received AA2024 cylindrical bars.

Fig. 3.2 shows the scanning electron microscope (SEM) microstructures of the AA2024 matrix powder, used in the cold compaction and SPS. The AA2024 powder was mounted, polished and etched according to standard metallographic procedure and its microstructure was observed under an optical microscope. Fig. 3.2 (a) indicates the SEM microstructure of the as received AA2024 powder, whereas Fig. 3.2 (b) indicates that of the etched AA2024 powder particles.
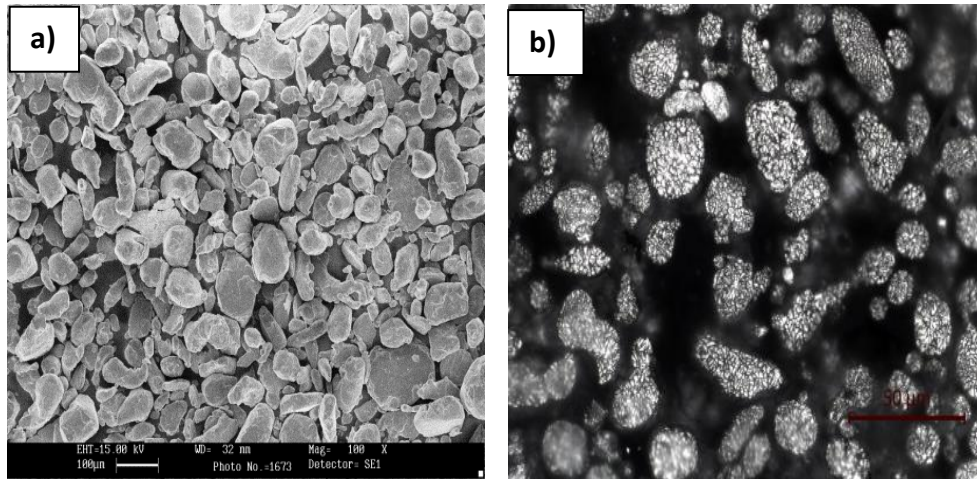
Fig. 3.2 SEM microstructures of (a) as-received AA 2024 powder, (b) etched AA2024 powder particles.

Fig. 3.2 (a) reveals the AA2024 powder with a near spherical morphology and having an average particle size of 60 µm. It can be clearly seen from Fig. 3.2 (b) that the powder particles exhibit dendrite structure comprising dendrite grains of size approximately 6-8 µm. The dendrite structure was developed due to rapid solidification of the particles from the liquid melt during inert gas atomization.

3.1.2 Preparation of reinforcing materials

Fig. 3.3 shows the SEM microstructures of the as-received powders which were used as the reinforcements in the present study. Fig. 3.3 (a) indicates the SEM microstructure of the as-received yttrium powder, wheras Fig. 3.3 (b) indicates that of the as-received TiB_2 powder. Fig. 3.3 (a) reveals the microstructure of loose yttrium powder particles which look like curled chips/whiskers with three different dimensions and traces of brittle fractures along the edges of its length.
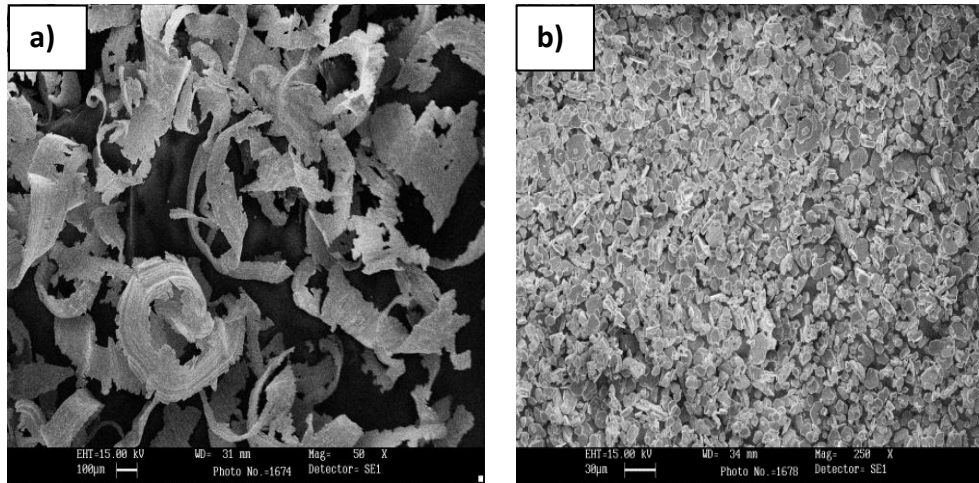
Fig. 3.3 SEM microstructures of the as-received reinforcement powder (a) yttrium (b) titanium boride.

Fig. 3.3 (b) reveals that the TiB_2 powder particles have the form of discs with approximate hexagon shape having average particle size of 10 µm. Fig. 3.4 shows the Transmission Electron Microscope (TEM) nanostructure of nano yttrium. The as-received yttrium powder was reduced to nano size by ball milling for 60 hours using steel jar and hardened steel balls, using a High Energy Ball Mill (HEBM). Fig. 3.4 reveals the agglomerated nano yttrium particles in a cluster. The nano yttrium particles were agglomerated due to the procedure followed during sample preparation for TEM observations.
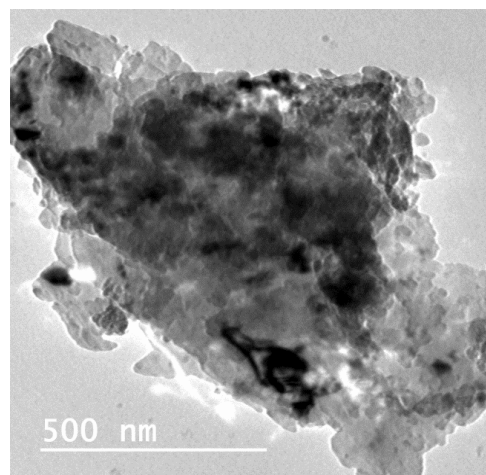
Fig. 3.4 TEM nanostructure of nano yttrium powder after 60 hours ball milling

3.1.3 Blending of powders

The powders were weighed and mixed according to the proportions shown in Table 3.2 and Table 5.1. A planetary ball mill was used for blending and uniform mixing of the composite sample powders. The ball mill was rotated at a speed of 50 RPM for 2 hours using a steel jar

coupled with hardened steel balls with a ball to powder ratios of 1:1 for blending and 10:1 for yttrium size reduction. The planetary ball mill used in the present work is shown in Fig. 3.5.

Fig. 3.5 High energy planetary ball milling machine.

Thermal analysis of the blended composite powders was done to indirectly observe if there was any oxidation and detect any change in their melting points. The analysis was done using a differential thermal analyzer (DTA) (Model: SII 6300 EXSTAR). The powder samples were kept in an alumina sample holder with 10° C/minute heating rate up to 700° C.

3.2 Development of composites

Five different composite samples with varying amounts of micro yttrium reinforcement were developed through stir casting, cold compaction and spark plasma sintering with the intended proportions shown in Table 3.2.

Table 3.2 Intended proportions of the composite samples.

Sample No	AA2024 proportion by weight (wt%)	Yttrium (micro/nano) proportion by weight (wt%)
1	99.9	0.1
2	99.8	0.2
3	99.7	0.3
4	99.6	0.4
5	99.5	0.5

3.2.1 Development of composites through stir casting

Fig. 3.6 shows the aluminium stir casting furnace set-up, used in the present investigation.

Fig. 3.6 Aluminium stir casting furnace set-up used in the present investigation.

The AA2024 bars were cut into 0.5 kg samples and melted in the stir casting furnace at 800°
C. After melting, pre heated micro yttrium powder at 700° C was gradually dropped into the
melt while stirring at a slow speed. Once all the yttrium was completely added, the stirring
speed was increased to 100 RPM and maintained for 15 minutes. Then the stirring was
gradually slowed down and the molten metal was released into a steel die fixed at the bottom.
After solidification, the casted composite samples were cut into pieces for characterization.
The casted composite samples were later artificially aged and characterized.

3.2.2 Development of composites through cold compaction

Five composite samples reinforced with varying amounts of micro yttrium powder were
developed by hydraullic pressing and conventional sintering method. An un-reinforced
AA2024 sample was also sintered as a benchmark to compare the effect of yttrium
reinforcement. The composite powder blend was heated to 100° C to remove the moisture and
make the powder free from humidity. Then the powder was poured in a hardened steel die and
the upper and lower punches were inserted by applying initial hand pressure and the die-punch
assembly was placed in a hydraullic press. A pressure of 50 MPa was applied gradually and
once the desired pressure was applied, it was left to dwell for 1 minute before the pressure was
gradually withdrawn. After gently removing the green compact from the die, it was sintered in
a tubular furnace at 550° C under flowing nitrogen gas for four hours.

3.2.3 Development of composites through spark plasma sintering

The blended powders were then seived and processed by SPS. It is worthwile to mention that it is a challenging task to optimize SPS conditions to obtain uncracked and dense composites. After a large number of trails, the following SPS conditions (shown in Table 3.3) were identified as the optimal processing conditions and the SPS cycle is shown in Fig. 3.7.

Table 3.3. Optimal SPS parameters employed to sinter the composite powders.

Temperature	450° C
Rate of temperature rise	50° C/ minute
Pressure	50 MPa
Holding time	180 seconds
Cooling rate	100° C
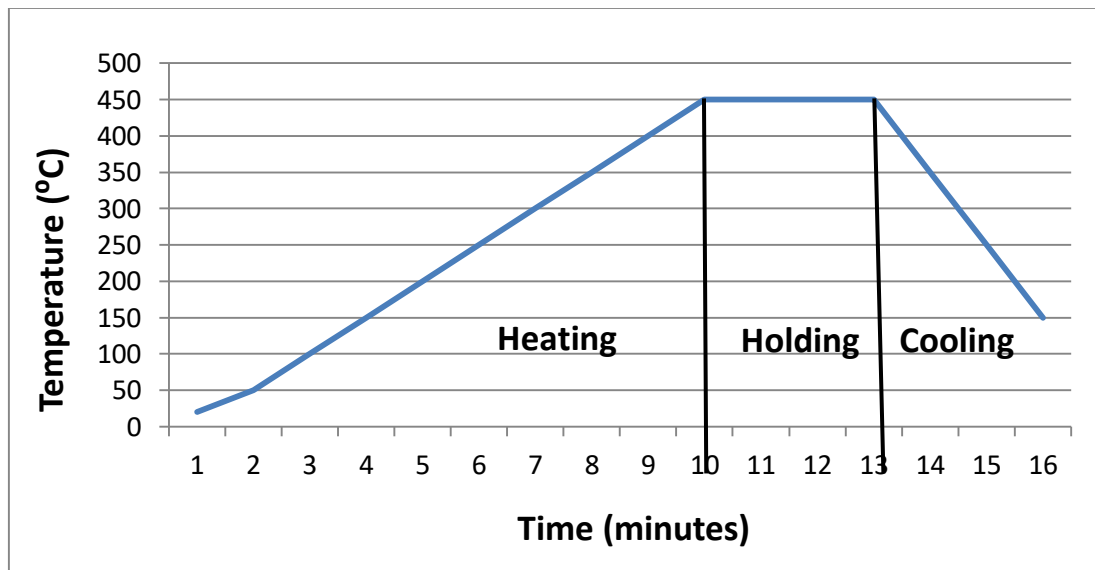
Fig. 3.7 SPS operating cycle.

The sintering of the composite powder sample was carried out using SPS apparatus (Model : Dr. Sinter SPS-625, Fuji Electronic Industrial Co. Ltd., Japan). The SPS equipment used in the present study is shown in Fig. 3.8.

Fig. 3.8 SPS equipment used in the present study.

Cylindrical composite discs having diameter 30 mm and thickness 7 mm were sintered using graphite die and punches through SPS. The schematic diagram of the intended spark plasma sintered composite sample is shown in Fig. 3.9.

7 mm

30 mm
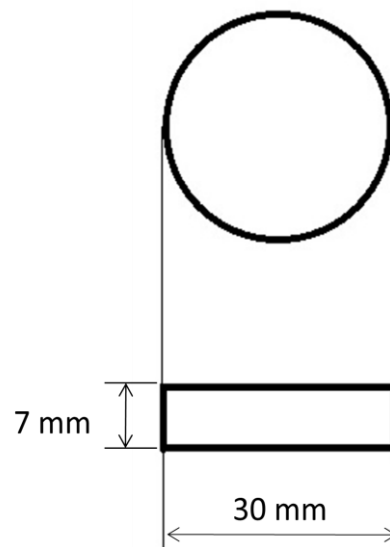
Fig. 3.9 Schematic diagram of the intended spark plasma sintered composite sample.

The composite powder blend was heated up to 100⁰ C temperature to remove any moisture present. The bottom punch was inserted into the die and the pre-heated powder was poured. Then the upper punch was inserted tightly by applying hand pressure. The die and punches used in the present study are shown in Fig. 3.10.

Fig. 3.10 Die and punches used to develope the composite samples.

The die-punch combination set up was placed inside the SPS chamber with appropriate graphite spacers and a uni-axial pressure of 50 MPa was applied throughout the sintering cycle. After sufficient vacuum was created, argon gas was introduced into the chamber. During SPS cycle, temperature was raised at a rate of 50° C/minute up to 450° C and held there for 3 minutes using a preset heating program. After final stage of holding, the power was turned off and the sample was left to cool at the rate of 100° C/minute, while maintaining the sintering pressure. The sintering temperature was monitored and regulated using a thermocouple, which was inserted into the graphite die. The sintering behavior was monitored by measuring the change in axial dimension of the compact.

3.2.4 Development of composite through cryogenic rolling

The composite samples i.e. AA2024 reinforced with 0.1 to 0.5 wt% micro yttrium along with pure AA2024 sample, processed through SPS were cryo rolled to 50% reduction at -196° C. The samples were rolled several times with 5% reduction in each pass. After each pass, the composite samples were immersed in liquid nitrogen to attain and maintain the cryogenic temperature. The rolling machine used in the present study is shown in Fig. 3.11.

Fig. 3.11 Rolling machine used for cryo rolling.

3.3 Evaluation of physical properties

3.3.1 Density

The density of the sintered composite samples was measured by applying Archimedes principle, according to ASTM B962-08 standard. The relative densities of the composite samples were determined by calculating their theoretical densities according to the linear rule of mixtures, shown in equation 3.1.

$\rho_{composite} = V_{matrix} \times \rho_{matrix} + V_{reinforcement} \times \rho_{reinforcement}$ ---------------- Equation (3.1)

Where,

$\rho_{composite}$ = density of the composite,

ρ_{matrix} = density of the matrix,

$\rho_{reinforcement}$ = density of the reinforcement,

V_{matrix} = volume fraction of the matrix,

$V_{reinforcement}$ = volume fraction of the reinforcement.

3.3.2 Green and sintered densities of preforms

The densities of the green compacts obtained after cold compaction and those of the preforms obtained after sintering were determined by weights and volume method. An electronic weighing balance recorded the weights of the green compacts and preforms, with an accuracy of 0.1 mg (Make: AUW10^{TM} *Shimadzu*, Japan). Dimensions of the samples were carefully measured using a digital Vernier calipers to an accuracy of 0.01 mm (Make: MITITOYO^{TM}, 150 mm measuring range). Measurements were repeated at least 6 times for each case and the

average values of weight and volume were taken to calculate green densities of the powder compacts/preforms.

The green and sintered densities were further confirmed by Archimedes principle / water displacement technique with oil-impregnation using the ASTM standard B962-08 method. According to the ASTM standards, the densities were calculated by using the following formula:

$$\text{Density} \quad D = \frac{A\rho}{B-(C-E)}$$
------------------------ (Eq. 3.2)

All densities were reported in gcm^{-3}

A   = the mass of the green part or test piece in air, grams.

B   = the mass of the oil-impregnated green part or test piece, grams.

C   = the mass of the oil –impregnated part/test specimen and specimen support immersed in water, grams.

E = the mass of the oil –impregnated part/test specimen support immersed in water, grams.

P   = the density of water, g/cm^3.

3.3.3 Densification parameter

The densification parameter (Ψ) was calculated by using the following formula:

$$\Psi = \left(\frac{\rho_s - \rho_g}{\rho_t - \rho_g}\right)$$
------------------------ (Eq. 3.3)

Where, ρ_s, ρ_g, and ρ_t are sintered, green and theoretical densities respectively.

Ψ is a dimensionless parameter, expressed as a percentage number which is useful in capturing the effect of net density progression activated by sintering. Positive values are an indication of density enhancement due to sintering (shrinkage) and negative values indicate a final expansion of the sample after sintering.

3.4 Evaluation of metallurgical properties

Investigations on microstructure like optical microscopy (OM), field emission scanning electron microscopy (FE-SEM), high resolution transition electron microscopy (HRTEM) and

X-ray diffraction (XRD) analysis were carried out for relevant composite samples including the unreinforced AA2024 sample, developed through stir casting, cold compaction and SPS.

The composite samples were cut into small pieces, ground and then polished on 1/0, 2/0, 3/0 and 4/0 silicon carbide emery papers. The polished samples were further polished on a mechanical rotating coarse cloth disc with fine Al_2O_3 powder particles until the visible scratches were removed. Finally, the coarse cloth on the rotating disc was replaced by a fine cloth and the samples were polished with a nano size diamond particle paste until the fine scratches were removed and a mirror like finish was obtained. After that, the samples were thoroughly washed and cleaned with water and dried using a hot air dryer. The dried samples were etched with modified Keller's reagent for 30-40 seconds. Then the composite samples have been thoroughly examined by OM, FE-SEM and HRTEM.

3.4.1 Optical microscopy

The optical microscope used in this study was LEICA DMI 5000M (Model: Leica Microsystems, Baffalo Grove, IL) microscope. The microstructures were captured at 100 X and the average grain sizes were determined by linear intercept method taking 20 images per each sample. The microstructure-property relationship was determined for all composite samples. The optical microscope used in the present study is shown in Fig. 3.12.

Fig. 3.12 Optical microscope used in the present study.

3.4.2 Scanning electron microscopy

The scanning electron microscope (SEM) (Model: Zeiss EVO18® LaB6 filament) coupled with energy dispersive analysis of X-rays (EDX) was used for the present study. The composite

specimens were prepared in the same manner as they were prepared for OM. The starting powders and fractured samples were analyzed by SEM. The SEM used in the present study is shown in Fig. 3.13.

Fig. 3.13 SEM used in the present study.

3.4.3 FE-SEM

A field emission scanning electron microscope (FE-SEM) (Model: Carl Zeiss ultra plus) equipped with EDX was used for the present investigations. All the sintered composite samples were polished and etched by conventional technique before observing them under FE-SEM. It was used to identify different phases and precipitation that were formed in the sintered composite samples. The FE-SEM used in the present study is shown in Fig. 3.14.

Fig. 3.14 FE-SEM used in the present study.

The approximate chemical compositions of different phases were acquired using EDX. Compared to SEM, FE-SEM could achieve higher magnification, resolution and back scattering, which were necessary to identify different phases that were formed in the composite samples during sintering. X-ray elemental mapping of the selected area was also carried out to analyse the distribution of various elements in that particular area of interest and their atomic percentages.

3.4.4 Transmission electron microscopy

Different phases in the composite samples were observed by means of high resolution transmission electron microscope (HR-TEM). Samples for TEM analysis were prepared by slicing thin sections from the cross section of the composite samples by slow diamond cutting and further thinning down to 30 microns by slow hand process. The HR-TEM used in the present study is shown in Fig. 3.15.

Fig. 3.15 HRTEM used in the present study.

Circular discs of 3 mm diameter were cut from the thinned slice and the discs were further thinned by using a dimple grinder with diamond paste. Finally, the dimpled discs were electro polished using a twin-jet electro polishing set-up with 75% CH_3OH and 25% HNO_3 solution at 12 Volts and -35° C.

3.4.5 X-ray diffraction

The blended composite powders as well as the developed composite samples were studied through X-ray diffraction (XRD). The XRD instrument used in the present study is shown in Fig. 3.16.

Fig. 3.16 X-ray diffractometer used in the present study.

All the measurements were done by using Burker X-ray diffractometer (Model: D8-Advance). The goniometer was set at 0.5°/minute through an angle range of 10° to 90° (2 theta). The new phases, crystal sizes and micro strains that were formed during fabrication were identified and analysed using expert high score and tiny tools software.

3.5 Evaluation of mechanical properties

Different types of mechanical testing viz. hardness and tensile strength were carried out for all the developed composite samples and also the unreinforced AA2024 samples to evaluate their strength and performance. The test specimens were cut from the composite according to the ASTM standards.

3.5.1 Hardness

The effects of reinforcement and the processing conditions on hardness for all the sintered composite samples were evaluated by measuring micro hardness using a computerized Vickers hardness testing machine (Model: FIE VM 50 PC). All the specimens were mirror polished and observed under a microscope, which was coupled to the machine. The Vickers hardness testing machine used in the present study is shown in Fig. 3.17.

Fig. 3.17 Computerized Vickers hardness testing machine.

A diamond pointer was placed on the sample and a load of 5 kg was applied for a dwell time of 10 seconds and then removed. The size of the indentation caused by the diamond pyramid pointer on the sample was inversely proportional to the hardness of the corresponding samples. Ten hardness measurements were taken randomly at several places for each sample for better accuracy and also to observe the precession. The average values and standard deviations of the results were calculated and reported. The hardness was measured in the transverse direction, which was perpendicular to the applied load during sintering.

3.5.2 Tensile strength

Tensile test was performed to evaluate the effect of reinforcement and processing methods on the tensile strength and elongation of all the composite samples. The tests were conducted on a universal testing machine (UTM) (Model: H 75 KS) at a strain rate of 0.003/second. The UTM used in the present study is shown in Fig. 3.18.
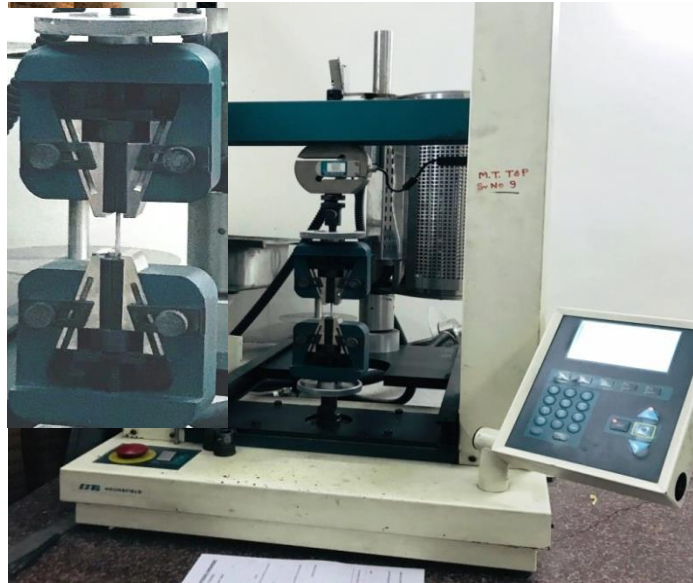
Fig. 3.18 UTM used for tensile testing.

Three tensile specimens were cut from each sintered sample and the average values and standard deviations were reported. The tensile specimens were cut using a wire cut electric discharge machine (EDM) according to ASTM E8 standards. Fig. 3.19 (a) shows the size of a standard specimen and (b) shows the specimen cut from a composite sample. The tensile test samples were cut in the transverse direction, which was perpendicular to the applied force during sintering.
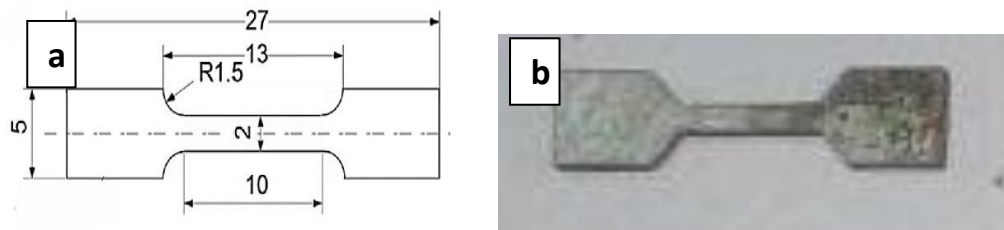
Fig. 3.19 Tensile specimen (a) ASTM E8 standard and (b) Specimen cut from a composite sample.

DEVELOPMENT OF AA2024 + YTTRIUM COMPOSITES

This chapter presents the details of investigations carried out to develop AA2024 matrix composites reinforced with varying amounts of micro yttrium through stir casting, cold compaction and spark plasma sintering. It also present the details of investigations carried out to develop AA2024 matrix composites reinforced with varying amounts of nano yttruium through SPS. Finally it reveals the effect of cryo rollig on SPS processed AA2024 matrix composites reinforced with micr yttrium.

4.1 Development of AA2024 + micro yttrium composites using stir casting

In this section, the first batch of composites comprising of five different composite samples were developed by reinforcing varying amounts of micro yttrium ranging from 0.1-0.5 wt% with AA2024 matrix. The composite samples were processed through stir casting. The results corresponding to density, metallurgical characterization, mechanical properties testing are presented in detail. Various results are discussed in the light of improvement in mechanical properties of the composites developed. At the end, the conclusions drawn from the present work are presented.

4.1.1 Experimental work

Cylindrical bars of AA2024 (99% purity) and yttrium powder (99.6% purity), shown in Fig. 3.1 (a) and (b), were procured from Alfa Aesar, United States. The as-received AA2024 cylindrical bars consisted of the following composition, as shown in Table 4.1.

Table 4.1 Chemical composition of as-received AA2024 cylindrical bar.

Element wt%	Si	Fe	Cu	Mn	Mg	Cr	Zn	V	Al
Minimum			3.80	0.30	1.20				
Maximum	0.50	0.50	4.90	0.90	1.80	0.10	0.25	0.005	Balance

The composite samples were stir cast by the procedure discussed in section 3.2.1. First the AA2024 pieces were melted in a furnace at 700º C. Once the pieces are melted and liquified, the pre-heated yttrium powder folded in aluminium foil was introduced into the melt. The

stirring speed was gradually increased and the temperature was increased to 800° C to compensate the cooling effect developed during stirring. After 10 minitues of stirring at 100 RPM, the liguid composite melt was allowed to flow from furnace chamber into a steel die placed underneath the furnace and left to cool down. The entire process was carried out at normal atmosphere and pressure (no special atmosphere was used and no degassing was done). After the liquid composite melt was solidified and cooled down to room temperature, the composite samples were removed from the steel die. Then the composite samples were cut into pieces for further mechanical and metallurgical investigations. After the composite samples were cut for characterization, the remains of each composite sample were stored in a refrigrator to avoid any natural ageing. Further, all the composite samples were subjected to artificial ageing. Initialy, all the composite samples were solutionized by heating them to a solid solution temperature of 500˚ C and quenched to room temperature by water. Next, each solutionized composite sample was cut into ten pieces and then placed in a furnace until the furnace reached a temperature of 190˚ C. Once all the pieces of all the composite samples in the furnace reached 190˚ C, time was noted. One hour after the noted time, one piece from each composite sample was taken out for characterization. In order to evaluate the effect of heating time on the hardening of the composite samples, corresponding pieces from each composite sample were taken out with an interval of one hour upto 10 hours.

4.1.2 Results

4.1.2.1 Density measurement

The composite samples developed through the above said stir casting process were cut into small pieces of equal size for measurement of experimental density. The theoretical and experimental densities of the composite samples were calculated by the procedure discussed in section 3.3.1. The relative density was calculated using the theoretical and experimental densities and its variation with respect to yttrium reinforcement is shown in Fig. 4.1.
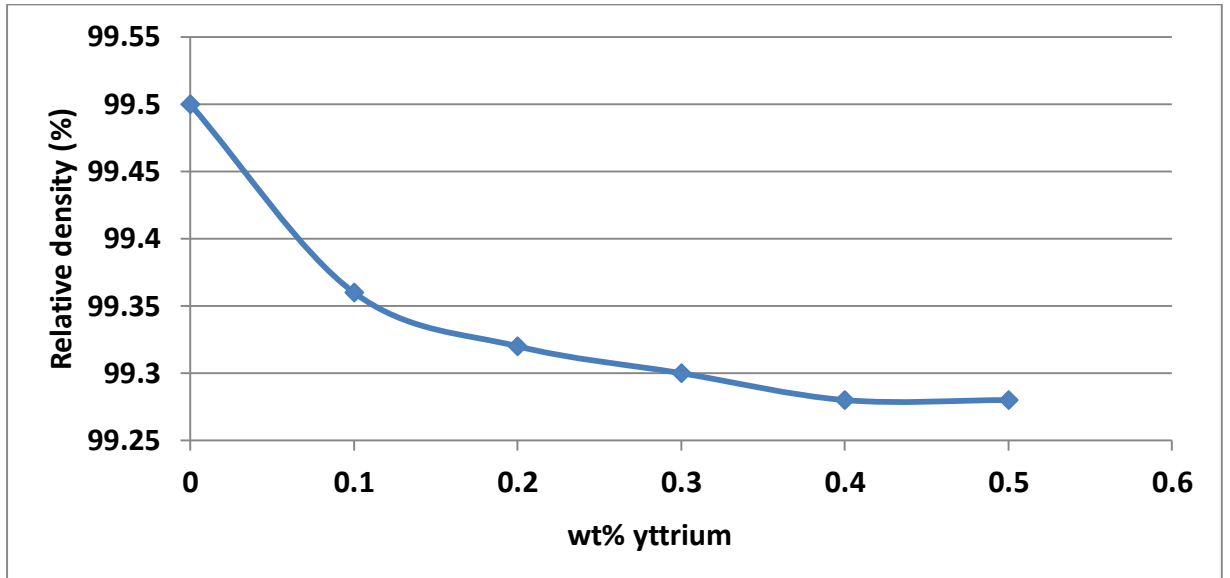
Fig. 4.1 Variation of relative density of the stir cast composite samples with varying amounts of reinforced yttrium.

Yttrium reinforcement to AA2024 matrix has decreased the relative density of the composite samples compared to the as-received AA2024 ingots. From Fig. 4.1, it can be observed that the relative density of the composite samples decreased steeply up to 0.3 wt% of yttrium reinforcemrnt. Upon further increase in yttrium reinforcement, the decrease in relative density is not significant.

4.1.2.2 Investigation of microstructure

The pieces that were cut from each composite sample were throughly polished and etched for further metallurgical characterization through FE-SEM and EDX, as discussed in section 3.4.3. Fig. 4.2 shows the FE-SEM microstructures of the stir cast composite samples with different reinforcements of micro yttrium.
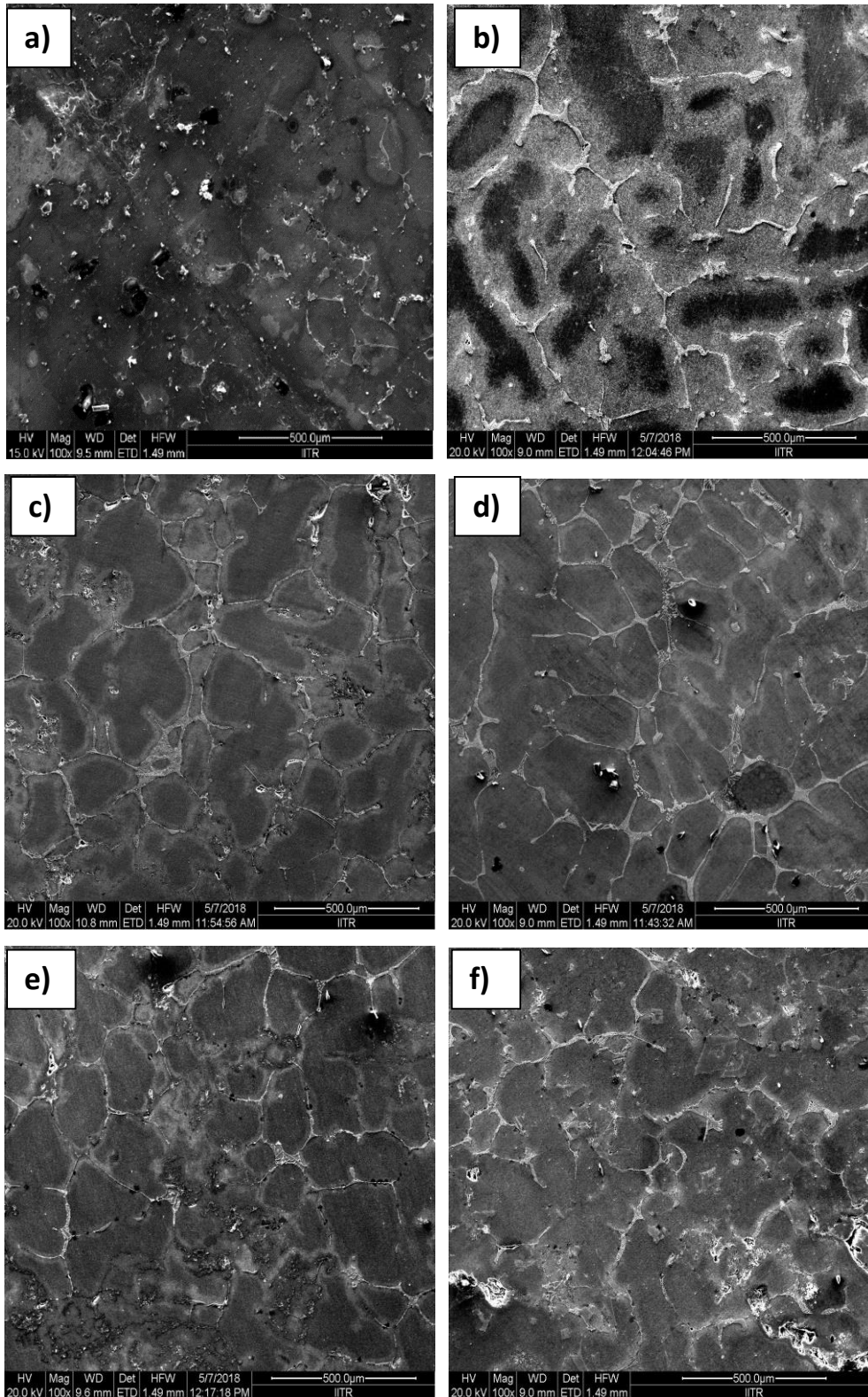
Fig. 4.2 FE-SEM microstructures of the stir cast composite samples reinforced with (a) 0.0 wt% micro Y, (b) 0.1 wt% micro Y, (c) 0.2 wt% micro Y, (d) 0.3 wt% micro Y, (e) 0.4 wt% Y and (f) 0.5 wt% micro Y.

From Fig. 4.2, it can be observed from the microstructures that the grain refinement of the aluminium matrix took place gradually with the increase in the reinforcement of yttrium compared to that of the the unreinforced AA2024 microstructure. The formation of the intermetallic compound (Al-Cu-Y) lead to the formation of grains in the matrix by creating nucleating sites. As the yttrium wt% increased upto 0.3 wt%, there was a positive response to grain refinement. Gradually the grains started to form, leading to grain refinement. Upon further increase in yttrium wt%, the grain refinement and grain size reduction was not evident.

For further investigation, the composite samples were examined through FE-SEM in back-scatter mode at higher magnification to observe the intermetallic phase formation and its transformation in the matrix. The back-scattered FE-SEM microstructures are shown in Fig. 4.3. The microstructures exhibit two distinct types of secondary phases in the α-Al matrix, which play an important role in the variation in strength of the composite samples. From Fig. 4.3, it is evident that the reinforcement of 0.1 wt% yttrium forms a chinese script in the matrix. EDX analysis shows that the chinese script has the composition rich in Al, Cu and Y. Apart from the chinese script, another phase comprising Al and Cu as major elements can also be seen in the matrix. As the yttrium reinforcement increases upto 0.3 wt%, the chinese script becomes finer. Upon further increase, the chinese script coarsens along with the Al-Cu phase, which is encircled in red.
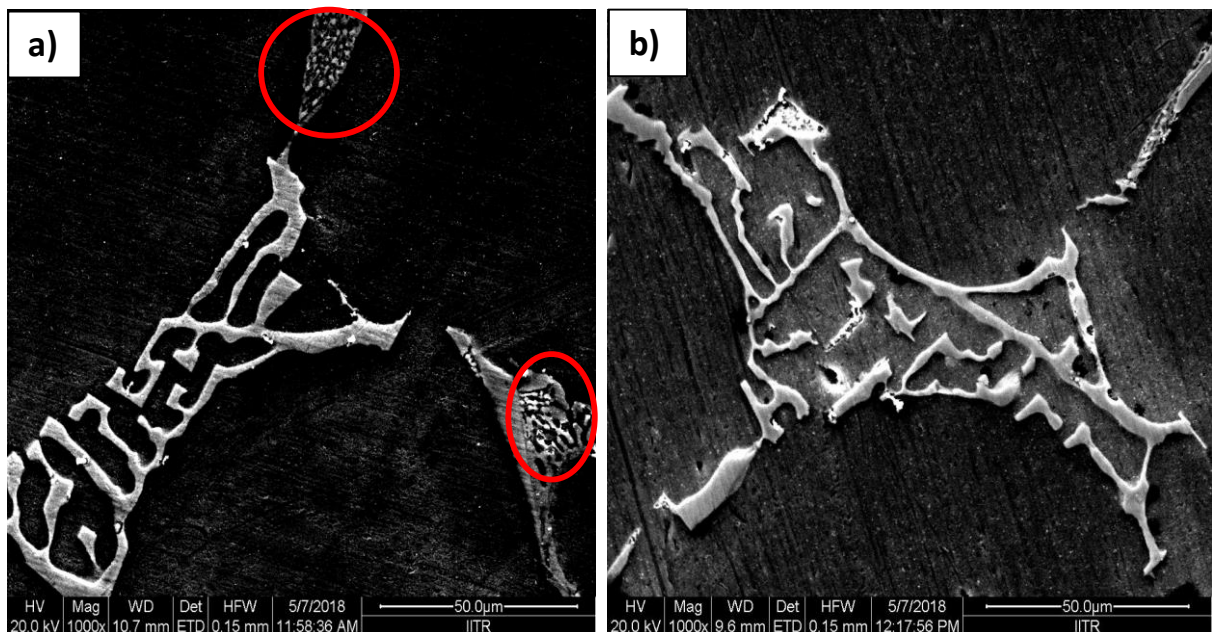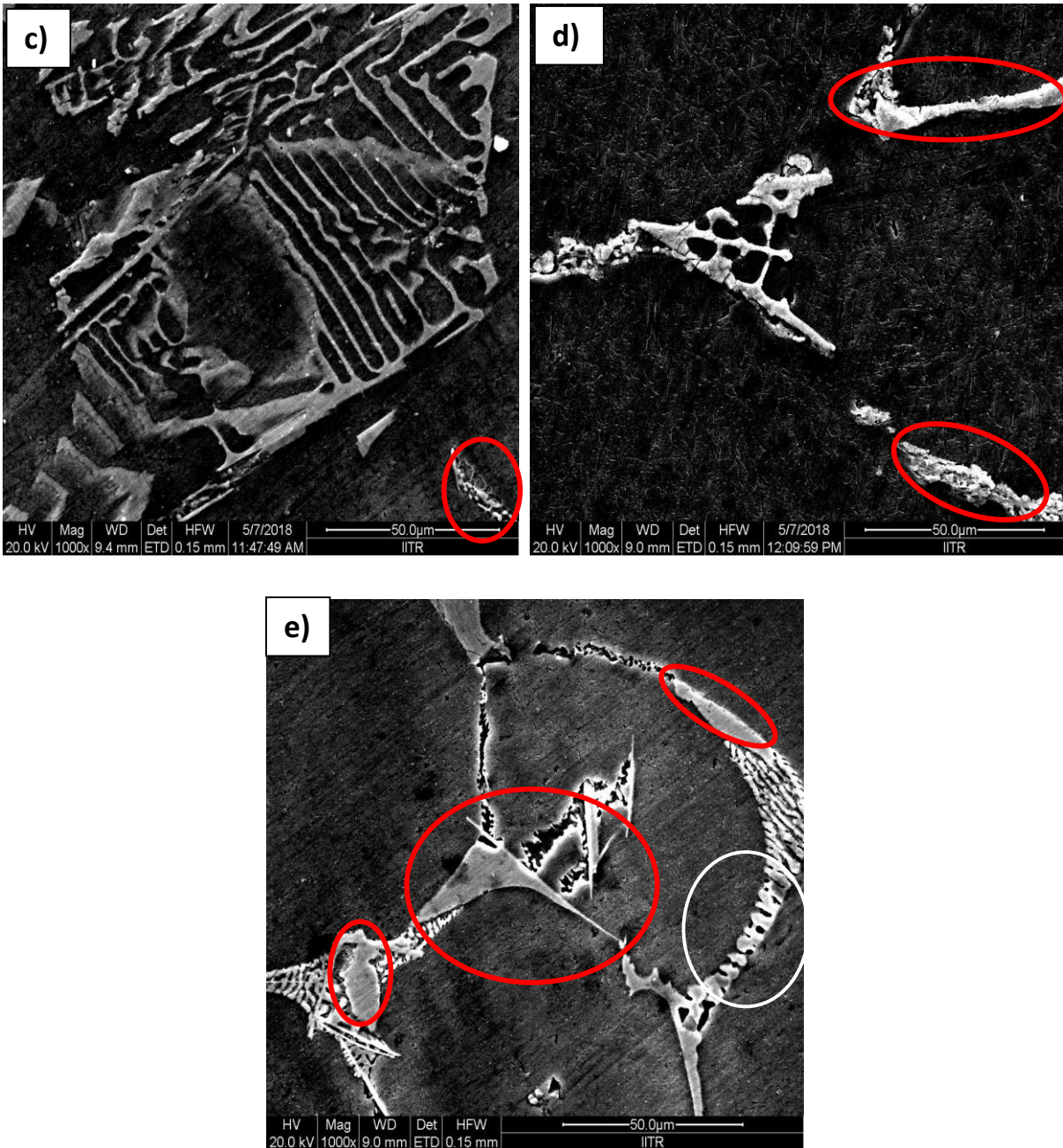
Fig. 4.3 FE-SEM back scattered microstructures at higher magnification showing secondary phases and intermetallic transformation in the stir cast composite samples reinforced with a) 0.1 wt% micro Y, b) 0.2 wt% micro Y, c) 0.3 wt% micro Y, d) 0.4 wt% micro Y and e) 0.5 wt% micro Y.

The SE-SEM microstructure showing the Al-Y-Cu intermetallic formation of the composite sample reinforced with 0.3 wt% yttrium is shown in Fig. 4.4. Fig. 4.4 (a) shows the FE-SEM microstructure, whereas Fig. 4,4 (b) shows the higher magnification of Fig. 4.4 (a) focusing on the intermetallic formation.

80
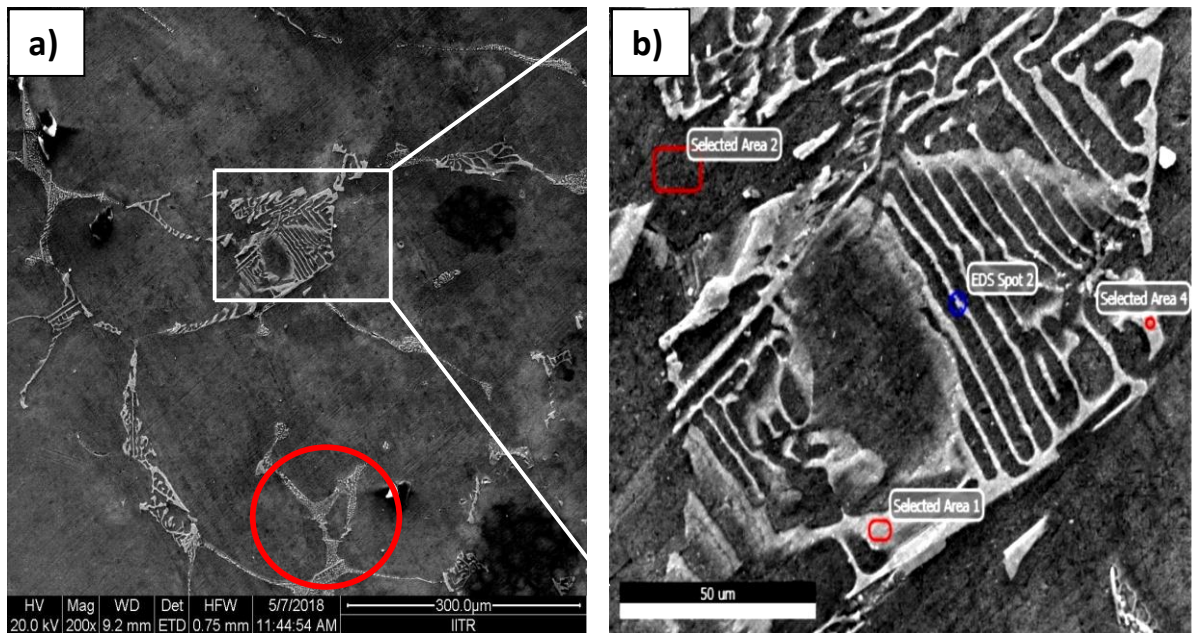
Fig. 4.4 FE-SEM microstructure of (a) Stir cast composite sample reinforced with 0.3 wt% micro Y, (b) Higher magnification of selected area in (a).

From Fig. 4.4 (a), it can be clearly observed that two distinct types of phases are present in the matrix. They constitute an intermetallic Al-Y-Cu phase resembling chinese script, out lined in a white rectangle, and an Al-Cu phase encircled in red. Fig. 4.4 (b) shows the intermetallic chinese script at a higher magnification showing the selected ponts for EDX elemental graph analysis.

Further, EDX analysis was carried out to quantify various elements present in the respective phases in the matrix, which are shown in Fig. 4.5. Table 3.2 shows the approximate weight percentage of different elements at various selected points in the said composite sample. The maximum temperature reached during stir casting is 800⁰ C and the melting point of yttrium is 1526⁰ C. Therefore, the loss of yttrium during melting might be as little as negligible. Fig. 4.5 (a), (b), (c) and (d) show the elemental graphs of the selected points shown in Fig. 4.4 (b). The elemental graphs show the intensity of the elements present in the selected points of interest in the microstructure.
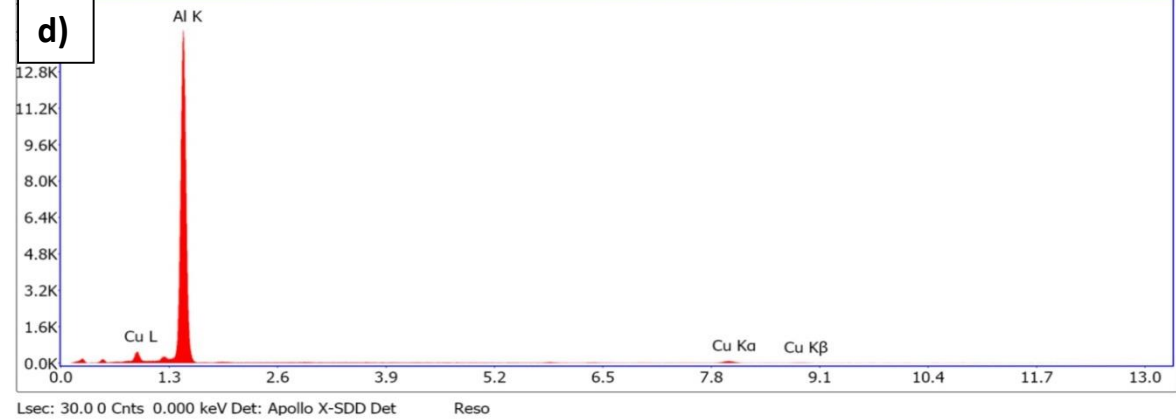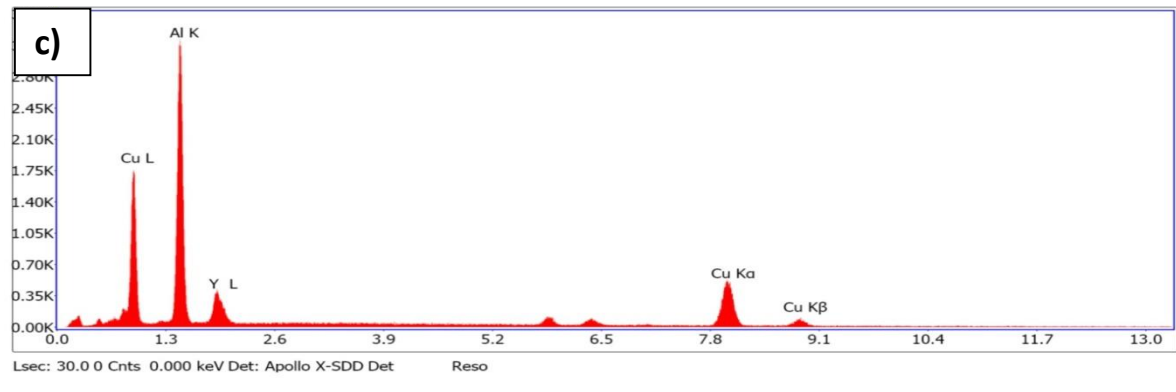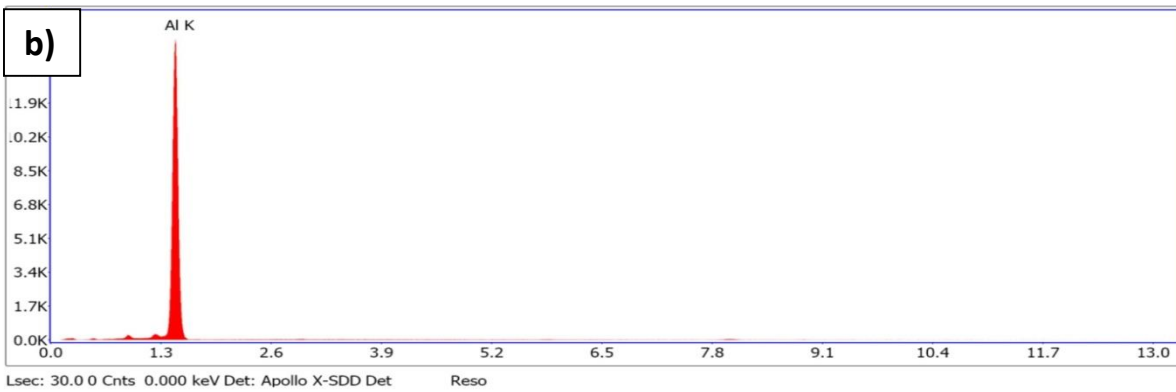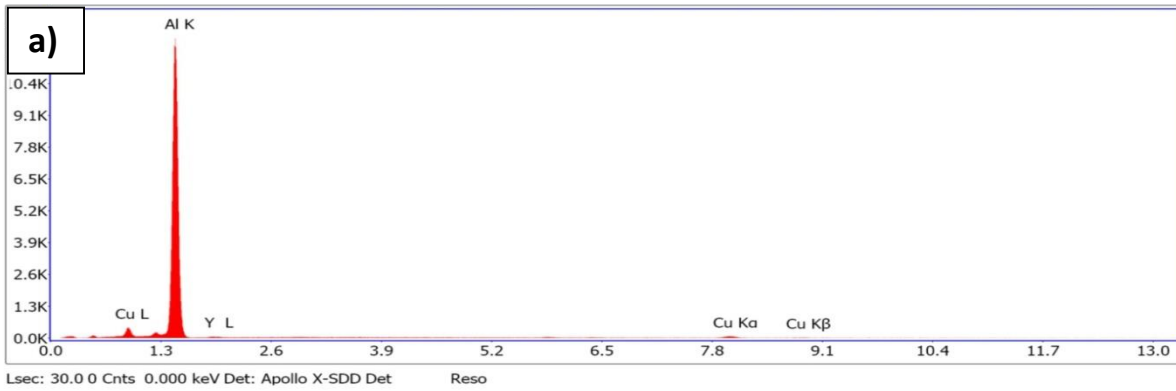
Fig. 4.5 EDX elemental graph of the 0.3 wt% micro Y reinforced composite sample shown in
Fig. 4.4 (b) (a) Selected area 1, (b) Selected area 2, (c) Spot 2 and (d) Selected area 4.

Table 4.2 Approximate composition of the elements in the composite sample with 0.3 wt% yttrium, calculated by EDX.

Elements	Selected area 1	Selected area 2	Spot 2	Selected area 4
Al	91.17	99.5	42.22	92.99
Y	0	0	12.4	1.2
Cu	8.83	0.5	45.38	5.82

Small pieces of all the composite samples were artifically aged at 190⁰ C for 1 to 10 hours with a time interval of 1 hour. Before the artificial ageing treatment, the sample pieces were solutionized at 500⁰ C and water quenched to room temperature. The FE-SEM microstructures of the composite samples artificially aged for 5 hours at 190⁰ C are shown in Fig. 4.6.
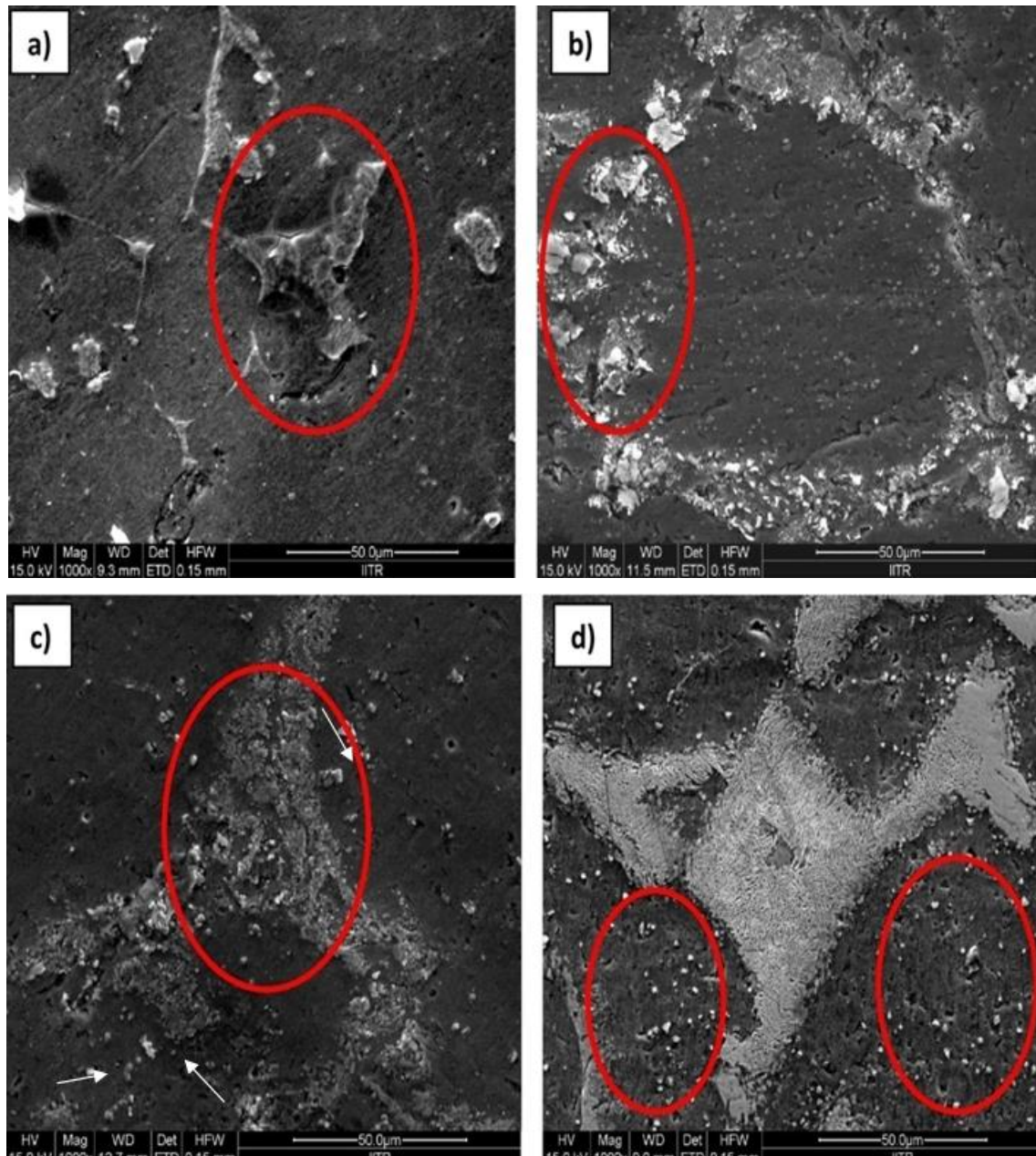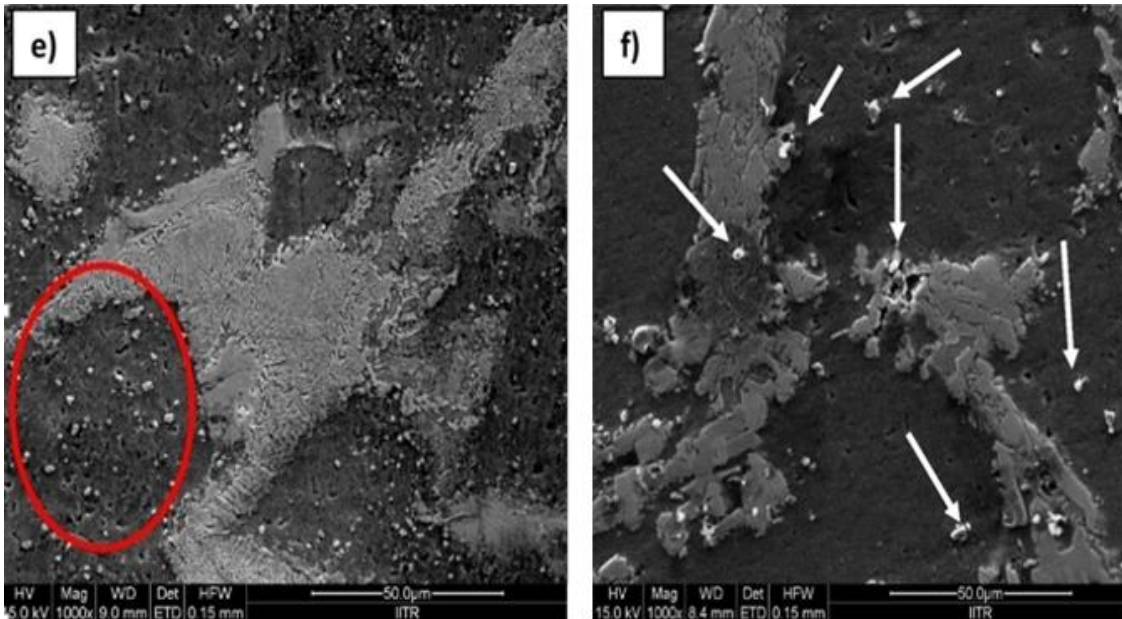
Fig. 4.6 FE-SEM back scattered microstructures of the stir cast composite samples artificially aged at 190° C for 5 hours (showing secondary phases) reinforced with a) 0.0 wt% micro Y, b) 0.1 wt% micro Y, c) 0.2 wt% micro Y, d) 0.3 wt% micro Y, e) 0.4 wt% micro Y and f) 0.5 wt% micro Y.

From Fig. 4.6, two different kinds of phases can be observed, which are indicated with circles and arrows in the microstructures. Due to heat treatment, evidence of precipitation is seen in the microstructures of the composite samples. The fibrous phase is an Al-Cu-Y intermetallic compound and the small white spots are Al_2Cu precipitates occured due to heat treatment. As the reinforcement of yttrium wt% increases, the fibrous intermetallic phase consisting of Al, Cu, Y and Al_2Cu precipitation also increase in the α-Al matrix. Beyond 0.3 wt% yttrium reinforcement, both the fibrous intermetallic phase and Al_2Cu precipitation coarsen.

4.1.2.3 Evaluation of mechanical properties

The mechanical properties like hardness, UTS, YS and elongation of the stir cast composites were evaluated, as described in sections 3.6.1 and 3.6.2. All the composite samples were mirror polished and tested for hardness by a computerized Vicker's hardness testing machine with a diamond point intender. The hardness variation of the composite samples with the reinforcement of yttrium is shown in Fig. 4.7. From Fig. 4.7, it can be observed that the hardness of the composite samples increased upto 0.3 wt% yttrium reinforcement and decreased thereafter. A clear trend of increase and decrease can be seen with yttrium reinforcement, compared to unreinforced AA2024.
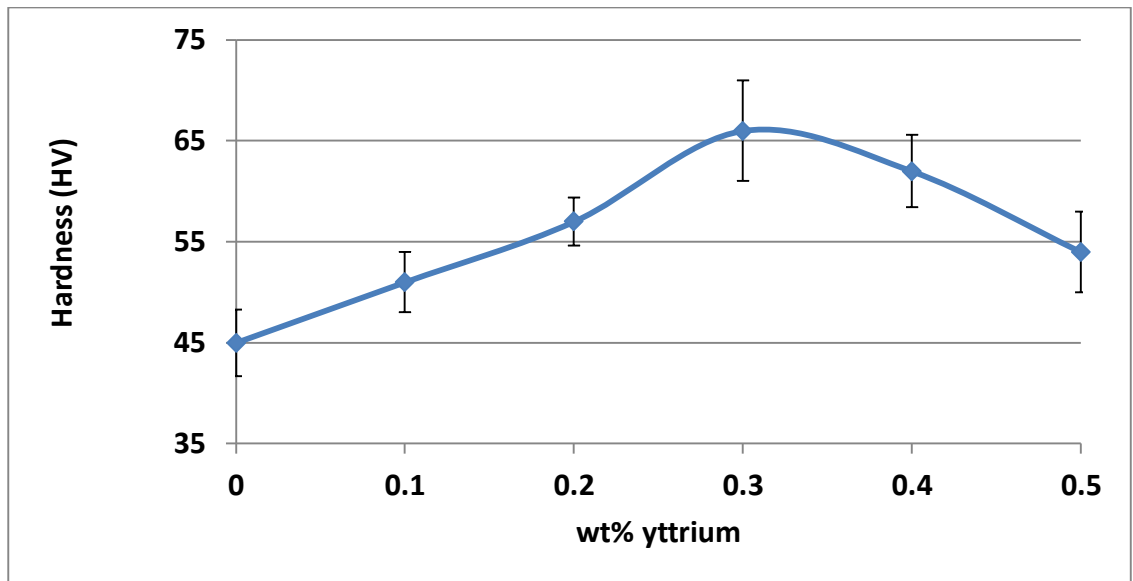
Fig. 4.7 Variation of hardness of the stir cast composite samples reinforced with varying amounts of micro yttrium.

The hardness of the composite samples artificially aged at 190⁰ C for various time periods is shown in Fig. 4.7. The samples were taken out of the furnace at each time interval, water quenched and polished to determine the hardness.
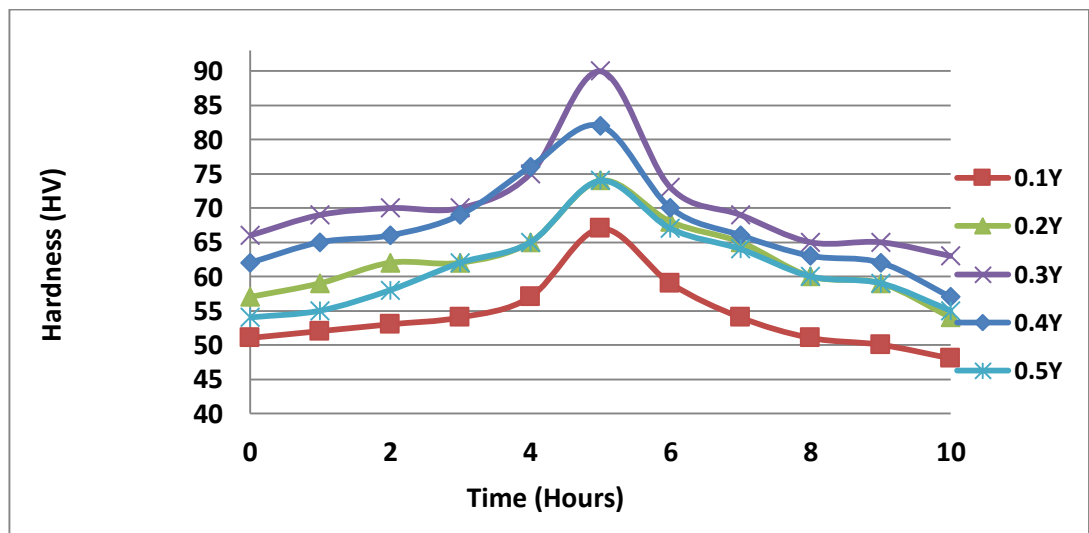
Fig. 4.8 Variation of hardness variation of the stir cast composite samples artificially aged at 190⁰ C with respect to time and variation in micro yttrium wt% reinforcement.

All the composite samples reached peak hardness within 5 hours of heat treatment at 190⁰ C irrespective of the yttrium reinforcement, as observed in Fig. 4.8. After 5 hours of heat

treatment, the samples got over-aged and before 5 hours, they were under-aged. However, the composite sample with 0.3 wt% yttrium reinforcement shows highest hardness compared to the other composite samples at the peak ageing time of 5 hours.

Three tensile specimens were cut from each composite sample including the as-received unreinforced AA2024 stir cast samples for tensile testing and the average values of the UTS and YS are plotted with error bars denoting the highest and lowest values. Fig. 4.9 shows the variation of UTS and YS of the stir cast composite samples with yttrium reinforcement. The tensile test was conducted on an UTM according to the procedure discussed in section 3.6.1. From Fig. 4.9, it can be observed that the UTS and YS of the composite samples follow the same trend as that of the hardness. There is a clear trend of increase in UTS and YS of the samples reinforced with yttrium compared to the as-received AA2024 sample. The UTS and YS increase upto 0.3 wt% yttrium reinforcement and tend to decrease upon further increase in yttrium reinforcement.
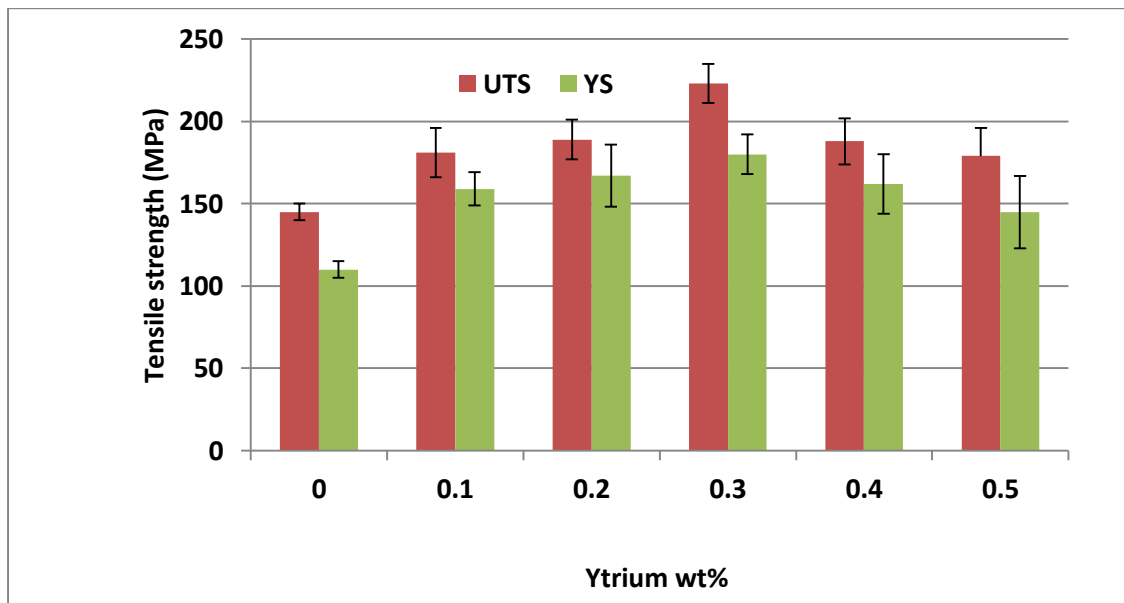
Fig. 4.9. Variation of UTS and YS of the stir cast composite samples reinforced with varying amounts of micro yttrium.

Fig. 4.10 shows the variation of elongation percentage of the composite samples reinforced with varying amounts of yttrium. From Fig. 4.10, an initial drop in elongation percentage can be observed compared to the as-received AA2024 sample. Yttrium reinforcement decreases the ductility of the samples. However, the elongation increased upto 0.3 wt% yttrium reinforcement and then tended to decrease. The elongation of the composite sample with 0.3

wt% yttrium reinforcement is observed to be higher than that of the unreinforced as-received AA2024 sample.
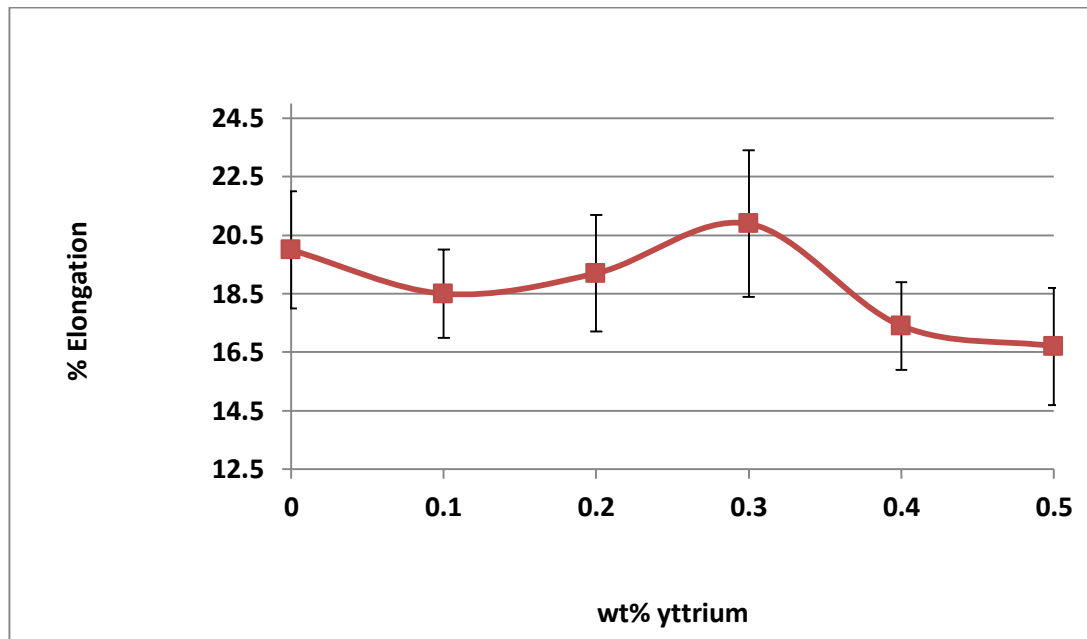
Fig. 4.10 Variation of elongation % of the stir cast composite samples reinforced with varying amounts of micro yttrium.

4.1.3 Discussion

Reinforcement of yttrium caused a steep drop in the density of the composite samples. The drop in the relative density can be explained by the action of stirring during the stir casting process. During the process, as the stirring was increased when yttrium was introduced into the melt, micro air bubbles were formed as a result of stirring. Since no de-gassing was done in the present work, it was difficult for the air bubbles to escape naturally from the liquid melt either during stirring or solidification. Reinforcement of yttrium hinders the release of air bubbles into the atmosphere. Hence, there was a decrease in the relative density of the composite samples as the yttrium reinforcement increased. However, the trend of decrease in relative density of the comosite samples beyond 0.3 wt% yttrium reinforcement is not understood clearly from this study, which needs to be further investigated.

Through other studies, it is observed that the modification of microstructure by grain refinement was achieved by reinforcing very little amount of rare earth elements that could effectively improve the overall mechanical properties of various aluminium alloys [164-169]. Reinforcement of rare earth metal (yttrium) in very small amounts to the molten AA2024 sample brought significant changes in the microstructure by changing the morphology of the matrix metal from dentric to spherical grains, as observed from Fig. 4.2. Yttrium reinforcement

is acompanied by grain modification and an increased tendency to form a non-dentric grain structure. The effect of yttrium reinforcement is manifested in the form of grain size modification, which affects the mechanical properties of the composite samples via Hall-Petch relation.

A closer look at the microstructures at higher magnification, as shown in Fig. 4.4, revealed a secondary phase, which resembeled a chinese script. From the EDX spectrum shown in Fig. 4.f (c) and the approximate elemental proportion shown in Table 4.2, the chinese script can be expected to be an Al-Cu-Y intermetallic [169]. As the yttrium wt% increases, this Al-Cu-Y intermetallic chinese script gets finer and also increases in amount up to 0.3 wt%. Upon further increase in yttrium wt%, the chinese script coarsens. Another secondary phase is also observed in the microstructure having composition rich in Al and Cu. The EDX spectrum of the phase is shown in Fig. 4.4 (a) and its approximate elemental proportion as detected by EDX is shown in Table 4.2. The secondary phases provide strength to the composite by obstructing the dislocation movement. Finer intermetallic and secondary phase present in the matrix could effectively resist the dislocation movement and hence modify the mechanical properties of the composite. Mechanical properties of the composite samples like hardness, UTS, YS and elongation depend on the size and amount of the secondary phases present in the matrix of the composite and their ability to resist slipping and dislocation movement. The mechanical properties of the stir cast composite samples increase with an increase in the reinforcement of yttrium wt%. However, as the yttrium wt% increases beyond 0.3, the secondary phases become coarser and their effectiveness in resisting the dislocation decreases. Instead of offering dispersion strengthening to the composite, the coarse secondary phase, intermetallic phase and precipitation start to behave like grains and hence the mechanical properties deteriorate. This phenomenon could be due to the fact that the matrix alloy contains a variety of alloying elements like Cu, Mg, Mn, Fe, etc,.

Liu et al., [167] reported that when the amount of rare earth reinforcement exceed certain value, the rare earth element will get segregated at the front of the solidification interface, as shown in Fig. 4.3 (d) and (e) (encircled in red colour) and prevent the diffusion of other alloying elements into the solid phase. This causes the solid solubility of alloying elements in α-Al matrix to decrease and hence increases the number of eutectic phases, causes segregation and reunion, hinder the refinement effect and make the entire organization begin to deteriorate.

2xxx series aluminium alloys are a class of heat treatable or age hardenable alloys. AA2024 is very responsive to heat treatment. The widely used heat treatments to this alloy are T-3 (solution artificially aged (SHT), cold worked and naturally aged), T-4 (SHT and naturally aged) and T-6 (SHT and artificially aged). Natural ageing requires a lot of time to get substantially stable condition and it follows an exponential trend. Hence, T-6 stands out to be a good alternative to T-3 and T-4 processes. The stir cast composite samples were artificially aged from 1 to 10 hours at 190°C. From Fig. 4.8, we can observe that the peak hardness was achieved in the samples artificially aged for 5 hours irrespective of the wt% of yttrium addition. Yttrium reinforcement has accelerated the ageing kinetics [168] and brought down the peak age hardening time to 5 hours, compared to standard 10 hours treatment. The phenemenon of acceleration of age hardening kinetics can be attributed to the increase in dislocation density due to thermal mis-match between the matrix and the reinforcing material. During quenching from solutionizing temperature, high density of dislocations along with excess vacancies are formed at the interface, which accelerate the kinetics of difussion process and cause the nucleation of precipitates [169]. Precipitates with approximate composition of Al_2CuMg were observed in the microstructures of peak hardened composite samples [168]. The precipitates become finer and increase in number as the yttrium wt% is increased and offer Orowan strengthening or precipitation strengthening to the composite samples. Beyond 0.3 wt% yttrium reinforcement, the precipitates coarsen, as shown in Fig. 4.6 and the strengthening decreases, leading to a drop in hardness. Before 5 hours of heat treatment, the composite samples were in under-aged condition and after 5 hours, they were in over-age condition.

4.1.4 Conclusions

The following conclusions are made from the results obtained from the afore said experimental work.

- Five composite samples with varying amounts of yttrium reinforcement were sucessfully developed using stir casting method.

- Addition of yttrium decreased the relative density of the composite samples.

- The microstructure analysis revealed that the reinforcement of yttrium to α-Al matrix refined the grains upto 0.3 wt% by changing the morphology of secondary dentric arm spacing (SDAS) and reducing the grain size. Beyond 0.3 wt% yttrium reinforcement, the grain refinement is not significant.

- Through EDX analysis, two types of secondary phases rich in Al-Cu-Y and Al-Cu were identified in the matrix. The phase rich in AL-Cu-Y resembled a chinese script and became finer and increased in amount as the yttrium reinforcement increased to 0.3 wt%. Upon further increase in yttrium reinforcement, the script as well as the Al-Cu phase coarsen.

- The main strengthening mehanisms in the composite samples were solid solution strengthening by Al-Cu phase, grain refinement and dispersion strengthening by Al-Cu-Y phase.

- Peak hardness of the artificially aged composite samples was achieved within 5 hours. Yttrium reinforcement reduced the heat treatment time to 5 hours compared to standard 10 hours at 190°C. Al_2Cu precipitation occured due to heat treatment and the shape and size of the precipitation occured at 5 hours heat treatment, depending on the variation of yttrium reinforcement. The precipitation provided dispersion strengthening to the composite samples.

- A highest hardness of 66 HV was achieved for the composite sample with 0.3 wt% yttrium reinforcement and without any heat treatment. Simillarly, a highest hardness of 90 HV was achieved for the same composite sample with heat treatment for 5 hours. The hardness achieved for the same composite sample with and with out heat treatment were 146% and 200% respectively compared to that of the as-received unreinforced and non-artificially aged AA2024 sample.

- Highest UTS and YS achieved were 223 MPa and 180 MPa for the composite sample with 0.3 wt% yttrium reinforcement. The highest UTS and YS achieved were 153% and 131% higher respectively compared to that of the as-received AA2024.

- Reinforcement of yttrium initially decreased the elongation but it increased with further increase in yttrium reinforcement upto 0.3 wt%. The highest elongation achieved was 20.9%, which is 104% higher compared to that of the as-received AA2024 sample. However, the elongation decreased beyond 0.3 wt% yttrium reinforcement.

- From the results, it can be concluded that the optimum amount of yttrium reinforcement to AA2024 matrix is 0.3 wt%, which can create suitable conditions for the strengthening mechanisms to achieve highest mechanical properties.

4.2 Development of AA2024 + micro yttrium composites using cold copaction

In this section, second batch of composites comprising of five different composite samples were developed by reinforcing varying amounts of micro yttrium ranging from 0.1-0.5 wt% to the AA2024 matrix. An unreinforced sample was also developed as a bench mark to evaluate the effect of yttrium reinforcement. The composite samples were processed through cold compaction. The details of the materials, instruments and experimentation procedures have been already furnished in the chapter 3. The results corresponding to density, metallurgical characterization, mechanical evaluation are presented in detail. Various results are discussed in the light of improvement in mechanical properties of the composites developed. At the end, the conclusions drawn from the present work are presented.

4.2.1 Experimental work

In this work, the materials chosen were the powders of 2024 aluminium alloy and micro yttrium, shown in Fig. 3.1 and 3.2. The chemical composition of the as-received aluminium 2024 alloy powder is shown in Table 4.3. This AA2024 powder (99% purity) was procured from Alfa Aesar, United States, which was fabricated through atomization. The average particle size was 60 microns.

Table 4.3 Chemical composition of the as-received Al 2024 alloy powder.

Element	Si	Cu	Fe	Zn	Mg	Ti	V	Mn	Al
Wt%	0.16	4.67	0.47	0.14	1.71	0.05	0.001	0.8	Balance

Yttrium particles of average size 400 microns were used as the reinforcement. This yttrium powder (99.6% purity) was also procured from Alfa Aesar, United States. Five AA2024+Y composite samples with varying amounts of yttrium addition, as shown Table 3.2 were developed through cold compaction. The as received AA2024 sample was also sintered to compare with the composite samples and to evaluate the effect of yttrium reinforcement. The composite samples were cold compacted and sintered as per the procedure discussed in the section 3.2.2.

The blended powder samples were subjected to thermal analysis using DTA. Before the measurements were recorded, the system was introduced with argon gas. The powder samples

were kept in alumina sample holders with a heating rate of 10°C/minute and were heated up to 700° C. Fig. 4.11 shows the DTA results with respect to temperature.
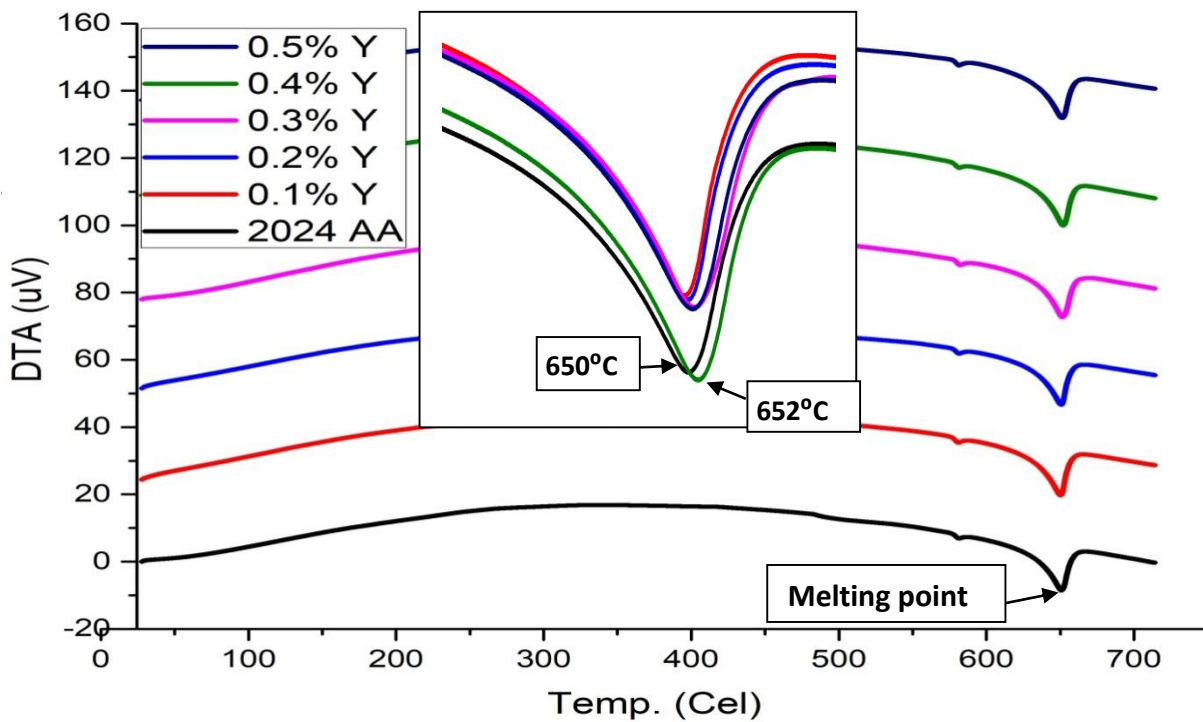
Fig. 4.11 DTA of blended powder samples.

From Fig. 4.11, it can be seen that all the powder blend samples follow the same endothermic trend. The DTA results show an endothermic peak at 650° C, which corresponds to the melting point of pure AA2024 powder and an endothermic peak at 652° C, which corresponds to the melting point of AA2024 blended with 0.4 wt% yttrium. Another samall endothermic peak can be observed at 575° C which could be an indication of a meta-stable phase or an unstable phase. The difference between the melting points of pure and yttrium blended AA2024 is only 2° C, which can be ignored since ± 5° C tolerence is generally allowed for melting points. Although the melting point of yttrium is higher than that of aluminium, its proportion (in wt%) is very less, so it did not have any effect on the melting point.

4.2.2 Results

4.2.2.1 Investigation of microstructure

The specimens for investigating microstructure were prepared according to the procedure discussed in section 3.4.1. Fig. 4.12 shows the optical microstructure of the composite samples with varying wt% of yttrium. The microstructure shows clear grain boundaries and good

packing of grains. The pores and void spaces increased as yttrium wt% increase while a clear trend of grain size reduction is observed. With 0.3 wt% yttrium, pores became smaller but with further increase in yttrium wt%, pores and grains grew larger. The pores are indicated in Fig.4.12 by pointed arrows. Un-dissolved secondary phase also increased beyond 0.3 wt% yttrium reinforcement.
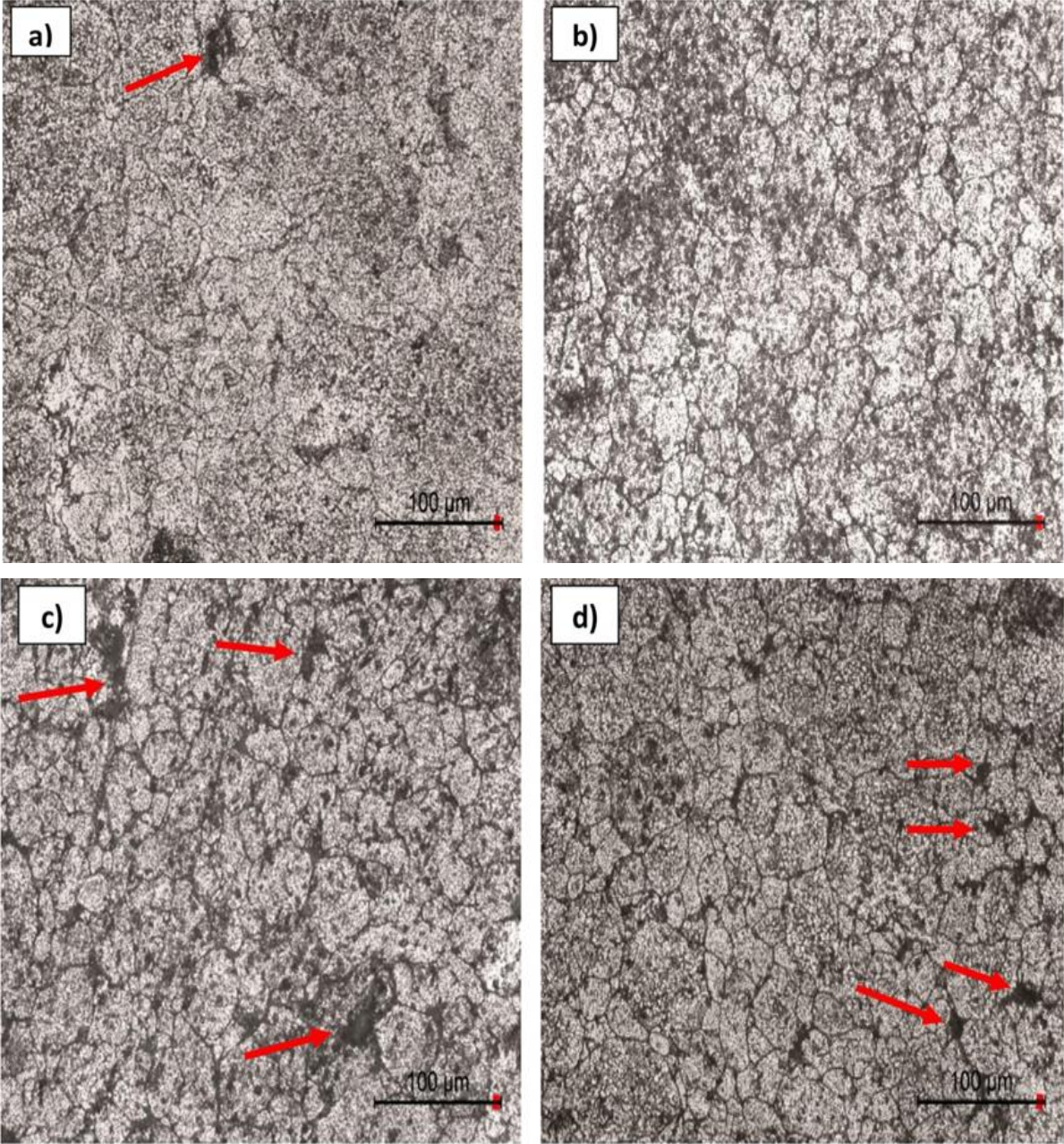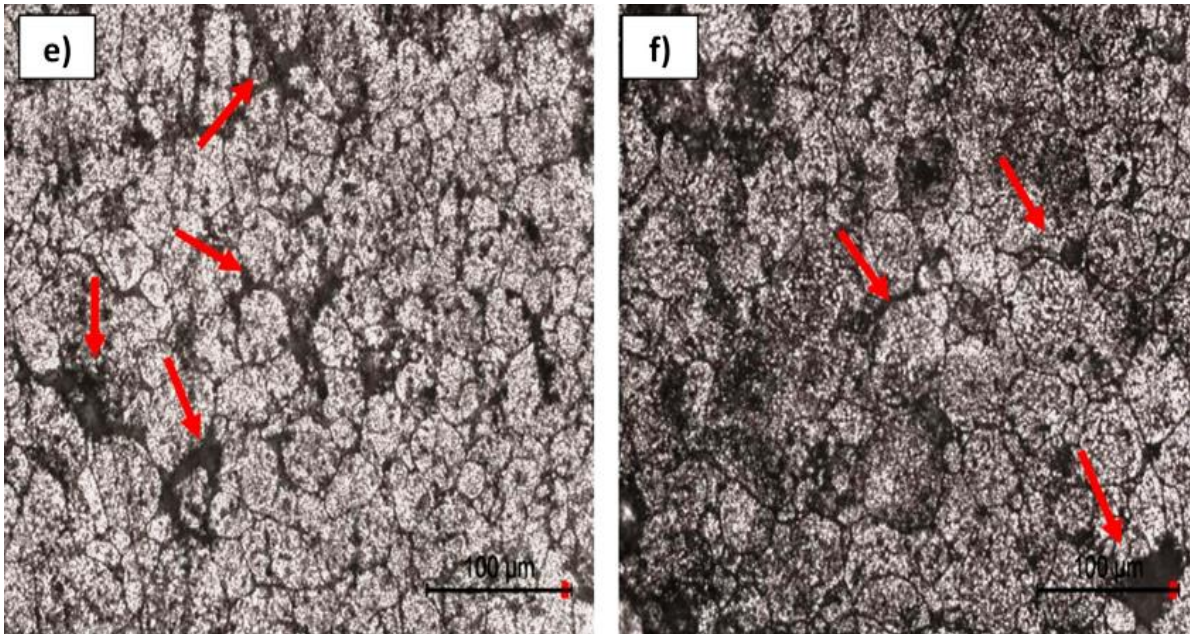
Fig. 4.12 Optical microstructures of unreinforced/cold compacted composite samples reinforced with (a) 0.0 wt% micro Y, (b) 0.1 wt% micro Y, (c) 0.2 wt% micro Y, (d) 0.3 wt% micro Y, (e) 0.4 wt% micro Y and (f) 0.5 wt% micro Y.

4.2.2.2 Density measurement

The properties of the composite samples mainly depend on the density and percentage of porosity. The green density, densification parameter and relative densities wee calculated for each unreinforced/composite sample reinforced with the yttrium, using standard methods and formulae, as discussed in section 3.3.

Relative green density is the ratio of green density of the compact (calculated after compaction) to experimental density. Fig. 4.13 shows the relative green densities of the unreinforced AA2024 compact and also those of compacts with varying wt% of yttrium before sintering. From Fig. 4.13 it can be seen that the green density decreases with an increase in the reinforcement of yttrium.
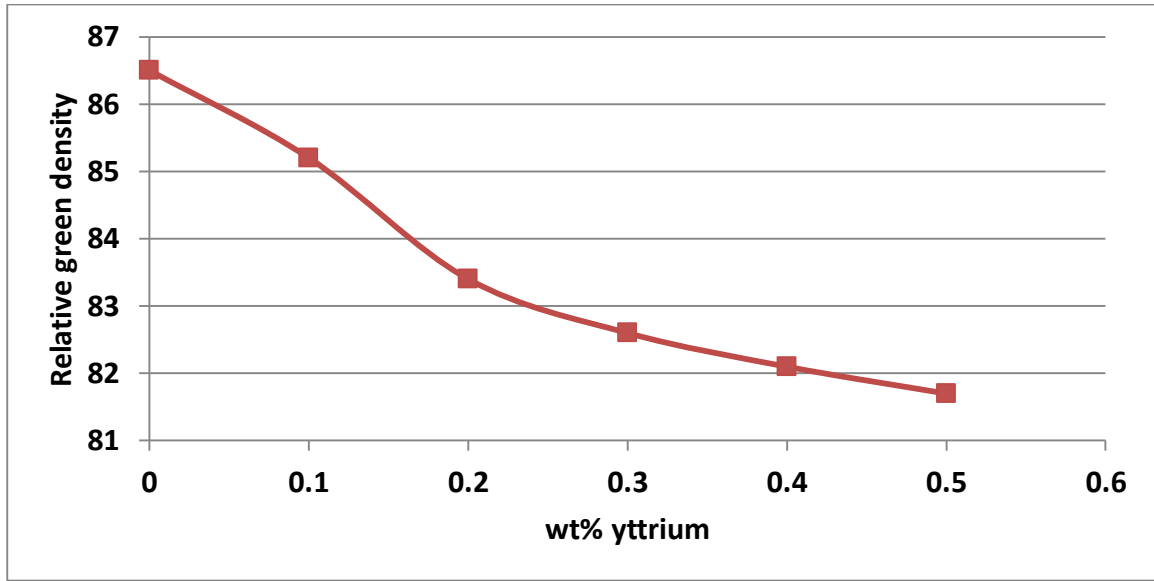
Fig. 4.13 Variation of green density of the cold compactsunreinforced/ reinforced with varying amounts of micro yttrium.

After the cold compaction, the green compacts were sintered to promote diffusion between the powder particles. Fig. 4.14 shows the variation of relative sintered densitiy of the composite samples with an increase in the reinforcement of micro yttrium. From Fig. 4.14, it can be observed that sintering density decreases with an increase in yttrium addition. However, the sintered density is higher than the green density for each case of the reinforcement.
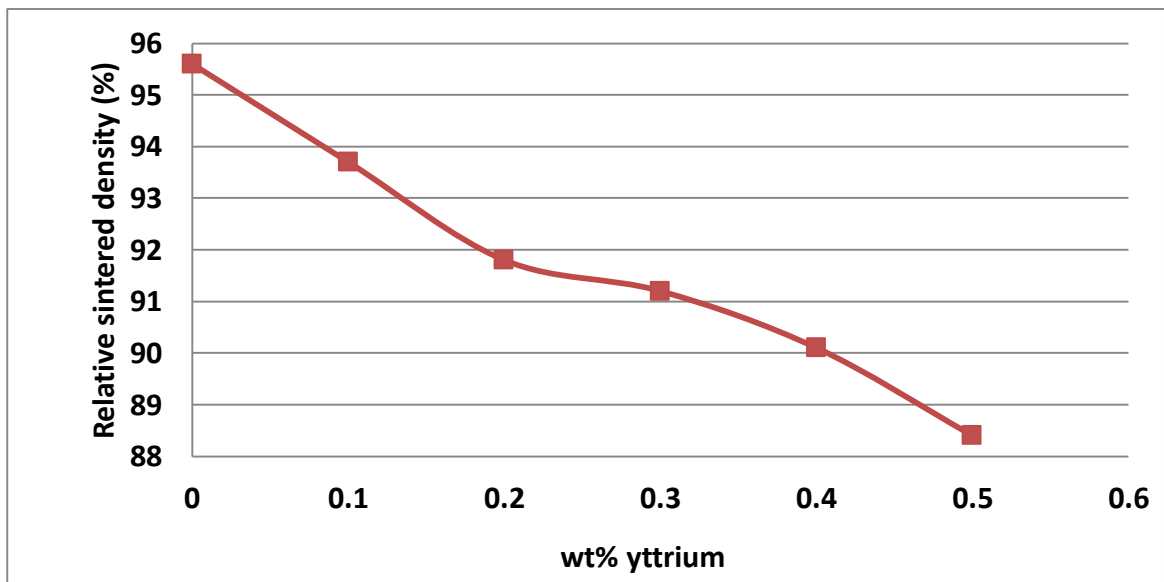
Fig. 4.14 Variation of relative sintered density of the cold compacted unreinforced/composite samples reinforced with varying amounts of micro yttrium.

Fig. 4.15 shows the variation of densification parameter with an increase in the reinforcement of yttrium. Densification parameter (Ψ) signifies the rate and intensity of densification achieved in the composite samples during sintering. In other words, densification parameter indicates how well the densification took place. It can be clearly seen from the graph that the densification parameter decreased with an increase in yttrium reinforcement. Though, the variation was less, it can be said that yttrium did not favour the densification process.
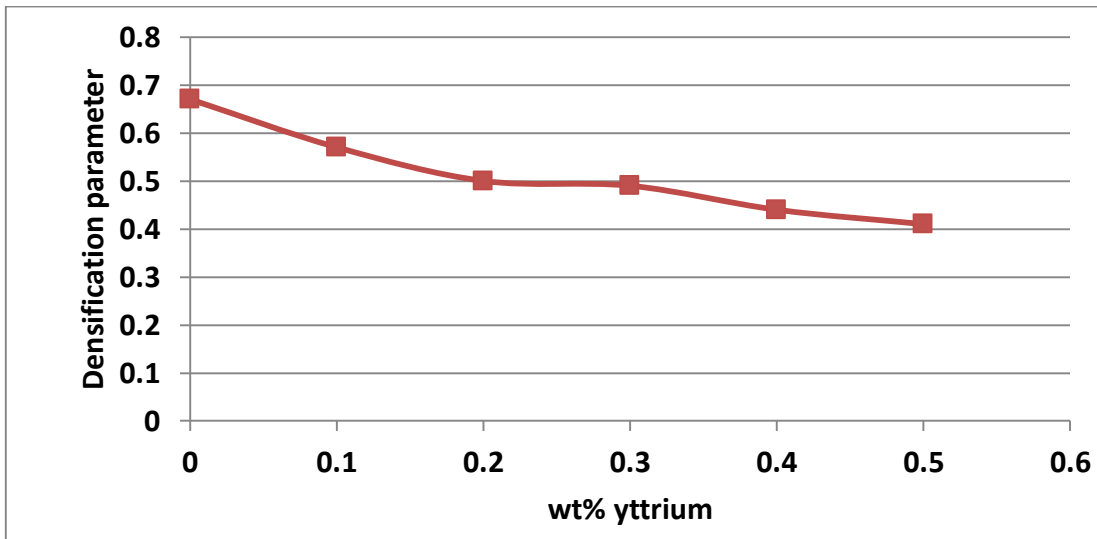
Fig. 4.15 Variation of densification parameter of the cold compacted unreinforced/composite samples reinforced with varying amounts of micro yttrium.

4.2.2.3 Evaluation of mechanical properties

The mechanical properties of the composite samples like hardness, UTS, YS and elongation were tested by the procedures discussed in the section 3.5. Ten measurements were taken for each sample in the case of hardness and three measurements in the case of tensile strength and the average values of the readings are furnished with error bars, showing highest and lowest values.

Fig. 4.16 shows the variation of hardness with an increase in the reinforcement of yttrium wt%. From Fig. 4.16, it can be seen that the hardness increased with the reinforcement of yttrium upto 0.3 wt% and decreased with further reinforcement. There is a clear trend of increase and decrease in the hardness for the composite samples with the reinforcement of yttrium.
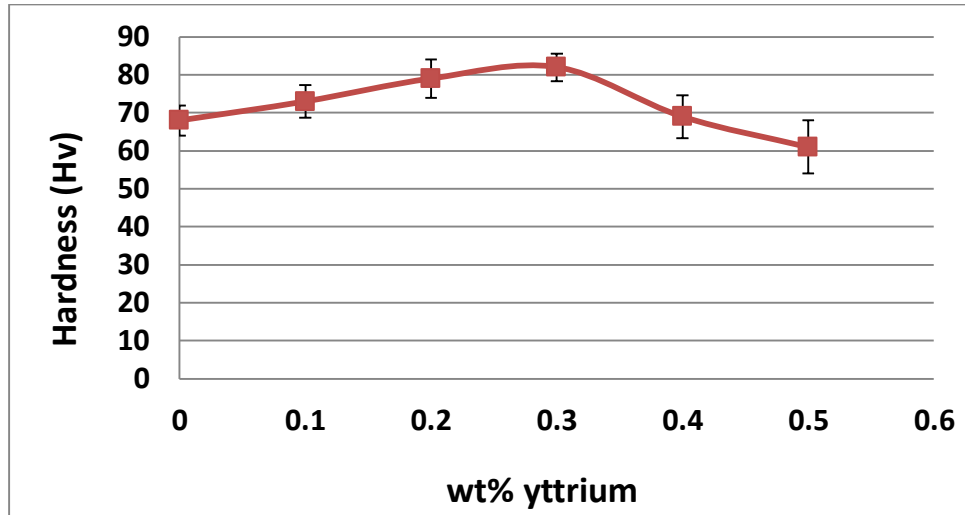
Fig. 4.16 Variation of hardness in the cold compacted unreinforced/composite samples reinforced with varying amounts of micro yttrium.

Fig. 4.17 shows the variation of UTS and YS in the sintered composite samples with an increase in the reinforcement of yttrium. The UTS and YS also followed the same trend of variation as the hardness. Obviously, UTS and YS increase upto 0.3 wt% yttrium reinforcement and decreased with further reinforcement. However, the average difference between UTS and YS decreased when the yttrium reinforcement increased beyond 0.3 wt%.
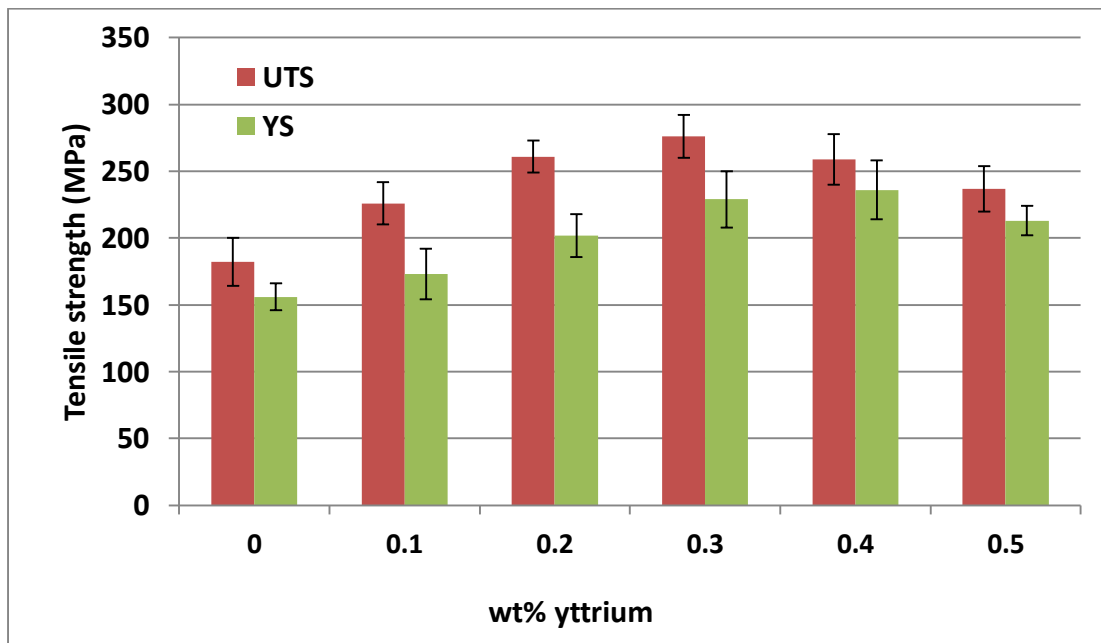
Fig. 4.17 Variation of UTS and YS of the cold compacted unreinforced/composite samples reinforced with varying amounts of micro yttrium.

Fig. 4.18 shows the variation of elongation at fracture with the reinforcement of yttrium. Elongation at fracture is a measure of the composite's ductility. Poor sintering causes the samples to fail at much lower loads with less elongation. The elongation of the composite samples in the present case also followed the same trend as the other mechanical properties.
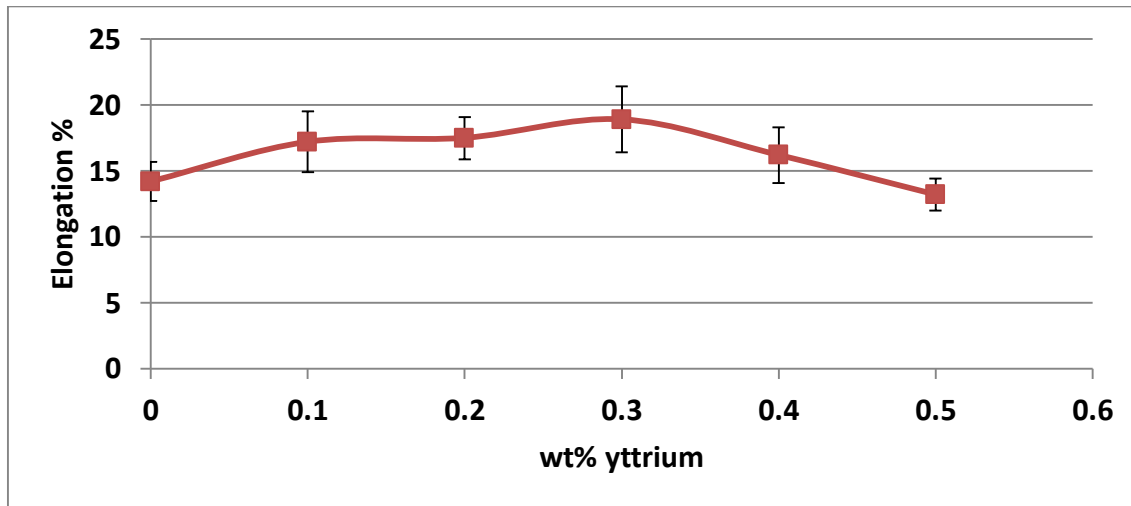
Fig. 4.18 Variation of elongation in the cold compacted unreinforced/composite samples reinforced with varying amounts of yttrium.

4.2.3 Discussion

The reinforcement of yttrium decreased the relative green density. The morphology of AA2024 powder particles could be the reason for such low green densities. As the void spaces increased, the density decreased. The increase in void spaces may be due to the irregular and random alignment of matrix powder paricles. In reinforcement to that, aluminium powder got oxidized forming an oxide layer when exposed to atmosphere. Each aluminium alloy powder particle was covered with an oxide layer leading to an increase in the deviation from theoritical density. Although the reinforcement of yttrium is very less, its reinforcement might have decreased the green density as its powder particles were larger than the matrix powder particles, moving the matrix particles much apart while accommodating themselves, creating more void spaces and thus decreasing the relative green density.

The relative densities of the green compacts were increased after sintering. However, the composites did not attain full theoretical density. It can also be observed that the reinforcement of yttrium had a negative influence on the relative density of the composites even after sintering. Many factors can be held responsible for the failure of composite samples to attain full theoretical density. Firstly, the oxide layer that forms on each aluminium powder particle

98

due to atomospheric exposure hinders the particle-particle contact and decreases the diffusion and densification during sintering. During compaction, the applied pressure breaks the oxide layers on the particle surfaces, favoring good particle-particle contact. Secondly, as the temperature increases, necking starts at particle-particle contact points and grows with an increase in the temperature, leading to the densification of the composite sample. The decrease in relative density of the sintered composites can be explained by the inability of the applied pressure to completely break the oxide layers. Thirdly, the morphology of the aluminium alloy powder paricles and their random orientation, which create void spaces at tripple and quadruple points. The reinforcement of yttrium might have further hindered the necking and diffusion, decreasing the densification of the composite samples. So, the relative density of the sintered composite samples decreased gradually with an increase in yttrium wt%. In order to accommodate themselves among the matrix particles, yttrium could have pushed them apart causing large voids and decrease in particle-particle contact. As the yttrium wt% increased, the particle-particle contact points and neck growth decreased, causing a drop in densification parameter.

The variation in the trend of hardness can be explained by the dispersion strengthening caused by the yttrium particles. Reinforcement of yttrium caused a strain field in the matrix around it due to the huge difference in their co-efficient of thermal expansion. The strain fields caused an increase in dislocation density and the yttrium particles hindered the dislocation motion (dispersion strengthening) when a load is applied on the composite sample and hence increase the hardness. Solid solution hardening also plays a role as the solid solution containing dissolved copper creates a strain field around it because of the difference in their atomic sizes. Since copper atoms are smaller than aluminium atoms, a tensile strain field is caused in the lattice. The dislocations have a strain field at their core due to the distortion in lattice. The copper solute atoms with a tensile strain field will diffuse to the dislocation core to nullify a part of compressive strain field and hence reduces the strain field.

This hinders the dislocation motion and hence hardness is increased. However, the hardness falls beyond 0.3 wt% yttrium. This can be explained by the tendency of yttrium particles to agglomerate as its wt% increases. The agglomerated yttrium acts as a grain itself and its dispersion hardening effect decreases. However, the solid solution hardening remains same for all the samples.

Multiple mechanisms control the strength of a composite. While the strength achieved by grain size and solid solution strengthening are same for all the composite samples, the variation caused in the strength can be attributed to yttrium and cummulative effect of the strengthening mechanism. Yttrium particles offer dispersion strengthening by obstructing the movement of dislocations when a load is applied. Reinforcement of yttrium also causes an increase in dislocations density, which further increases the strength by causing hinderence to the motion of neighbouring dislocations. Apart from the strengthening mechanisms discussed, decrease in sintering parameters and relative density also played a part in the decrease in elongation of the composite samples. Hence, a specific amount of yttrium reinforcement (0.3 wt%) to AA2024 matrix could create optimum conditions in the composite sample and achieve superior mechanical properties.

4.2.4 Conclusions

Based on the aforesaid investigations and results, the following conclusions can be drawn.

- Five different composite samples reinforced with varying amounts of yttrium reinforcement along with unreinforced AA2024 sample were sucessfully developed through hydraulic cold compaction and subsequent conventional sintering.

- Reinforcement of yttrium decreased the relative green density, relative sintered density and densification parameter.

- Hardness, UTS, YS and elongation of the composite samples were improved upto 0.3 wt% yttrium reinforcement and then decreased with further yttrium addition. The hardness, UTS, YS and EL were found to be 68 HV, 182 MPa, 156 MPa and 14.2% respectively for the unreinforced AA2024 sample.

- The highest hardness, UTS, YS and Elongation were found to be 82 HV, 276 MPa, 229 MPa and 18.9% respectively for the composite sample with 0.3 wt% yttrium addition.

- It was observed that the reinforcement of 0.3 wt% yttrium to the AA2024 matrix creates favorable conditions for the strengthening mechanisms and to show its best effect on the composite sample, leading to superior mechanical properties.

4.3 Development of AA2024 + micro yttrium composite using spark plasma sintering

In this section, third batch of composites comprising of five different composite samples were developed by reinforcing varying amounts of micro yttrium ranging from 0.1-0.5 wt% to the AA2024 matrix. An unreinforced sample was also developed as a bench mark to evaluate the effect of yttrium reinforcement. The composite samples were processed through SPS. The results corresponding to density, metallurgical characterization, mechanical properties testing are presented in detail. Various results are discussed in the light of improvement in mechanical properties of the composites developed. At the end, the conclusions drawn from the present work are presented.

4.3.1 Development of the composites
4.3.1.1 Experimental work

In the present work, the matrix and the reinforcing materials selected were the powders of AA2024 and yttrium respectively. The details of the starting powders used in the present study have already been discussed in the section 4.2.1. The approximate elemental composition of the as-received AA2024 starting powder has already been shown in Table 3.1.

Five AA2024 matrix composite samples reinforced with different proportions of yttrium were developed along with an unreinforced AA2024 sample. The intended proportions of the composite samples are already shown in Table 3.2. A planetary ball milling machine was used for uniform mixing of both matrix and reinforcement powders. The planetary ball mill was operated at 50 RPM for 2 hours with a ball to powder ratio 1:1. Fig. 4.19 shows the blended powders with varying amounts of micro yttrium. From Fig. 4.19, we can observe that the powder particles were not deformed plastically but were mixed thoroughly during milling.
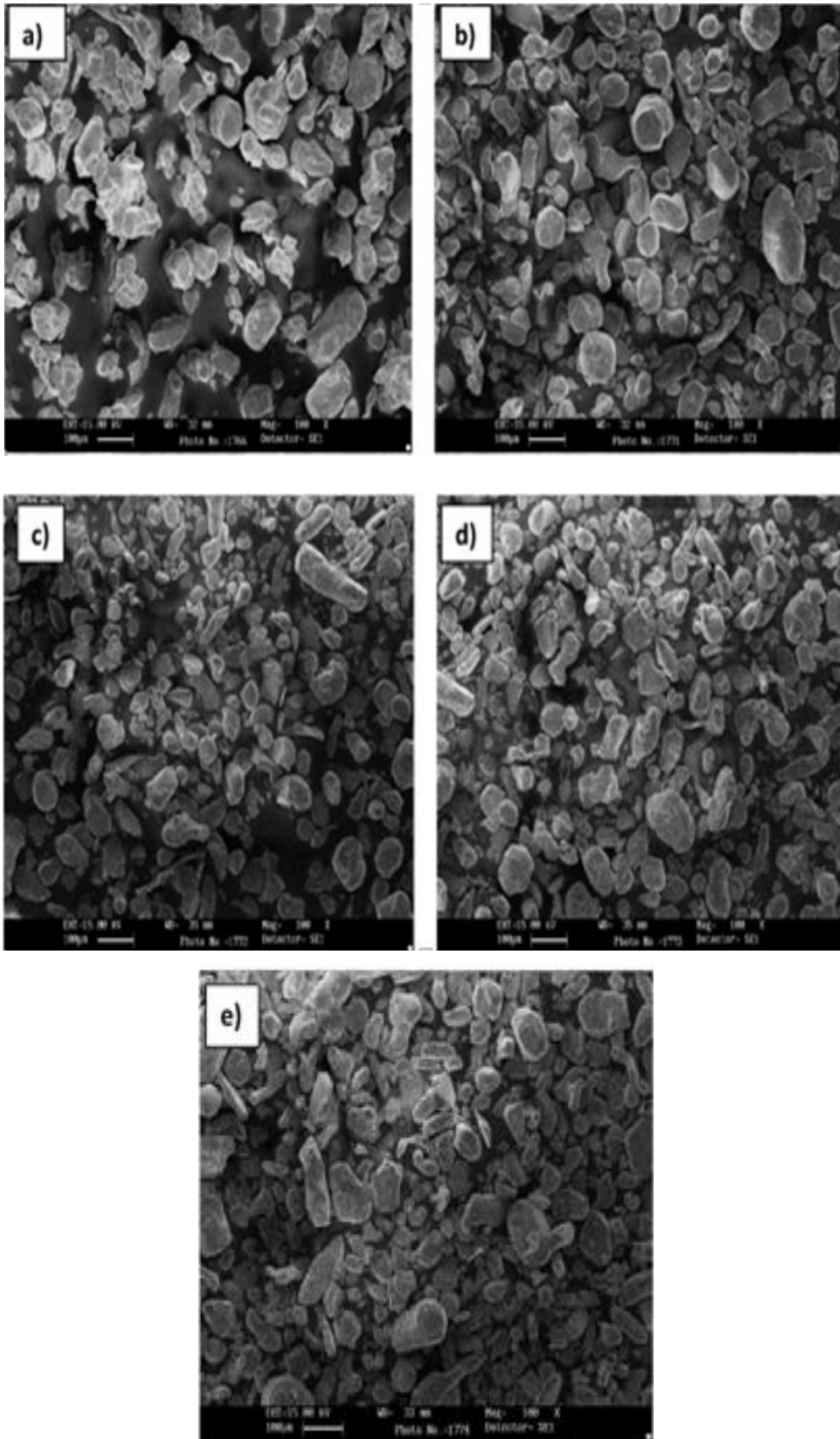
Fig. 4.19 SEM microstructures of the blended powders of AA2024 with (a) 0.1 wt% micro Y, (b) 0.2 wt% micro Y, (c) 0.3 wt% micro Y, (d) 0.4 wt% micro Y and (e) 0.5 wt% micro Y.

The blended composite powders were consolidated by SPS with the parameters shown in Table 3.3. The composite samples developed by spark plasma sintering are shown in Fig. 4.20, starting from pure AA2024 sample at the top left followed by AA2024 matrix composite reinforced with yttrium ranging from 0.1 to 0.5 wt%.

Fig. 4.20 SPSed composite samples reinforced with varying amounts of yttrium.

4.3.1.2 Results

4.3.1.2.1 Density measurement

The experimental and relative densities were calculated for each composite sample developed. The theoretical density was calculated by the rule of mixtures and the experimental density was calculated by standard Archimedes principle. The variation of relative density of the spark plasma sintered composite samples with respect to yttrium reinforcement is shown in Fig. 4.21. From Fig. 4.21, it can be observed that the densities of these samples reached very close to the theoretical density and then tended to saturate to full density after 0.2 wt% reinforcement of yttrium.
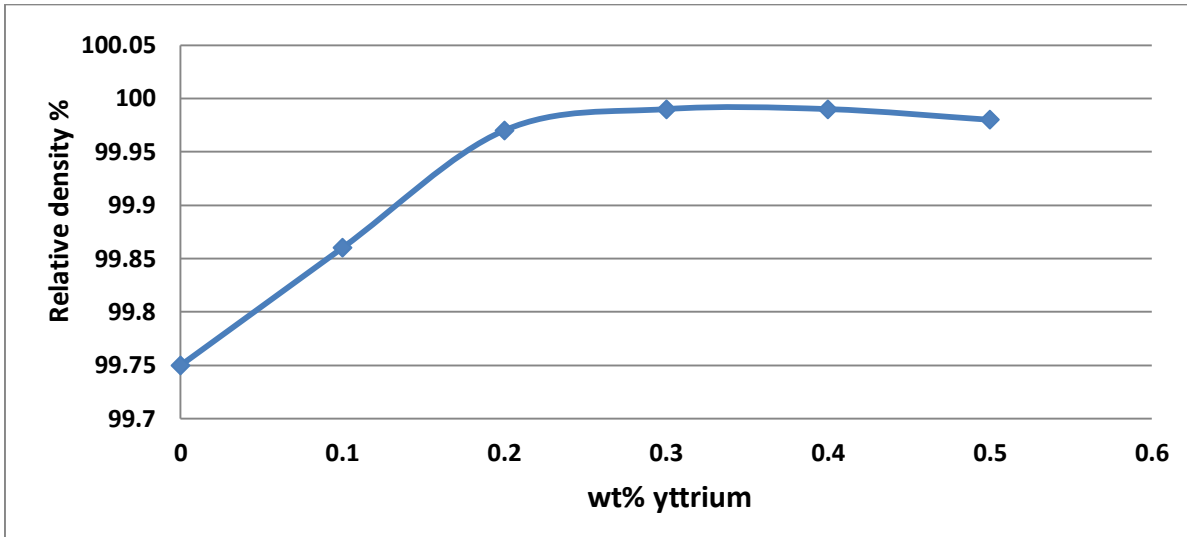
Fig. 4.21 Variation of relative density of the SPSed unreinforced/composite samples reinforced with varying amounts of micro yttrium.

4.3.1.2.2 Investigation of microstructure

The microstructures of the SPSed composite samples are shown in Fig. 4.22. The average grain sizes of the composite samples were measured using 'Image J' software and the corresponding linear intercepts were found to be 60, 52, 41, 37, 46 and 49 µm for the samples reinforced with 0.0, 0.2, 0.2, 0.3, 0.4 and 0.5 wt% micro yttrium respectively. The grain size was reduced with an increase in the reinforcement of yttrium, but after 0.3 wt% of yttrium reinforcement , the grains tend to grow. The distinction of the grain boundaries slowly dissappeared in the samples with 0.4 wt% and 0.5 wt% yttrium, which might be due to the intermetallic agglomeration at the grain boundaries.
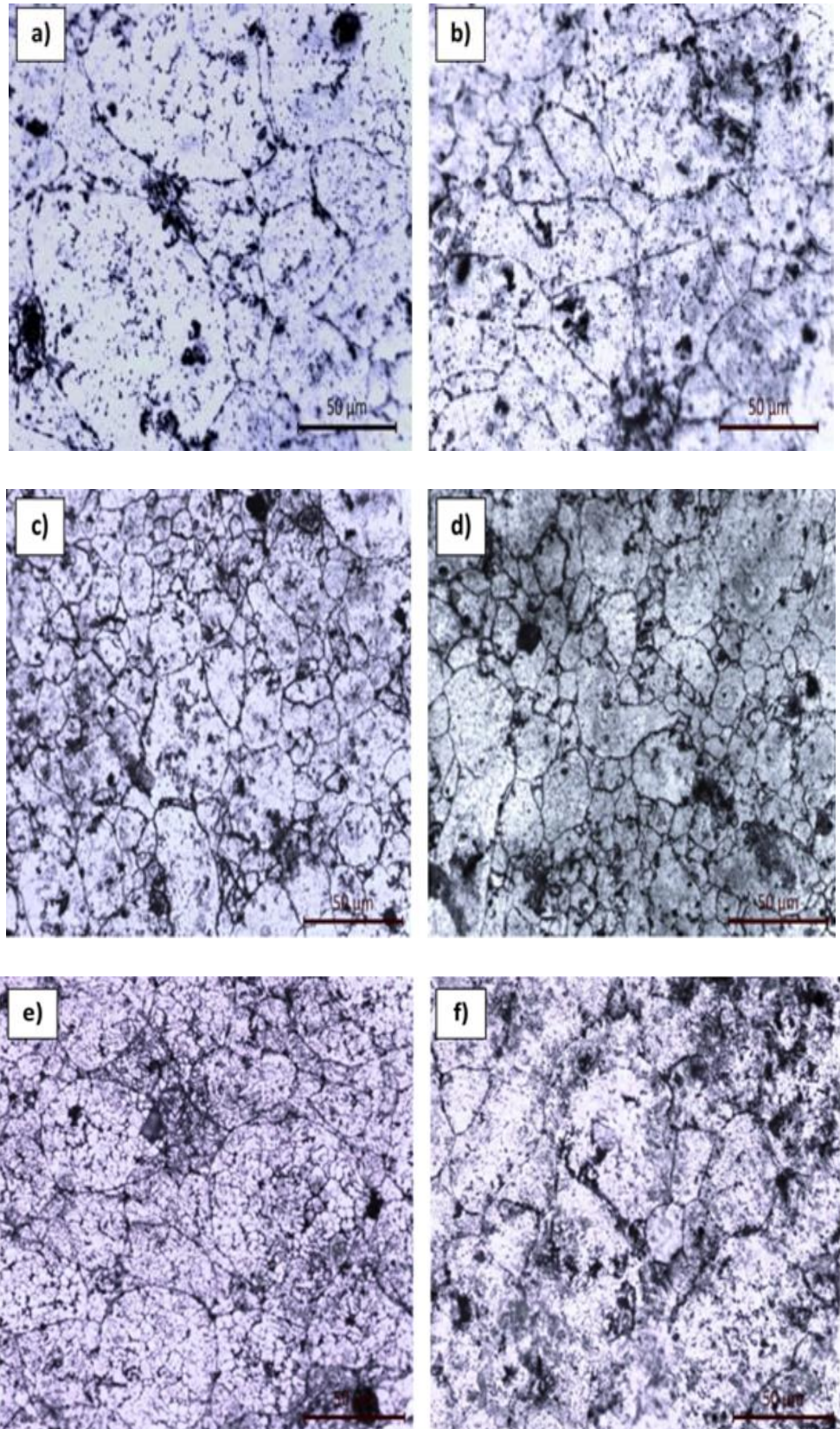
Fig. 4.22 Optical microstructures of the SPSed unreinforced/composite samples reinforced with (a) 0.0 wt% micro Y, (b) 0.1 wt% micro Y, (c) 0.2 wt% micro Y, (d) 0.3 wt% micro Y, (e) 0.4 wt% micro Y and (f) 0.5 wt% micro Y.

To clearly observe the secondary phase precipitates, the samples were observed under FE-SEM in the back scattered mode. The microstructures are shown in Fig. 4.23. From Fig. 4.23, it can be observed that the Al-Cu precipitates grow in number up to 0.3 wt% reinforcement of yttrium and tend to increase in size and agglomerate as the amount of yttrium further increases. The white spots are the precipitates and the grey colour indicates the matrix, while the black spots are the voids, as indicated by the arrows.
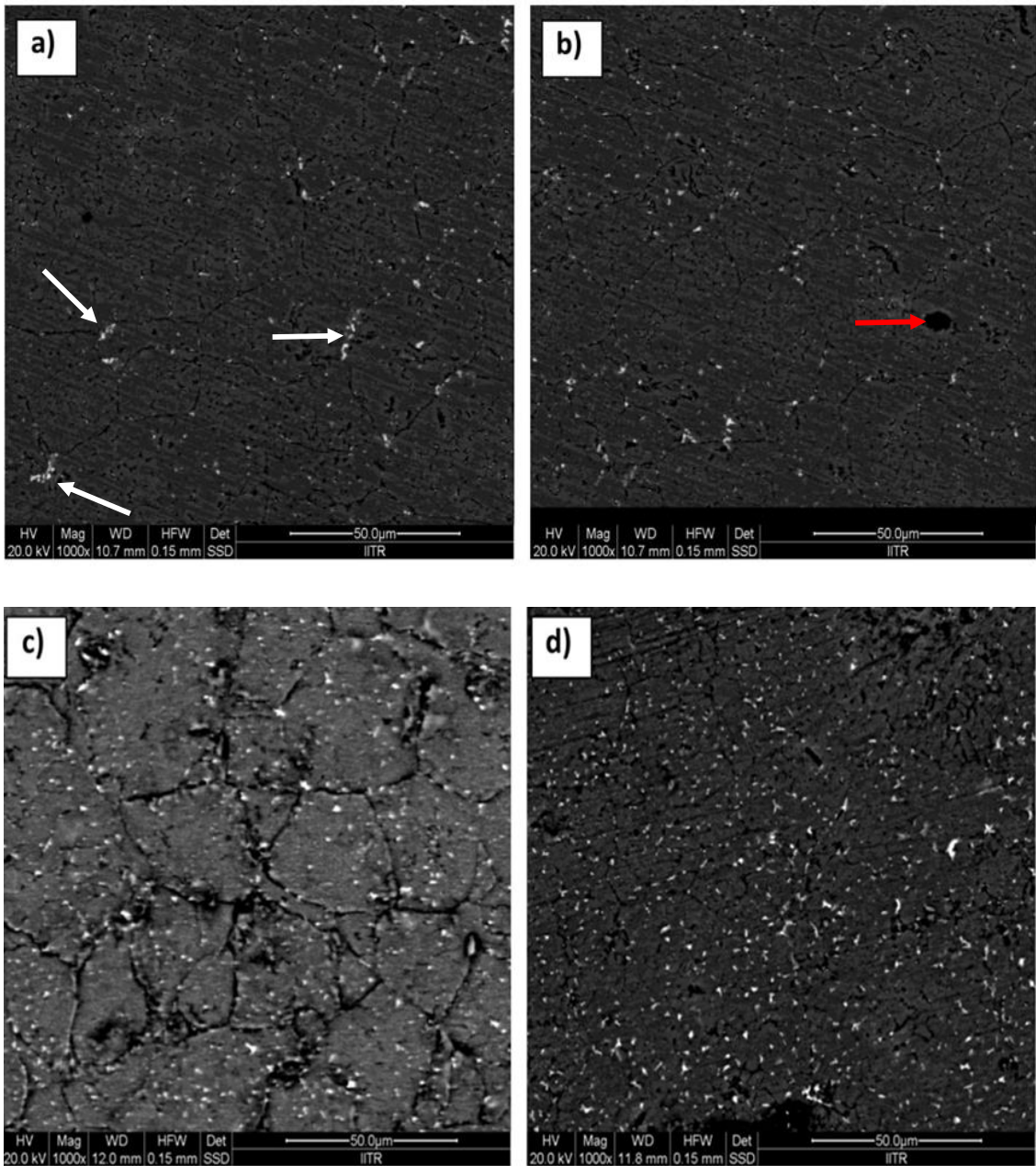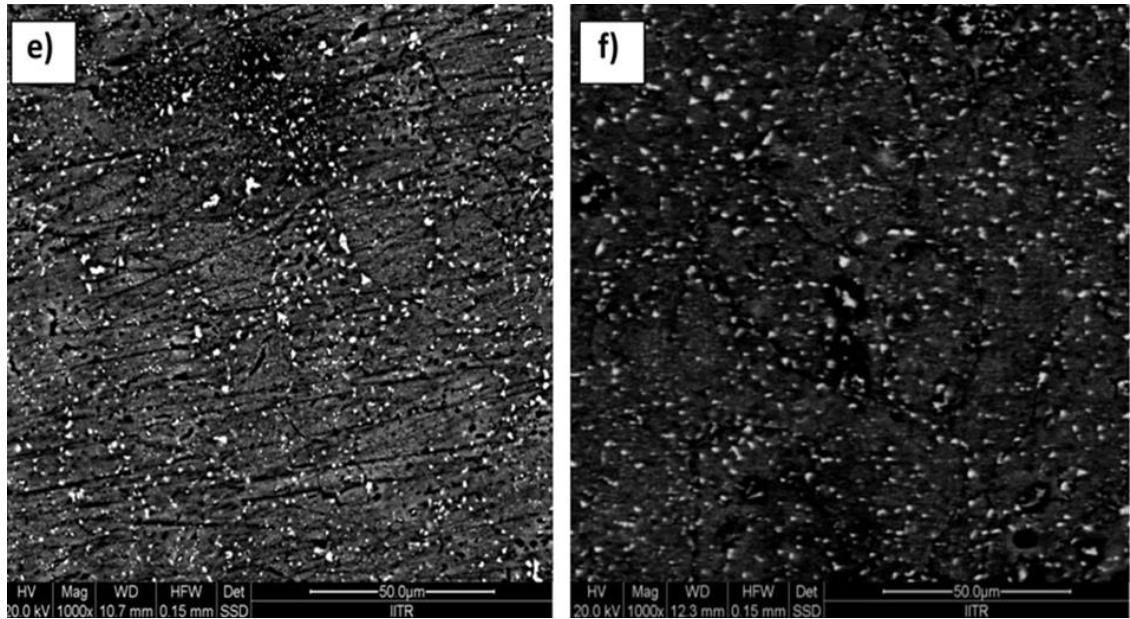
Fig. 4.23 FE-SEM microstructures showing precipitation of Al-Cu in AA2024 matrix composite samples reinforced with (a) 0.0 wt% micro Y, (b) 0.1 wt% micro Y, (c) 0.2 wt% micro Y, (d) 0.3 wt% micro Y, (e) 0.4 wt% micro Y and (f) 0.5 wt% micro Y.

Fig. 4.24 shows the FE-SEM microstructure of the composite sample reinforced with 0.3 wt% yttrium, and X-Ray mapping of different elements present in the same composite sample. It can be observed that the elements Al, Cu, Mg and Y were distributed uniformly. This uniform distribution of elements can be an evidence of improved mechanical properties of the composite samples. Yttrium was mainly distributed along the grain boundaries. The way the elements were distributed could be an indication that intermetallic Al-Cu-Mg and Al-Y phases were possible as the yttrium reinforcement increases.
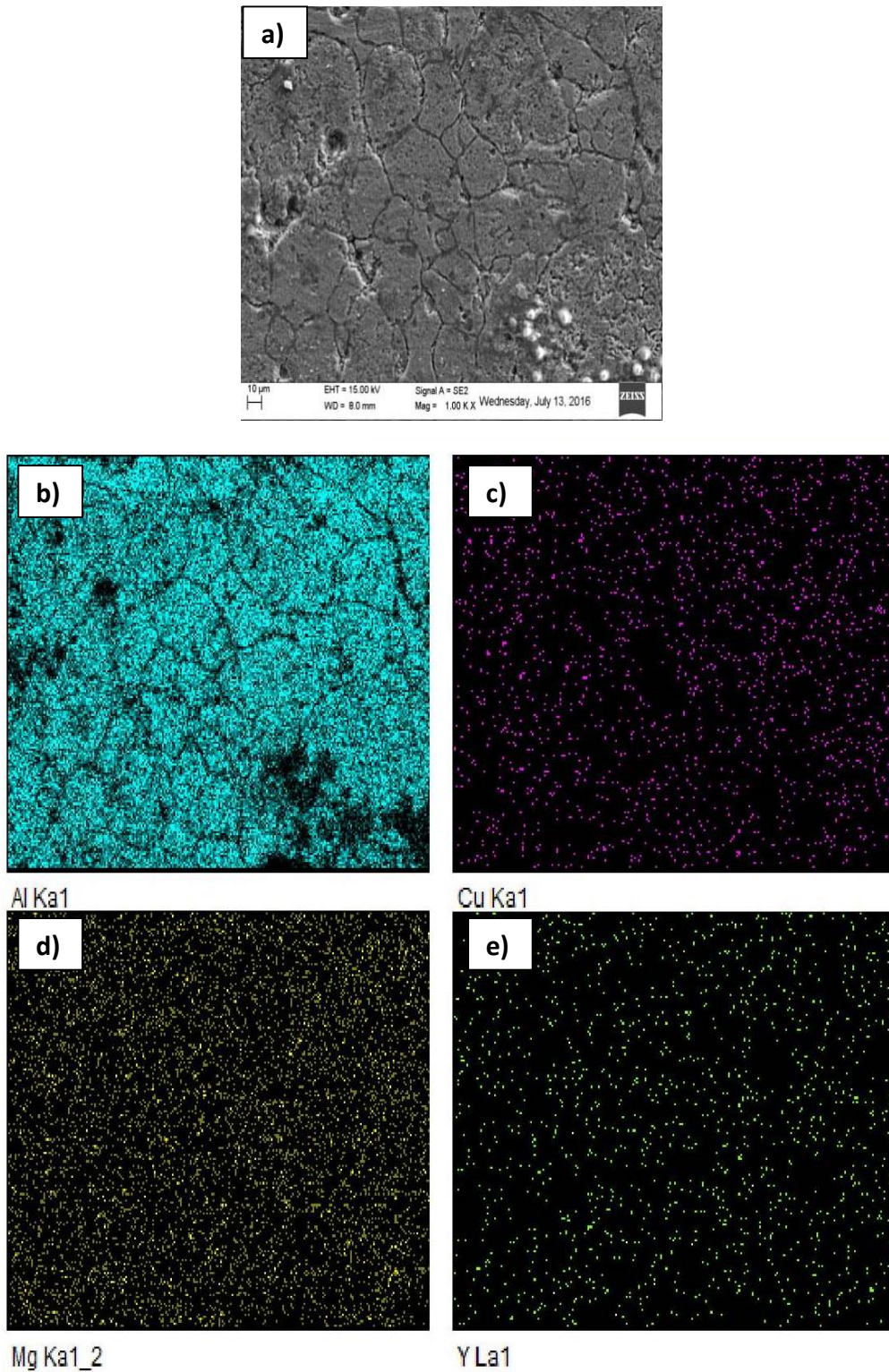
Fig. 4.24 X-ray elemental mapping of the composite sample with 0.3 wt% yttrium reinforcement using EDX (a) selected FE-SEM microstructure, (b) aluminium, (c) copper (d) magnesium and (e) yttrium.

Fig. 4.25 shows the intensity of various elements present in the microstructure shown in Fig. 4.24 (a).
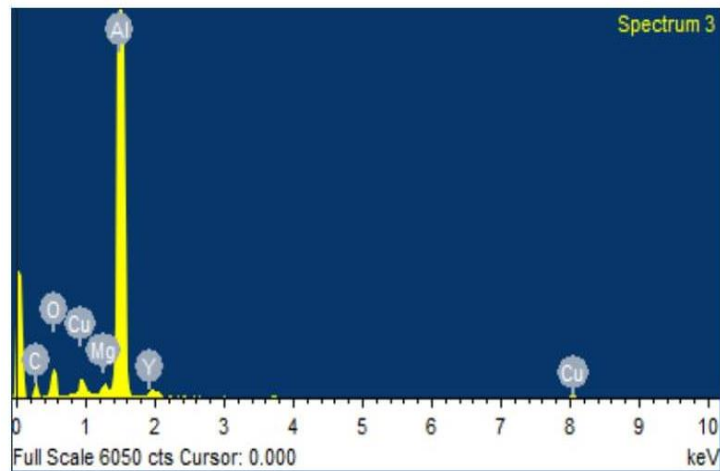
Fig. 4.25 EDX elemental graph of the microstructure shown in Fig. 4.24 (a).

The orientation and interaction of yttrium powder particles with AA2024 matrix is shown in Fig. 4.26. The interface of yttrium and AA2024 matrix contain certain amount of diffusion between them, which could lead to the formation of intermetallics, as shown in Fig. 4.27 by line EDX. The approximate percentages and intensities of various elements present at various spots in the microstructure shown in Fig. 4.26 are shown in Fig. 4.27 (a), (b), (c) and (d).
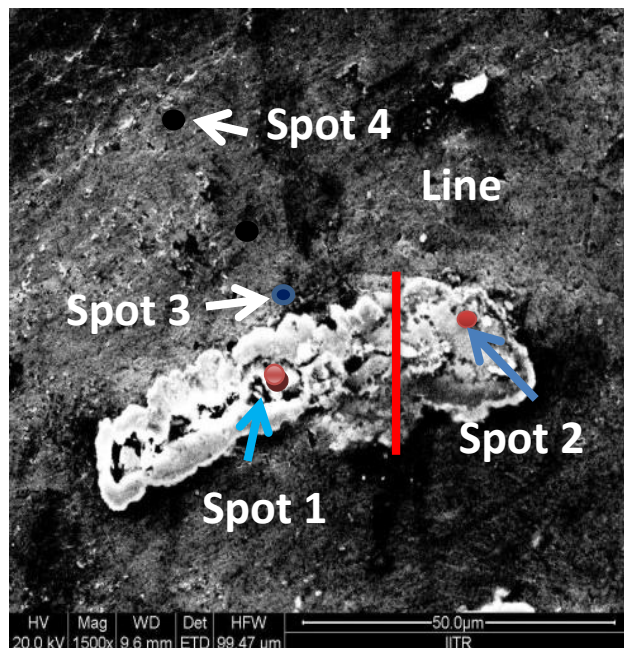
Fig. 4.26 FE-SEM microstructure of the spark plasma sintered composite sample showing the orientation and interaction of yttrium with the matrix.

Fig. 4.27 shows the intensities of Al, Cu and Y by EDX on the line drawn across the yttrium and matrix interaction as shown in Fig. 4. 26.
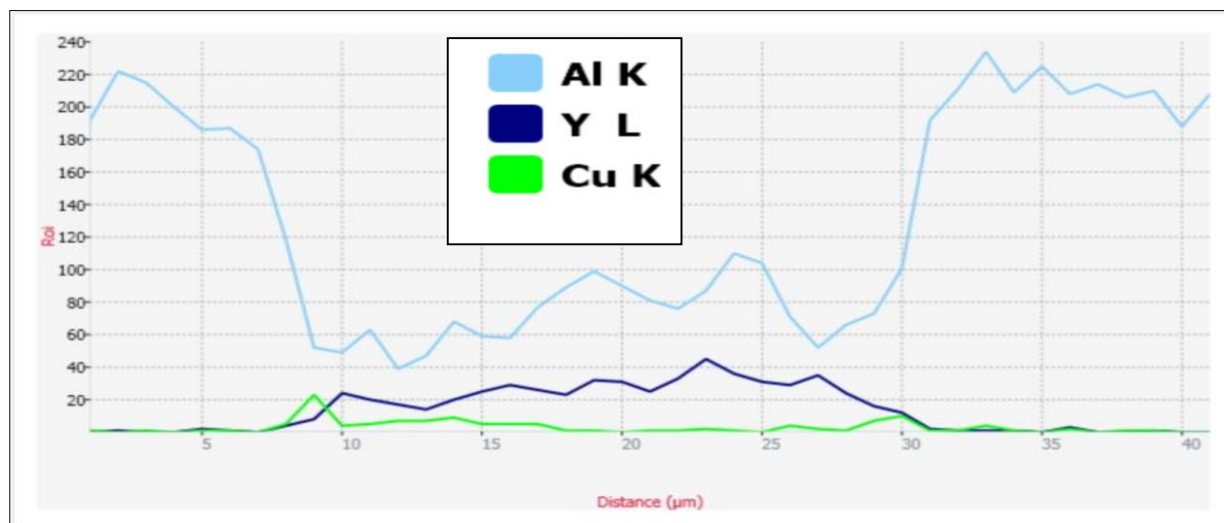
Fig. 4.27 EDX profile of the line drawn across the interaction of yttrium with the matrix as shown in Fig. 4.26.

Fig. 4.28 shows the EDX graphs showing the intensities of various elements present at particular points shown in Fig. 4. 26.

Element	Weight %	Atomic %	Net. Int	Error %
Al	3.94	11.91	13.2	2.3
Y	96.06	88.06	282.46	2.85

sec: 30.0 0 Cnts 0.000 keV Det: Octane Pro Det   Reso

110

b) Spot 2

Element	Weight %	Atomic %	Net. Int	Error %
Al	49.72	76.52	369	2.3
Y	50.28	23.48	113.11	2.12

Lsec: 30.0 0 Cnts 0.000 keV Det: Octane Pro Det   Reso

c) Spot 3

Element	Weight %	Atomic %	Net. Int	Error %
Al	95.3	97.18	1139.34	17.38
Y	1.12	1.27	13.85	2.46
Mg	3.58	1.55	6.27	30.57

Lsec: 30.0 0 Cnts 0.000 keV Det: Octane Pro Det   Reso

d) Spot 4

Element	Weight %	Atomic %	Net Int.	Error %
MgK	3.39	4.02	33.19	10.08
AlK	84.61	90.52	859.62	4.25
CuK	12	5.45	21.97	14.81

Lsec: 29.6 0 Cnts 0.000 keV Det: Octane Pro Det   Reso

Fig. 4.28 EDX elemental graphs and approximate percentages of elements present in (a) spot 1, (b) spot 2, (c) spot 3 and (d) spot 4 shown in Fig. 4.26.

111

The TEM nanostructures of the spark plasma sintered unreinforced/composite samples are shown in Fig. 4.29. From the nanostructures, the growth and distribution of Al-Cu precipitation can be observed. Two types of precipitates namely rod shape and disc shape along with nano precipitation were observed. The precipitates grew in number and were finely distributed up to 0.3 wt% yttrium addition. Beyond 0.3 wt% yttrium addition, the precipitates agglomerated and coarsened. Dislocation colonies were also observed.
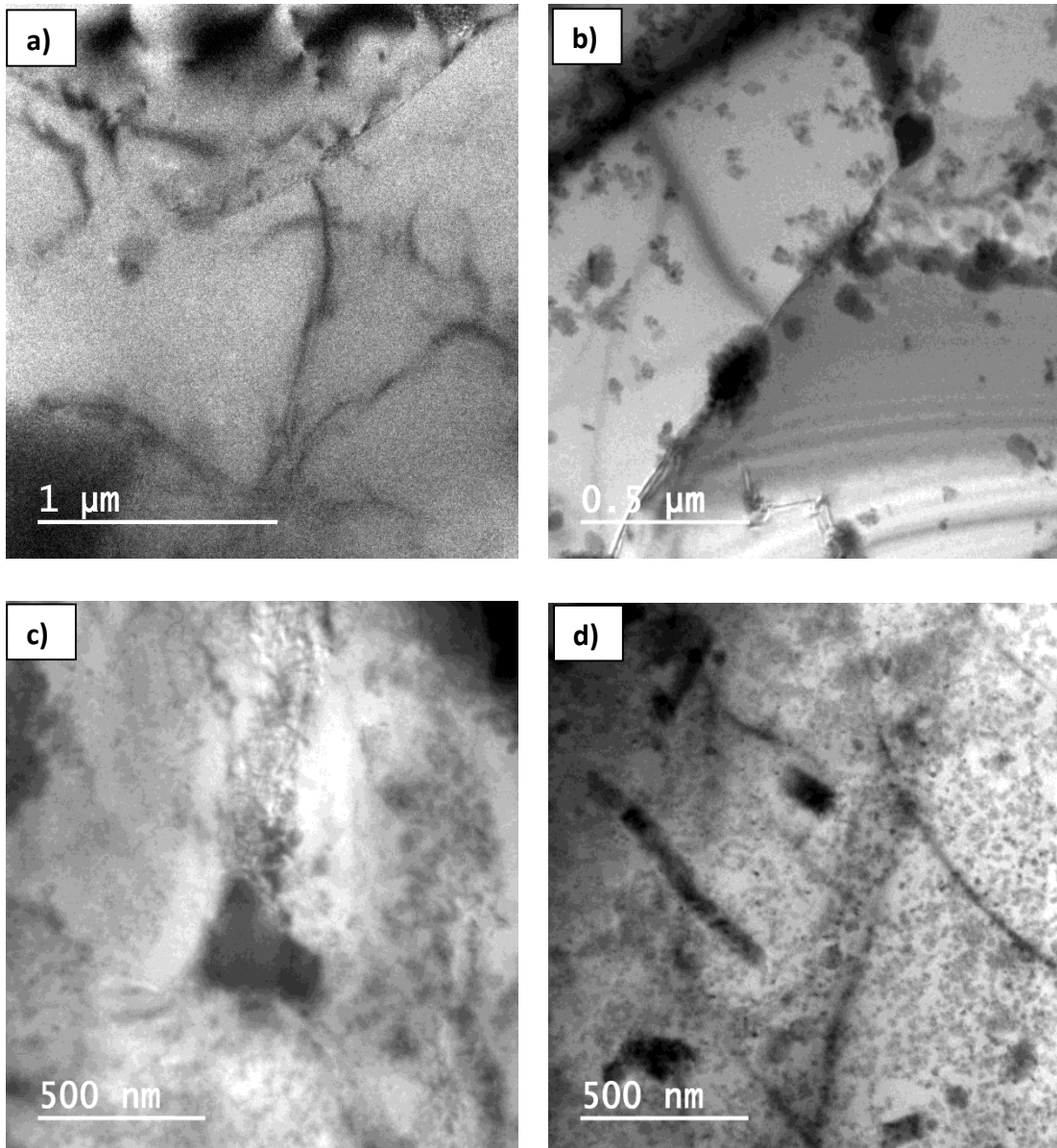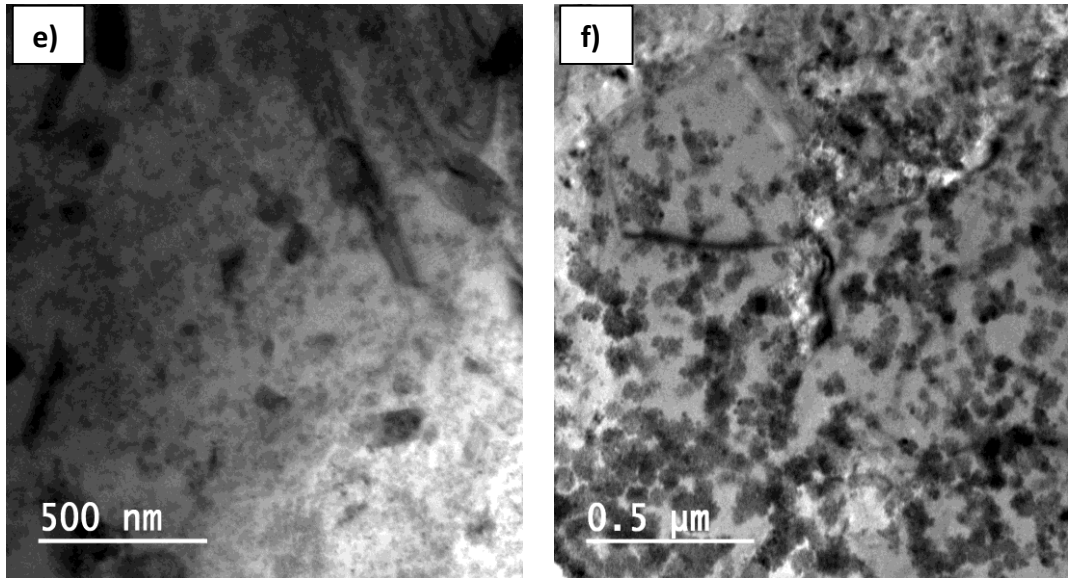
Fig. 4.29 TEM nanostructures of SPSed AA2024 unreinforced/composie samples reinforced with (a) 0.0 wt% micro Y, (b) 0.1 wt% micro Y, (c) 0.2 wt% micro Y, (d) 0.3 wt% micro Y, (e) 0.4 wt% Y and (f) 0.5 wt% micro Y.

Fig. 4.30 shows the microstructures of the tensile fractured surfaces of the composite samples. As the yttrium content increased, the number of dimples and its depth increases. The samples underwent ductile fracture up to 0.3 wt% yttrium reinforcement that can be observed from Fig. 4.30 (a), (b), (c) and (d), in which there is a fair number of fine and deep dimples. As the yttrium reinforcement increased beyond 0.3%, the dimples gradually increased in size with a decrease in depth and also inter granular fracture, which led to ductile-brittle fracture, as shown in Fig. 4.30 (e) and (f).
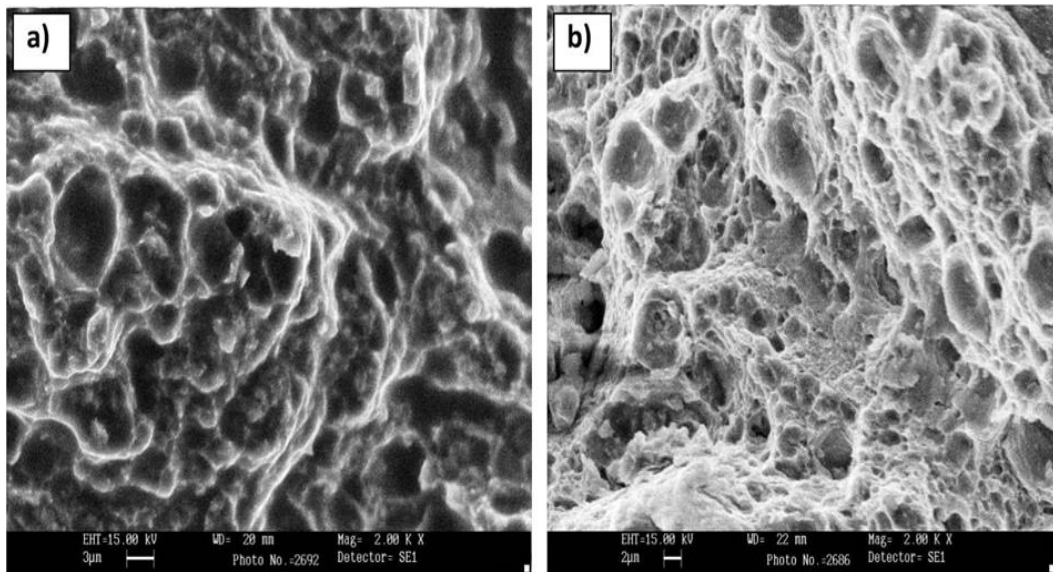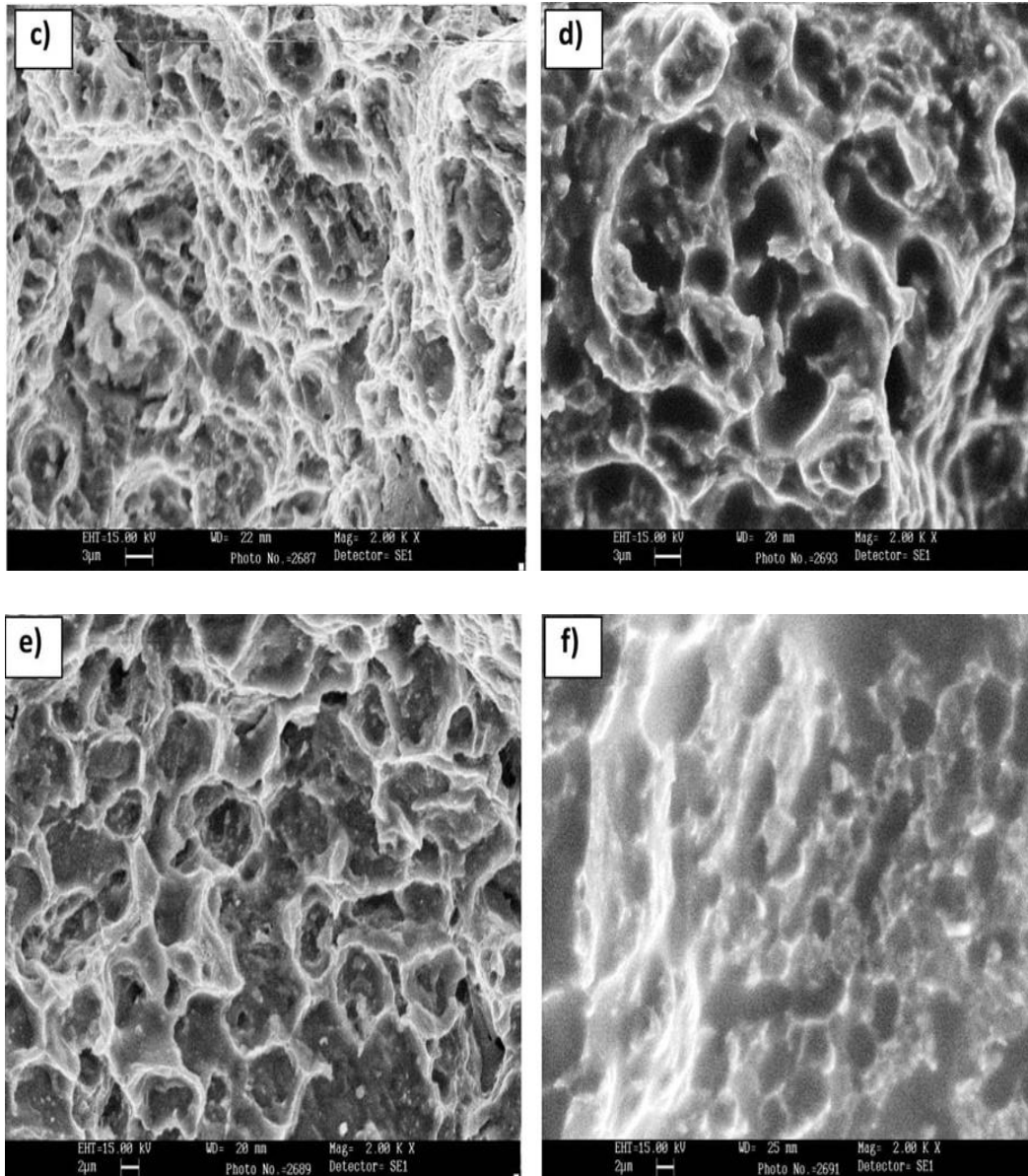
Fig. 4.30 SEM microstructures of fractured surfaces of SPSed unreinforced/reinforced composite samples with (a) 0.0 wt% micro Y, (b) 0.1 wt% micro Y, (c) 0.2 wt% micro Y, (d) 0.3 wt% micro Y, (e) 0.4 wt% micro Y and (f) 0.5 wt% micro Y.

4.3.1.2.3 Evaluation of mechanical properties

The SPSed composite samples were mirror polished and the hardness was measured by a computerized Vickers testing machine with a load of 5 Kg. Ten readings were taken for each composite sample and the average hardness for each sample was reported. Fig. 4.31 shows the variation of Vickers hardness of different samples with an increase in yttrium reinforcement. As a result of yttrium reinforcement, nearly full relative density of the composite samples, remarkably high hardness is achieved. However, beyond 0.3% reinforcement of yttrium, the hardness decreased.
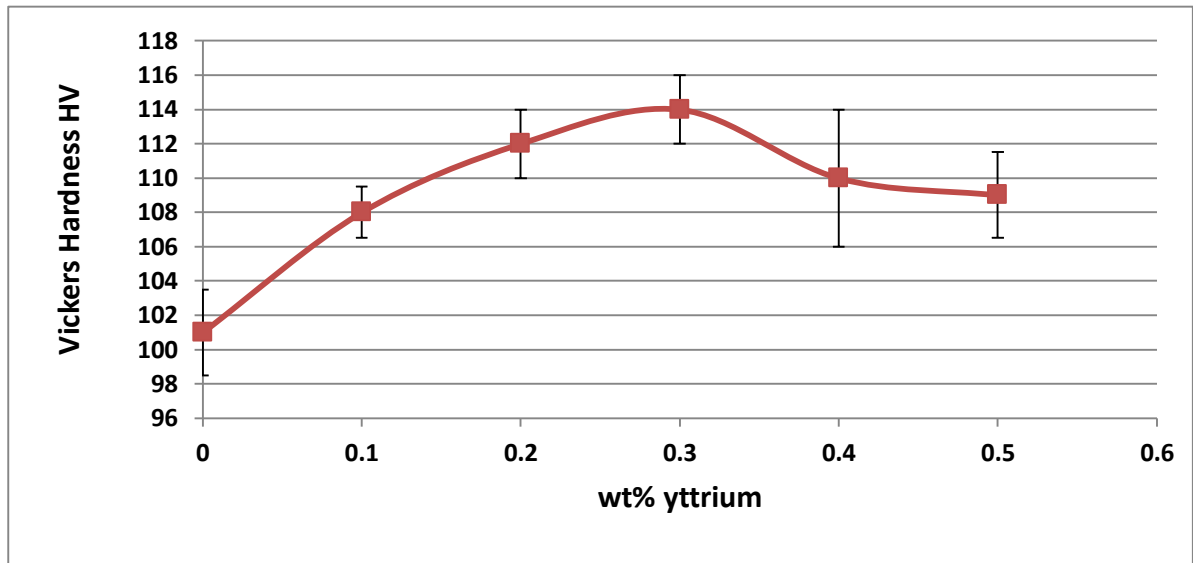
Fig. 4.31 Variation of hardness the SPSed unreinforced/reinforced composite samples with varying amounts of micro yttrium.

Tensile specimens were cut from each SPSed composite sample and tested for tensile strength, using a universal testing machine (Model, 75KS). Three tensile specimens were cut from each composite sample. The average values of ultimate tensile strength, yield strength and elongation for each composite sample were recorded. Fig. 4.32 shows the variation of YS and UTS with an increase in yttrium reinforcement. The highest YS and UTS achieved were 343 MPa and 388 MPa respectively for the sample with 0.3 wt% yttrium reinforcement. Both the tensile and yield strengths followed the same trend in the increase as well as the decrease. Beyond 0.3 wt% reinforcement of yttrium, the difference between the tensile and yield strengths decreased. Ductility of a material can be calculated by its strain or elongation at a particular point. In the present study, strain at fracture was taken into consideration to analyse the effect of yttrium reinforcement on the ductility of AA2024 matrix composite.
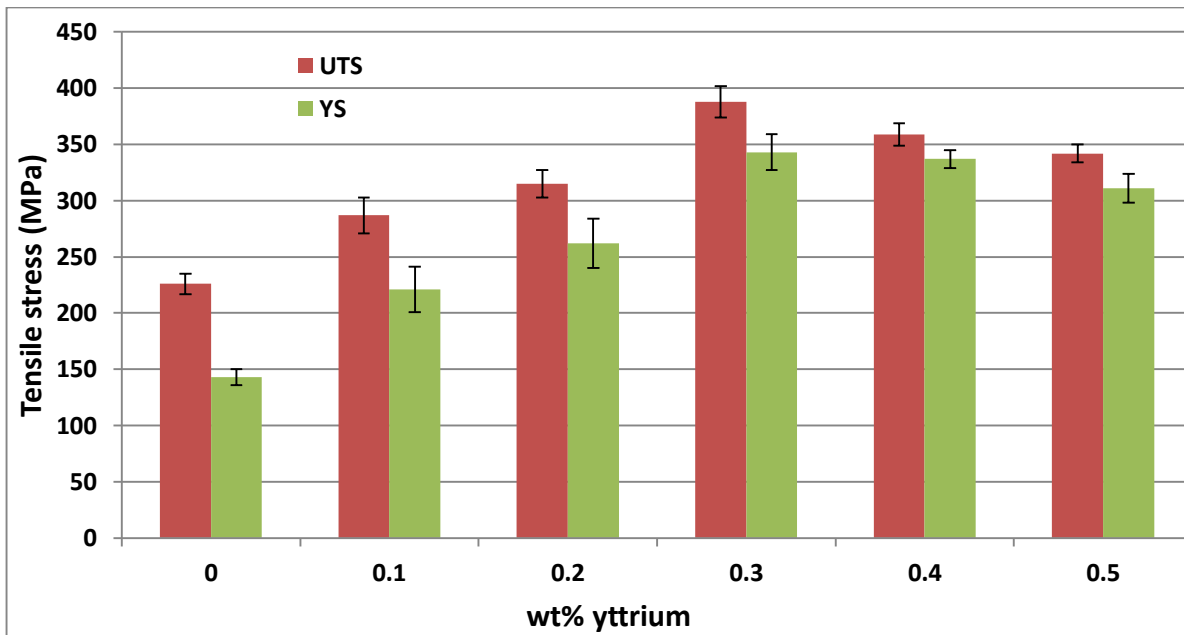
Fig. 4.32 Variation of UTS and YS in the SPSed unreinforced/reinforced composite samples with varying amounts of micro yttrium.

Fig. 4.33 shows the variation of percentage elongation with an increase in the reinforcement of yttrium. The elongation increased gradually up to 0.3 wt% yttrium reinforcement and then decreased. The highest elongation recorded was 18.4% for the composite sample with 0.3 wt% reinforcement of yttrium.
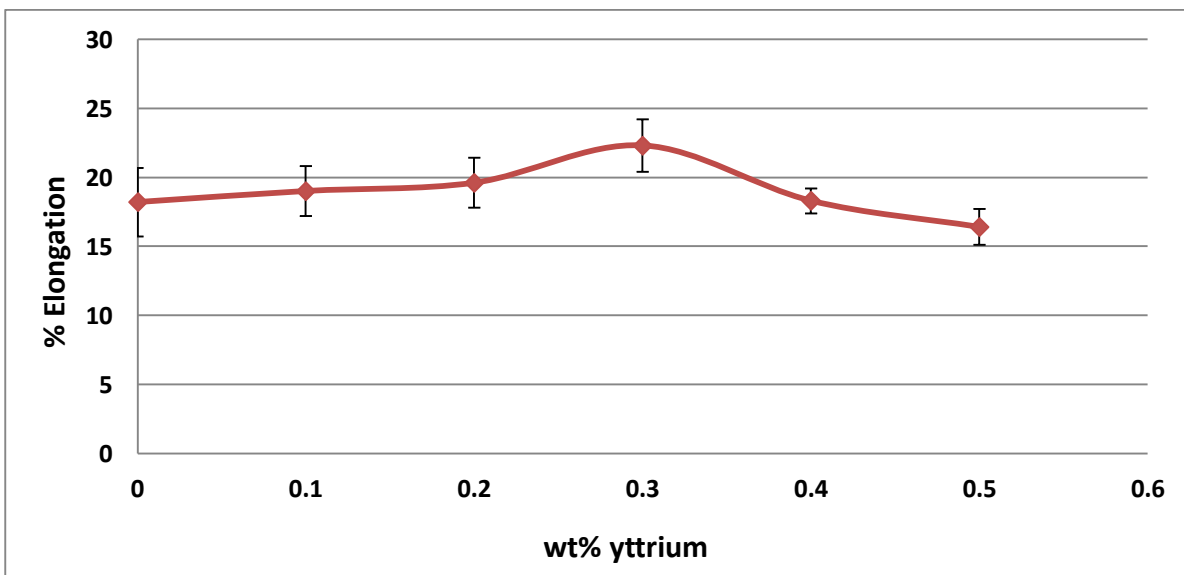
Fig. 4.33 Variation of percentage elongation of the SPSed unreinforced/reinforced composite samples with varying amounts of micro yttrium.

116

The percentage elongation also followed the same trend as the other mechanical properties. The fractured specimens are shown in Fig. 4.34.

Fig. 4.34. Fractured tensile specimens reinforced with varying wt% of yttrium (starting from minimum yttrium at the top to maximum yttrium at the bottom).

4.3.1.2.4 XRD analysis

Fig. 4.35 shows the XRD patterns of the sintered composite samples with varying amounts of yttrium reinforcement.
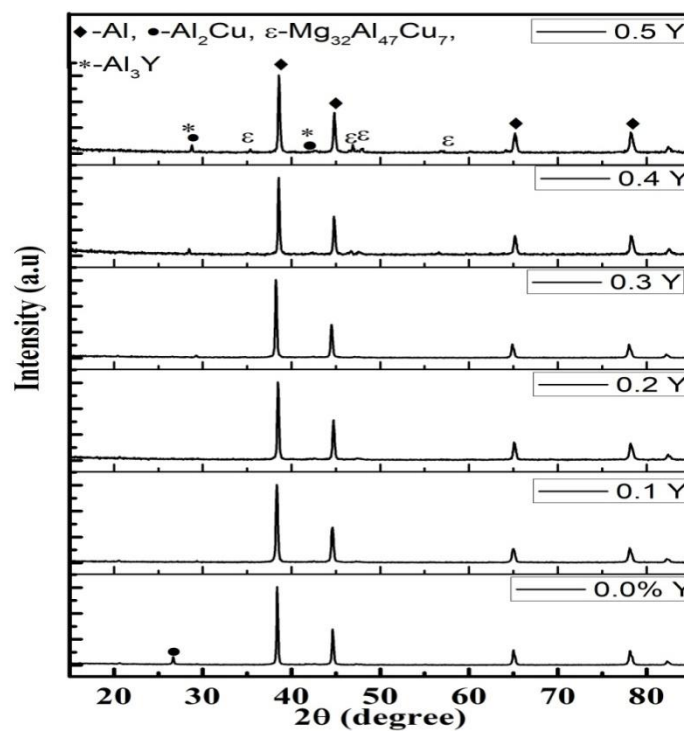
Fig. 4.35 XRD patterns of SPSed unreinforced/composite samples reinforced with varying amounts of micro yttrium.

The XRD of the composite samples is done using Burker X-ray diffractometer (Model: D8-Advance). The goniometer was set at 0.5º/minute through an angle range of 10º to 90º (2θ), as discussed in the section 3.5. The new phases, crystal sizes and micro strains that were formed during spark plasma sintering were identified and analysed using 'Xpert Highscore software'.

It can be observed from Fig. 4.35 that five distinct peaks of aluminium matrix (α-Al) are clearly visible for all the samples. As the yttrium reinforcement increases, small peaks of precipitation and intermetallic phases appeared. The Al_2Cu phase in supersaturated solid solution of pure AA2024 sample was also identified. Many intermetallic phases consisting of Al, Y, Cu and Mg were not detected due to the limitation of the XRD instrument in detecting phases of low intensities. The phases identified were α-Al, Al_2Cu, $Mg_{32}Al_{47}Cu_7$ and Al_3Y. The crystallite size and micro-strains in the sample were calculated using 'Tiny Tools' (Scherrer equation) software and are shown in Table 4.4.

It can be seen that the variation in crystallite sizes match with the grain size variation. As the crystallite size decreased, the lattice strain increased and peak shift and broadening were observed for all the sintered samples with respect to AA2024 (α-Al) peaks. The peak shift and broadening are the indications of an increase in dislocation density and micro strain in the composite samples.

Table 4.4 Crystallite size and lattice-strain of the unreinforced/reinforced composite samples with varying wt% of yttrium.

Sample No.	Proportion of Yttrium (wt%)	Position (2θ)	Full width at half maximum (FWHM)	Average crystallite size (nm)	Lattice-strain ($\varepsilon \times 10^{-6}$)
1	0.0	38.3711	0.1392	63.14	0.0017
2	0.1	38.3315	0.3424	25.66	0.0043
3	0.2	38.4631	0.4524	19.43	0.0057
4	0.3	38.2426	0.4872	18.03	0.0061
5	0.4	38.5756	0.4176	21.06	0.0052
6	0.5	38.5834	0.4176	25.66	0.0043

4.3.1.3 Discussion

The density variation of the composite samples with an increase in yttrium content is shown in Fig. 4.21. Relative densities (>99.75%) were achieved through SPS. The SPS parameters employed in this study could yield densities up to 99.8, as reported by other researchers [170, 171]. Since the AA2024 powder was obtained by rapid solidification in an inert gas atmosphere, we can observe a dendrite structure and eutectic phase consisting of Al_2Cu, which might have affected the sintering quality of the sample.

Due to Joule heating and electric discharge, high heating rates were generated at the particle boundaries during SPS. Consequently, local temperature of the contact points increased and eutectic melting occurred along the particle boundaries (necking) closing up the voids, resulting in high relative densities. Also, the pressure applied could break the oxide film on the powder particles, and the particles deformed plastically, giving a way to an increase in particle-particle contact, which made the diffusion easier. One of the underlying reasons behind the increase in relative density with an increase in yttrium content could be due to the morphology of yttrium particles.

Yttrium particles are like chips or ribbons and are bigger in size than those of the 2024 AA powder particles. The possibility of yttrium particles getting into the voids (triple points) of aluminium particles was very less. So the yttrium particles might have enveloped the aluminium particles making an aluminium-yttrium-aluminium particle sandwich, which might have increased with an increase in yttrium reinforcement. Since the sintering phenomenon is mainly based on the diffusion mechanism, the yttrium between aluminium particles was assumed to have hindered the diffusion causing a drop in density. However, on the other hand, yttrium is a metal, which is not as good as aluminium in conducting electric current and offer more resistance to the current flow during SPS, which intensifies heat between the sandwiches and lead to better diffusion. Moreover, with the applied pressure, the yttrium ribbons or chips that are flat could have accommodated themselves within the available void space without pushing the aluminium particles much apart.

In the SPSed composite samples, the hardness variation can be attributed to various hardness mechanisms, such as solid solution hardening, dispersion hardening (Orowan bowing), strain hardening, precipitation hardening and hardening by grain size reduction (Hall-Petch). Although AA2024 contains copper, which could cause precipitation hardening in the samples,

119

it cannot contribute as much as it should after 0.3 wt% yttrium reinforcement, because the precipitates coarsen and behave like grains themselves and their dispersion strengthening effect decreases. **Cooke et al.,** [171] reported that the samples get over aged during SPS, but in the present work, yttrium reinforcement altered the ageing kinetics of the composites leading to variation in strength. Since the SPS parameters for all the composite samples were kept similar, the hardness variations were directly or indirectly influenced by yttrium alone. The presence of yttrium contributed to an increase in the hardness by dispersion hardening, but the contribution might be less because of its larger particle size. From Fig. 4.22, it can be observed that the grain size reduced as the yttrium reinforcement increased up to 0.3 wt%, beyond 0.3 wt%, grains become coarser.

From Fig. 4.23 and 4.29, it can be observed that the precipitates started to coarsen and the hardness dropped as the proportion of yttrium was increased beyond 0.3 wt%. This could be due to the alteration of age hardening kinetics, achieved by yttrium reinforcement. The precipitation effectively hindered the dislocation movement and as the grain size reduced, the grain boundaries increased, creating more barriers. So the strength achieved was because of the rate and size of the precipitation and grain size. This precipitation behavior could be attributed to the heterogeneous nucleation capacity of meta-stable phases on yttrium particles and high dislocation density induced by the mismatch [172, 173]. In addition, the difference between the coefficients of thermal expansion of Al (23.5×10^{-6}/K) and yttrium (10.6×10^{-6}/K) caused a strain field at the interface of the matrix and reinforced particles, which led to an increase in dislocation density. During precipitation, these dislocations could act as nucleating sites.

The variation of tensile strength and percentage elongation were depicted in Fig. 4.32 and 4.33. A considerable increase in tensile properties is evident up to 0.3 wt% yttrium reinforcement. Increase in yttrium reinforcement beyond 0.3 wt% decreased the tensile properties. SPS processing was able to transform the initial dendrite structure into finer grains. Finer precipitates and smaller grains hindered the dislocation movement, increasing the mechanical properties of the SPSed samples. However, excessive reinforcement of yttrium (more than 0.3 wt%) could decrease the strength, as it could form intermediate compounds like Al-Cu-Y, decreasing the solid solubility of Cu in Al, and hence coarsening the precipitates, as seen in Fig. 4.29. Therefore, the mechanical properties of the samples decreased when the yttrium content increased beyond 0.3 wt%, as also reported by **Hui et al.,** [174]. However, in aluminium alloys without copper alloying, only AlY intermetallic phase agglomerates along

the grain boundaries, which enables grain boundaries to hinder dislocation motion or slipping [175].

The variations in the tensile properties were mainly due to the combined effect of the formation of precipitates (as discussed in the previous section 4.1.3), grain size reduction and inter-metallic compounds (Al-Cu-Mg) and Al-Y growth near the particle boundaries. Since yttrium has better resistance than aluminium, Joule heat generated from the resistance offered by yttrium simply adds to the total heat. As the yttrium reinforcement increased, the heat input to the powder sample increased and the precipitation of the samples also changed. The grain refinement was due to the high-intensity of pulse current that led to melting/vaporization at the particle interface and recrystallization took place during necking. The SPS processing time was so less that it did not give enough time for the newly formed grains at the interface to grow [150]. However, on the other hand, **Chen et al.,** [185] gave an alternative explanation to grain refinement achieved by high intensity pulsed electric field through thermo-mechanical fatigue effect, which plastically deforms and breaks the grains into number of smaller grains. The yield strength of a material is dependent on the grain size, as proposed by **Hall-Petch** [188]. According to Hall-Petch equation, the yield strength is inversely proportional to the square root of the grain size.

The inter-metallic Al-Cu (Mg, Y) growth near the particle boundaries is due to inter-atomic diffusion. Many researchers have investigated the inter-atomic diffusion at lower temperatures between dissimilar metals having a difference in their melting points using SPS. **Ruidi et al.,** [176] investigated the atomic diffusion of Fe-Al system under SPS conditions and concluded that the current increases the growth rate of Al_5Fe_2 and $Al_{13}Fe_4$ at 550 and 600º C. However, the question arises whether such diffusion took place in the present investigation or not. But according to literature, the atomic diffusion is improved by a considerable increase in the density of lattice defects, such as dislocation and vacancies. As discussed earlier, lattice defects are expected at the Al-Y interface due to the mismatch between them, leading to diffusion. Fig. 4.26 shows the diffusion of yttrium to the AA2024 matrix in the specimen reinforced with 0.3 wt% yttrium.

The line EDX shown in Fig. 4.27 shows the diffusion of aluminium-yttrium. In Fig. 4.28, spot 1 shows the yttrium in the matrix, spot 2 shows the diffusion of aluminium and yttrium, spot 3 shows the matrix and spot 4 shows the precipitate. The UTS of the unreinforced 2024 AA

sample is 226 MPa and those of the composites samples varied from 287 to 388 MPa with the highest elongation of 18.4%. The variation of UTS followed a similar trend as in the case of hardness and density. The microstructure clearly shows that Al matrix consists of a combination of small and large grains. The smaller grains contribute to the strength while the larger ones contribute to the ductility. As the yttrium content increases, we can observe deep dimples and a huge number of dislocations piled up near the grain boundaries. As the yttrium content increased beyond 0.3 wt%, we can see that the dimples gradually disappeared and inter granular fracture took place, which led to a near brittle fracture, as shown in Fig. 4.29 (e) and (f).

4.3.1.4 Conclusions

In the present study, five composite samples with AA2024 as the matrix material and varying wt% of micro yttrium as the reinforcement were developed using SPS. Pure AA2024 sample was also sintered to compare the effect of yttrium reinforcement on the mechanical properties of AA2024 matrix composites. The following major conclusions have been made based on the present investigations.

- Five AA2024 matrix composite samples reinforced with varying proportions of yttrium were successfully developed through SPS with nearly full density. The high density of the composites is attributed to the effective diffusion of powder particles achieved by Joule heating and simultaneous high pressure provided by SPS.

- Though it is widely known that grain refinement is not possible via powder metallurgy route, the reinforcement of micro yttrium to 2024 AA matrix has modified the microstructure by effectively changing the grain size and increasing the secondary phase precipitates by accelerating the age hardening kinetics, which are the major strengthening mechanisms. This credit of grain refinement achieved in the composite samples is attributed to the reinforcement of yttrium and sintering mechanism of SPS.

- X-Ray mappng and EDS analysis showed a uniform distribution and diffusion of yttrium in the 2024 AA matrix, which has improved the mechanical properties. Therefore, ball milling could be considered as a convenient means of mixing the powders before consolidating through SPS.

- The pulse current in SPS caused grain refinement and diffusion of Al and Y particles, leading to intermetallic growth near particle boundaries, which has improved the strength

of the composite samples up to 0.3% yttrium reinforcement. The strength then decreased as the intermetallic phase coarsed along with Al-Cu precipitation with further increase in yttrium reinforcement.

- The mechanical properties of the composite samples were in close agreement with the microstructures and grain sizes. As a result of near full density of the samples, reasonably good hardness was obtained. The highest hardness recorded was 114 HV with 0.3% reinforcement of yttrium, which was 112% that of the unreinforced 2024 AA sample. However, with a further reinforcement of yttrium, the hardness decreased. The highest YS and UTS achieved were 343 MPa and 388 MPa respectively with 0.3% reinforcement of yttrium with 18.4% elongation. These values of YS, UTS and elongation were 239, 171 and 128% compared to those of the unreinforced 2024 AA sample.

- Reinforcement of yttrium altered the age hardening and precipitation kinetics by providing favourable conditions like promoting dislocation density, creating strain field and providing nucleating sites for precipitation. Precipitation of Al_2Cu, the growth of intermetallic compound Al_3Y and grain size played an important role in the variation of mechanical properties of the composite samples. It was found that an optimum amount of yttrium reinforcement (0.3 wt%) could create favorable conditions for optimum precipitation, grain refinement and intermetallic growth in the composite sample, which led to peak mechanical properties.

- A new theory on the mechanism of grain refinement in the spark plasma sintered composites is hereby proposed from the present study. This theory explains the combined effect of recrystallization caused by melting/vaporization at the particle interface and the thermo-mechanical fatigue that occurred in the matrix due to plastic deformation, during sintering of the composites. Both these mechanisms together could refine the grains of the composites throughout the matrix.

4.3.2 Effect of cryo rolling on spark plasma sintered AA2024 + micro yttrium composites.

The micro composite samples developed through SPS with AA2024 as the matrix material and varying wt% of yttrium as the reinforcement (discussed in section 4.3) were further subjected to severe plastic deformation (SPD) to improve their strength. The method of SPD employed in the present study was rolling at cryogenic temperature (cryo-rolling).

4.3.2.1 Experimental work

The details of SPS, cryo-rolling and the related experimental methods are already discussed in sections 3.2.3, 3.2.4, 3.4 and 3.5. The cryo-rolled composite samples were further subjected to metallurgical characterization and mechanical testing. The metallurgical characterization like optical microscopy, FE-SEM, TEM, XRD and mechanical testing like hardness, UTS, YS, elongation have been done according to the procedures discussed in sections 3.4, 3.5 and 3.6.

4.3.2.2 Results

4.3.2.2.1 Investigation of microstructure

The cryo-rolled composite samples were polished, etched and observed under various microscopes according the procedures discussed in the section 3.4. Fig. 4.36 shows the FE-SEM microstructures of the cross sections of the cryo-rolled composite sample with varying amounts of yttrium.
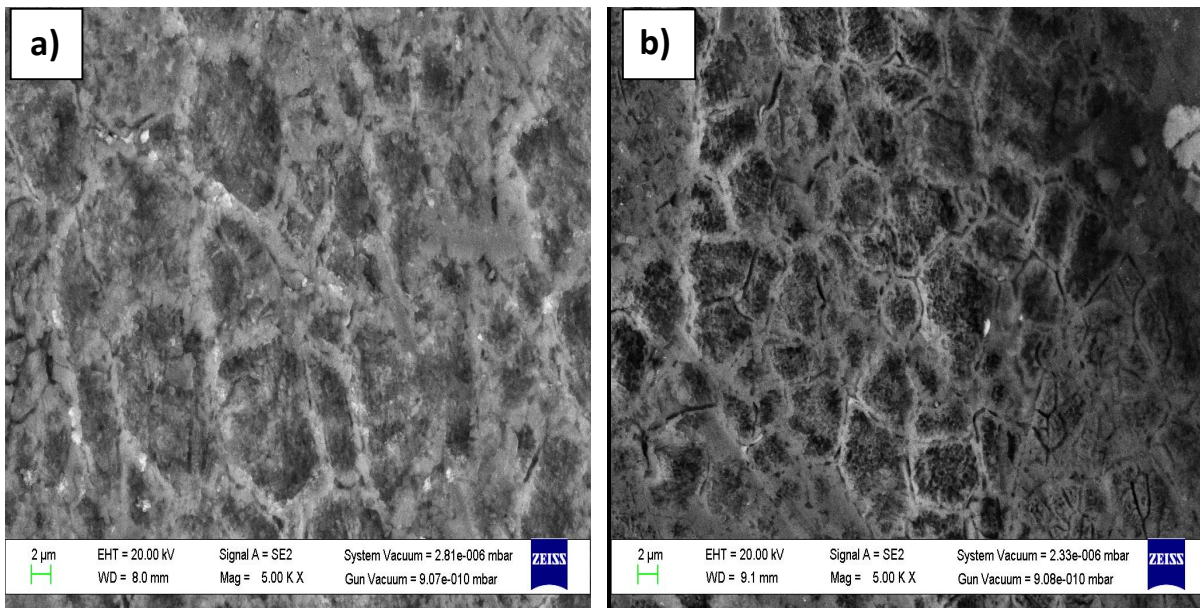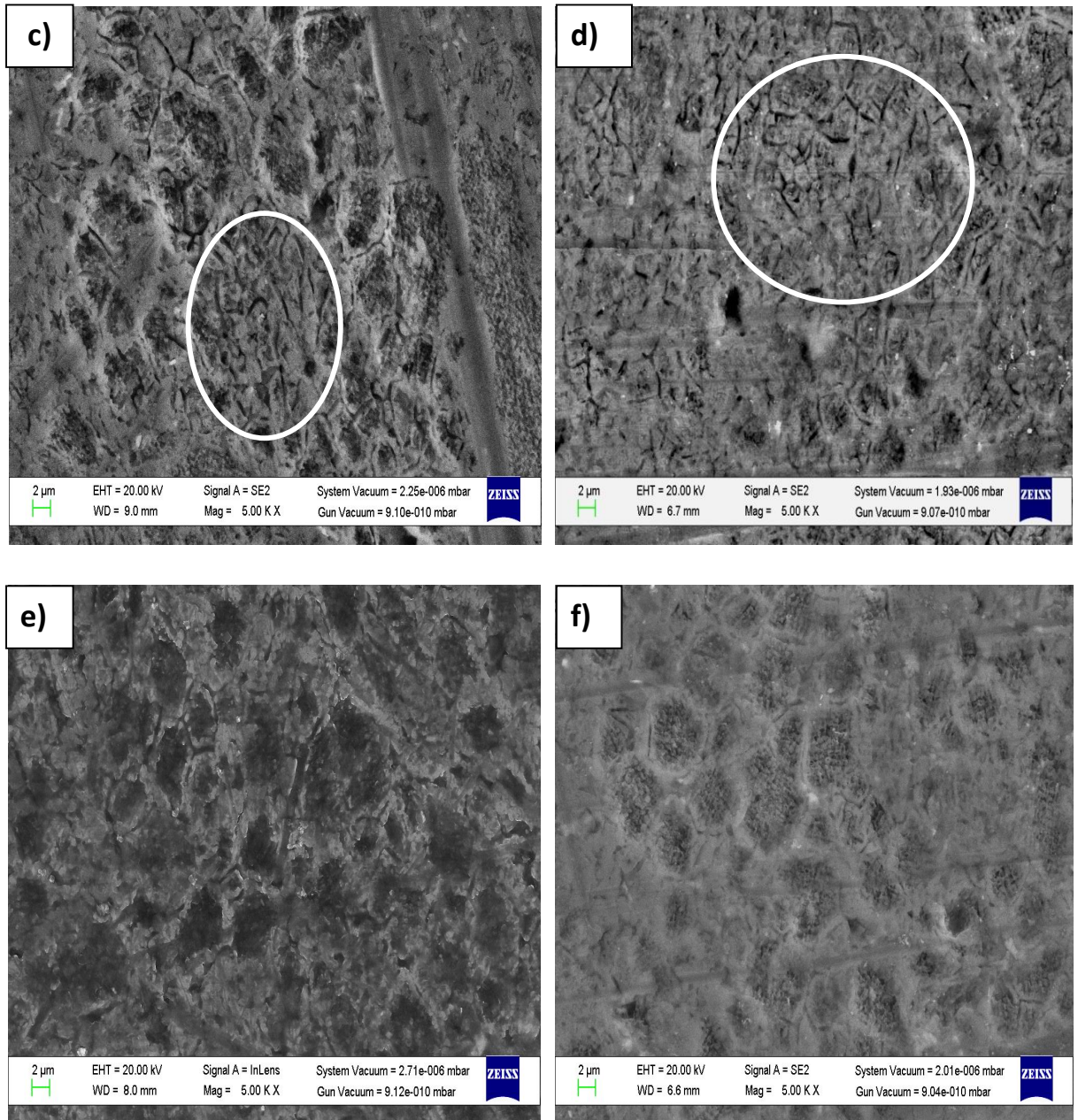
Fig. 4.36 FE-SEM microstructures of the cross sections of the SPSed and cryo-rolled unreinforced/composite samples in the direction perpendicular to rolling, reinforced with (a) 0.0 wt% micro Y, (b) 0.1 wt% micro Y, (c) 0.2 wt% micro Y, (d) 0.3 wt% micro Y, (e) 0.4 wt% micro Y and (f) 0.5 wt% micro Y.

It can be observed from the above Fig. 4.36 that cryo-rolling induced severe stress and strain through the action of compression in the composite samples. The grains were compressed and took the shape of a honeycomb with an approximate hexagonal structure. Almost all the grains were of similar shape and size in each composite samples. Cryo rolling also introduced high dislocation density, which can be seen along the grain boundaries. From Fig. 4.36 (c), it can be observed that the matrix grains tended to become smaller with 0.2 wt% yttrium reinforcement

as encircled in white on the microstructure. As the yttrium reinforcement reached 0.3 wt%, the number of smaller grains increase and spread throughout the matrix, as observed in Fig. 4.36 (d) encircled in white. With further increase in yttrium wt%, the smaller grains disappeared. The grain sizes of the cryo-rolled composite samples were calculated by linear intercept method and confirmed by Image J software. The calculated grain sizes were 8, 4, 3, 1, 4 and 5 µm for the samples starting from pure AA2024 to AA2024 + 0.5 wt% yttrium reinforcement respectively. Fig. 4.37 shows the optical microstructures of the longitudinal sections of the unreinforced composite samples.
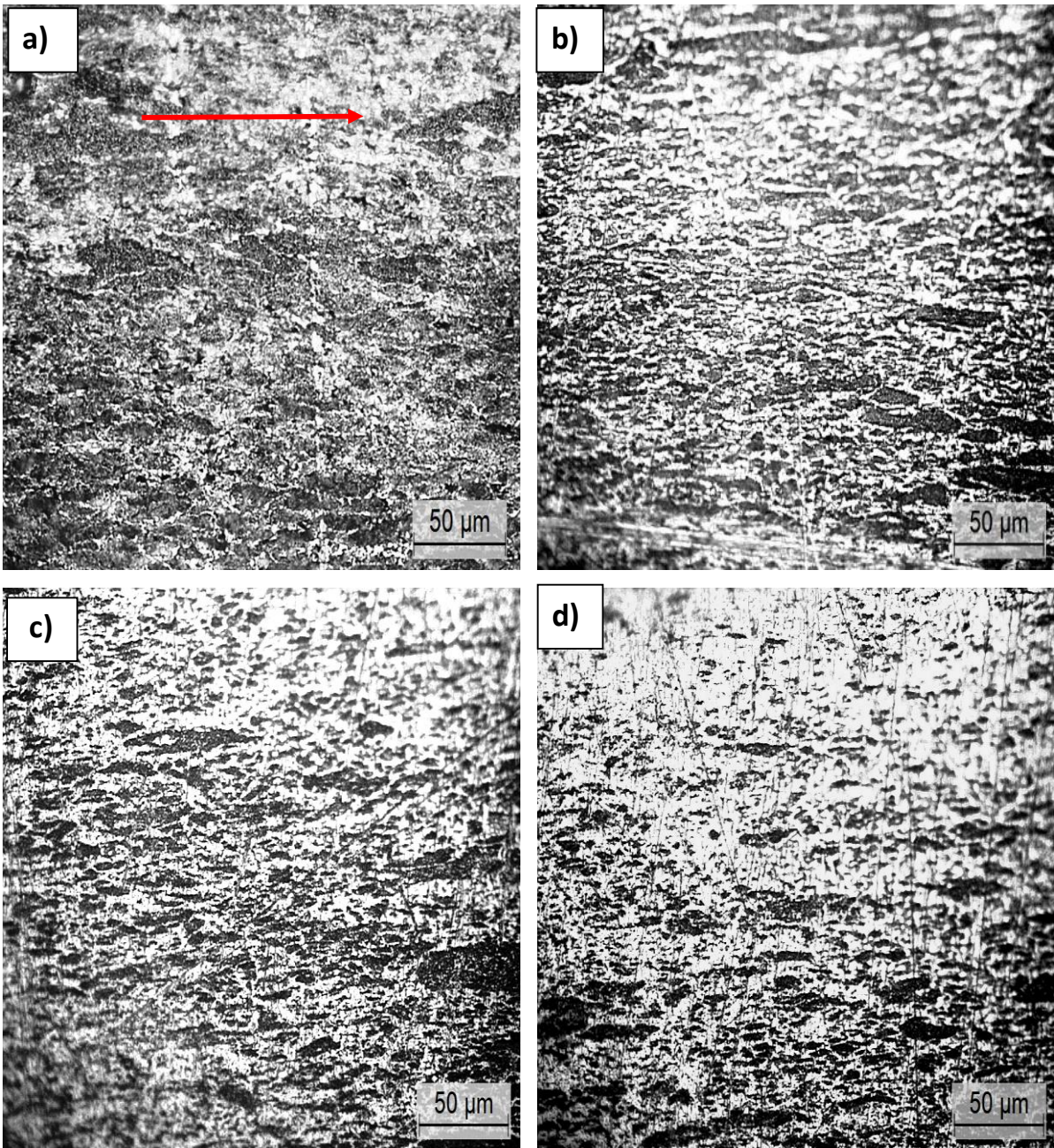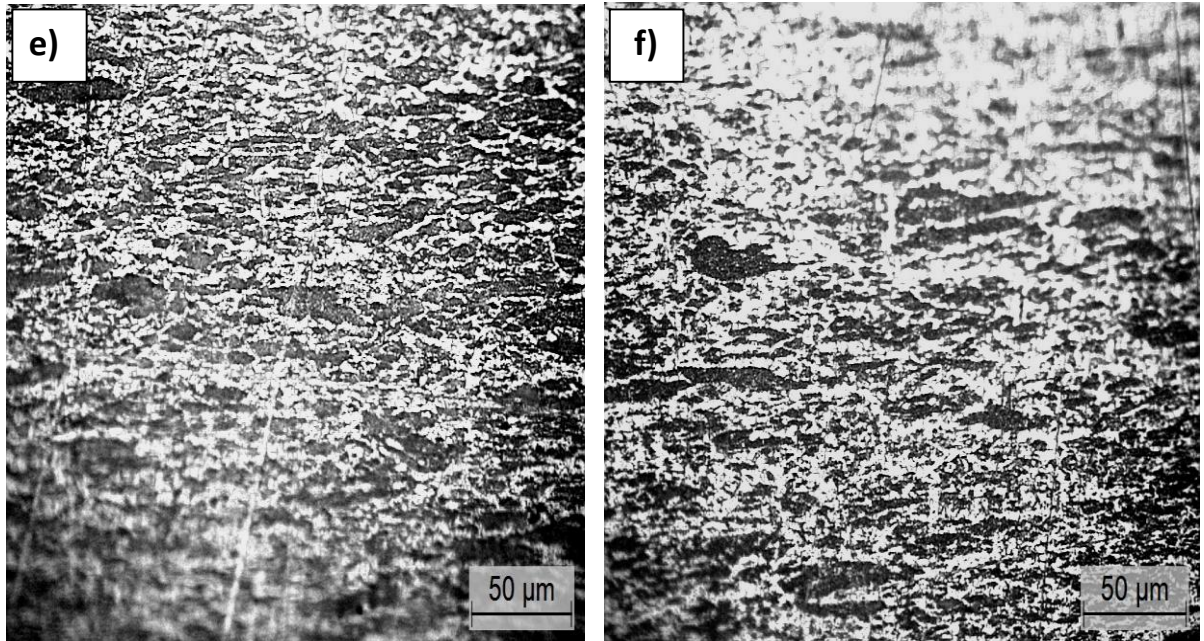
Fig. 4.37 Optical microstructures of the SPSed and cryo rolled composite samples in longitudinal rolling direction, reinforced with (a) 0.0 wt% micro Y, (b) 0.1 wt% micro Y, (c) 0.2 wt% micro Y, (d) 0.3 wt% micro Y, (e) 0.4 wt% micro Y and (f) 0.5 wt% micro Y.

From Fig. 4.37, it can be observed that the grains were elongated in the rolling direction (shown by a red arrow) in Fig. 4.37 (a) and the strain induced was also able to cut the elongated grains as the yttrium wt% was increased up to 0.3 wt%. Rolling induced high number of dislocations in the composite samples and the dislocations generated piled up at the grain boundaries as observed in the microstructures. The elongated grain size tended to decrease in the composite samples up to 0.3 wt% yttrium reinforcement. Upon further increase in yttrium reinforcement, the grain size increased.

For further analysis, FE-SEM microstructure of the composite sample reinforced with 0.3 wt% yttrium was considered. The microstructure was taken in the direction perpendicular to the rolling direction, as shown in Fig. 4.38. Severe plastic deformation, achieved in the composite sample by cryo-rolling, compressed the grains and the sub grains. As a result of compression action in the composite sample, sub grains were formed within the grains and nano grains were formed within the sub grains. Since the cryo-rolling process suppressed the dynamic re-crystallization, the shape and size of the grains were retained.
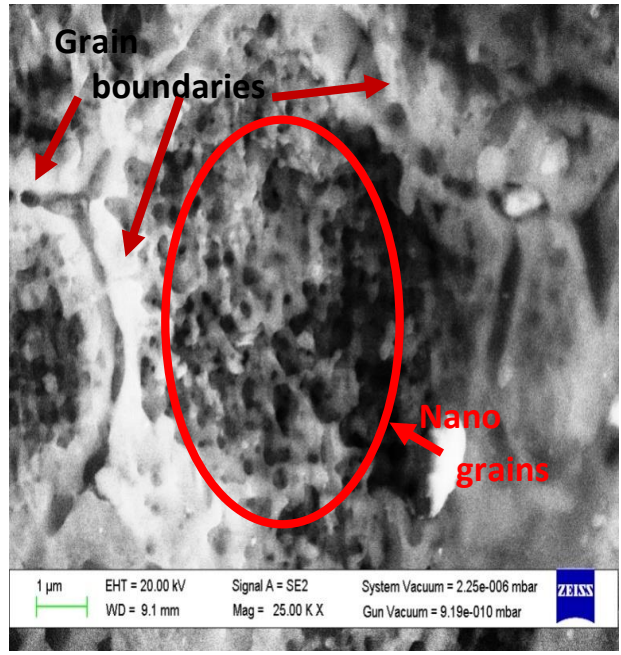
Fig. 4.38 FE-SEM microstructure of the SPSed and cryo rolled composite sample reinforced with 0.3 wt% micro yttrium taken perpendicular to the rolling direction showing the formation of nano grains.

Fig. 4.39 shows the TEM nanostructure of the cryo-rolled composite samples with varying amount of yttrium reinforcement.
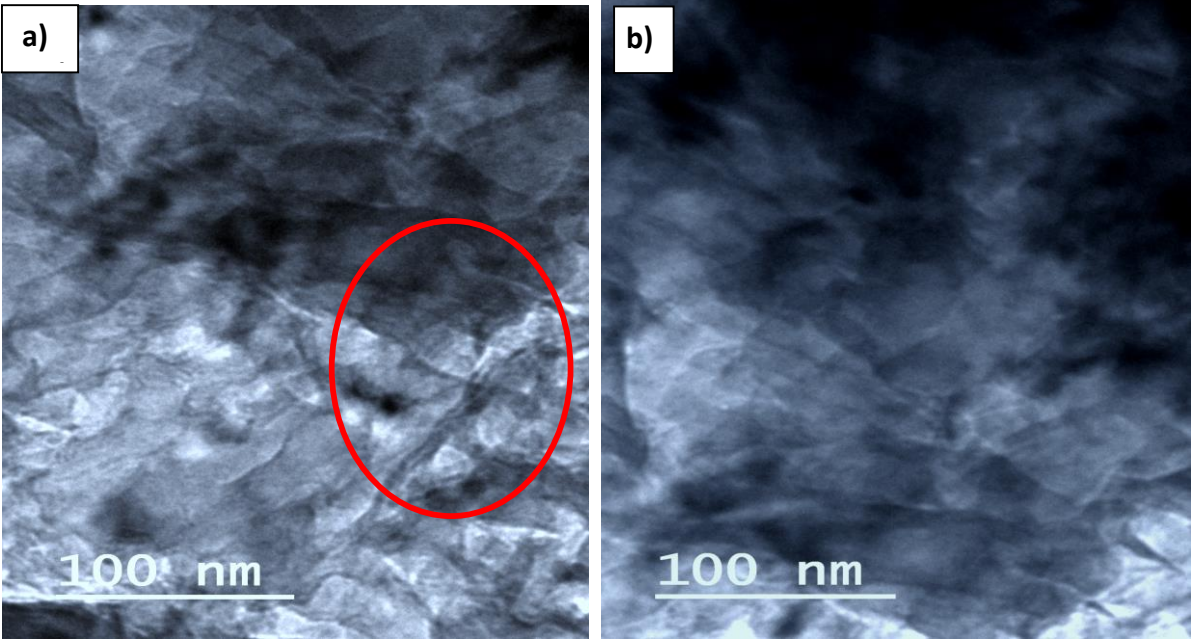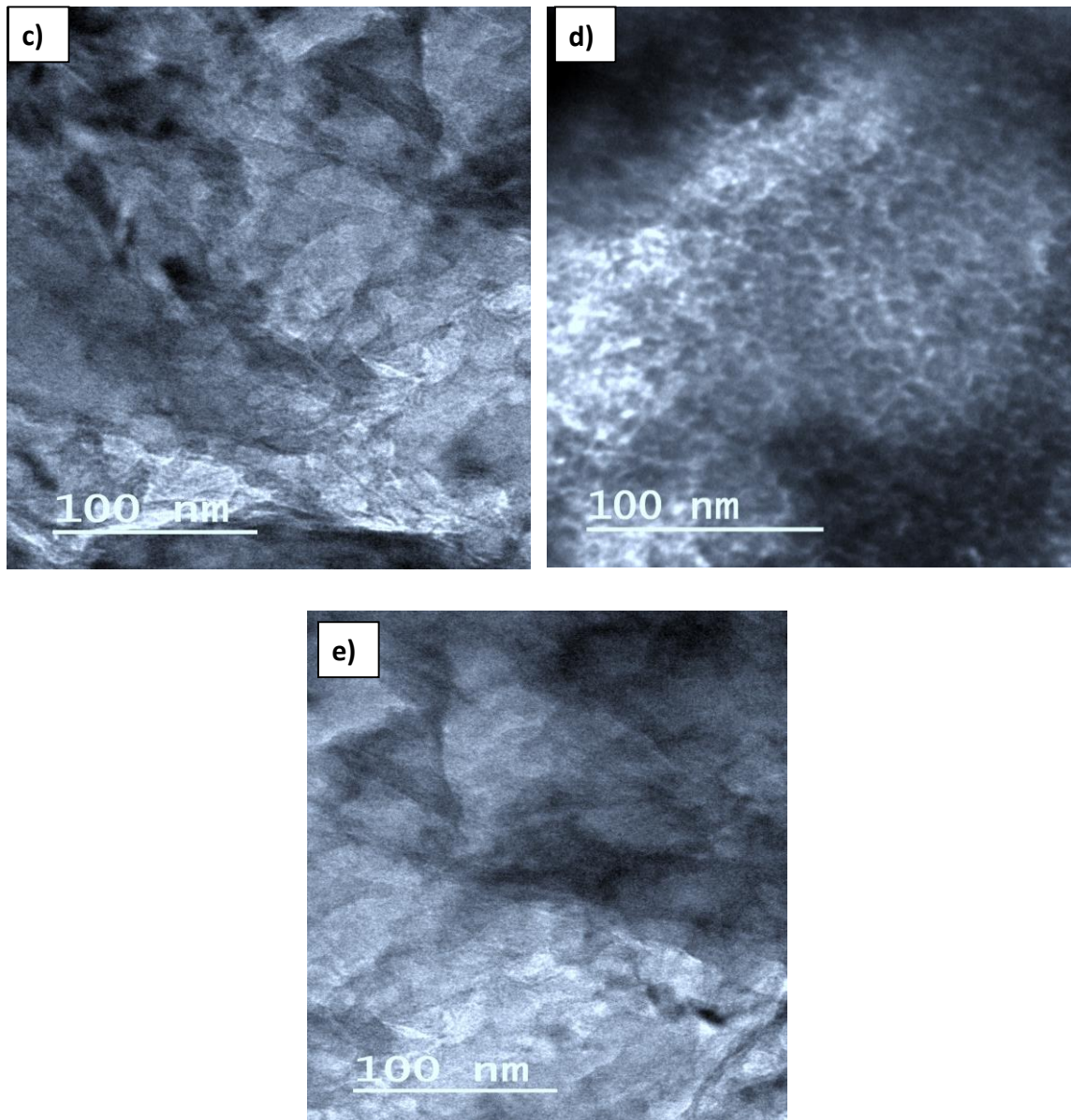
Fig. 4.39 TEM nanostructures of cross sections of SPSed and cryo-rolled micro composite samples in the direction perpendicular to rolling, reinforced with (a) 0.1 wt% micro Y, (b) 0.2 micro wt% Y, (c) 0.3 wt% micro Y, (d) 0.4 wt% micro Y and (e) 0.5 wt% micro Y.

From Fig. 4.39, it can be clearly observed the formation of nano grains due to cryo-rolling. The nano grain size decreases from a few tens of nano meters to a few nano meters with variation in yttrium reinforcement from 0.1 to 0.3 wt%. With further increase in the yttrium reinforcement, the grains tend to coarsen. The dislocation density achieved in the composite samples by cryo-rolling can be observed as dark clouds in the nanostructures.

For further investigation of the shape and size of the nano grains, TEM nanostructure of the composite sample with 0.3 wt% yttrium reinforcement was taken at a higher magnification.

Fig. 4.40 shows the TEM nanostructure of the composite sample with 0.3 wt% yttrium reinforcement at higher magnification.
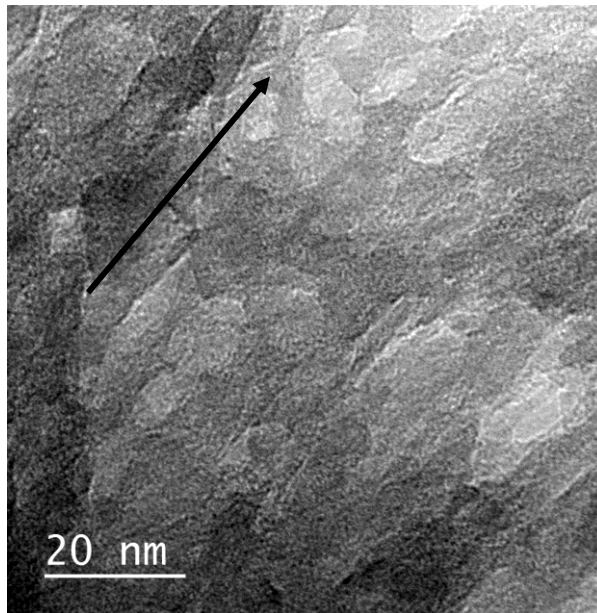
Fig. 4.40 TEM nanostructure of the SPSed and cryo rolled composite sample reinforced with 0.3 wt% micro yttrium at a higher magnification.

The black arrow on the nanostructure indicates the cryo-rolling direction. From the nanostructure in Fig. 4.40, it can be observed that the nano grains have an ellipsoid shape and are about 10 nm in size. Almost all the grains have acquired similar shape and size.

4.3.2.2.2 Evaluation of mechanical properties
The mechanical properties of the cryo-rolled composite samples such as hardness, UTS, YS and elongation were determined as per the procedures discussed in section 3.5. The hardness was taken on the rolled surfaces and the tensile testing was done on the samples in the rolling direction.

Fig. 4.41 shows the hardness variation of the cryo-rolled composite samples with varying amounts of yttrium. Rolling induced a large number of dislocations in the composite, whose movement became difficult with reduction in grain size, dispersion of reinforcement and precipitates, hence increased the hardness of the composite samples. The cryogenic temperature played an important role in suppressing the re-crystallization and grain growth, retaining the grain size during and after rolling by absorbing the heat energy responsible for grain growth.
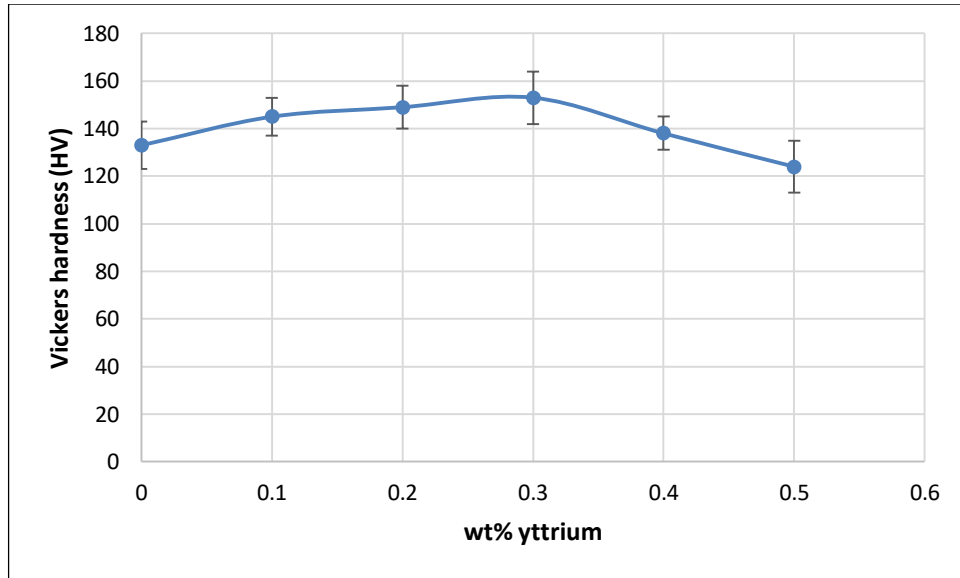
Fig. 4.41 Hardness variation in SPSed and cryo-rolled composite samples reinforced with micro yttrium.

The hardness of the cryo-rolled composite samples followed the same trend as the hardness of the composite samples developed through other processing techniques, discussed earlier. The hardness achieved can be attributed to the increase in dislocation density due to rolling. A highest hardness of 153 HV is achieved for the spark plasma sintered and cryo-rolled composite sample with 0.3 wt% yttrium addition. With further increase in yttrium reinforcement, the hardness tended to decrease. Compared to the hardness of the composite samples developed through stir casting, cold compaction and spark plasma sintering, cryo-rolled composite samples exhibited significant increase in hardness.

Tensile samples were cut from the spark plasma sintered and cryo-rolled composite samples and the tensile test was done according to the procedure discussed in the section 3.6. The UTS and YS of the cryo-rolled composite samples are shown in Fig. 4.42. It can be noted that both the hardness and tensile properties of the cryo-rolled composite samples followed the same trend of variation as the un-rolled composites samples. The UTS and YS of the spark plasma sintered composite samples increased remarkably by cryo-rolling. Compared to unrolled spark plasma sintered composite samples, there was an increase in both UTS and YS of the cryo-rolled composite samples. However, unlike the un-rolled composite samples, the decrease in tensile strength was steep.

The highest UTS and YS reached up to 572 MPa and 539 MPa respectively for the cryo-rolled composite sample with 0.3 wt% yttrium reinforcement. With further increase in yttrium reinforcement, the UTS and YS decreased. The variation in the elongation of the cryo-rolled composite samples with respect to yttrium addition is shown in Fig. 4.43.
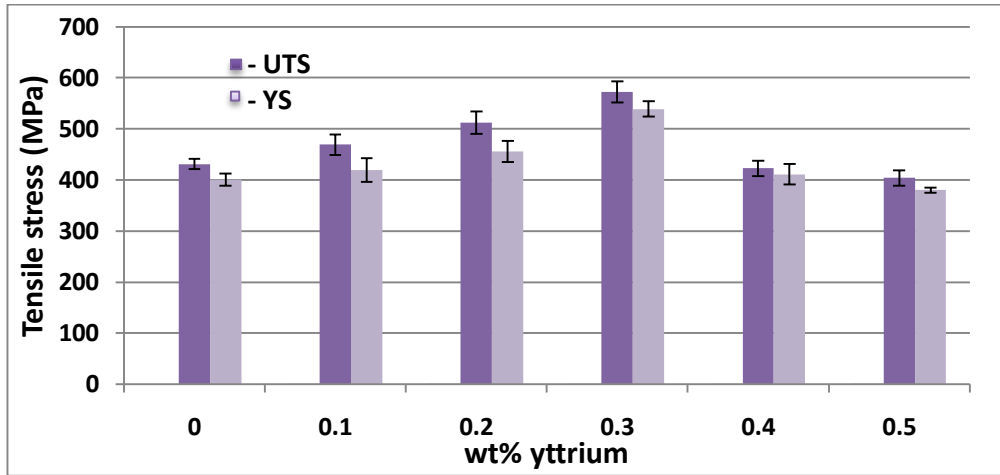
Fig. 4.42 Variation of UTS and YS for the SPSed and cryo-rolled composite samples reinforced with varying amounts of micro yttrium.

From Fig. 4.43, it can be observed that the elongation increased up to 0.3 wt% yttrium reinforcement and tended to decrease thereafter. The highest elongation achieved in the cryo-rolled composite sample with 0.3 wt% yttrium reinforcement was 4.6%. Compared to the un-rolled spark plasma sintered composite samples and the composite samples developed through stir casting and cold compaction, the elongation of the cryo-rolled composite samples at fracture was considerably less. Hence, cryo-rolling should be followed by heat treatment to increase the ductility of the composite samples to a reasonable level.
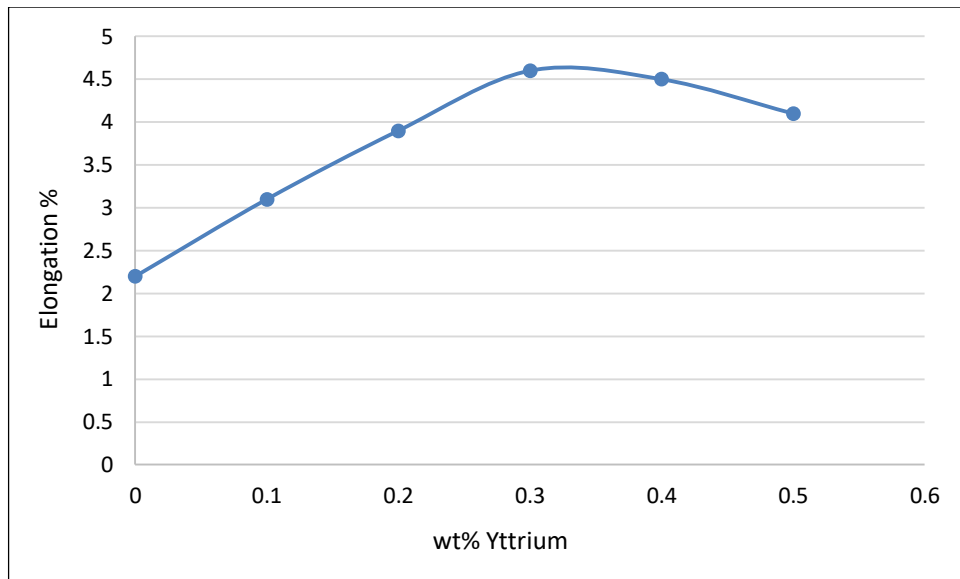
Fig. 4.43 Variation of percentage elongation of SPSed and cryo rolled composite samples reinforced with varying amounts of micro yttrium wt%.

4.3.2.3 Discussion

The use of cryogenic treatment to improve the mechanical properties of metals and alloys has been developed during the period 1960-70. Recently, the application of cryo treatment, especially cryo rolling, has spread in developing various composite materials.

The main drawback encountered in the products processed through powder metallurgy is porosity. Decrease in green density due to improper application of pressure and decrease in sintered density due to poor sintering conditions lead to increase in porosity and decrease in density. Consolidation of the AA2024 + micro yttrium powders through spark plasma sintering has dramatically increased the density of composite samples as discussed in section 4.3. Further, cryo rolling of these spark plasma sintered composites led to the suppression of the voids and hence, full densification could be achieved.

From Fig. 4.36, the grains and grain boundaries of the composite samples after cryo rolling can be observed. Compared to the starting powder, it has an average size of 60 μm, the cryo rolled grains exhibit typical hexagonal shape due to rolling. The hexagonal structures of the grains denote the uniform pressure/compression applied during rolling. The formation of smaller and equal sized grains increased the strength of the composite according to the Hall Petch relation. Rolling includes compressive stress on the material, which crushes the larger grains into several smaller grains. The grains also tended to elongate in the direction of rolling and broke into

133

number of smaller grains, as shown in Fig 4.37. During rolling, high amount of heat was developed in the material, which helped the grains to retain their size and shape to an extent, by the dynamic re-crystallization, followed by grain growth. In cryo rolling, the material was at cryogenic temperature and, hence, all the heat developed during rolling was dissipated according to the third law of the thermodynamics, supressing the dynamic recrystallization step.

It has been observed from the previous section 4.3 that the reinforcement of yttrium to AA2024 matrix and processing through spark plasma sintering caused grain size reduction in the composite samples. The same composite samples after cryo rolling also exhibited a great deal of grain size reduction. The hardness of the cryo-rolled composite samples increased with an increase in the yttrium reinforcement up to 0.3 wt% and tended to decrease with further increase. There was a clear trend of increase and subsequent decrease in the hardness since the cryo rolling parameters were same for all the composite samples. Hence, the change in the hardness was clearly because of the yttrium reinforcement. The effect of yttrium reinforcement on the mechanical properties was discussed in the previous sections 4.3.3 and 4.4.3. However, the hardness variation can be explained by the Hall Petch relation [188]. The grain size of the cryo rolled samples reduced with the reinforcement of yttrium up to 0.3 wt% and hence the hardness increased. Beyond 0.3 wt% yttrium reinforcement, the grain size tended to increase and so the hardness decreased.

There have been various strengthening mechanisms that contribute to the increase of the strength of the cryo-rolled composite samples. The following are the strengthening mechanisms that are active in the present cryo rolled composite samples.

a) Solid solution strengthening
b) Strengthening by grain refinement or grain boundary strengthening
c) Dislocation strengthening
d) Dispersion strengthening

It is well known that the above mentioned strengthening mechanisms do not contribute equally in the composite samples, but the overall strength of the composite is the cumulative effect of all the strengthening mechanisms. However, calculating the strength induced by the each

mechanism individually is complicated as the composite has a complex structure and more number of variables.

From Fig. 4.42, it can be observed that the UTS and YS also have increased remarkably by cryo rolling. The tensile strength achieved in the cryo rolled composite samples were almost twice the tensile strength of the un-rolled composite samples. Due to cryo rolling, homogeneous microstructure was achieved with equal size grains throughout. The main mechanisms involved in the strengthening of the cryo-rolled composites were grain boundary strengthening and dislocation strengthening. Both the mechanisms were greatly initiated and activated by cryo-rolling. Cryo-rolling decreased the grain size and induced high density of dislocations in the composites.

Yttrium also plays an important role in the matrix by providing dispersion strengthening but the contribution is very little, as the reinforcement of yttrium is very less.

From Fig. 4.39, we can observe the dislocation density and increase in grain boundaries in the composite samples subjected to cryo-rolling. Fig. 4.40 shows a decrease in grain size and uniform distribution of grains with the reinforcement of 0.3 wt% yttrium. As discussed in previous sections 4.3.3 and 4.4.3, an optimum amount of yttrium reinforcement to the AA2024 matrix creates favourable conditions for the cryo-rolling to modify the grain structure to ultrafine and nano structure and activate the strengthening mechanisms within the composite to achieve superior mechanical properties.

The percentage of elongation of the composite samples decrease dramatically due to cryo-rolling effect. The strength of the composites is achieved at the cost of ductility.

4.3.2.4 Conclusions

The following conclusions can be drawn from the results obtained in the present experimental work.

- Five composite samples including the un-reinforced AA2024 sample developed through SPS were successfully cryo-rolled to 50% reduction.

- Cryo-rolling induced high amount of dislocation density and significantly decreased the grain sizes throughout the microstructures of the composite samples.

- Dual grains of different sizes were observed in the cryo-rolled composite samples. A combination of ultrafine grains and nano grains were present together in the microstructures.

- The grain sizes of both the ultrafine grains and nano grains got reduced with the reinforcement of yttrium up to 0.3 wt%. With further increase in yttrium reinforcement, both the grains tended to coarsen.

- The mechanical properties of the composite samples increased due to cryo-rolling. The hardness, UTS and YS of the composite samples varied with the variation in respective grain sizes.

- The highest hardness, UTS and YS achieved were 153 HV, 572 MPa and 539 MPa respectively for the cryo-rolled composite sample reinforced with 0.3 wt% yttrium.

- The highest hardness, UTS and YS achieved for the cryo-rolled composites were 115%, 132% and 134% higher compared to those of the unreinforced cryo-rolled sample and 134%, 147% and 157% higher compared to those of the unrolled composite reinforced with 0.3 wt% yttrium.

- The mechanical properties of the cryo-rolled composite samples increased at the cost of ductility. The ductility of the composites decreased dramatically by cryo-rolling.

4.4 Development of AA2024 + nano yttrium composites using spark plasma sintering

In this section, fourth batch of composites comprising of five different composite samples were developed by reinforcing varying amounts of nano yttrium ranging from 0.1-0.5 wt% to the AA2024 matrix. An unreinforced sample was also developed as a bench mark to evaluate the effect of yttrium reinforcement. The composite samples were processed through spark plasma sintering. The results corresponding to density, metallurgical characterization, mechanical evaluation are presented in detail. Various results are discussed in the light of improvement in mechanical properties of the composites developed. At the end, the conclusions drawn from the present work are presented.

4.4.1 Experimental work

Using spark plasma sintering, another set of composite samples were developed by reinforcing nano yttrium to AA2024 matrix. Five AA2024 matrix nano composites were developed with varying wt% of nano yttrium reinforcement. The intended compositions of the nano composites are shown in Table 3.2. The as-received micro yttrium was ball milled for 60 hours to reduce its size to nano level. The constituent powders were blended in a planetary ball milling machine at low speed to uniformly mix both the powders, as discussed in the section 3.1.3.

The blended powder samples were sintered using SPS with the parameters as discussed in section 3.2.3. The spark plasma sintered nano composite samples are shown in Fig. 4.44.

Fig. 4.44 Spark plasma sintered nano composite samples starting from top left.

4.4.2 Results

4.4.2.1. Investigation of microstructure

The composite specimens were polished, etched and observed under an optical microscope. Fig. 4.45 shows the optical microstructures of the composite samples, which show clear grain boundaries and black speckles that were formed due to corrosion and exfoliation of the intermetallic phases after metallographic etching. The grain size of the nano composite samples reduced with an increase in reinforcement of yttrium. However, after 0.3 wt% of yttrium reinforcement, the grain size tended to increase. The secondary Al-Cu phase and the intermetallic phases that were formed during sintering, played an important role in altering the mechanical properties of the composites.

138
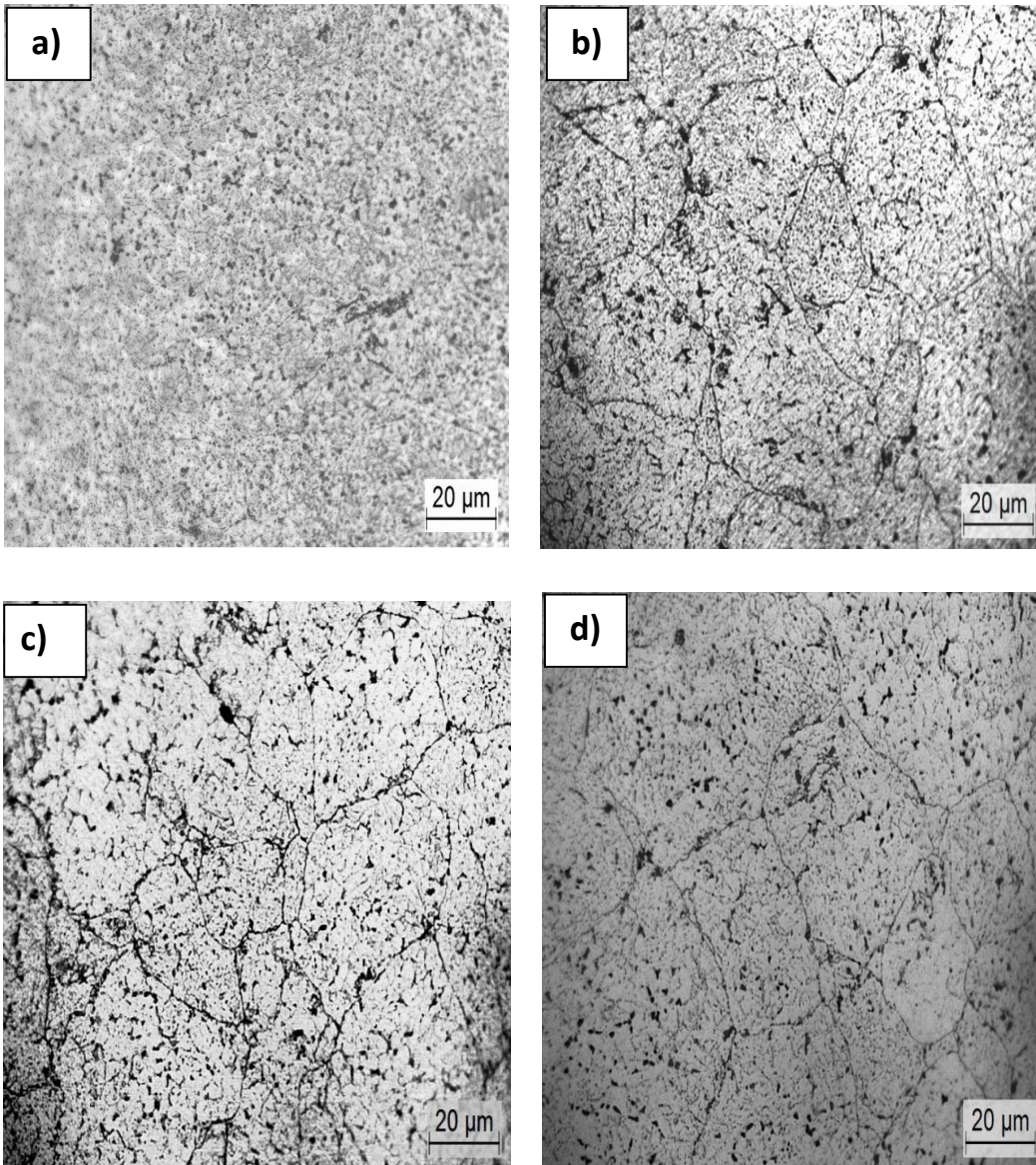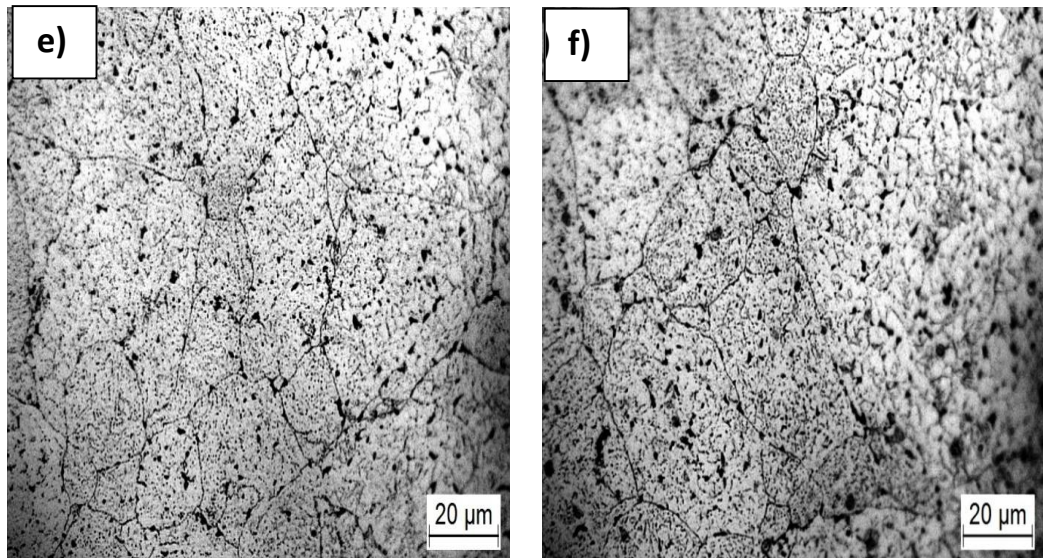
Fig. 4.45 Optical microstructures of spark plasma sintered AA2024 matrix unreinforced/nano composites reinforced with (a) 0.0 wt% nano Y, (b) 0.1 wt% nano Y, (c) 0.2 wt% nano Y, (d) 0.3 wt% nano Y, (e) 0.4 wt% nano Y and (f) 0.5 wt% nano Y.

The FE-SEM microstructures of the composite samples are shown in Fig. 4.46. The microstructures were captured in back-scatter mode to focus on the precipitation and other associated intermetallics that were formed during sintering including the growth, size and distribution of the precipitates in AA2024 matrix. The presence of yttrium particles in the composites caused strain concentrations and non-uniform dislocations at the Al/Y interface and in the matrix region close to the interface. These dislocations could provide pipe diffusion paths for the solute atoms and thus altered the ageing corresponding kinetics.
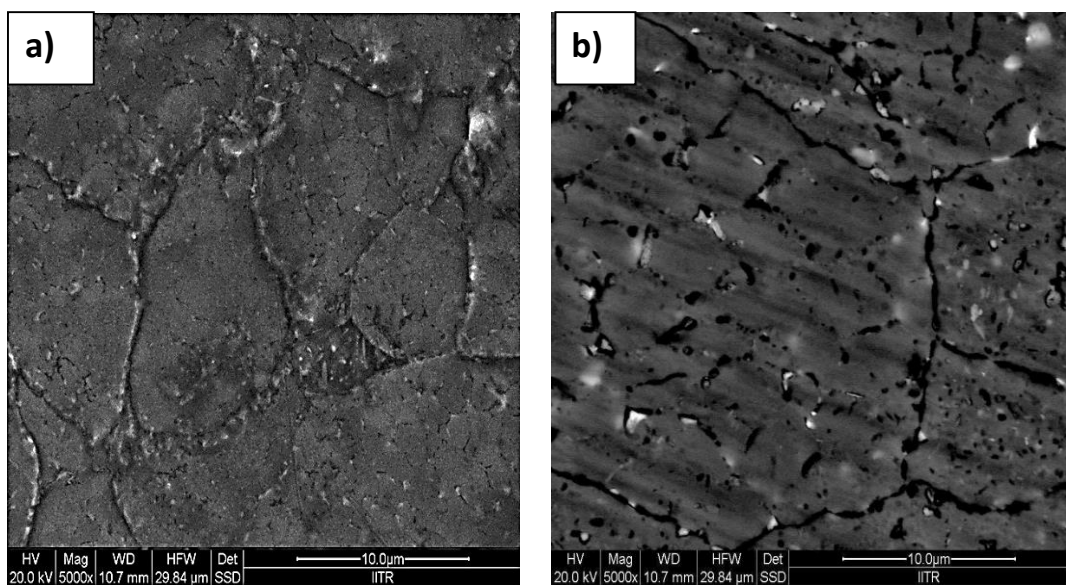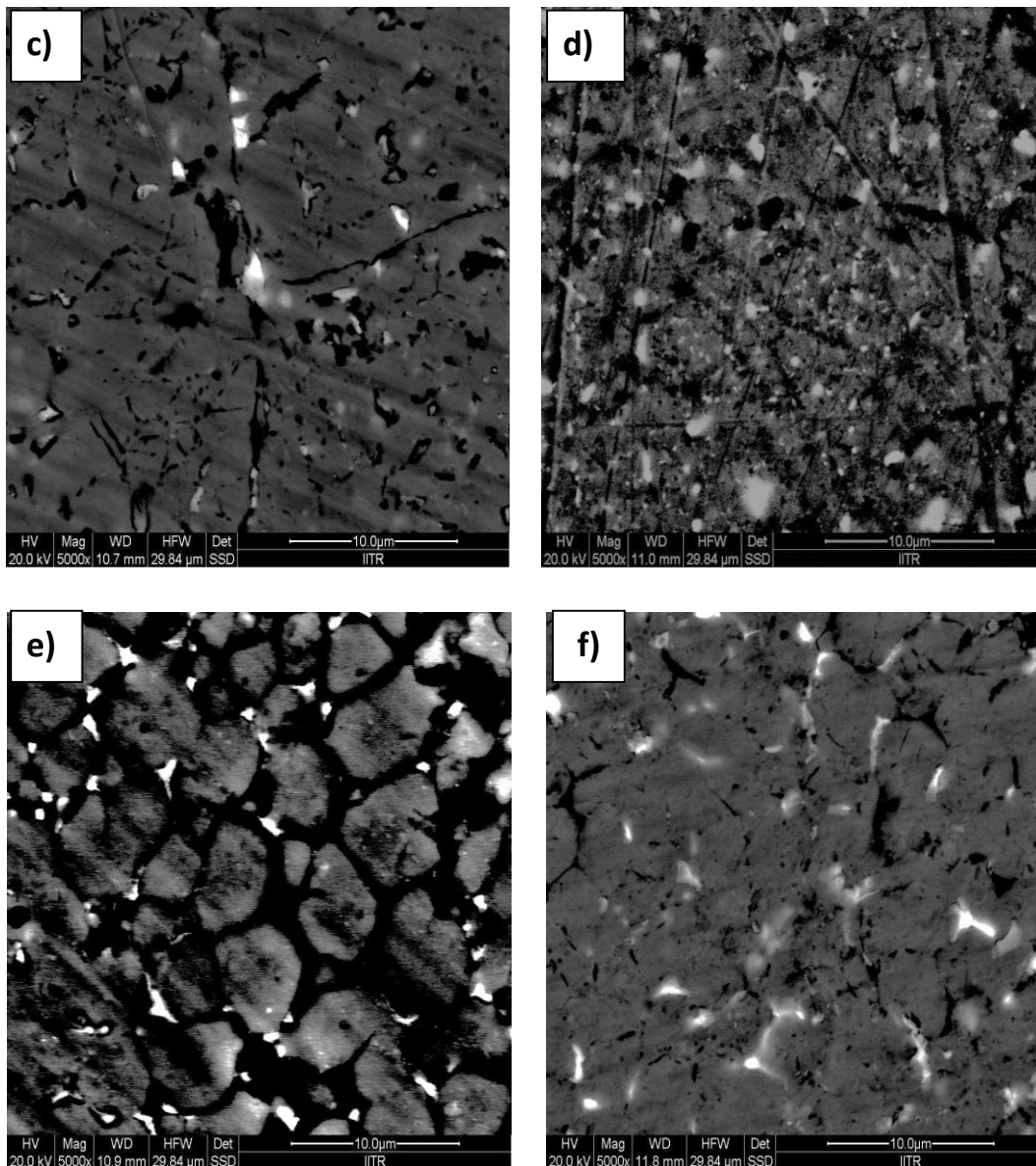
Fig. 4.46 FE-SEM microstructures showing precipitation and grain refinement in AA2024 matrix unreinforced/nano composites reinforced with (a) 0.0 wt% nano Y, (b) 0.1 wt% nano Y, (c) 0.2 wt% nano Y, (d) 0.3 wt% nano Y (e) 0.4 wt% nano Y and (f) 0.5 wt% nano Y.

The precipitation increased as the yttrium reinforcement was increased up to 0.3 wt% and started to coarsen with further increase. It is surprising to observe that the composite specimens exhibited grains of size about 10µ much smaller than the starting powders confirming that the initial dentric structure of the aluminium particles has been refined. It is contradictory to the fundamentals of sintering and densification, which state that during sintering, the powder particles diffuse together leading to grain growth [10-17]. The Al_2Cu precipitation increased from less than a micron to a few microns as the yttrium reinforcement increased above 0.3

wt%. The intermetallic growth and its agglomeration around the grain boundaries can also be seen contracting in the microstructures.

After tensile testing, the fractured surfaces of the composite specimens were examined by SEM and the corrsponding microstructures are shown in Fig. 4.47. The specimens exhibited a combination of both ductile and brittle failures up to 0.3 wt% yttrium reinforcement. Beyond 0.3 wt% yttrium reinforcement, the specimens exhibited failure, which was of more brittle in nature (shown in black circles). However, cracks (pointed out with red arrows) and grain pull out (shown in red circles) were observed in all the samples.
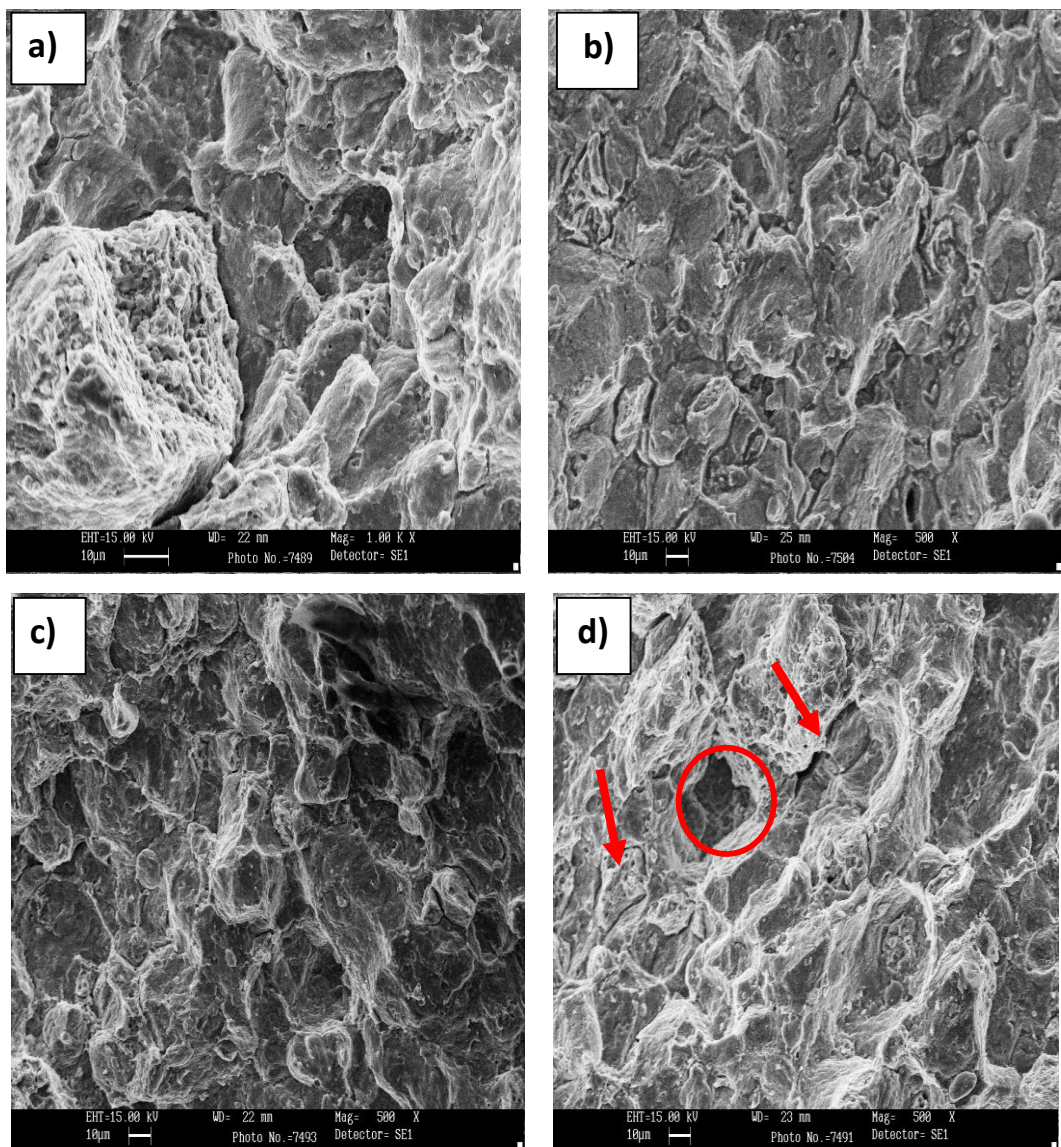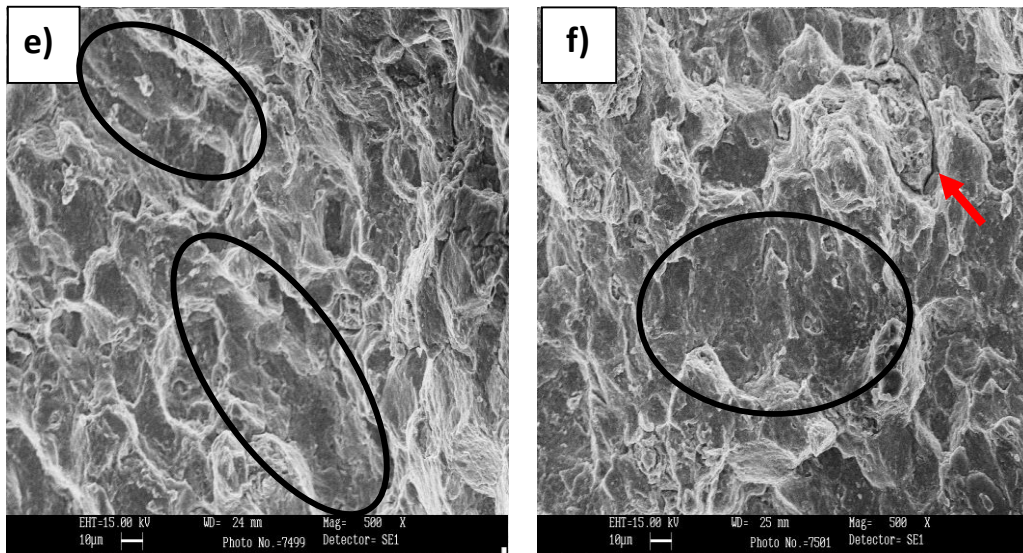
Fig. 4.47 SEM images of fractured surfaces of AA2024 matrix nano composite samples reinforced with (a) 0.0 wt% nano Y, (b) 0.1 wt% nano Y, (c) 0.2 wt% nano Y, (d) 0.3 wt% nano Y, (e) 0.4 wt% nano Y and (f) 0.5 wt% nano Y.

4.4.2.2 Density measurement

The composite samples have achieved almost full densification as seen in Fig. 4.40. Though there is a slight variation in the relative densities of the composite samples, the variation can be neglected as it is very small. However, relative densities of these nano yttrium reinforced composites are slightly lower than those of the composites reinforced with micro yttrium. Agglomeration of yttrium nano particles during processing and consolidation might be the reason for density drop. Since both the aluminium and yttrium are conducting powder materials, it is the intense Joul heating effect from the electric pulsed current that led to neck formation. If at all there is spark/plasma, it plays a role of cleaning the particle contact surfaces, thus providing favorable path to the electric current, leading to better densification. The relative density tended to increase with an increase in reinforcement of nano yttrium up to 0.4 wt% and then decreased. However, the relative density of the nano composites increased when ccompared to that of the unreinforced SPSed composite which was 99.75.
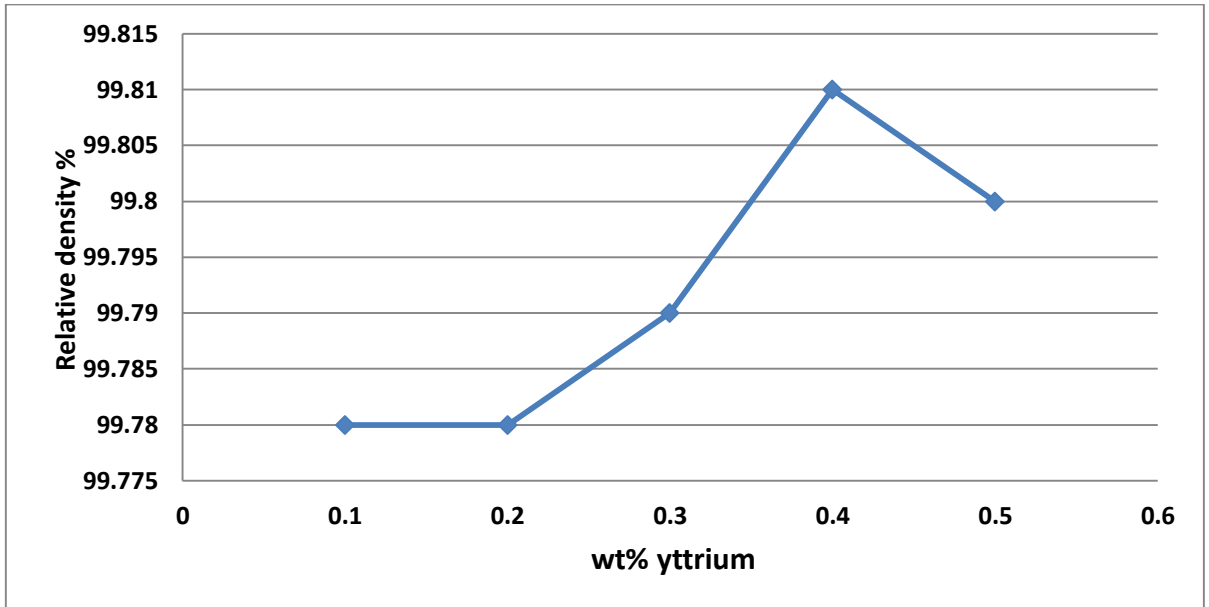
Fig. 4.48 Variation of relative density of the spark plasma sintered composite samples reinforced with varying amounts of nano yttrium.

4.4.2.3 Evaluation of mechnical properties

Fig. 4.49 shows variation of hardness of the composite samples with yttrium reinforcement. The Vikers hardness increased with an increase in reinforcement of nano yttrium up to 0.3% by weight and tended to decrease as the yttrium reinforcement was increased further. The Vickers hardness of unreinforced SPSed sample was 101 HV. It is intresting to observe that the hardness of the nano yttrium reinforced composites followed the same trend as that of the micro yttrium reinforced composites. The variation of hardness in the nano composite samples can be attributed to a number of hardening mechanisms. The decrease in grain size through grain refinement also contributed to the hardening effect by resisting dislocation movement.
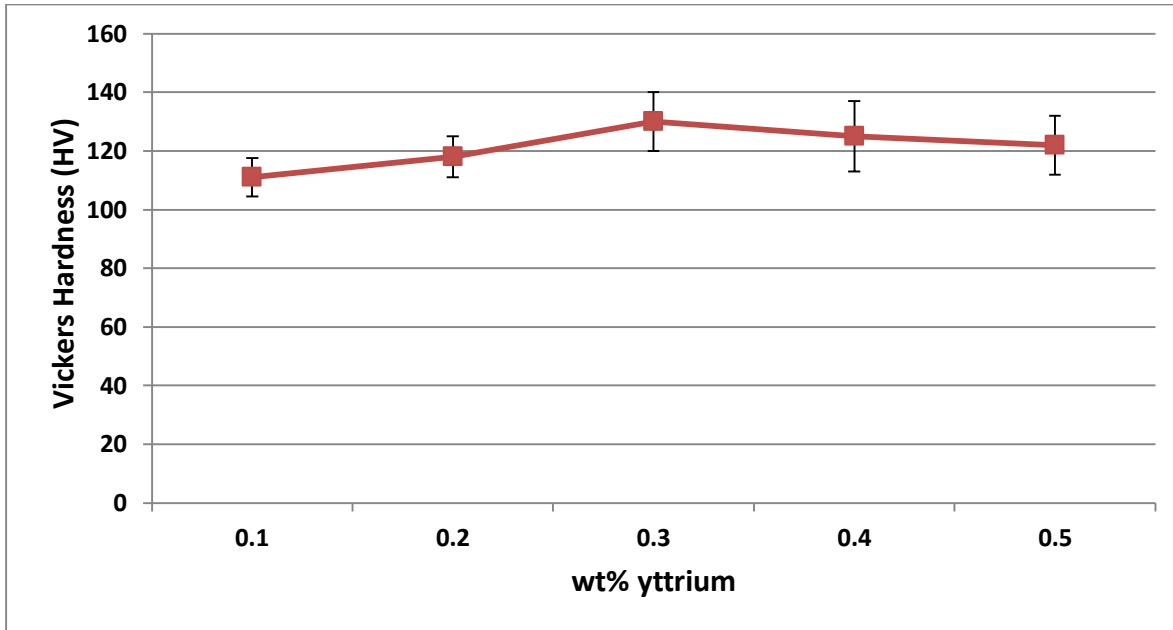
Fig. 4.49 Variation of hardness of the spark plasma sintered composite samples reinforced with varying amounts of nano yttrium.

Fig. 4.50 shows the tensile behaviour of the nano composite samples with varying reinforcement of nano yttrium. The values of tensile strength at fracture (Ultimate tensile strength) and the yield strength at 0.2% offset strain are shown together for each composite sample.
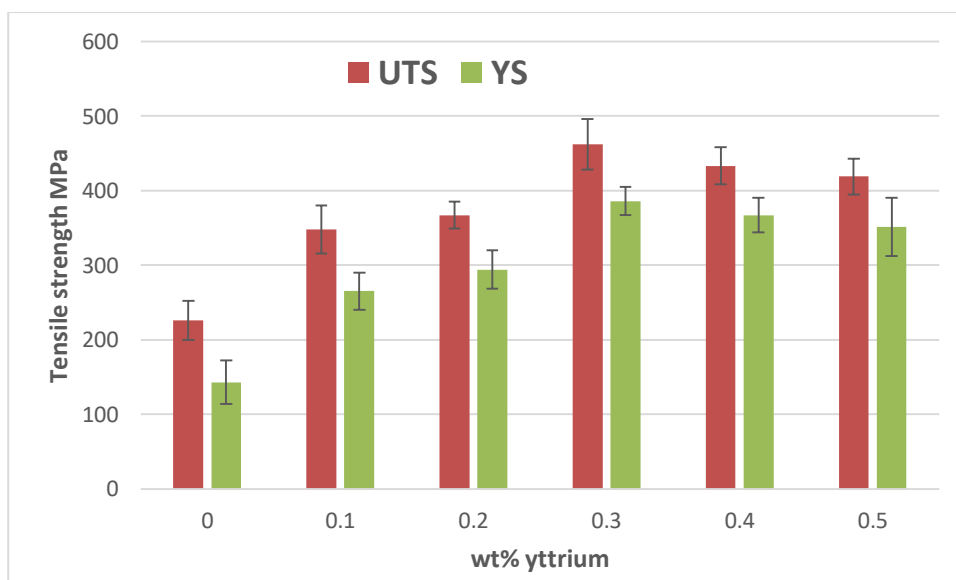
Fig. 4.50 Variation of UTS and YS of the spark plasma sintered composite samples reinforced with varying amounts of nano yttrium.

The UTS and YS increased with an increase in nano yttrium reinforcement up to 0.3% by weight and decreased with further reinforcement. The UTS and YS of the composites followed the same trend, followed by its micro yttrium reinforced counterparts. Fig. 4.51 shows a comparison between UTS of the composite samples reinforced with micro yttrium and nano yttrium, processed through SPS.
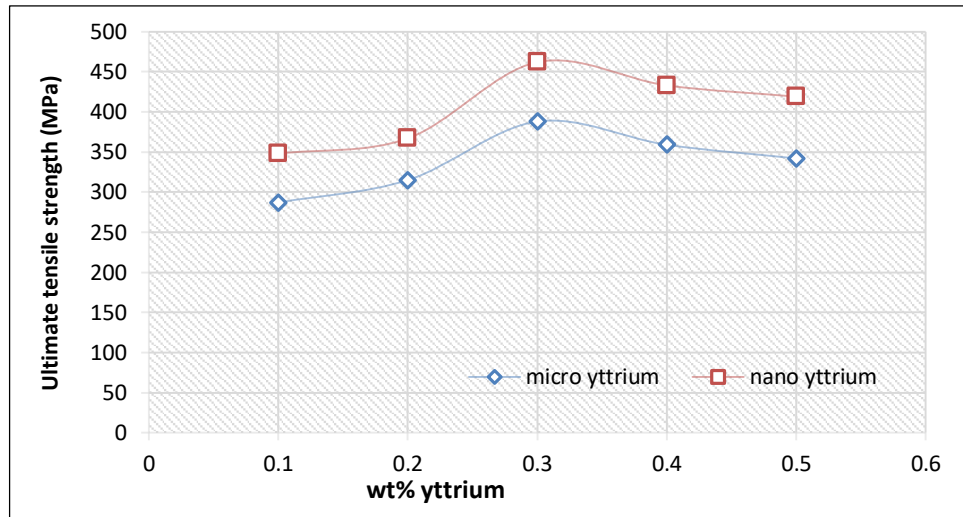
Fig. 4.51 Comparison between UTS of the SPSed composite samples reinforced with varying amounts of micro yttrium and nano yttrium.

Fig. 4.52 shows a comparison between YS of the composite samples reinforced with micro yttrium and nano yttrium, processed through SPS.
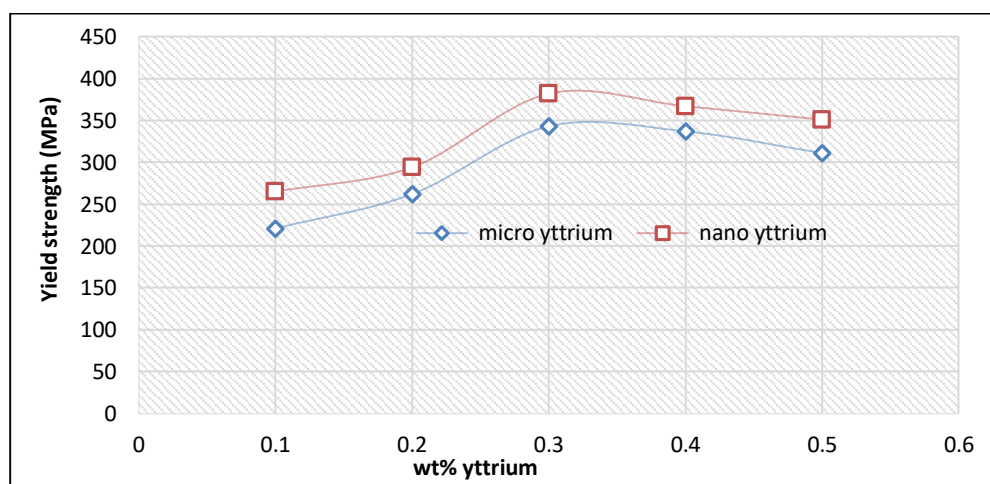
Fig. 4.52 Comparison between YS of the SPSed composite samples reinforced with varying amounts of micro yttrium and nano yttrium.

From Fig. 4.51 and 4.52, it can be observed that the nano composites show better strength than their micro yttrium reinforced counterparts for the same wt% of yttrium reinforcement.

Fig. 4.53 shows the variation of elongation% of the SPSed composite samples with the reinforcement of nano yttrium. Compared to their micro yttrium reinforced counterparts, the elongation of the nano composites has decreased. However, the trend of variation did not change. The formation of aluminium-yttrium based intermetallic compounds and Al_2Cu precipitations from the matrix made the nano composite samples brittle, owing to a decrease in ductility.
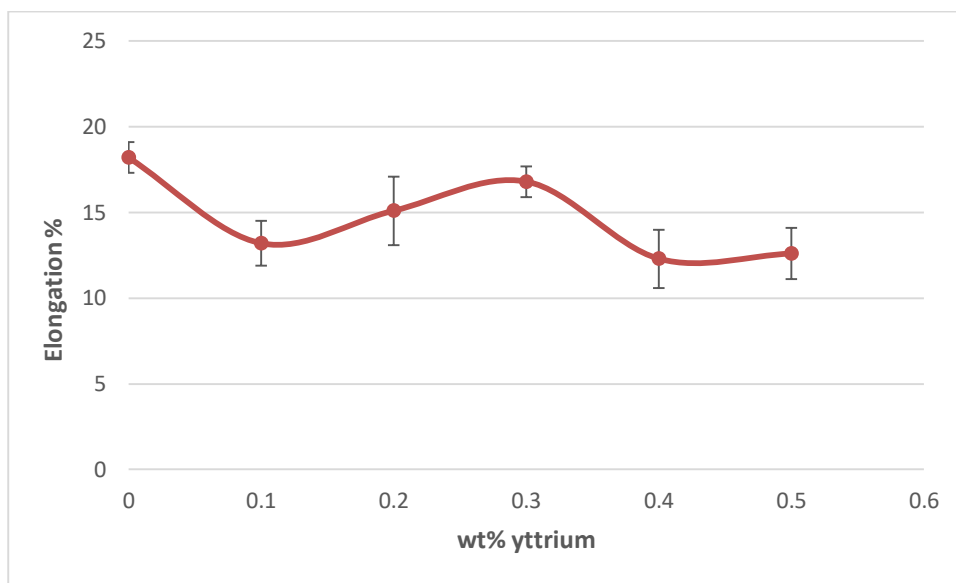
Fig. 4.53 Variation of % elongation of spark plasma sintered AA2024 matrix unreinforced/nano composite samples reinforced with varying amounts of nano yttrium.

4.4.3 Discussion

Due to the extremely high temperature generated at the particle interface, melting/vaporization of the particle-contact zones occured that led to rapid formation of necks at sintering temperatures much lower than the conventional sintering [176-178]. Consequently, the temperature raise very fast and densification was completed within a few minutes. The simultaneous application of pressure along with the temperature raise mobilize the powder particles to freely flow until they hit the neighbouring particles and hence minimised voids in the sintered composite sample. **Song et al.,** [150] proposed a self adjusting mechanism for conducting powders that controls the uniform distribution of neck growth through out the composite sample by re-distributing the current intensity.

As discussed earlier about the trend of variation in hardness, the important underlying reason for the trend in the present nano composites is the tendency of nano yttrium particles to agglomerate as the nano yttrium reinforcement increase beyond 0.3% by weight. Due to agglomeration, the particles became too large to offer dispersion hardening. Though the precipitates were hard and brittle in nature, as their size increased, their hardening effect fades away. For the same percentage of yttrium reinforcements, nano yttrium reinforced composites showed higher values of hardness compared to their micro yttrium reinforced counterparts. Excessive reinforcement of nano yttrium caused non-homogeneous dislocation density regions in the matrix due to nano particles clustering, resulting in an increase in the internal stress at the particle interface and decrease in the hardness. The highest hardness was achieved in the nano composite with 0.3 wt% yttrium reinforcement, which is 130 HV.

The strength variation mechanisms for the nano composites can be explained in the same lines as the hardness values i.e. the increase dislocation formation, due to difference in coefficient of thermal expansion values of the matrix and reinforcement, as the reason for the increase in the hardness. The tendency of nano yttrium to form agglomeration at higher volume fractions is the reason for the decrease in hardness beyond 0.3 wt% yttrium reinforcement. It is well known that for a given weight percent, the number of particles in the nano size is much higher than those in the micro size. Since the number of particles is very high in nano yttrium powder, they could cause a large amount of dislocation formation, depending on their distribution in the matrix. These dislocations became nucleating sites for precipitation and the strain field caused diffusion of Al_3Y at the interface.

Reinforcement of nano yttrium refined and modified the microstructure and reduced the grain size to less than 10 μm in the nano composite samples, while micro yttrium reinforcement had little effect on grain refinement. The additional strength achieved in the nano composite samples could be justified by grain size reduction, by referring to the standard Hall-Petch equation [188]. The equation suggests that the strength is indirectly proportional to the grain size. However, the previous studies on various composites sintered through SPS reveal that grain refinement is quite possible and this possibility is attributed to the pulsed high current used in SPS.

While the mechnism of SPS is not yet completely understood, it is generally accepted that the sintering/densification in SPS process is due to the sparks induced by the electric field at

weakly linked particles of the green compact, such as pores and micro cracks. The sparks are likely to increase the temperature to several thousand degrees celsius for a brief moment, which could cause the particles to melt and join together. The extremly high temperature and temperature gradient cause rapid mass transport and densification.

With this sintering mechanism, it is clearly evident from the analysis in previous section that the reinforcement of micro yttrium refined the microstructure to some possible extent. Therefore, the reinforcement of nano yttrium played an enhanced role in the microstructure refinement. Although, the role of nano yttrium in the refinement of microstructure is yet to be clearly understood, a reasonable explanation can be derived from a simillar work done by other researchers using SPS. The refinement in microstructure could be due to a melting re-crystalization process. The particle is first melted at the surface by spark and then recrystalized into smaller grains due to short sinterting time employed in SPS. The entire SPS processing lasted for less than 20 minutes, which is sufficient to avoid the growth of the newly formed smaller grains. This sintering process gives raise to a combination of smaller grains at the particle-particle contact point and bigger grains within the particle. The pulse high current used in SPS can generate a local electric discharge, which momentarily releases a large amount of electrons that have accumulated on the surface of the particles. This forms a momentary electric current within these localized areas. It is known that a material carrying the electric current experiences the Lorentz force and thermal stress due to joule heating. This force/stress can cause a strain field and deform the material and this deformation could be severe plastic deformation. It is possible that the microstructure refining results from such a fatigue process, which in situ ''shatters'' the large starting particles into smaller grains [178, 179]. Owing to the random distribution of the sparks, the stresses are uniformly applied on the material at random time intervals, leading to the formation of the smaller grains.

The intermetallic compounds that are formed due to diffusion of aluminium and yttrium and the compounds precipitated from the matrix play an important role in the variation of UTS and YS of the nano composite samples. The thermal changes caused by the reinforcement of nano yttrium during sintering play a significant role in the grain refinement and phase transformation. Although yttrium is a metal and is a conductor of electricity and heat, compared to aluminium its conductivity is less. During sintering, when high intensity pulsed current is introduced, Joule heating takes place with the heat developed by the resistance offered by the composite powder to pulsed current. Since yttrium has better resistance than aluminium, Joule

heat generated from the resistance offered by yttrium simply adds to the total heat generated. As the yttrium reinforcement increases, the heat input to the powder sample increases and the precipitation of the samples also change. However, the heat developed by yttrium depends on the amount, size and distribution of the yttrium particles. It can be seen from the Fig. 4. 46 that the precipitation from the matrix starts in the composite sample with 0.1 wt% yttrium reinforcement and grows as the yttrium reinforcement increases. The sequence of natural ageing phenomenon in aluminium-copper alloys starts with the super saturation copper atoms in the solid solution. With time, the solute atoms precipitate out from the super saturated solution and the precipitates start to grow. This precipitation can be achieved artificially by supplying heat to the material. The growth of these precipitates entirely depends on the temperature and time interval of the current. Increase in temperature accelerates the growth of these precipitates artificially, but after certain time (known as peak ageing time), coarsening of the precipitates occur.

AA2024 powder is produced through nitrogen gas atomization, in which fine liquid drops undergo rapid solidification to form into powder. The starting powders with which the composite samples are made of already contain super saturated solid solution of aluminium and copper. During SPS, the powder particles simply undergo artificial ageing and densification through necking and plastic deformation. However, **Cooke et al.,** [171] reported that aluminium-copper alloy samples get over aged through SPS. Hence, in the present study it can be understood that the reinforcement used in AA2024 has decelerated the ageing kinetics, which is in agreement with the findings of **Feng et al.,** [180].

Peak UTS and YS are seen in the sample with 0.3 wt% yttrium in which the precipitates are finer and uniformly distributed. Beyond 0.3 wt% yttrium, the precipitates grow in size due to over ageing.

4.4.4 Conclusions

The following conclusions are drawn from the results of the present experimental investigations.

- Five composite samples with AA2024 as the matrix material and varying amounts of nano yttrium as the reinforcement were developed successfully using SPS.

- Reinforcement of nano yttrium was able to refine the microstructure and grain size better than micro yttrium, yielding better mechanical properties in the nano composite samples.

- Highest hardness, UTS, YS and elongation achieved were 130 HV, 462MPa, 382 MPa and 16.8% respectively for the composite with 0.3 wt% yttrium reinforcement. These values were 117%, 120%, 144% and 127% higher respectively compared to the unreinforced AA2024 sample.

- Nano yttrium also altered the precipitation kinetics by increasing Joules heating and dislocation density, which contributed to the improvement of mechanical properties.

- In the present study, it was observed that an optimum reinforcement of nano yttrium (0.3 wt%) created peak precipitation hardening effect, dispersion strengthening and intermetallic strengthening, which lead to highest mechanical properties in the composite sample.

DEVELOPMENT OF AA2024 + YTTRIUM + TiB$_2$ HYBRID COMPOSITE

In this chapter, fifth batch of composites comprising of five different composite samples were developed by reinforcing a constant amount of 1.0 wt% TiB$_2$ and various amounts of nano micro yttrium ranging from 0.1-0.5 wt% with AA2024 matrix. The composite samples were processed through SPS. The details of the materials, instruments and experimentation procedures are incorporated. The results corresponding to density, metallurgical characterization, mechanical evaluation are presented in detail. Various results are discussed in the light of improvement in mechanical properties of the composites developed. At the end, the conclusions drawn from the present work are presented.

5.1. Development of AA2024 + nano yttrium + TiB$_2$ hybrid composite using spark plasma sintering

5.1.1 Experimental work

Five different hybrid composite samples with the intended compositions shown in Table 5.1 are developed by spark plasma sintering through the procedure discussed in section 3.2.3.

Table 5.1 Intended compositions of different composite samples.

Sample No	Micro AA2024 proportion by weight (%)	Nano yttrium proportion by weight (%)	Micro titanium boride proportion by weight (%)
1	98.9	0.1	1
2	98.8	0.2	1
3	98.7	0.3	1
4	98.6	0.4	1
5	98.5	0.5	1

Various metallurgical investigations like SEM, FE-SEM, TEM and mechanical tests like hardness, UTS, YS and elongation have been done according to the procedures discussed in the sections 3.4 and 3.6.

5.1.2 Results

5.1.2.1 Density measurement

Fig. 5.1 shows the variation of density of the hybrid composite samples with an increase in yttrium reinforcement. The theoretical and experimental densities were calculated using the rule of mixtures and Archimedes principle respectively, as discussed in the section 3.3.1. From Fig. 5.1, it can be observed that the relative density of the composite samples decreased (from 99.78 to 99.69%) with an increase in the yttrium reinforcement. However, the decrease was very low and well above 99.5%.
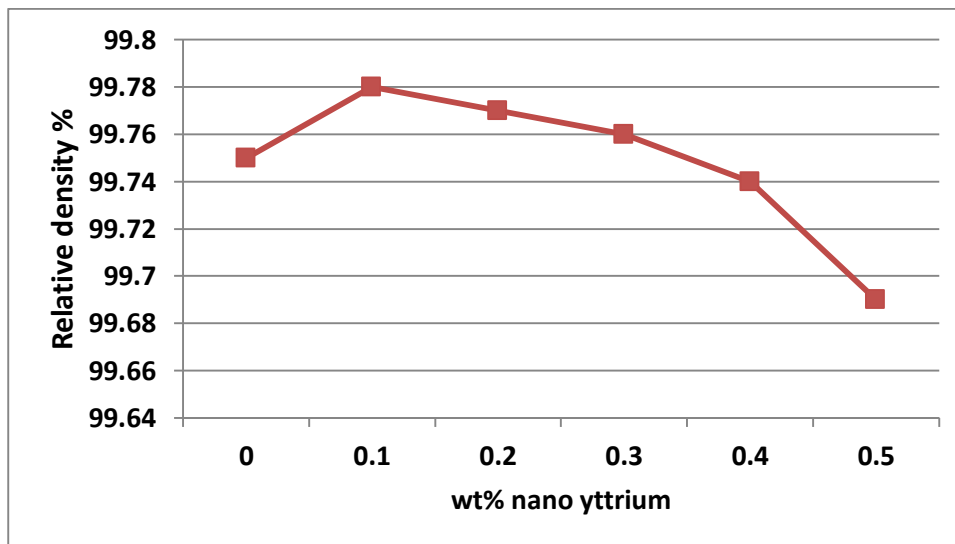
Fig. 5.1 Variation of relative density of unreinforced/hybrid AA2024 composite samples reinforced with 1.0 wt% TiB_2 and varying amounts of nano yttrium.

5.1.2.2 Investigation of microstructure

The hybrid composite specimens were prepared by polishing and etching as discussed in the previous section 3.4 and observed under an optical microscope. The optical microstructures are shown in Fig. 5.2. From Fig. 5.2, some changes in microstructure with the reinforcement of 1.0 % TiB_2 and varying amounts of nano yttrium can be observed.
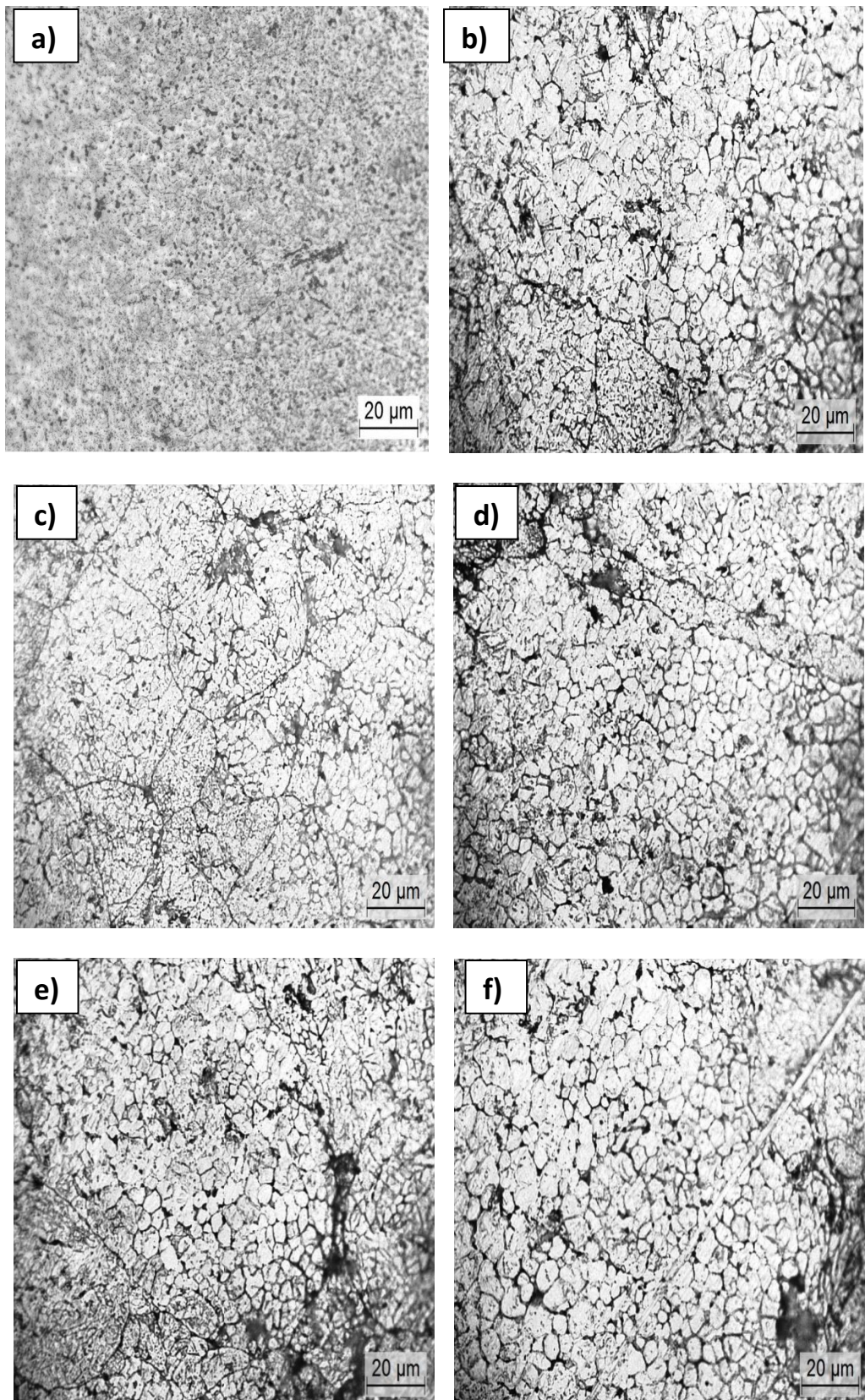
Fig. 5.2 Optical microstructure of unreinforced/hybrid composites reinforced with of 1.0 wt% TiB$_2$ and (a) 0.1% nano Y, (b) 0.2% nano Y, (c) 0.3% nano Y, (d) 0.4% nano Y and (e) 0.5% nano Y.

From the optical microstructures shown in Fig. 5.2, it can be observed that there is a definite grain refinement in all the composite samples. All the hybrid composite samples were reinforced with 1.0 wt% TiB_2 powder of average size 10 μm. Hence, the variation in grain size must be caused by the change in yttrium reinforcement. As it can be seen from the microstructures, the refinement is enhanced with an increase in yttrium % by weight. However, reinforcement of yttrium beyond 0.3% by weight led to grain coarsening. The black spots in the microstructures are observed to be the secondary phases rich in Al and Cu that were formed inside and around the grains during sintering. The original AA2024 grains and the sub-grains formed inside the grains during sintering are clearly visible. Both the particle boundaries and sub-grain boundaries are also visible in the optical microstructures.

Further, the hybrid composite samples have been analysed by FE-SEM and TEM for better understanding. The FE-SEM microstructures of the hybrid composite samples are shown in Fig. 5.3. From these microstructures, the grain refinement at higher magnification that took place in after the sintering can be observed.
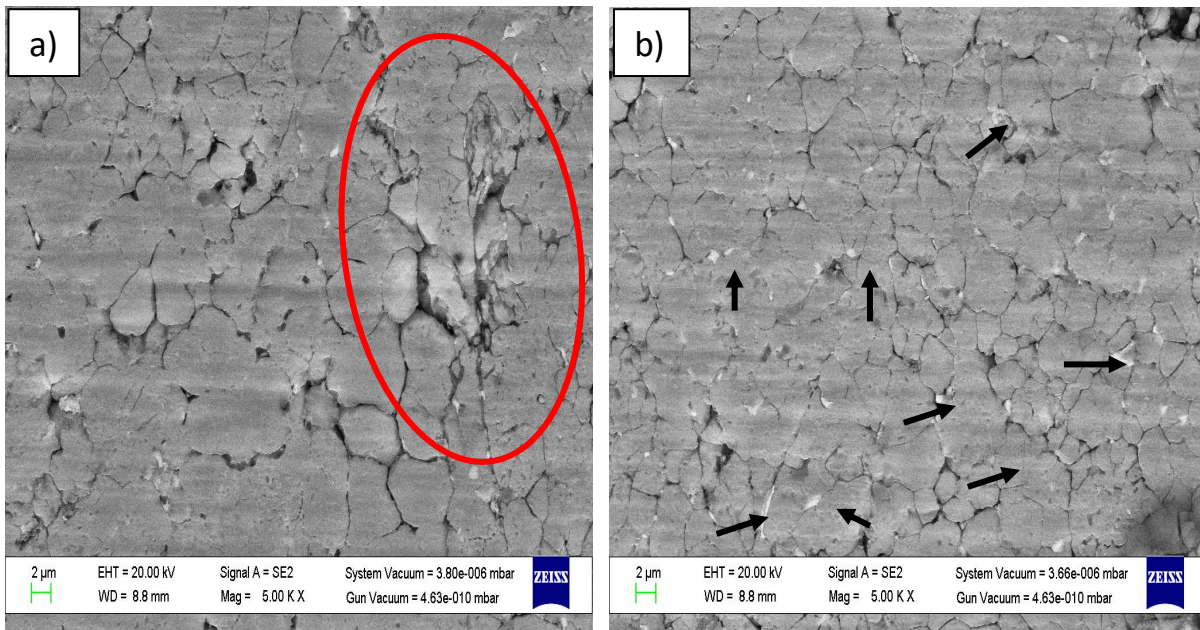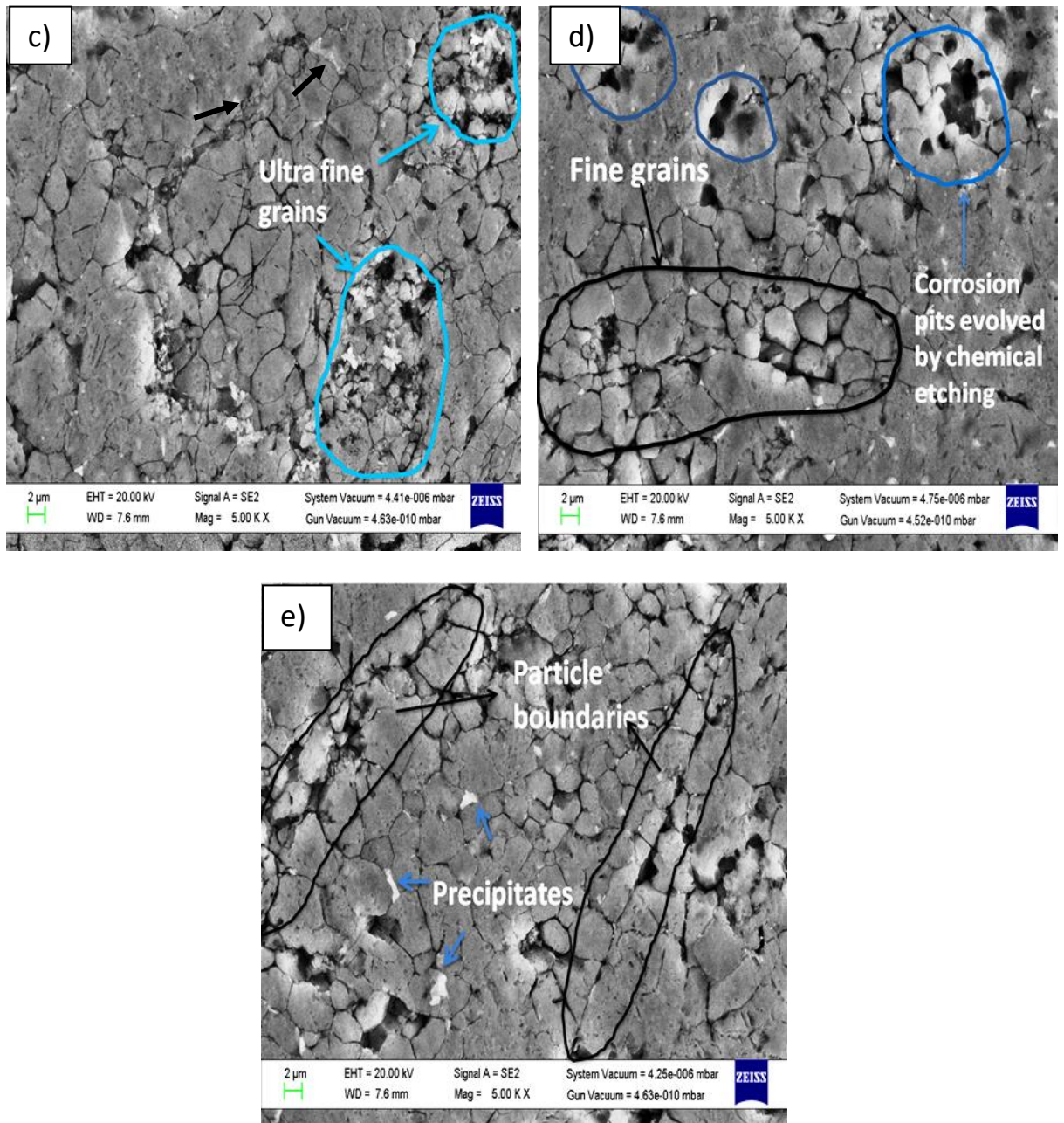
Fig. 5.3 FE-SEM micrographs of AA2024 + 1.0 wt% TiB$_2$ hybrid composite samples sintered with nano (a) 0.1 wt% nano Y, (b) 0.2 wt% nano Y, (c) 0.3 wt% nano Y, (d) 0.4 wt% nano Y and (e) 0.5 wt% nano Y.

From Fig. 5.3 (a), (b) and (c), it can be observed that the effect of grain refinement increased as the yttrium wt% increased. Fig. 5.3 (c) shows that the structure near the particle boundary has transformed into ultra-fine grain region as marked in light blue colour circles. Beyond 0.3 wt% yttrium reinforcement, the ultra-fine grain structure was not found. However, beyond 0.3 wt% yttrium reinforcement, sub-grains are formed and are finely distributed along the particle boundaries as shown in Fig. 5.3 (d), (e). The corrosion pits caused due to

chemical etching can also be seen (encircled in light blue). Fig. 5.3 (e) shows the particle boundaries and sub grains within the particle. The arrows indicate the precipitation growth along the sub-grain boundaries. It can be observed that the ultra-fine grains were developed at the particle-particle interface and spread.

Fig. 5.3 (c) shows the ultra-fine grain formation in the hybrid composite sample reinforced with 0.3 wt% nano yttrium. Fig. 5.4 shows the microstructure of ultra-fine grains formed in the same hybrid composite sample at a higher magnification. The microstructure reveals the presence of different size grains i.e., coarse and ultrafine grains along with grains having intermediate size, indicated in red colour outline. The ultrafine grains are indicated in white colour outline, surrounded by coarse grains and intermediate grains. However, ultra-fine grain structure could not be achieved throughout the matrix.

Fig. 5.4 shows the TEM nanostructures of hybrid composite sample reinforced with 0.3 wt% yttrium.
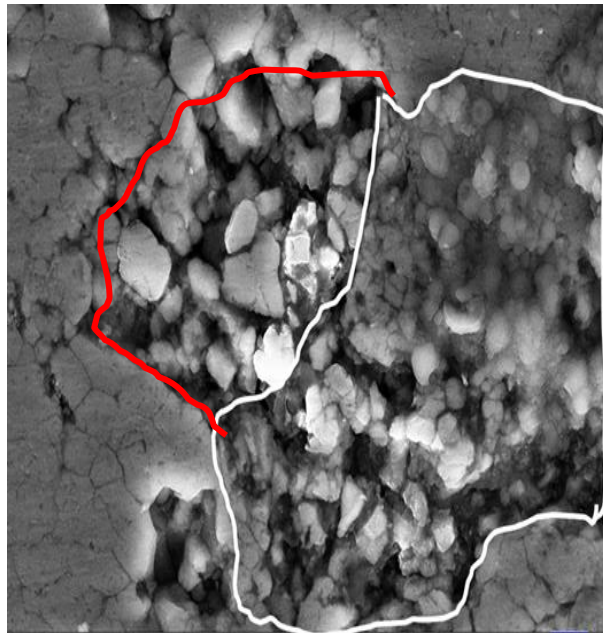
Fig. 5.4 FE-SEM micrograph of AA2024 + 1.0 wt% TiB_2 reinforced hybrid composite with 0.3 wt% nano yttrium showing the formation of ultra-fine grains.

Fig. 5.5 shows the TEM nanostructures of the composite sample reinforced with 1 wt% TiB_2 and 0.3 wt% yttrium. TEM examination reveals that the composite sample reinforced with 0.3 wt% nano yttrium consists of nano grains along with three different kinds of nano precipitates, which are pointed out with different colour arrows. The rod shaped precipitates θ′, indicated with red arrows and the circular platelet precipitates θ″, indicated with light

blue arrows, are coherent and semi-coherent with the matrix. The precipitates, both rod shape and circular platelets have an approximate chemical composition of Al_2CuMg. The hexagonal platelet precipitates Ω, indicated with dark blue arrows, are comparatively bigger in size than the rod shape or circular platelet precipitates. The Ω precipitates are coherent with the matrix and have an approximate chemical composition of Al_2Cu.
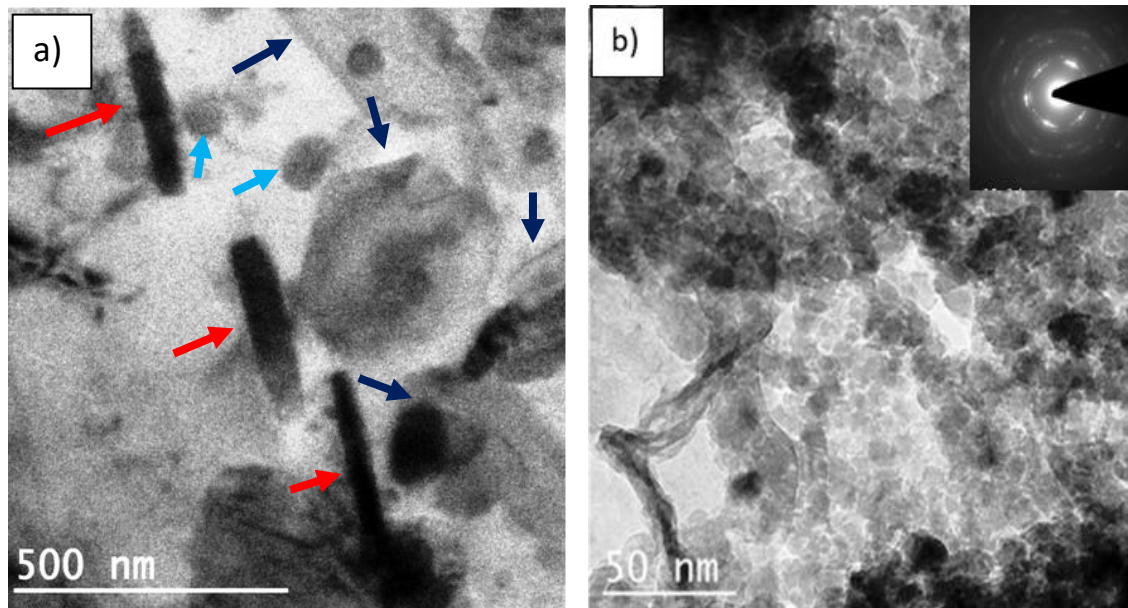
Fig. 5.5 TEM nanostructure of AA2024 + 1.0 wt% TiB_2 hybrid composite reinforced with 0.3 wt% nano yttrium showing (a) different precipitates and (b) nano size grains at higher magnification (insert shows the Selected Area Difraction (SAD) pattern).

Fig. 5.6 shows the TEM nanostructure of hybrid composite sample reinforced with 1 wt% TiB_2 and 0.4 wt% yttrium. From the nanostructure shown in Fig. 5.6 (a), it can be observed that the hexagonal precipitates Ω and the circular platelet θ'' precipitates that were found in the composite sample with 1 wt% TiB_2 and 0.3 wt% yttrium reinforcement have now disappeared. Moreover, only coherent rod shaped precipitates show up and also the Al-Cu-Y intermetallic tended to agglomerate around the rod shaped precipitates, as shown in Fig. 5.6 (a).
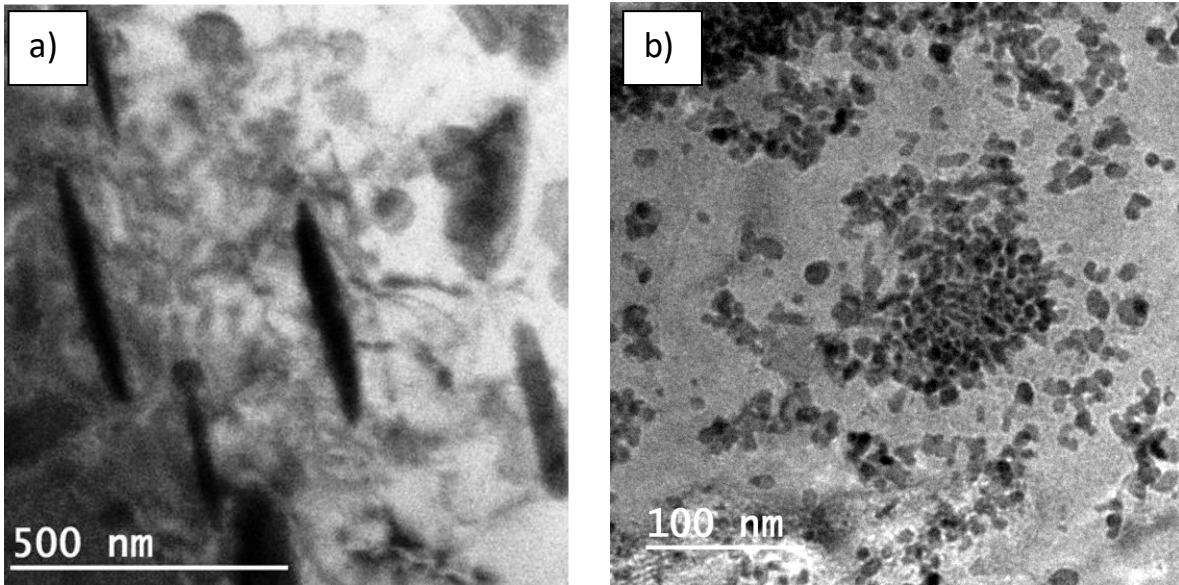
Fig. 5.6 TEM nanostructure of AA2024 + 1.0 wt% TiB$_2$ hybrid composite reinforced with 0.4 wt% nano yttrium showing (a) precipitates and (b) Al-Cu-Y intermetallic agglomeration at higher magnification.

The orientation and interaction between TiB$_2$ powder particles and the AA2024 matrix is shown in Fig. 5.7 (a). Fig. 5.7 (b) shows the intensity graph of the elements shown in Fig. 5.7 (a). Fig. 5.7 (c) shows the cummulative mapping of various elements present in Fig. 5.7 (a). Fig. 5.7 (d), (e), (f) and (g) shows the mapping of the elements titanium, boron, aluminium and copper respectively.
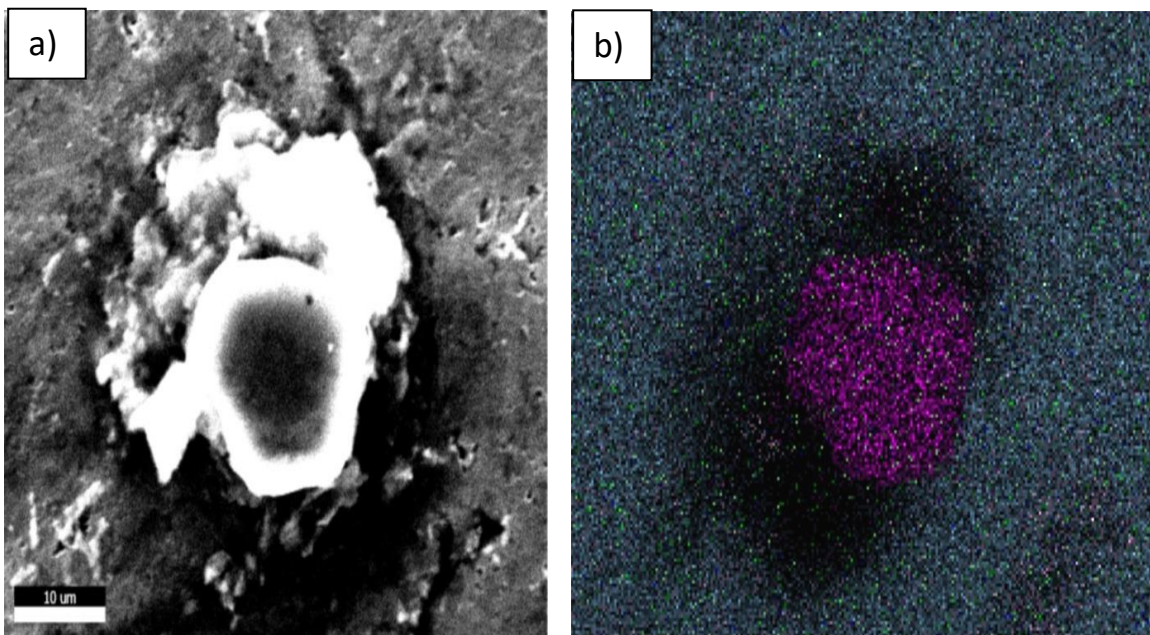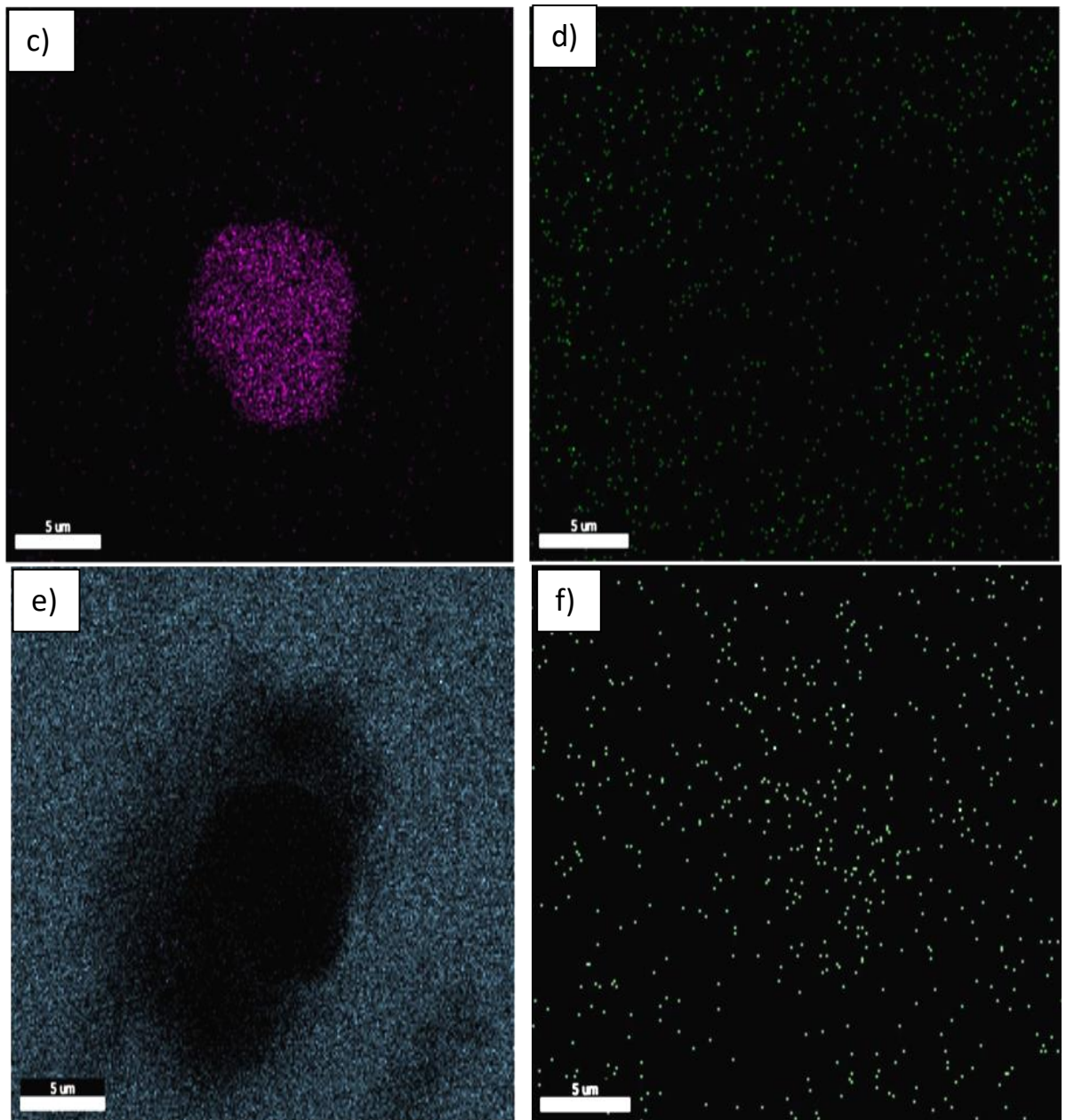
Fig. 5.7 SEM and EDX analysis of the composite showing (a) microstructure showing orientation of TiB$_2$ particle in AA2024 matrix, (b) cumulative mapping of all the elements, elemental mapping of (c) titanium, (d) boron, (e) aluminium and (f) copper.

Table 5.2 shows the approximate weight percentages of various elements present in Fig. 5.7 (a) detected by EDX. Elements like titanium, boron, aluminium, copper, magnesium and yttrium were expected to be present in the area of the sample shown in Fig. 5.7 (a).

Table 5.2 Approximate weight percentages of various elements present
in the area under consideration in Fig. 5.7 (a).

Compound	Weight %	Atomic %	Net Int.	Net Int. Error
B K	51.53	73.85	5.2	0.04
MgK	1.03	0.66	20.7	0.03
AlK	41.27	23.7	857.9	0
Y L	0.16	0.03	1	0.12
TiK	3.75	1.21	34.4	0.02
CuK	2.26	0.55	7	0.11

5.1.2.3 Evaluation of mechanical properties

The mechanical properties of the spark plasma sintered hybrid composite samples such as hardness, UTS, YS and elongation were tested by the procedure discussed in section 3.6. The hardness of the nano hybrid composites with varying amounts of yttrium is shown in Fig. 5.8. From the Figure 5.8, it can be seen that the hardness of the composite samples increased with an increase in yttrium wt% up to 0.3 (137 HV). Upon further increase in yttrium reinforcement, hardness tended to decrease. The Vickers hardness of the unreinforced SPSed sample is 101 HV.
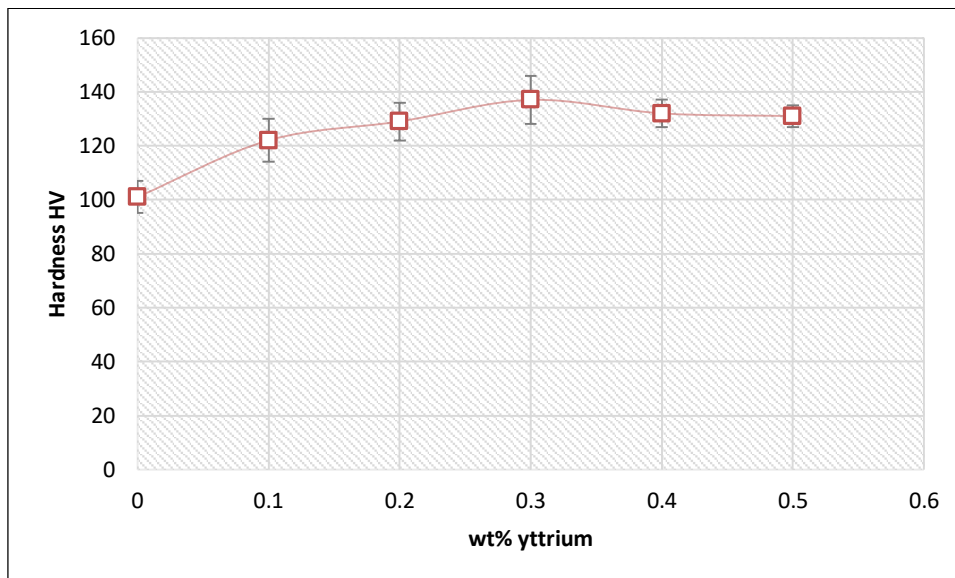
Fig. 5.8 Hardness variation of the AA2024+1.0 wt% TiB_2 hybrid composite samples reinforced with varying amounts of nano yttrium.

The tensile and elongation test results are plotted and shown in fig. 5.9 and 5.10 respectively. The tensile properties of the hybrid composites have increased significantly and their variation

with nano yttrium reinforcement followed a trend similar to the composites developed by stir casting, cold compaction and SPS. The UTS and YS of the unreinforced SPSed samples are 143 MPa and 126 MPa respectively. - The elongation of the hybrid composite samples also followed a similar trend. Both UTS and YS of the hybrid composite samples increased up to 0.3 wt% yttrium reinforcement (496 MPa and 458 MPa) and then started to decrease upon further increase in yttrium reinforcement. Due to the grain refinement, formation of nano grains, dispersion strengthening caused by reinforcements along with micro and nano precipitation strengthening, the hybrid composites yielded better mechanical properties. However, the elongation reduced remarkably as expected.
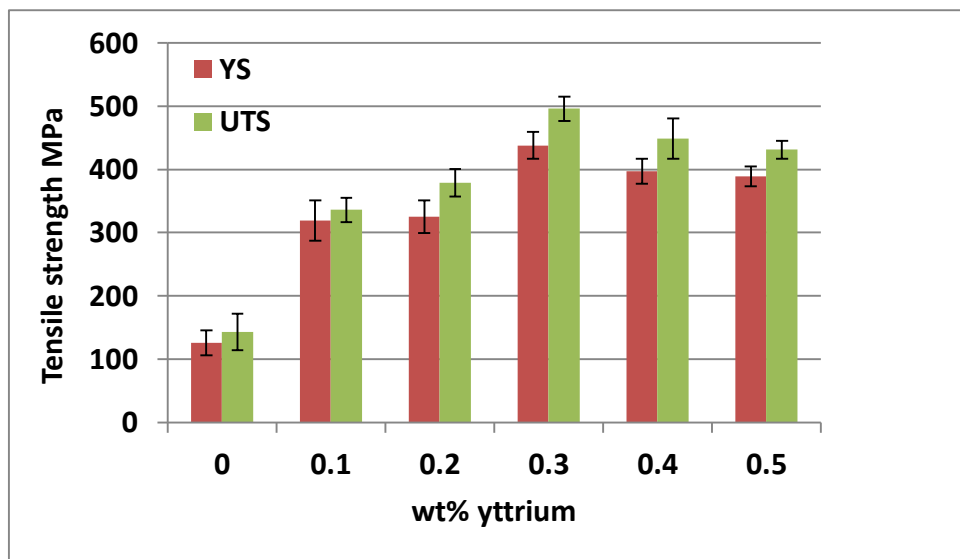
Fig. 5.9 Variation of UTS and YS of the AA2024 hybrid composite samples reinforced with 1.0 wt% TiB_2 and varying amounts of nano yttrium.

The tensile strength was improved at the cost of ductility. Fig. 5.10 shows the variation of elongation with the reinforcement of yttrium. The elongation achieved in the present hybrid composites is lesser when compared to that of the stir cast cold compacted, and spark plasma sintered (micro and nano) composite samples. A highest elongation percentage (15.7%) at fracture was recorded for the sample with 0.3 wt% yttrium reinforcement.
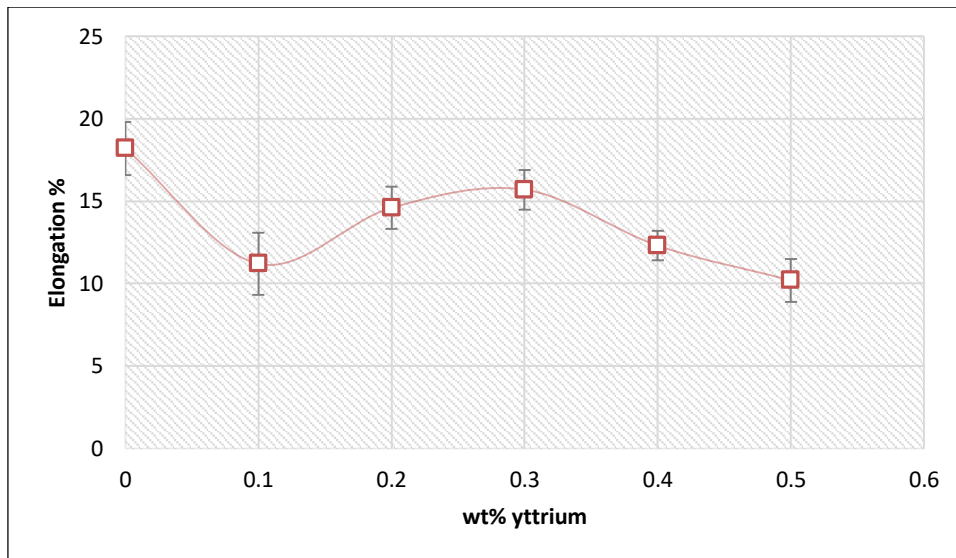
Fig. 5.10 Variation of elongation % of the hybrid composite samples reinforced with 1.0 wt% TiB$_2$ and varying amounts of nano yttrium.

5.1.3 Discussion

At low temperature and low pressure, the powder particles have the tendency to fill the void spaces by adjusting themselves within the die space without much deformation. The starting powder (AA2024) has particles with different sizes with an average particle size of 60 µ.Due to the non-uniform particle size distribution of starting powders and the pressure exerted at the start of the SPS process, bigger particles may come in contact with several smaller particles. Therefore, there will be a local distribution of the current intensity among the particles when pulsed current passes through them. As the current preferably chooses the path, which has less resistance, the distribution of the current intensity depends only on the resistances of various current paths. Due to the self-adjusting mechanism of current intensity, proposed by **Song et al.,** [150], the current intensity is uniformly distributed leading to a better densification. As the pressure is increased, the oxide layers on the aluminium particles are broken and good diffusion between particle-particle interfaces is achieved. In the beginning stages of sintering when the temperature is low, there is little change in the electrical resistivity, so the effect of the area on the local resistance is dominant. Thus, the resistance of the contact with a larger cross-sectional area is lower than that with a smaller area.

Further, as the temperature is increased, the powder particle boundaries get disturbed due to particle softening and the particles plastically flow and fill in the void spaces, increasing the density. However, the decrease in relative density in the present study can be explained by the

162

reinforcement of 1.0 wt% hard ceramic TiB_2 particles to all the samples, which might have caused small void spaces around them because of the shape misfit. The other reason might be the tendency of nano yttrium to agglomerate as its proportion increases, which leads to porosity. Though, the relative density of the hybrid composite samples decreased with an increase in the proportion of yttrium, the densities (> 99.6) were well above the densities achieved by other sintering techniques.

Reinforcement of TiB_2 and nano yttrium to AA2024 matrix brought remarkable changes in the microstructure and mechanical properties. The main hardening mechanism in the present hybrid composites was the dispersion strengthening provided by TiB_2 and nano yttrium particles. Other mechanisms like precipitate hardening and hardening due to grain size reduction also might have played a significant role. The reinforcement of 1.0 wt% TiB_2 ceramic particles to all the samples seems to have contributed equal hardness to all the hybrid composite samples. Hence, the trend of variation can be attributed to nano yttrium reinforcement. The refinement of grains, and the formation of ultra-fine and nano grains led to the increase in hardness up to 0.3 wt% yttrium reinforcement. However, yttrium reinforcement beyond 0.3 wt% led to agglomeration of nano yttrium and corresponding intermetallic Al-Cu-Y compounds at the grain boundaries which in turn deteriorated the hardness.

Both UTS and YS of the hybrid composite samples got increased with an increase in yttrium reinforcement up to 0.3 wt% and then decreased upon further reinforcement of yttrium. The main characteristic feature of SPS for effective sintering and densification is its Joules heating through high intensity pulsed current. Joules heating also known as ohmic heating and resistive heating, is basically heat developed due to resistance when current is passed through a material. Although both aluminium and yttrium are metals and conductors of electricity and heat, there is a resistance potential between them which give rise to an increase in Joules heating during sintering. On the other hand, TiB_2 being a hard ceramic powder and non-conductor of current, highly resists the pulse current and generates heat due to resistance and thus promotes Joules heating in the hybrid composite samples. Hence, the distribution of heat in the composite sample powders during sintering entirely depends on the distribution of both yttrium and TiB_2 powder particles in the AA2024 matrix. As the reinforcement of nano yttrium powder increased, it became a highly difficult to handle the powders due to agglomeration which led to a decrease in tensile strength as the dispersion strengthening ability decreased. Compared to UTS, YS of the hybrid composite samples were improved. TiB_2 has been considered as an

effective grain refiner in aluminium alloys, as the intermetallic compound Al_3Ti acts as nucleation site and promotes grain refinement. However, later, efforts were made by many researchers to suppress the formation of brittle Al_3Ti, as it degrades the mechanical properties of the alloy and makes it more brittle by reducing its ductility. In the present study, Al_3Ti formation was not encountered anywhere in the composites developed as shown in Fig. 5.7. However, intermetallic compounds rich in aluminium and boron were detected.

It is well known that TiB_2 has emerged as an effective grain refiner in aluminium castings [181, 182] and its application as reinforcement is also extended to aluminium hybrid composites [183, 184]. However, in powder metallurgy, there is only a little or no scope for grain refinement. However, in the present study, grain refinement to the extent of formation of nano grains was observed. All the hybrid composite samples contained 1 wt% TiB_2 powder with 10 µm average particle size and thus the contribution of TiB_2 in grain refinement was constant in all the composite samples. Hence, the variation in grain size was a cumulative effect of variation in reinforcement of nano yttrium and a constant contribution from TiB_2 particles. As we can see from Fig. 5.2, the grain refinement was enhanced with an increase in yttrium reinforcement. However, yttrium reinforcement beyond 0.3 wt% led to grain coarsening. The formation of new ultra-fine grains was due to Joule's heating, which created high-localized instantaneous heat at particle interface leading to instantaneous local melting of the contact particle surfaces (necking zones,) followed by rapid solidification. The process was so quick that the dynamic re-crystallization of the newly formed grains was suppressed, preventing the grain growth [185].

On the other hand, **Kepi et al.,** [179] explained the formation of nano grains during SPS as a thermo-mechanical fatigue process, which ''shatters'' the large powder particles into nano-sized grains. The ultra-fine structure was not achieved throughout the matrix but has spread around the necking zones as evident from Fig. 5.3. However, a combination of both the above said mechanisms can be observed from Fig. 5.4. Hence, in the present study it can be concluded that the formation of nano grains is attributed to the combined effect of melting and rapid solidification at necking zones due to Joule heating and the formation of sub-grains is attributed to the thermo-mechanical fatigue process.

Grain refinement, formation of nano grains, dispersion strengthening, micro and nano precipitation strengthening induced better mechanical properties in all the hybrid composites

developed. With yttrium reinforcement beyond 0.3 wt%, nano grain structure disappeared. However, the grains were finely distributed along the particle boundaries (encircled in black), as shown in Fig. 5.2 (d). The corrosion pits caused due to melting and evaporation at the particle interface due to increased pressure and heat during sintering can also be seen (encircled in light blue) [186]. Fig. 5.3 (e) shows the particle boundaries and sub grains within the particles and the arrows indicate the precipitation growth along the sub-grain boundaries. TEM examination revealed that the sample reinforced with 0.3 wt% yttrium had nano grains. However, three kinds of nano precipitates (rod shape, circular platelets and hexagonal platelets) were appearing which are indicated with different colour arrows.

Melotti et al., [187] reported that the reinforcement of TiB_2 and silver to 2xxx series aluminium alloy greatly reduced the activation energy for the formation of Ω phase (hexagonal precipitates), while the activation energy for the formation of the GP zones is unchanged. The Ω phase contributes to the strength of the 2xxx series alloy as it nucleates on the $\{1, 1, 1\}$ planes which is the slip planes, of the aluminium matrix.

Fig. 5.10 shows the variation of elongation with an increase in yttrium reinforcement. As the load was applied to the composite sample, the strengthening mechanisms became active and effective, the dislocation movement became difficult and plastic deformation did not take place at normal and regular applied loads. Therefore, the composite material fails at a much lesser strains making it brittle. However, the elongation at failure achieved in the present hybrid composites was better than the previous findings by the other researchers due to the existence of dual grains (nano and sub micro) in the microstructure and the suppression of brittle Al_3Ti phase. The ultra-fine grains contributed to the improvement in strength while the coarse grains contributed to the improvement in ductility.

5.1.4 Conclusions
From the present experimental study and results, the following conclusions can be made.

- Reinforcement of 1 wt% TiB_2 in all the hybrid composite samples has made remarkable modifications in the microstructures of the hybrid composite samples. Even though TiB_2 is not considered as a grain refiner in powder metallurgy and only used for dispersion strengthening, SPS processing created favourable conditions for TiB_2 to refine grains in its vicinity.

- The formation of nano grains is attributed to the combined effect of melting and rapid solidification at necking zones due to Joule's heating and thermo-mechanical fatigue process.

- Formation of nano grains, three different types of nano precipitates along with micro precipitates and dispersion strengthening caused by both nano yttrium and TiB_2 improved the mechanical properties of all the hybrid composite samples.

- The highest hardness, UTS and YS were achieved in the hybrid composite sample reinforced with 1 wt% TiB_2 and 0.3 wt% yttrium. The highest hardness, UTS and YS were 137 HV, 496 MPa, 438 MPa respectively, which were 135%, 219% and 306% higher than compared to the spark plasma sintered AA2024 sample.

- The strength achieved in all the hybrid composite samples was complimented with ductility (elongation percentage) with 15.7% highest elongation for the composite sample with 1wt% TiB_2 and 0.3 wt% yttrium, due to the formation of dual size grains.

- Formation of brittle Al_3Ti intermetallic has been suppressed in the present composite developed, due to the quick processing time of SPS, which did not give enough time for its formation.

- Reinforcement of 0.3 wt% yttrium seems to create a favourable condition in the nano hybrid composite sample to yield superior mechanical properties.

In the present work, some investigations are carried out with an objective to develop AA2024 matrix composites with minor reinforcements of yttrium and TiB_2.

The properties of a composite mainly depend on some factors like reinforcement material and processing method. Though the reinforcing material has the potential to improve the properties of a composite, the drawbacks and challenges encountered during the production stage deteriorate the properties of the end product. Unfortunately, very well-known and popular conventional processing techniques like stir casting and PM possess certain drawbacks while processing aluminium metal matrix composites. On the other hand, over the years, utilization of various types of reinforcing materials in aluminium metal matrix composites has increased. However, with an increase in the reinforcement wt% in the composite, certain factors like agglomeration, formation of undesirable phases, ductility reduction and cost increase. Hence, the present research is emphasized on the influence of a few factors like processing techniques, minor reinforcements of a rare earth element (yttrium) and a ceramic material (TiB_2) on the mechanical properties of AA2024 matrix composites.

The present study revealed that the reinforcement of yttrium (micro) in small amounts has improved the mechanical properties of AA2024 matrix composites. It is worthwhile to note that the AA2024 matrix composites with minor reinforcements of nano yttrium showed better mechanical properties compared to those of the composites with micro yttrium reinforcement. As mentioned in the literature review (chapter 2), a few researchers have used rare earth metals as reinforcements to enhance the mechanical properties of aluminium alloys. For example, reinforcement of small amounts of Sm [64], Ce [62, 65] Cd [67], Nd [71], Yb [72-75], Sc [76], Y [70, 78, 79], etc., are reported to improve the mechanical properties, promote grain refinement and accelerate precipitation kinetics of various aluminium alloys.

Present investigations too confirmed that the reinforcement of rare earth element (yttrium) in small amounts to an aluminium matrix significantly improves its mechanical properties through grain refinement and acceleration of precipitation kinetics. Present investigations

reassures the metallurgists that the rare earth elements act as vitamins for light metals in improving their mechanical properties.

The existing literature shows that enough investigations have been done on improving the mechanical properties of various aluminium alloys through reinforcement with TiB_2. However, in most of the cases, formation of brittle Al_3Ti phase is observed, which deteriorated the ductility of the composites. Later, some researchers have put efforts in suppressing the formation of such phases and succeeded. Present investigations on AA2024 + TiB_2 + yttrium can be regarded as one of such successful efforts to eliminate the formation of brittle Al_3Ti phase. These composites exhibited strength better than that of the micro/nano reinforced composites. The composites have not only exhibited better strength but also improved ductility.

In the present study, influence of processing techniques in the development of AA2024 + yttrium composites with respect to grain refinement and precipitation kinetics is investigated. In stir casting, due to high processing temperature, yttrium formed an intermetallic phase in the matrix, which refined the grains and hence improved the tensile strength. However, the composites developed through stir casting revealed a considerable decrease in their densities, due to the air bubbles and flue gasses entrapped in the matrix as a result of stirring. Composites developed through cold compaction showed improved mechanical properties when compared to those of the composites developed through stir casting. However, the composites failed to reach full densification in spite of sintering them in a nitrogen atmosphere at 500˚ C for 4 hours. SPS on the other hand has sintered the composites to full density at 450˚ C with 3 minutes holding time. Based on the present work, the processing methods can be rated as SPS > cold compaction > stir casting with respect to the mechanical properties attained in the composites.

From the available literature, it can be noticed that the possibilities of grain refinement in PM were very less. However, **Song et al.,** [149] reported that SPS is able to refine the grains by melting and re-crystallization during sintering and **Kepi et al.,** [178] explained the formation of nano grains in a bulk material due to thermo-mechanical fatigue during SPS. A combination of both the grain refinement mechanisms discussed above is observed in the present hybrid composites developed through SPS. In addition, due to the unique sintering mechanism of SPS, the precipitation in the composite samples is accelerated and nano precipitation is also observed. However, SPS also has certain limitations and challenges such as difficulty in sintering larger size samples and samples with complex shapes.

Additional investigations on the cryo rolling of composite samples processed through SPS showed nano grain structure and significant improvement in the tensile strength. However, the ductility of the composite samples decreased drastically.

6.1 General conclusions

The general conclusions drawn from the present work are as follows.

1) Three batches of each comprising five different AA2024 matrix composites are sucessfully developed reinforced with varying amounts of micro yttrium ranging from 0.1 to 0.5 wt% through stir casting, cold compaction and SPS. The mechanical properties of the composite samples with respect to the processing method can be rated as SPS > cold compaction > stir casting.

2) Among the different processing techniques used to develop the composite samples reinforced with micro yttrium, the composite samples processed through SPS showed improved strength. Among the SPSed composite samples, the composite reinforced with 0.3 wt% micro yttrium showed highest values of hardness, UTS, YS and EL which were found to be 114 HV, 315 MPa, 262 MPa and 22.3% respectively. The composite samples reinforced with micro yttrium and processed through SPS showed densities more than 99.6% and upto 99.97%. The densities reached in all the composites with respect to the processing methods can be rated as SPS > cold compaction > stir casting.

3) In a simillar way, five composites reinforced with varying amounts of nano yttrium ranging from 0.1 to 0.5 wt% to AA2024 matrix are also developed through SPS. The composite reinforced with 0.3 wt% nano yttrium showed better properties among the other nano composite samples. Highest hardness, UTS, YS and EL are found to be 130 HV, 462 MPa, 382 MPa and 16.8% respectively for the composite reinforced with 0.3 wt% nano yttrium.

4) Five composites reinforced with 1.0 wt% TiB_2 and varying amounts of nano yttrium ranging from 0.1 to 0.5 wt% are also developed through SPS. The formation of brittle Al_3Ti phase is supressed and the ductility is retained. The composite reinforced with 1.0 wt% TiB_2 and 0.3 wt% nano yttrium showed better properties. Highest hardness, UTS, YS and EL were found to be 137 HV, 496 MPa, 438 MPa and 15.8% respectively for the composite reinforced with 1.0 wt% TiB_2 and 0.3 wt% nano yttrium.

5) Cryo rolling of the composite samples processed through SPS reinforced with varying amounts of micro yttrium ranging from 0.1 to 0.5 wt% improved their strength remarkably, but at the cost of ductility.

6) Reinforcement of 0.3 wt% yttrium seems to create a favourable condition for all the composite samples processed through stir casting, cold compaction and SPS to yield superior mechanical properties.

6.2 Scope for future work

Scope for future work in the area of development of aluminium metal matrix composites is limitless. However, based on the gap areas identified and the investigations carried out in the present work, some extension of work can be carried out with the following themes.

In the present investigations, its is observed that the reinforcement of rare earth element (yttrium) could speed up precipitation kinetics and improve the mechanical properties of AA2024 matrix. However, there is an ample scope to investigate the effect of other rare earth elements on the mechanical properties of AA2024 matrix. Also, heat treatment response of cold compacted and SPSed composite samples can be investigated for further improvement of mechanical properties.

The evaluation of mechanical properties of the composites developed in the present work is limited only to hardness and tensile strength. However, other properties like compression strength, wear, toughness, creep, corrosion, coefficient of thermal expansion, etc., can also be evaluated in order to increase the application range of the composites developed.

In the present investigations, both micro and nano yttrium is used individually as reinforcement to develop AA2024 matrix micro and nano composites. However, there is an ample scope to develop composites by varying the size of AA2024 (matrix) powder as well in addition to the size of yttrium (reinforcement) powder through ball milling and subsequent SPS process.

In one of the present investigations, TiB_2 is used as the second reinforcement to develop AA2024 matrix hybrid composites. However, reinforcement with other ceramic materials like boron carbide, silicon carbide, silicon nitride, alumina, etc., which are less denser and cheaper

than TiB_2 can be tried to develop such hybrid composites. Heat treatment response and evaluation of other mechanical properties of these hybrid composites can also be investigated.

In the cryo rolled composite samples, though the tensile strength has increased, the main drawback is that their ductility decreased drastically. However, the cryo rolled composite samples can be further subjected to heat treatment processes like annealing, solution treatment, artificial ageing, etc., to relieve the stresses induced due to severe plastic deformation (SPD) during cryo rolling. For example, cryo rolling followed by annealing of aluminium metal matrix composites could result in a good combination of high strength and improved ductility. Apart from cryorolling, other severe plastic deformation techniques such as forging, Equi-Channel Angular Pressing (ECAP), hot rolling, etc., can also be employed on the composite samples with subsequent heat treatment to achieve superior mechanical properties.

****

REFERENCES

1) M. Kumar and C. Samuel. Selection of best renewable energy source by using vikor Method. Technology and Economics of Smart Grids and Sustainable Energy, Vol 2(1), 2017, pp 8-17.

2) G.B. Veeresh Kumar, C.S.P. Rao and N. Selvaraj. Mechanical and tribological behavior of particulate reinforced aluminium metal matrix composites–a review. Journal of Minerals and Materials Characterization and Engineering, Vol 10(9), 2011, pp 59-65.

3) Van Suchetclan and Philips Res. Product properties: A new application of composite materials. Material Reports, Vol 27, 1972, pp 28-39.

4) Kelly Tyson. The determination of interfacial shear strength in short fibre reinforced poly ethylene terephthalate by theory. Open Journal of Composite Materials, Vol 7, 2017, pp 218-226.

5) http://www.mar-bal.com/language/en/applications/advantages-of-composites/.

6) K.G. Harish, Ketan Verma, Alakesh Manna and Rajesh Kumar. Hybrid metal matrix composites and further improvement in their machinability- A review. International Journal of Latest Research in Science and Technology, Vol 1(1), 2012, pp 36-44.

7) Drozdov and Andrey. Aluminium: The thirteenth element. 2007, Rusal Library. ISBN 978-5-91523-002-5.

8) http://en.wikipedia.org/wiki/Aluminium.htm on date1/4/2011.

9) D. Vojtich. Challenges for research and development of new aluminium alloys. Metabk, Vol 49(3), 2010, pp 181-185.

10) P.N. Rao. Manufacturing technology - Foundry, forming and welding. Vol 1, Fourth edition, Tata Mc Graw Hill education.

11) M.K. Surappa. Aluminium matrix composites: challenges and opportunities. Sadhana, Vol 28(1–2), 2003, pp 319-334.

12) B. Vijaya Ramnath and C. Elanchezhian. Aluminium metal matrix composites - A review. Reviews on Advance Material Science, Vol 38, 2014, pp 55-60.

13) D.L. Danels. Analysis of stress-strain fracture and ductility behaviour of aluminium matrix composites containing discontinuous silicon carbide reinforcement. Metallurgical Transactions, Vol 16A, 1985, pp 1105-1115.

14) M. Taya, K.E. Lulay and D.J. Lloyd. Strenghening of a particulate metal matrix composite by quenching. Acta Metallurgica, Vol 39, 1991, pp 73-87.

15) K.P. Gowda, J.N. Prakash, S. Gowda, and B.S. Babu. Effect of particulate reinforcement on the mechanical properties of Al 2024-WC MMCs. Journal of Minerals and Materials Characterization and Engineering, Vol 3, 2015, pp 469-476.

16) I. Sevim, S. Sahin, H. Cug, E. Cevik, F. Hayat and M. Karal. Strength of Materials, Vol 46(2), 2014, pp 190-197.

17) Manoharan and M. Gupta. Effect of silicon carbide volume fraction on the work hardening behaviour of thermo mechanically processed aluminium-based metal matrix composites. Composites Part B, Vol 30, 1999, pp 107-112.

18) Fathima Patham, Kader mohideen, Senthil Kumar Anantharajan, M. Rahman and H.S. Lim. A study on wear mechanism and wear reduction strategies in grinding wheels used for ELID grinding. Wear, Vol 254(12), 2003, pp 1247-1255.

19) H.S. Arora, H. Singh, B.K. Dhindaw and H.S. Grewal. Effect of microstructural evolution on the properties of friction stir processed al 6061 alloy. Advance Materials Research, Vol 620, 2012, pp 77–81.

20) S. Ray. M. Tech Dissertation (Indian Institute of Technology, Kanpur, 1969).

21) D.B. Karunakar, Ram Naresh Rai, Suprakas Patra, G.L. Datta. Effect of grain refinement and residual element on hot tearing in aluminium casting. The International Journal of Advanced Manufacturing Technology, Vol 45, 2009, pp 851-858.

22) F.A. Girot, L. Albingre, J.M. Quenisset and R. Naslain. Discontinuously reinforced aluminium matrix composites. Journal of Metals, Vol 30, 1987, pp 155-184.

23) M.K. Surappa. Microstructure evolution during solidification of discontinuously reinforced metal matrix composites. Journal of Material Processing Technology. Vol 63, 1997, pp 325-333.

24) R.W. Messler. An industrially sponsored research programme in PIM. Metal Powder Report, 1990, pp 363-369.

25) Wang, Hongtao, Fang, Zhigang, Sun and Pei. A critical review of mechanical properties of powder metallurgy titanium. International Journal of Powder Metallurgy, Vol 46, 2010, pp 45-57.

26) Natarajan Nanjappan, Krishnaraj Vijayan, J. Paulo Davim. Metal matrix composites. Applied Sciences and Technology, 2015, pp 21-34.

27) Sai Mahesh Yadav Kaku, Asit Kumar Khanra and M.J. Davidson. Strain hardening behaviour and its effect on properties of zrb_2 reinforced al composite prepared by powder metallurgy technique. Journal of the Institution of Engineers (India): Series D, Vol 99(1), 2018, pp 115-124.

28) Nouari Saheb et al. Spark plasma sintering of metals and metal matrix nano composites: A review. Journal of Nanomaterials, Vol 1, 2012, pp 1-13.

29) V. Mamedov. Spark plasma sintering as advanced PM sintering method. Powder Metallurgy, Vol 45(4), 2002, pp 322-328.

30) U. Anselmi Tamburini, S. Gennari, J.E. Garay, and Z.A. Munir. Fundamental investigations on the spark plasma sintering/synthesis process-2, modelling of current and temperature distributions. Material Science and Engineering A, Vol 394 (1–2), 2005, pp 139-148.

31) Palukuri Nageswararao, Amrita Kaurwar, Dharmendra Singh and Rengaswamy Jayaganthan. Enhancement in strength and ductility of al-mg-si alloy by cryorolling followed by warm rolling. Proceedia Engineering, Vol 75. 2013, pp 151-157.

32) https://www.3m.com/.

33) M.D. Bermudez, G. Martinez-Nicolas, F.J. Carrion, I. Martinez-Mateo, J.A. Rodriguez and E.J. Herrera. Dry and lubricated wear resistance of mechanically alloyed aluminium base sintered composites. Wear, Vol 248, 2001, pp 178-186.

34) T. Miyajima and Y. Iwai. Effects of reinforcements on sliding wear behaviour of aluminium matrix composites. Wear, Vol 255, 2003, pp 606-616.

35) Y. Sahin and S. Murphy. Wear performance of aluminium alloy composites containing uni-directionally-oriented silicon carbide coated boron fibres. Wear, Vol 197, 1996, pp 248–254.

36) A. Kalkanli and S. Yilmaz. Synthesis and characterization of aluminium alloy 7075 reinforced with silicon carbide particulates. Materials and Design, Vol 29, 2008, pp 775-780.

37) R.L. Deuis, C. Subramaniun and J.M. Yell Up. Abrasive wear of aluminium composites-A review. Wear, Vol 201, 1996, pp 132-144.

38) Q. Fang, P. Sidky and M.G. Hocking. Erosive wear behaviour of aluminium based composites. Materials and Design, Vol 18 (4/6), 1997, pp 389-393.

39) K.B. Lee, H.S. Sim, S.H. Kim, K.H. Han and H. Kwon. Fabrication and characteristics of AA 6061/SiCp composites by pressureless infiltration technique. Journal of Material Science, Vol 36, 2001, pp 3179-3188.

40) G.B. Veeresh Kumar, C.S.P. Rao and N. Selvaraj. Mechanical and dry sliding wear behavior of Al 7075 alloy-reinforced with SiC particles. Journal of Composite Materials, Vol 46(10), 2012, pp 1201-1209.

41) T.F. Klimowicz and K.S. Vecchio. The Influence of aging condition on the fracture toughness of alumina-reinforced aluminium composites and fundamental relationships between microstructure and mechanical Properties of metal matrix composites. Conference Proceedings, TMS, 1990, pp 112-117.

42) I.B. Deshmanya and G. Purohit. Development of mathematical model to predict micro-hardness of Al 7075/Al_2O_3 composites produced by stir casting. Journal of Engineering Science and Technology Review, Vol 5(1), 2012, pp 44-50.

43) V. Jayaram and S.K. Biswas. Wear of Al_2O_3-SiC-(AlSi) melt oxidised ceramic composites. Wear, Vol 225, 1999, pp 1322-1326.

44) G.B. Veeresh Kumar, C.S.P. Rao, N. Selvaraj and M.S. Bhagyashekar. Studies on Al 6061-SiC and Al 7075-Al2O3 metal matrix composites. Journal of Minerals and Materials Characterization and Engineering. Vol 9(1), 2010, pp 43-55.

45) M. Selvaganesan and S. Suresh. Production and characterization of Al 6061- TiB_2 metal matrix composites. International Journal of Engineering Research and Technology, Vol 2(11), 2013, pp 3154-3159.

46) K. Ravikumar, K. Kiran and V.S. Sreebalaji. Characterization of mechanical properties of aluminium/tungsten carbide composites. Measurement, Vol 102, 2017, pp 142-149

47) Cun-Zhu Nie, Jia-Jun Gu, Jun-Liang Liu and Di Zhang. Production of boron carbide reinforced 2024 aluminium matrix composites by mechanical alloying. Materials Transactions, Vol 48(5), 2007, pp 990-995.

48) Nie, Jinfeng, Wang, Fang, Li, Yusheng, Cao, Yang, Liu, Xiangfa, Zhao, Yonghao, Zhu and Yuntian. Microstructure evolution and mechanical properties of al-TiB_2/TiC in situ aluminium-based composites during accumulative roll bonding (ARB) process. Materials, Vol 10, 2017, pp 109.

49) K.K. Alaneme and A.O. Aluko. Fracture toughness (K1C) and tensile properties of as-cast and age-hardened aluminium 6063–silicon carbide particulate composites. Scientia Iranica, Vol 19(4), 2012, pp 992-996.

50) T.G. Durai, Karabi Das and Siddhartha Das. Synthesis and characterization of Al matrix composites reinforced by in-situ alumina particulates. Materials Science and Engineering A, Vol 445-446, 2007, pp 100-105.

51) S. Jain, K. Chandra, and V. Agarwala. Microstructure and mechanical properties of vacuum hot pressed p/m short steel fiber reinforced aluminium matrix composites. International Scholarly Research Notices-Materials Science, Vol 2014, 2013, pp 1-9.

52) Desalegn Wogaso Wolla, M.J. Davidson and A.K. Khanra. Studies on the formability of powder metallurgical aluminium–copper composite. Materials and Design, Vol 59, 2014, pp 151-159.

53) Sai Mahesh Yadav Kaku, Asit Kumar Khanra and M.J. Davidson. Effect of deformation on densification and corrosion behaviour of Al-ZrB_2 composite. Metallurgical and Materials Engineering, Vol 23(1), 2017, pp 47-63.

54) Manikanta, S.S. Sharma and U. Sathish Rao. Characteristic study and enhancement of mechanical properties of Al 2024 gray cast iron powder reinforced MMC by heat treatment.

International Journal of Advance Research Ideas and Innovations in Technology, Vol 2(6), 2016, pp 1-3.

55) M. Haribabu, P. Chandrasekhar and D. Venkatesh. Fabrication, characterization and damping studies of AA2024/Cu particulate reinforced composites for naval applications. International Journal of Advances in Mechanical and Civil Engineering, Vol 4(2), 2017, pp 121-128.

56) Xiaorui Wang, Sergio Scudino and Jürgen Eckert. Production and characterization of Al 2024 matrix composites reinforced with β-Al_3Mg_2 complex metallic alloy particles. MRS Proceedings, 2013, pp 1517-1521.

57) Jinwen Qian, Jinglong Li, Jiangtao Xiong, Fusheng Zhang and Xin Lin. In situ synthesizing Al_3Ni for fabrication of intermetallic-reinforced aluminium alloy composites by friction stir processing. Materials Science and Engineering A, Vol 550, 2012, pp 279-285.

58) C.J. Hsu, Po-We Kao and N.J. Ho. Intermetallic-reinforced aluminium matrix composites produced in situ by friction stir processing. Materials Letters, Vol 61, 2007, pp 1315-1318.

59) A. Uma Jayanthi, K. Krishna Kishore, G. Sudhakar and L. Prakasa rao. Production, characterization and analysis of AA2024, reinforced with ternary alloy. International Journal of Scientific and Engineering Research, Vol 7(7), 2016, pp 90-97.

60) Z. Changzhong and L. Zhonghan. Rare-earth metals and their applications in aviation 1984, pp 7-8. http://www.dtic.mil/dtic/tr/fulltext/u2/a144410.pdf.

61) Y.L. Liu, L. Luo, M.Z. Shun, L. Zhang, Y.H. Zhao and B.L. Wu. Microstructure and mechanical properties of Al–5.5Fe–1.1V–0.6Si alloy solidified under near-rapid cooling and with Ce addition. Rare Metals, 2016, pp 1-6.

62) J. Chang, I. Moon and C. Choi. Refinement of cast microstructure of hypereutectic Al-Si alloys through the addition of rare earth metals. Journal of Material Science, Vol 33, 1998, pp 5015-5023.

63) H. Qiu, H. Yan and Z. Hu. Effect of samarium (Sm) addition on the microstructures and mechanical properties of Al–7Si–0.7Mg alloys. Journal of Alloys and Compounds, Vol 567, 2013, pp 77-81.

64) P. Kaur, D.K. Dwivedi, P.M. Pathak and S.H. Rodriguez. The effect of electromagnetic stirring and cerium addition on dry sliding reciprocating wear of hypereutectic aluminium–silicon alloy. Proceedings of Institute of Mechanical Engineers Part J, Engineering Tribology, Vol 226, 2011, pp 251-258.

65) R.S. Rana, Rajesh Purohit and S. Das. Reviews on the Influences of alloying elements on the microstructure and mechanical properties of aluminium alloys and aluminium alloy composites. International Journal of Scientific and Research Publications, Vol 2(6), 2012, pp 01-07.

66) B.T. Sofyan, K. Raviprasad and S.P. Ringer. Effects of micro alloying with Cd and Ag on the precipitation process of Al-4Cu0.3Mg (wt%) alloy at 200˚ C. Micron, Vol 32, 2001, pp 851-856.

67) S.P. Ringer, K. Hono, I.J. Polmear and T. Sakural. Nucleation of precipitation in aged Al-Cu-Mg-(Ag) alloys with high Cu: Mg ratios. Acta Materialia, Vol 44(5), 1996, pp 1883-1898.

68) D.L. Gilmore and E.A. Starke Jr. Trace element effects on precipitation processes and mechanical properties in an Al-Cu-Li alloy. Metallurgical and Materials Transactions A, Volume 28(7), 1997, pp 1399–1415.

69) F. Barlat and J. Liu. Precipitate-induced anisotropy in binary A1-Cu alloys. Materials Science and Engineering A, Vol 257, 1998, pp 47-61.

70) H.Z. Li, X.P. Ling, F.F. Li, F.F Guo, Z. Li and X.M. Zhang. Effect of Y on microstructure and mechanical properties of 2519 aluminium alloy. Transaction of Nonferrous Metals Society of China, Vol 17(6), 2007, pp 1191-1198.

71) X.M. Zhang, W.T. Wang, B. Liu, M.A. Chen, Y. Liu, Z.G. Gao, L.Y Ye and Y.Z. Jia. Effect of Nd addition on microstructures and heat-resisting properties of 2519 aluminium alloy. The Chinese Journal of Nonferrous Metals, Vol 19(1), 2009, pp 15-20. (In Chinese).

72) D.H. Xiao and B.Y. Huang. Effect of Yb addition on precipitation and microstructure of Al-Cu-Mg-Ag alloys. Transactions of Nonferrous Metals Society of China, Vol 17(6), 2007, pp 1181-1185.

73) H.C. Fang, K.H. Chen, Z. Zhang and C.J. Zhu. Effect of Yb addition on microstructures and properties of 7A60 aluminium alloy. Transactions of Nonferrous Metals Society of China, Vol 18(1), 2008, pp 28-32.

74) K.H. Chen, H.C. Fang, Z. Zhang, X. Chen and G. Liu. Effect of Yb, Cr and Zr additions on recrystallization and corrosion resistance of Al-Zn-Mg-Cu alloys. Materials Science and Engineering A, Vol 497, 2008, pp 426-431.

75) Fang Hua-chan, Chen Kang-hua, Zhang Zhuo and Zhu Chang-jun. Investigation of the Effect of Yb additions on microstructures and properties of 7A60 aluminium alloy. Transition Non Ferrous Metals Society China, Vol 18, 2008, pp 28-32.

76) Ying Pio Lim, Wei Hong Yeo, and Azliana Masita. Effect of heat treatment on gravity die-cast Sc-A356 aluminium alloy. Manufacturing Revolution, Vol 4, 2017, pp 3-9.

77) Y.J. Zhang et al. A new technology to improve the elongation of A356 alloy. Solid State Phenomena, Vol 217-218, 2015, pp 450-454.

78) Ying Pio Lim and Wei Hong Yeo. Effect of yttrium addition on the mechanical properties of A356 aluminium alloy. Proceedings of the World Congress on Mechanical, Chemical, and Material Engineering (MCM 2015) Barcelona, Spain, 2015, pp 93-97.

79) B. Wang et al. Effects of yttrium on microstructure and mechanical properties of in situ (al$_2$o$_3$+al$_3$zr)p/a356 composites. Advanced Materials Research, Vol 152-153, 2011, pp 1083-1087.

80) F.A. Girot, L. Albingre, J.M. Quenisset and R. Naslain. Journal of Metals, Vol 39, 1987, pp 18-21.

81) N. Harnby, M.F. Edward and A.W. Nienow. Mixing in process industries, Butterworths, London, 1985.

82) B.T. Ramesh. Fabrication of stir casting setup for metal matrix composite. International Journal for Scientific Research and Development. Vol 5, 2017, pp 2321-2613.

83) Pardeep Sharma, G. Chauhan and Neeraj Sharma. Production of AMC by stir casting - an overview. International Journal of Controlled Practice, Vol 2, 2005, pp 23-46.

84) V. Agarwala and D. Dixit. Fabrication of aluminium base composite by foundry technique. Transactions of the Japan Institute of Metals, Vol 22(8), 1981, pp 521-526.

85) S. Ray. Casting of metal matrix composites. Key Engineenng Materials, vol (104-107), 1995, pp 417-446.

86) A.D. Sable and S.D. Deshmukh. Preparation of MMCs by stir casting method. International Journal of materials Engineering Technology, 2012, pp 3-11.

87) S. Poria, G. Sutradhar and P Sahoo. wear and friction behavior of stir cast Al-TiB$_2$ metal matrix composites with various lubricants. Tribology in Industry, Vol 38 (4), 2016, pp 508-521.

88) Qi Gao, Shusen Wu, Shulin Lü, Xuecheng Duan and Ping An. Preparation of in-situ 5vol% TiB$_2$ particulate reinforced Al–4.5Cu alloy matrix composites assisted by improved mechanical stirring process. Materials and Design, Vol 94, 2016, pp 544-552. doi:10.1016/j.matdes.2016.01.023.

89) Nanjappan, Natarajan, Vijayan, Krishnaraj and J. Davim. Machinability of metal matrix composites. Springer Briefs in Applied Sciences and Technology, 2015, pp 67-85.

90) S.M. Suresh, Debadutta Mishra, A. Srinivasan, R.M. Arunachalam and R. Sasikumar. Production and characterization of micro and nano Al$_2$O$_3$ particle-reinforced LM 25 aluminium alloy composites. Journal of Engineering and Applied Sciences, Vol 6(6), 2011, pp 255-263.

91) A. Sreenivasan, S. Paul Vizhian, N.D. Shivakumar, M. Muniraju and M. Raguraman. A study of microstructure and wear behaviour of TiB$_2$/Al metal matrix composites. Latin American Journal of Solids and Structures, Vol 8, 2011, pp 1-8.

92) Jasmi Hashim. The production of cast metal matrix composite by a modified stir casting Method. Journal of Technology, Malaysia, 2007, pp 9-20.

93) Nabil Fat-Halla, Pascal Secordel and Michel Suery. Microstructure and mechanical properties of modified and non-modified stir-cast Al-Si hypoeutectic alloys. Journal of Materials Science, Vol 23, 1988, pp 2419-2423.

94) V. Jayaseelan, K. Kalaichelvan, M. Kannan and S. Vijay Ananth. Extrusion characterizes of al/sic by different manufacturing process. International Journal of Applied Engineering Research, Vol 1(1), 2010, pp 194-199.

95) K.K. Alanemea, B.O. Ademilua and M.O. Bodunrin. Mechanical properties and corrosion behaviour of aluminium hybrid composites reinforced with silicon carbide and bamboo leaf ash. Tribol Ind, Vol 35(1), 2013, pp 25-35.

96) S. Gopalakrishnan and N. Murugan. Production and wear characterisation of AA 6061 matrix titanium carbide particulate reinforced composite by enhanced stir casting method. Composites Part B-engineering, Vol 43, 2012, pp 103-112.

97) S. Naher, D. Brabazon and L. Looney. Simulation of the stir casting process. Journal of Materials Processing Technology, Vol 166, 2005, pp 430-439.

98) M. Mahendra Boopathi, K.P. Arulshri, N. Iyandurai, and P. Shanmughasundaram. Dry sliding wear, co-efficient of friction and corrosion behaviour of aluminium alloy 2024 reinforced with silicon carbide and fly ash hybrid metal matrix composites. International Journal of Mechanical and Mechatronics Engineering, Vol 14(4), 2012, pp 44-52.

99) James Johny, K. Venkatesan, P. Kuppan, Radhakrishnan and Ramanujam. Comparative study of composites reinforced with SiC and TiB_2. Procedia Engineering, Vol 97, 2014. doi:10.1016/j.proeng.2014.12.378.

100) S.K. Ravesh and T.K. Garg. Preparation and analysis for some mechanical property of aluminium based metal matrix composite reinforced with SiC and fly ash. International Journal of Engineering Research Applications, Vol 2(6), 2012, pp 727-731.

101) Gaurav Mahajan, Karve, Nikhil, Patil, Uday, P. Kuppan and K. Venkatesan. Analysis of microstructure, hardness and wear of Al-SiC-TiB_2 hybrid metal matrix composite. Indian Journal of Science and Technology, Vol 8, 2015, pp 101-109.

102) K.R. Ramkumar, Habtamu Bekele, and S. Sivasankaran. Experimental investigation on mechanical and turning behavior of al 7075/x% wt TiB_2-1% Gr in situ hybrid composite. Advances in Materials Science and Engineering, vol 2015, 2015, pp 1-14.

103) Suswagata Poria, Sutradhar, Goutam, Sahoo and Prasanta. Wear and friction behavior of Al-TiB_2-nano-Gr hybrid composites fabricated through ultrasonic cavitation assisted stir casting. Materials Research Express, Vol 5, 2018, pp 1-10.

104) Bhargavi Rebba and N. Ramanaiah. Studies on mechanical properties of 2024 al – b_4c composites. Advanced Materials Manufacturing and Characterization, Vol 4(1), 2014, pp 42-46.

105) B. Bhaskar and Abdul Sharief. Effect of solutionizing on dry sliding wear of al2024-beryl metal matrix composite. Journal of Mechanical Engineering and Sciences, Vol 3, 2012, pp 281-290.

106) M. Rajaram Narayanan and S. Nallusamy. Experimental analysis of aluminium alloy metal matrix composite with tungsten carbide by in-situ method using SEM. Journal of chemistry, Vol 11(1), 2018, pp 355-360.

107) A. Canakci, F. Arslan and T. Varol. Effect of volume fraction and size of B_4C particles on production and microstructure properties of B_4C reinforced aluminium alloy composites. Materials Science and Technology, Vol 29(8), 2013, pp 954-960.

108) K. Punith Gowda, J.N. Prakash and K. Channakeshavalu. Evaluation of wear properties of Al 2024 reinforced with tungsten carbide particulate metal matrix composites. International Journal of Advance Research in Science and Engineering, Vol 6(12), 2011, pp 1139-1142.

109) Ajit Bhandakkar, R.C. Prasad and M.L. Shankar Sastry. Fracture toughness of AA2024 aluminium fly ash metal matrix composites. International Journal of Composite Materials, Vol 4(2), 2014, pp 108-124.

110) J. Babu Rao, D. Venkata Rao, I. Narasimha Murthy and N.R.M.R. Bhargava. Mechanical properties and corrosion behaviour of fly ash particles reinforced AA2024 composites. Journal of Composite Materials, Vol 46(12), 2011, pp 1393-1404.

111) Vijayalakshmi and M. Balaji. Deformation behaviour of AA2024 alloy fly ash composites by using FEM. International Organization of Scientific Research-Journal of Engineering, Vol 04(9), 2014, pp 46-48.

112) Inampudi Narasimha Murthy, Nallabelli Arun Babu and Jinugu Babu Rao. Comparative studies on microstructure and mechanical properties of granulated blast furnace slag and fly ash reinforced AA2024 composites. Journal of Minerals and Materials Characterization and Engineering, Vol 2, 2014, pp 319

113) Y.M Shivaprakash, K.V. Sreenivasa Prasad and Yadavalli Basavaraj. Dry sliding wear characteristics of fly ash reinforced AA2024 based stir cast composite. International Journal of Current Engineering and Technology, Vol 3(3), 2013, pp 911-921.

114) S. Pitchi Reddy and A. Chennakesava Reddy. Synthesis and characterization of zirconium carbide nano particles reinforced AA2024 alloy matrix composites cast by bottom-up pouring. 7th International Conference on Composite Materials and Characterization, Bangalore, 2009, pp 211-215.

115) M. Boopathi, K.P. Arulshri and N. Iyandurai. Evaluation of mechanical properties of aluminium alloy 2024 reinforced with silicon carbide and fly ash hybrid metal matrix composites. American Journal of Applied Science, Vol 10(3), 2013, pp 219-229.

116) G. Siva Karuna et al. Effect of blast furnace slag and red mud reinforcements on the mechanical properties of AA2024 hybrid composites. Advanced Materials Research, Vol 1148, 2018, pp 29-36.

117) A. Uma Jayanthi, K. Krishna Kishore, G. Sudhakar and L. Prakasa rao. Production, characterization and analysis of AA2024, reinforced with ternary alloy. International Journal of Scientific and Engineering Research, Vol 7(7), 2016, pp 90-97.

118) Z.W. Chen, S.R. Peck and C.J. Davidson. Semisolid casting using a vertical-injection squeeze casting machine: material flow and tensile properties of Al-7Si-0.3Mg alloy, International Journal of Cast Metals Research, Vol 12(2), 1999, 127-135, doi: 10.1080/13640461.1999.11819350.

119) R. Sagar and R. Purohit. Fabrication and testing of Al-SiCp composite valve seat inserts. International Journal of Advance Manufacturing Technology, Vol 29, 2006, pp 922-928.

120) M. Ramachandra, A. Abhishek, P. Siddeshwar and V. Bharathi. Hardness and wear resistance of zro_2 nano particle reinforced al nano composites produced by powder metallurgy. Procedia Materials Science, Vol 10, 2015, pp 212-219.

121) Meysam Tabandeh Khorshid, Emad Omarani, L.P. Menezes and P.K. Rohatgi. Tribological performance of self –lubricating aluminium matrix nano composites: Role of graphene nano platelets. Engineering Science and Technology, Vol 19, 2016, pp 463-469.

122) Hossein Abdizadeh, Reza Ebrahimifard and Mohammad Amin Baghchesara. Investigation of microstructure and mechanical properties of nano MgO reinforced Al composites manufactured by stir casting and powder metallurgy methods: A comparative study. Composites, Part B, Vol 56, 2014, pp 217-221.

123) E. Amal Nassar and E. Eman Nassar. Properties of aluminium matrix nano composites prepared by powder metallurgy processing. Journal of King Saud University – Engineering Sciences, Vol 5, 2015, pp 59-67.

124) A. Umma, M.A. Maleque, I.Y. Iskandar and Y.A. Mohammed. Carbon nano tube reinforced aluminium matrix nano-composite: A critical review. Australian Journal of Basic and Applied Sciences, Vol 6(12), 2012, pp 69-75.

125) Aoshuang Tan, Jie Teng, Xiang Zeng, Dingfa Fu and Hui Zhang. Fabrication of aluminium matrix hybrid composites reinforced with SiC micro particles and TiB_2 nanoparticles by powder metallurgy. Powder Metallurgy, Vol 60(1), 2017, pp 144-153.

126) T. Rajmohan, K. Palanikumar and S. Ranganathan. Evaluation of mechanical and wear properties of hybrid aluminium matrix composites. Transactions of Nonferrous Metal Society of China, Vol 23(9), 2013, pp 2509-2517.

127) B.V. Subrahmanyam, S.V. Gopla Krishna, C. Lakshmi Pornima and A.Srinivasa Rao. Evaluation of the mechanical properties on aluminium alloy 2024 -fly ash metal matrix

composite. International Journal of Advanced Mechanical Engineering, Vol 8(1), 2018, pp 1-11.

128) I. Ovali, H. Karakoç and H. Çinici. Optimization of the wear resistance of AA2024 matrix composites fabricated with hot pressing. Journal of Advanced Metals and Materials Engineering, Vol 79(1), 2016, pp 66-71.

129) C.H. Krishnama Raju and A. Srinivasa Ganapathi. Investigation of mechanical properties of aluminium based powder metallurgical composites reinforced with SiC and Al_2O_3. International Journal of Engineering Science and Invention, Vol 7(3), 2018, pp 62-67.

130) S. Vinoth kumar, K. Manisekar and P. Ravindran. Development and tribological performance of nano SiC particles on the AA2024 hybrid composites with the addition of nano graphite. 5th International and 26th All India Manufacturing Technology, Design and Research Conference (AIMTDR 2014), 2014, pp 173-176.

131) D.K. Das, P.C. Mishra, Saranjit Singh and R.K. Thakur. Properties of ceramic-reinforced aluminium matrix composites: A review. International Journal of Mechanical and Materials Engineering, Vol 9(12), 2014, pp 341-347. doi.org/10.1186/s40712-014-0012-9.

132) M.H. Enayati and M. Salehi. Formation mechanism of Fe_3Al and FeAl intermetallic compounds during mechanical alloying. Journal of Material Science, Vol 40, 2005, pp 3933-3945. https://doi.org/10.1007/s10853-005-0718-4.

133) Syed Ghazi Sarwat. Contamination in wet-ball milling, Powder Metallurgy, Vol 60(4), 2017, pp 267-272. doi: 10.1080/00325899.2017.1280647.

134) T. Pieczonka, Thomas Schubert, Stefan Baunack and Bernd Kieback. Sintering behaviour of aluminium in different atmospheres. 4th International Conference on Science, Technology and Applications of Sintering, Sintering 2005.

135) Guoqiang et al. Effect of interface behaviour between particles on properties of pure aluminium compacts by spark plasma sintering. Materials Transactions, Vol 42(9), 2001, pp 1846-1849.

136) A. Muthuchamy, A. Raja Annamalai, Swati Ghosh Acharyya, Nidhi Nagarajua and D.K. Agarwal. Microstructural and electrochemical behaviour of aluminium alloy composites produced using different sintering techniques. Materials Research, Vol 21(3), 2018, pp 1-7.

137) Ehsan Ghasali, Hossein Nuranian, Ali Rahbari, Houdsa Majidian, Masoud Alizadeh and Touradj Ebadzadeh. Low temperature sintering of aluminium-zircon metal matrix composite prepared by spark plasma sintering. Materials Research, Vol 19, 2016, pp 1-4. doi.org/10.1590/1980-5373-MR-2016-0395.

138) B. Mallik, Koushik Sikdar and Debdas Roy. Synthesis and characterization of aluminium base in situ metal matrix composites by spark plasma sintering. Journal of Materials Science Research, Vol 7(1), 2017, pp 14-19.

139) G.A. Sweet, M. Brochu, I.W. Donaldson and D.P. Bishop. Consolidation of aluminium-based metal matrix composites via spark plasma sintering. Materials Science and Engineering A, Volume 648, 2015, pp 123-133.

140) Ehsan Ghasali, Parvaneh Sangpour, AlirezaJam, Hosein Rajaei, Kamyar Shirvanimoghaddam and Touradj Ebadzadeh. Microwave and spark plasma sintering of carbon nanotube and graphene reinforced aluminium matrix composite. Archives of Civil and Mechanical Engineering, Vol 18(4), 2018, pp 1042-1054.

141) Ehsan Ghasali et al. Evaluation of microstructure and mechanical properties of al-tic metal matrix composite prepared by conventional, microwave and spark plasma sintering methods. Materials Vol 10(11), 2017, pp 1255-1262.

142) P. Cavaliere, B. Sadeghi and A. Shabani. Carbon nano tube reinforced aluminium matrix composites produced by spark plasma sintering. Journal of Material Science, Vol 52, 2017, pp 8618-8625.

143) Ridvan Yamaoglu and Eugene A. Olevsky. Consolidation of Al-nano SiC composites by spark plasma sintering. International Journal of Materials, Mechanics and Manufacturing, Vol 4(2), 2016, pp 119-122.

144) Kosty Firestein, S. Corthay, A.E. Steinman, Andrei Matveev, A.M. Sukhorukova, Irina Kovalskii, Dmitri Golberg and Dmitry Shtansky. High-strength aluminium-based composites reinforced with BN, AIB_2 and AIN particles fabricated via reactive spark plasma sintering of Al-BN powder mixtures. Materials Science and Engineering A, Vol 681, 2017, pp 1-9.

145) Behzad Sadeghi, Morteza Shamanian, Fakhreddin Ashrafizadeh, and Pasquale Cavaliere. Effect of processing parameters on microstructural and mechanical properties of aluminium–SiO_2 nano composites produced by spark plasma sintering. International Journal of Materials Research, Vol 109(5), 2018, pp 422-430.

146) Baisong Guo, Song Ni, Rujuan Shen, Zhonghu, Tang and Min Song. Microstructures and mechanical properties of carbon nanotubes reinforced pure aluminium composites synthesized by spark plasma sintering and hot rolling. Materials Science and Engineering A Volume 698, 20 June 2017, pp 282-288.

147) Ehsan Ghasali, Masoud Alizadeh and Touradj Ebadzadeh. TiO_2 ceramic particles-reinforced aluminium matrix composite prepared by conventional, microwave, and spark plasma sintering. Journal of composite materials, Vol 52(19), 2018, pp 2609-2619.

148) J. Liao, M.J Tan and I. Sridhar. Spark plasma sintered multi-wall carbon nano tube reinforced aluminium matrix composites. Materials and Design, Vol 31, 2010, pp 96-100.

149) Shijo Thomas and V. Umasankar. Effect on hardness and densification of CNT reinforced AA 2219 composites sintered in different methods. ARPN Journal of Engineering and Applied Sciences, Vol 12(6), 2017, pp 1701-1705.

150) W. Xiaoyan Song, Xuemei Liu, and Jiuxing Zhang. Neck formation and self-adjusting mechanism of neck growth of conducting powders in spark plasma sintering. Journal of American Ceramic Society, Vol 89(2), 2006, pp 494-500.

151) K. Rajeswari, M. Buchi Suresh, Dibyendu Chakravarty, Dibakar Das and Roy Johnson. Effect of nano-grain size on the ionic conductivity of spark plasma sintered 8YSZ electrolyte. International Journal of Hydrogen Energy, Vol 37(1), 2012, pp 511-517.

152) N. Naga Krishna, K. Sivaprasad and P. Susila. Strengthening contributions in ultra-high strength cryo rolled Al−4%Cu−3%TiB$_2$ in situ composite. Transactions of the Nonferrous Metal Society of China. Vol 24, 2014, pp 641-647.

153) M.V. Markushev, E.V. Avtokratova, I.Y. Kazakulov, S.V. Krymsky, M.Y. Mochalova, M.Y. Murashkin and O.S. Sitdikov. Microstructure and properties of an aluminium d16 alloy subjected to cryogenic rolling. Russian Metallurgy (Metally), Vol 4, 2011, pp 364-369.

154) Sushanta Kumar Panigrahi and R. Jayaganthan. Development of ultrafine-grained Al 6063 alloy by cryorolling with the optimized initial heat treatment conditions. Materials and Design, Vol 32, 2011, pp 2172-2180.

155) P. Das, R. Jayaganthan and I.V. Singh. Tensile and impact-toughness behaviour of cryorolled Al 7075 alloy. Materials and Design, Vol 32, 2011, pp 1298-1305.

156) S.K. Panigrahi, R. Jayaganthan and V. Pancholi. Effect of plastic deformation conditions on microstructural characteristics and mechanical properties of Al 6063 alloy. Materials and Design, Vol 30(6), 2009, pp 147-154.

157) Yu Hailiang et al. Enhanced mechanical properties of ARB-processed aluminium alloy 6061 sheets by subsequent asymmetric cryo rolling and ageing. Materials Science and Engineering A, Vol 674, 2016, pp 256-261.

158) S. Vigneshwarana, K.S.V.B.R. Krishnab, K. Chandra Sekhara, K. Sivaprasad, K. Venkateswarlud and R. Narayanasamy. A study on the work hardening and the effect of triaxiality on the fracture behaviour of some cryo rolled aluminium alloys. Materials Science and Engineering A, Vol 678, 2016, pp 165–177.

159) Fitsum Taye Feyissa and Digavalli Ravi Kumar. Enhancement of drawability of cryo rolled AA5083alloy sheets by hydro-forming. Journal Material Research Technology, Vol 24, 2018, pp 655- 663.

160) Vineet Kumara and Deepak Kumar. Investigation of tensile behaviour of cryo rolled and room temperature rolled 6082 Al alloys. Materials Science and Engineering A, Vol 691, 2017, pp 211–217.

161) Hailiang Yu, Ming Yan, Jintao Li, Ajit Godbole, Cheng Lu, Kiet Tieu, Huijun Li and Charlie Kongf. Mechanical properties and microstructure of a Ti-6Al-4V alloy subjected to cold rolling, asymmetric rolling and asymmetric cryo rolling. Materials Science and Engineering A, Vol 710, 2018, pp 10-16.

162) S. Vigneshwaran, K. Sivaprasad, R. Narayanasamy and K. Venkateswarlu. Formability and fracture behaviour of cryo rolled Al-3 Mg-0.25 Sc alloy. Materials Science and Engineering A, Vol 721, 2018, pp 14-21.

163) S. Kumar, V. Subramanya Sarma and B.S. Murty. The influence of room temperature and cryogenic temperature rolling on the aging and wear behaviour of Al–4Cu–5TiB$_2$ in situ composites. Journal of Alloys and Compounds, Vol 479, 2009, pp 268-273.

164) Yu-Lin Liu, Lei Luo, Ming-Ze Shun, Li Zhang, Yu-Hua Zhao and Bao-Lin Wu. Microstructure and mechanical properties of Al–5.5Fe–1.1V–0.6Si alloy solidified under near-rapid cooling and with Ce addition. Rare Metals, Vol 1, 2016, pp 1-6.

165) Joonyeon Chang, Inge Moon and Chongsool Choi. Refinement of cast microstructure of hypereutectic Al-Si Alloys through the addition of rare earth metals. Journal of material science, Vol 33(20), 1998, pp 5015- 5023.

166) Qiu Hongxu, Yan Hong and Hu Zhi. Effect of samarium (Sm) addition on the microstructures and mechanical properties of Al–7Si–0.7Mg alloys. Journal of Alloys and Compounds, Vol 567, 2013, pp 77-81.

167) Wei Liu, Hong Yan and Jian-Bin Zhu. Effect of the addition of rare earth element La on the tribological behaviour of AlSi5Cu1Mg alloy. Applied Sciences, Vol 163 (8), 2018, pp 1-14.

168) C. Tekmen and U. Cocean. The effect of Si and Mg on age hardening behavior of Al–SiCp composites. Journal of composite materials, Vol 37(20), 2003, pp 1791-1800.

169) Z.L. Hui, X.P. Liang, F.F. Li, F.F. Guo, L. Zhou and X.M. Zhang, Effect of Y content on microstructure and mechanical properties of 2519 aluminium alloy. Trans. Nonferrous Met. Soc. China, Vol 17(6), 2007, pp 1194-1198.

170) Y. Ridvan and A.O. Eugene. Consolidation of AL-nano SiC composites by spark plasma sintering. International journal of machining and machinability of materials, Vol 4(2), 2016, pp 119-122.

171) R.W. Cooke, and N.P. Kraus and D.P. Bishop. Spark plasma sintering of aluminium powders pre-alloyed with scandium additions. Materials Science and Engineering: A, Vol 657, 2016, 10.1016/j.msea.2016.01.053.

172) R. Ehsan and Syed. RSM Aging behavior and tensile behavior of squeeze cast Al SiC metal matrix composites. Iranian Journal of Science and Technology, Transactions A: Science, Vol 2, 2004, pp 392-397.

173) N.S. Miller and F.J. Humphery. Strengthening mechanisms in particulate metal matrix composites. Scripta Materila, Vol 25(1), 1991, pp 33-38.

174) Z.L. Hui, X.P. Liang, F.F. Li, F.F. Guo, L. Zhou and X.M. Zhang. Effect of Y content on microstructure and mechanical properties of 2519 aluminium alloy. Transactions of the Nonferrous Metal Society of China, Vol 17(6), 2007, pp 1194-1198.

175) Y.Y. Chen, Y.F. Si, F.T. Kong and et al. Effects of yttrium on microstructures and properties of Ti-17Al-27Nb alloy. Transactions of the Nonferrous Metal Society of China, Vol 16, 2006, pp 316-320.

176) L. Ruidi, Y. Tiechui, L. Xiaojun and Z. Kechao. Enhanced atomic diffusion of Fe–Al diffusion couple during spark plasma sintering. Scripta Materila, Vol 110, 2016, pp 105-108.

177) J.R. Groza. Field activation provides improved sintering. Powder Report, Vol 55, 2000, pp 16-18.

178) S. Kandukuri. A FAST winner for fully dense nano powders. Metal Powder Report, Vol 63, 2008, pp 22-27.

179) C. Kepi, Z. Xiaowen, W. Hui, Z. Ligong, Z. Jing, Y. Fuqian and A. Linan. Making Nano-structured ceramics from micrometer-sized powders via grain refinement during SPS Sintering. Journal of American Ceramic Society, Vol 91(8), 2008, pp 2475-2480.

180) Feng Qian, Eva Mørtsell, Calin Marioara, Sigmund Andersen and Li Yanjun. Improving ageing kinetics and precipitation hardening in an Al-Mg-Si alloy by minor Cd addition. Materialia, 2018, (accepted manuscript), doi:10.1016/j.mtla.2018.09.006.

181) K.T. Kashyap and T. Chandrashekar. Effects and mechanisms of grain refinement in aluminium alloys. Bulletin of Material Science, Vol. 24(4), 2001, pp 345-353.

182) V. Hotea1, J. Juhasz1 and F. Cadar. Grain refinement of 7075Al alloy microstructures by inoculation with Al-Ti-B master alloy, IOP Conf. Series: Materials Science and Engineering, 2017, pp 200-207.

183) Reza Barenji, khojastehnezhad, M. Vahid, H. Pourasl, Hamed, Rabiezadeh and Amin. Wear properties of Al–Al$_2$O$_3$/TiB$_2$ surface hybrid composite layer prepared by friction stir process, Journal of Composite. Vol 10, 2015, pp 120-129.

184) J. Nie, F. Wang, Y. Li, Y. Cao, X. Liu, Y. Zhao and Y. Zhu. Microstructure evolution and mechanical properties of Al-TiB$_2$/TiC in-situ aluminium-based composites during accumulative roll bonding (ARB) process. Materials, Vol 10(2), 2017, pp 109-117.

185) Chen Fei, Yang, Shuang, Wu, Junyan, Galaviz, Jorge, Shen, Qiang, M. Schoenung, Julie, Lavernia, Enrique and L. Zhang. Spark plasma sintering and densification mechanisms of conductive ceramics under coupled thermal/electric fields. Journal of the American Ceramic Society, Vol 98, 2014, pp 732-740.

186) S. Devaraj, R. Kumar, and S. Sankaran. Electric erosion induced microstructure and mechanical properties in spark plasma sintered Al-4.5 wt% Cu alloy. Materials Performance and Characterization, Vol 5(1), 2016, pp 54-65.

187) F. Melotti et al. Effects of TiB_2 particles and Ag on the activation energy of Ω phase in Al alloys. IOP Conference series, Material Science and Engineering A, Vol 76, 2016 pp 117-126.

188) E.O. Hall. The deformation and ageing of mild steel: III discussion of results. Proc. Phys. Soc., Sect. B, Vol 64(9), 1951, pp 747-755.

CH. SURESH VIDYASAGAR

Doctorate of Philosophy 2018

(submitted)

Indian Institute Technology, Roorkee

(IIT Roorkee)

E-MAIL

sureshvidyasagar@gmail.com

PHONE NO

 +917579076554

 +917983536101

COMPUTER SKILLS

- Auto-CAD, ANSYS 5.0, CATIA, Xpert Highscore
- Package:-M.S.Office, Exel.

AREAS OF INTEREST

- Material Science
- Nano materials
- Design and Production
- Building materials

OBJECTIVE :

To work in a collaborative and professional environment where I can enhance my acumen and add value to the organization.

PROFESSIONAL EXPERIENCE :

1) Worked as a **Teaching Assistant** in JBIET Hyderabad **from** 5th October 2009 to 14th July 2011.

ACADEMIC QUALIFICATIONS :

Submitted **Ph.D thesis** in **"DEVELOPMENT OF YTTRIUM / TiB_2 REINFORCED AA2024 MATRIX COMPOSITES WITH SUPERIOR MECHANICAL PROPERTIES"** in Department of Metallurgical and Material Science, Indian Institute of Technology, Roorkee (**IIT Roorkee**).

2) **M.Tech in Water Resource Development** From **Indian Institute of Technology, Roorkee** with CGPA **7.23** in **2013**

3) **B.Tech in Mechanical Engineering** from PBRVITS, Jawaharlal Nehru Technological University, Hyderabad with **58.54%** in **2008**

4) **Intermediate** from Sai Co-Operative Junior College, Nellore, Andhra Pradesh, **in 2004** with **75.2%.**

5) **High School** from Railway Boys High School **in 2002** with **58.33%.**

PROJECTS UNDERTAKEN :

6) Development of porous refractory ceramic materials for adsorbing Arsenic in staple drinking water, DST project in IIT Roorkee.

7) Development of yttrium / TiB_2 reinforced AA2024 matrix composites with superior mechanical properties during Ph.D program.

8) Experimental Study on the effects of porosity on the Ceramic Shells fabricated for casting Trunion Pin used in Radial Gates as a dissertation during M.Tech at IIT Roorkee.

9) Analysis of Hydraulically activated Mandrel, which holds hollow cylindrical work pieces for turning on Lathe Machine using ANSYS 5.0, during B.Tech.

INTERNATIONAL CONFRENCES ABROAD:

10) **Ch. Suresh Vidyasagar** and D.B. Karunakar, 'Synthesis and mechanical properties of spark plasma sintered 2024 AA reinforced with nano Yttrium" at 13th International Conference on Nanotek and Expo is going to be held during December 05-07, 2016 Phoenix, **USA.**

11) **Ch. Suresh Vidyasagar** and D.B. Karunakar, "Spark plasma sintering of pre alloyed 2024 AA and Yttrium powders" at International Conference on Recent Advances in Materials & Manufacturing Technologies (IMMT 2017) November 28-29, 2017, **Dubai, UAE**.

INTERNATIONAL CONFRENCES IN INDIA:

12) **Ch. Suresh Vidyasagar** and D.B. Karunakar, "Microstructure and Mechanical Properties of Spark Plasma sintered 2024 AA reinforced with Nano Yttrium" at International Conference on Hybrid and Composite Materials at St. Peters Engineering College, **Hyderabad**, India, from 25th- 27th October 2016.

13) Kashif Hasan Kazmi and **Ch. Suresh Vidyasagar**, "Simulation and experimental investigation of Mechanical properties of Aluminium-Copper Alloy" at IVth International Conference on Production and Industrial Engineering, **Allahabad,** December 2016.

14) Kashif Hasan Kazmi, B. Anand and **Ch. Suresh Vidyasagar**, "Synthesis of Al-Y composite by Spark Plasma sintering and Analysis of its Tensile properties by FEM" at AMPCO 2017, Metallurgy Department, **IIT Roorkee**, December 2017.

PUBLICATIONS :

1) **Ch.S. Vidyasagar** and D.B. Karunakar. Development of 2024 AA-Yttrium composites by spark plasma sintering. IOP Conf. Series: Materials Science and Engineering 346 (2018) 012050.

2) **Ch.S. Vidyasagar** and D.B. Karunakar. Improvement of mechanical properties of 2024 AA by reinforcing yttrium and processing through spark plasma sintering. Arabian Journal for Science and Engineering. https://doi.org/10.1007/s13369-019-03924-5.

3) **Ch.S. Vidyasagar** and D.B. Karunakar. Effects of yttrium addition and ageing on the mechanical properties of AA2024 fabricated through multi-step stir casting. Non-Ferrous Metal Society of China. TNMSC-2019-0390.R1 (**Addressing comments for revision**).

4) **Ch.S. Vidyasagar** and D.B. Karunakar. Development of Al-TiB2-Y hybrid composite with ultra-fine and nanograins through spark plasma sintering. Journal of Material Science, JMSC-D-19-04050. (**Under review**).

PERSONAL DESCRIPTION

I am a person having good logical & analytical ability with fast grasping power. My strength includes to effectively solving the problems with proper plans, schedules & with variety of solutions.

Date : ....

Place : ....…………

I hereby declare that all the information in this CV is correct

(CH. SURESH VIDYASAGAR)

Conference

1) **Ch.S. Vidyasagar** and D.B. Karunakar. Development of 2024 AA-Yttrium composites by spark plasma sintering. IOP Conf. Series: Materials Science and Engineering 346 (2018) 012050.

Journal

1) **Ch.S. Vidyasagar** and D.B. Karunakar. Improvement of mechanical properties of 2024 AA by reinforcing yttrium and processing through spark plasma sintering. Arabian Journal for Science and Engineering. (**Addressing comments for revision**).

2) **Ch.S. Vidyasagar** and D.B. Karunakar. Effects of yttrium addition and ageing on the mechanical properties of AA2024 fabricated through multi-step stir casting. Non-Ferrous Metal Society of China. TNMSC-2019-0390.R1 (**Addressing comments for revision**).

3) **Ch.S. Vidyasagar** and D.B. Karunakar. Development of Al-TiB2-Y hybrid composite with ultra-fine and nanograins through spark plasma sintering. Journal of Material Science, JMSC-D-19-04050. (**Under review**).